THE DESIGN, SYNTHESIS AND COMPLEXATION PROPERTIES OF BODIPY DERIVATIVE-BASED SIGNALING UNIT FOR CATION RECOGNITION; EXPERIMETAL AND THEORETICAL STUDIES

TASAWAN KEAWWANGCHAI

A thesis submitted in partial fulfillment of the requirements for
the degree of Doctor of Philosophy in Chemistry
Mahasarakham University
May 2012
Copyright of Mahasarakham University

THE DESIGN, SYNTHESIS AND COMPLEXATION PROPERTIES OF BODIPY DERIVATIVE-BASED SIGNALING UNIT FOR CATION RECOGNITION; EXPERIMETAL AND THEORETICAL STUDIES

TASAWAN KEAWWANGCHAI

A thesis submitted in partial fulfillment of the requirements for the degree of Doctor of Philosophy in Chemistry Mahasarakham University May 2012

Mahasarakham University

The examining committee has unanimously approved this thesis, submitted by Mrs. Tasawan Keawwangchai, as a partial fulfillment of the requirements for the Doctor of Philosophy degree in Chemistry, Mahasarakham University.

Examining Committee

Nadtanet Nunthaboot .... Chairman
(Nadtanet Nunthaboot, Ph.D.) (Faculty graduate committee)

Nongnit Morakot .... Committee
(Assoc. Prof. Nongnit Morakot, Ph.D.) (Advisor)

B. Wanno .... Committee
(Banchob Wanno, Ph.D.) (Co-advisor)

Chatthai kaewtong .... Committee
(Chatthai Kaewtong, Ph.D.) (Faculty graduate committee)

T. Tuntulani .... Committee
(Prof. Thawatchai Tuntulani, Ph.D.) (External expert)

Mahasarakham University has granted approval to accept this thesis as a partial fulfillment of the requirements for the Doctor of Philosophy degree in Chemistry.

La-orsri Sanoamuang .... _ _
(Prof. La-orsri Sanoamuang, Ph.D.) (Prof. Pradit Terdtoon, Ph.D.)
1 of the Faculty of Science Acting of the Faculty of Graduate Studies
Mahasarakham University ....May..29...... 2012

ACKNOWLEDGEMENTS

Tasawan Keawwangchai

ชื่อเรื่อง	การออกแบบ การสังเคราะห์ และสมบัติการเกิดสารประกอบเชิงซ้อน ของอนุพันธ์ของบอดีพาย สำหรับการตรวจจับแคตไอออน: การทดลอง และ การศึกษาเชิงทฤษฎี
ผู้วิจัย	นางทัศน์วรรณ แก้ววังชัย
ปริญญา	ปริญญาดุษฎีบัณฑิต **สาขาวิชา** เคมี
กรรมการควบคุม	รองศาสตราจารย์ ดร.นงนิตย์ มรกต
	อาจารย์ ดร.บรรจบ วันโน
มหาวิทยาลัย	มหาวิทยาลัยมหาสารคาม **ปีที่พิมพ์** 2555

บทคัดย่อ

ได้สังเคราะห์รีเซปเตอร์ที่เป็นอนุพันธ์ของ 4,4-ไดฟลูออโร-4-บอรา-3เอ,4เอ-ไดเอซา-เอส-อิน เดคซีน (บอดีพาย) 4 ตัว คือ 8-(4-ไฮดรอกซีฟีนิล)-1,3,5,7-เตตระเมทิล-บอดีพาย (**L1**), 8-(3,4-ไดไฮ ดรอกซีฟีนิล)-1,3,5,7-เตตระเมทิล-บอดีพาย (**L2**), 8-(4-(2-ไดเอทิลอะมิโน)-2-ออกโซเอทอกซี)ฟีนิล)- 1,3,5,7-เตตระเมทิล-บอดีพาย (**L3**) และ 8-(3,4-บิส(2-ไดเอทิลอะมิโน)-2-ออกโซเอทอกซี)ฟีนิล)- 1,3,5,7-เตตระเมทิล-บอดีพาย (**L4**) ผ่านปฏิกิริยาการคู่ควบระหว่างอนุพันธ์ของเบนซัลดีไฮด์กับ 2,4-ได เมทิลไพรโรล ได้ศึกษาการเกิดเป็นสารประกอบเชิงซ้อนระหว่างรีเซปเตอร์ที่สังเคราะห์ได้กับไอออน โซเดียม (Na^+) ไอออนโพแทสเซียม (K^+) ไอออนเงิน (Ag^+) ไอออนแคลเซียม (Ca^{2+}) ไอออนตะกั่ว (Pb^{2+}) ไอออนปรอท (Hg^{2+}) ไอออนโคบอลต์ (Co^{2+}) ไอออนนิเกิล (Ni^{2+}) ไอออนเหล็ก (Fe^{2+}) ไอออนสังกะสี (Zn^{2+}) ไอออนแคดเมียม (Cd^{2+}) ไอออนทองแดง (Cu^{2+}) ไอออนโครเมียม (Cr^{3+}) ไอออนอะลูมิเนียม (Al^{3+}) และไอออนเจอร์มาเนียม (Ge^{4+}) ด้วยเทคนิคยูวี-วิสิเบิล สเปกโทรสโกปีและฟลูออเรสเซนต์ สเปกโทรสโกปี ผลการศึกษาด้วยเทคนิคยูวี-วิสิเบิลสเปกโทรสโกปี แสดงการลดลงของค่าการดูดกลืน สูงสุดของรีเซปเตอร์ทั้งหมดเมื่อเติม Al^{3+} ยกเว้นรีเซปเตอร์ **L4** สเปกทราของฟลูออเรสเซนต์แสดงการ ลดลงของค่าความเข้มการคายแสงสูงสุด เมื่อเติม Al^{3+} สำหรับรีเซปเตอร์ **L2** และ **L3** และเมื่อเติม Cu^{2+} สำหรับรีเซปเตอร์ **L1** และ **L4** ตามลำดับ ได้ศึกษาการเกิดเป็นสารประกอบเชิงซ้อนของรีเซป เตอร์ที่เป็นอนุพันธ์ของบอดีพายที่มีอะตอมตัวให้เป็นออกซิเจน (**L1** - **L4**) และที่มีอะตอมตัวให้เป็น กำมะถัน กับ Na^+, Ag^+, Al^{3+} และ Cu^{2+} โดยใช้การคำนวณด้วยทฤษฎีฟังก์ชันความหนาแน่น ผลการ คำนวณแสดงให้เห็นว่ารีเซปเตอร์ทุกตัวสามารถเกิดเป็นสารประกอบเชิงซ้อนกับ Al^{3+} ได้ดีที่สุด เมื่อ เทียบกับแคตไอออนตัวอื่น

คำสำคัญ: การจดจำแคตไอออน ; อนุพันธ์ของบอดีพาย ; ตัวตรวจวัดฟลูออเรสเซนต์ ; ทฤษฎี ฟังก์ชันความหนาแน่น

TITLE	The Design, Synthesis and Complextion Properties of BODIPY Derivative-based Signaling Unit for Cation Recognition; Experimental and Theoretical Studies
AUTHOR	Mrs. Tasawan Keawwangchai

DEGREE   Doctor of Philosophy degree in Chemistry

ADVISORS   Assoc. Prof. Nongnit Morakot, Ph.D.

Banchob Wanno, Ph.D.

UNIVERSITY Mahasarakham University   **YEAR** 2012

ABSTRACT

Four 4,4-difluoro-4-bora-3a,4a-diaza-*s*-indacene (BODIPY) receptors, 8-(4-hydroxyphenyl)-1,3,5,7-tetramethyl-BODIPY (**L1**), 8-(3,4-dihydroxyphenyl)-1,3,5,7-tetramethyl-BODIPY (**L2**), 8-(4-(2-(diethylamino)-2-oxoethoxy)phenyl)-1,3,5,7-tetra methyl-BODIPY (**L3**) and 8-(3,4-bis(2-(diethylamino)-2-oxoethoxy)phenyl)-1,3,5,7-tetramethyl-BODIPY (**L4**) have been synthesized via a coupling between derivative of benzaldehyde and 2,4-dimethylpyrrole. Complexations between synthesized receptors and Na^+, K^+, Ag^+, Ca^{2+}, Pb^{2+}, Hg^{2+}, Co^{2+}, Ni^{2+}, Fe^{2+}, Zn^{2+}, Cd^{2+}, Cu^{2+}, Cr^{3+}, Al^{3+}, and Ge^{4+} ions were investigated using UV-vis spectroscopy and fluorescent spectroscopy techniques. The UV-visible results show the decreasing of maxima absorption of all receptors when addition of Al^{3+} ion except for receptor for **L4**. The fluorescent spectra show the decreasing of maxima emission intensity when successive addition of Al^{3+} ion for receptors **L2** and **L3** and when addition of Cu^{2+} ion for receptors **L1** and **L4**, respectively. The complexations of BODIPY derivative receptors containing oxygen donor atom (**L1** – **L4**) and containing sulphur donor atom with Na^+, Ag^+, Al^{3+} and Cu^{2+} ions were investigated using the density functional theory calculation. Calculation results point out that all of receptors show the strongest complexation with Al^{3+} ion comparing to the other cations.

Key Words : cation recognition ; BODIPY derivatives ; fluorescent sensor ; the
density functional theory

CONTENTS

Page

Page

LIST OF TABLES

LIST OF FIGURES

Page

Page

LIST OF SCHEMES

LIST OF ABBREVATIONS AND SIGNS

o	Degree
δ	Chemical shift
^{o}C	Degree Celsius
Δ	Delta
Å	Angstrom
au	Atomic unit
B3LYP	Becke's three parameter hybrid functional using the LYP correlation function
DFT	Density functional theory
E	Energy
eV	Electron volt
equiv.	Equivalent
g	Gram
G	Gibbs free energy
^{1}H-NMR	Proton nuclear magnetic resonance
H	Enthalpy
HOMO	Highest Occupied Molecular Orbital
Hz	Hertz
J	Coupling constant
K	Kelvin
K_a	Association constant
kcal	Kilocalorie
LUMO	Lowest unoccupied molecular orbital
LYP	Lee-Yang-Parr functional
M	Molar
mL	Milliliter
NBO	Natural bond orbital
ppm	Part per million
s, d, m	Splitting patterns of ^{1}H-NMR (singlet, doublet and multiplet)

CHAPTER 1

INTRODUCTION

1.1 Rationale and Background

Fluorescent chemosensors, capable of recognizing metal ions and organic cations as well as various anions and neutral molecules more and more selectively, have gained much research interest. The selective complexing ability of sensor molecules is based on the phenomenon of molecular recognition. These fluorescent ligands can be used as sensor molecules for constructing optical sensors. Recently fluorescent dryes have play were attractions. Bright colours and wide range of wavelengths make fluorescent dyes of interest in many fields of study such as biological chemistry, photochemistry, physical chemistry and optical engineering. Many such dyes are known. There are diversity of structures, spectroscopic properties, and chemical reactivities differentiating the dyes providing a huge variation of photochemical properties which can be used to select a dye for a particular purpose. [1] Reflecting this, there are many organic dyes in common use including fluorescein, [2] rhodamine, [3] cyanine, [4] alexa, [5] ethidium [6] and 4,4-difluoro-4-bora-3a,4a-diaza-s-indacene (BODIPY) as shown in Figure 1.1. These all tend to be relatively small molecules with absorption and emission bands in the rang of 300-800 nm. Given the nature of this project the remainder of this review focuses on BODIPY dyes.

fluorescein

rhodamine

alexa

ethidium bromide

cyanine
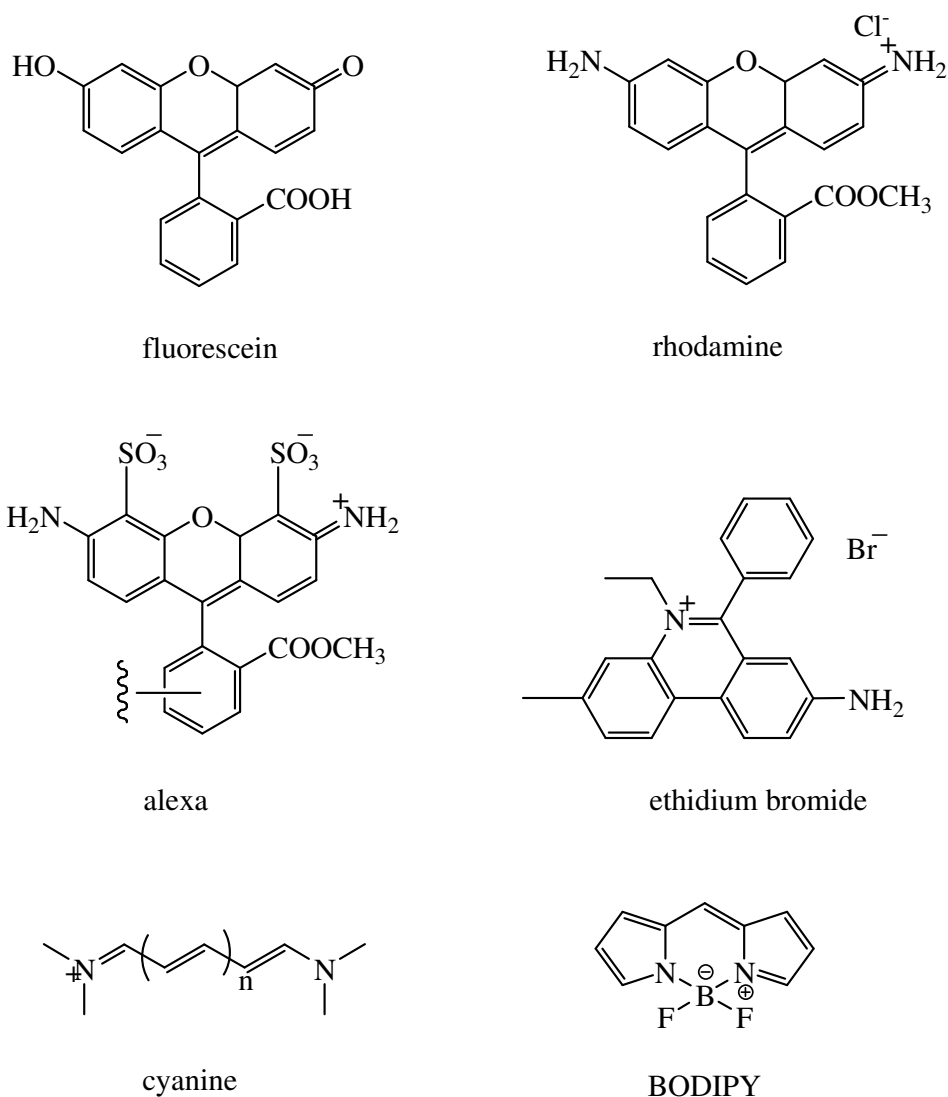
BODIPY

Figure 1.1 Organic fluorescent dye structures

1.2 BODIPY dyes

The BODIPY dye was first discovered in 1968 by Treibs and Kreuzer. [7] Since then, the BODIPY dye has become one of the most versatile organic fluorophore labels in use. These dyes have been used much and became popular in recent three decades because they have many excellent properties. One of their most important characteristics is that it is strongly UV (ultra violet) absorbing molecule and it emits radiation with high quantum yield; in addition it has sharp fluorescence peaks. Another property of this molecule is that it is relatively insensitive to polarity and pH of its

environment which means that its absorption and emission characteristics do not change much by changing the solvent. Also it is stable to physiological conditions. Furthermore, its fluorescence characteristics can be tuned by small modifications. In fact all positions (1–8) of a BODIPY skeleton as shown in Figure 1.2 are labile to chemical modifications. Especially, modifications on positions 2, 3, 5, 6 extend the conjugation and make it possible to obtain new dyes having absorption and emission maxima in red and near IR regions of the electromagnetic spectrum. Furthermore, functional units can also be attached with modifications to positions 4 and 8. Derivatization and functionalization of BODIPY dyes are still a challenge and research studies to that end are continuing.
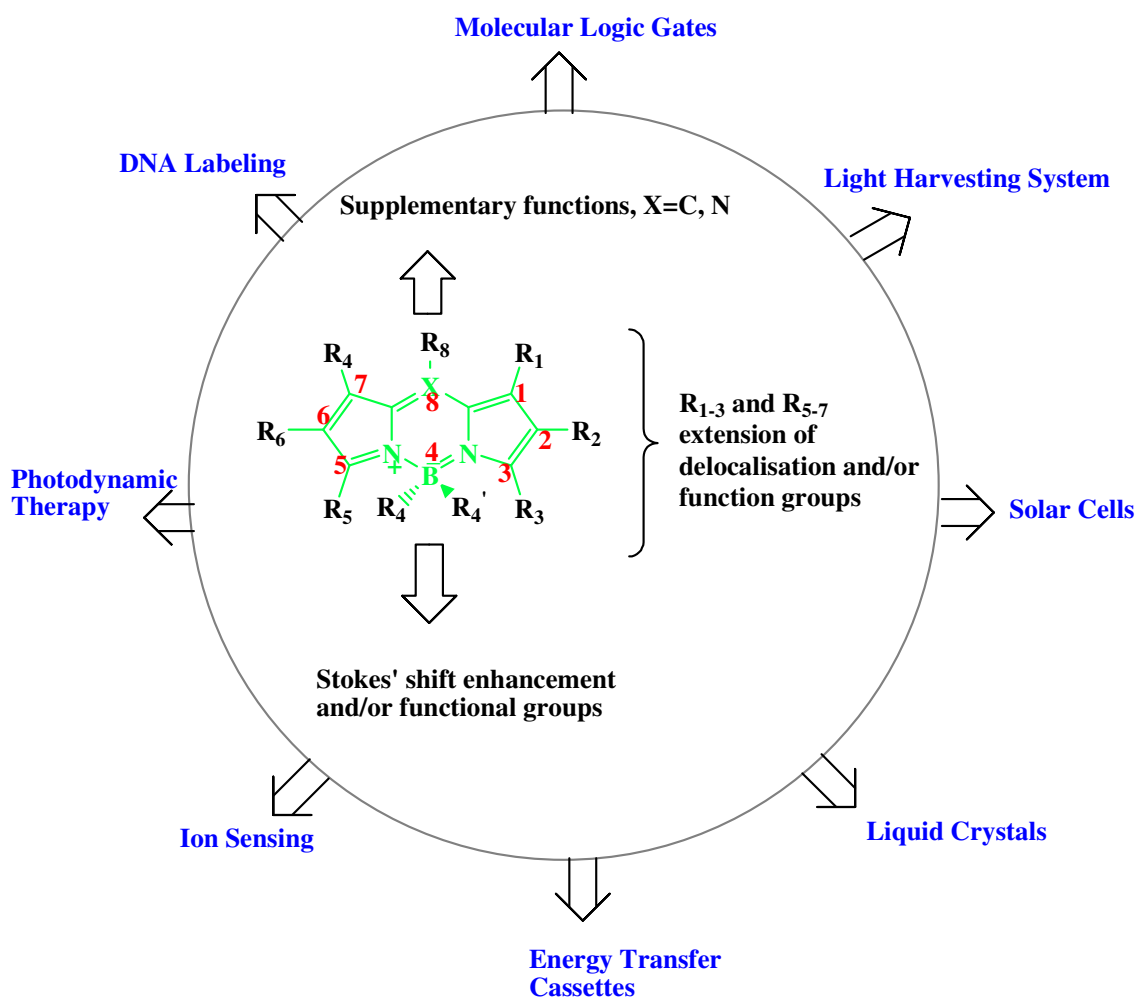
Figure 1.2 Potential applications of BODIPY dyes

Hence, now many research groups design new projects based on this small molecule and synthesize different types of it by changing its core. They have been widely used for monitoring biomolecules in living cells. [8] For instance, BODIPYs have been attached to both proteins, [9-10] and viruses. [11] Other uses include roles in laser dyes, [12-13] nanocrystals, [14] fluorescent switches, [15] and chemosensors. [16]

1.3 Objectives of Research

1. To design and synthesis novel BODIPY-based receptors for cation recognition.

2. To investigate the binding ability of BODIPY-based receptors with various cations by using UV-Vis and fluorescent spectrophotometries.

3. To study the binding energy and thermodynamic property change of complexation between BODIPY-based receptors and cations.

1.4 The Scope of Research

This project has been focused on the design and synthesis of BODIPY-based receptors for cation sensors as shown in Figure 1.3. The designed target sensors were contained BODIPY moieties as optical signaling unit. The hydroxyphenyl and 2-(diethylamino)-2-oxoethoxy)phenyl) groups at BODIPY meso-position were proposed for cation binding sites. The binding properties of the complexation between chemosensors and cations (K^+, Na^+, Ag^+, Ca^{2+}, Cu^{2+}, Cd^{2+}, Hg^{2+}, Pb^{2+}, Fe^{2+}, Zn^{2+}, Co^{2+}, Ni^{2+}, Fe^{3+}, Cr^{3+}, Al^{3+} and Ge^{4+}) were investigated by UV-Vis and fluorescent spectrophotometries. The computational calculation has been performed to investigate the geometrical structures of synthetic compounds, analogues sulfur compounds (Figure 1.4) and their complexes with cations. The binding energies and thermodynamic property changes of complexation between chemosensors and various cations were calculated using the density functional theory method (DFT). The experimental and computational results are compared.

Mahasarakham University
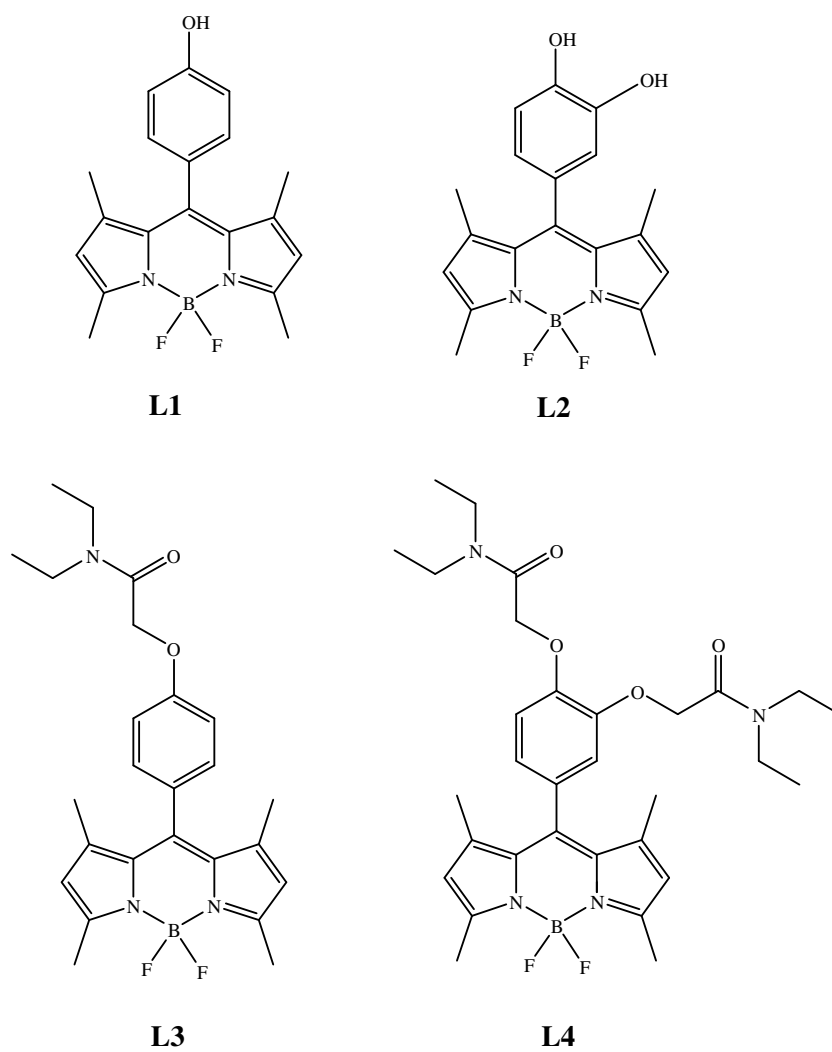
Figure 1.3 Target synthetic BODIPY-based on chemosensors.
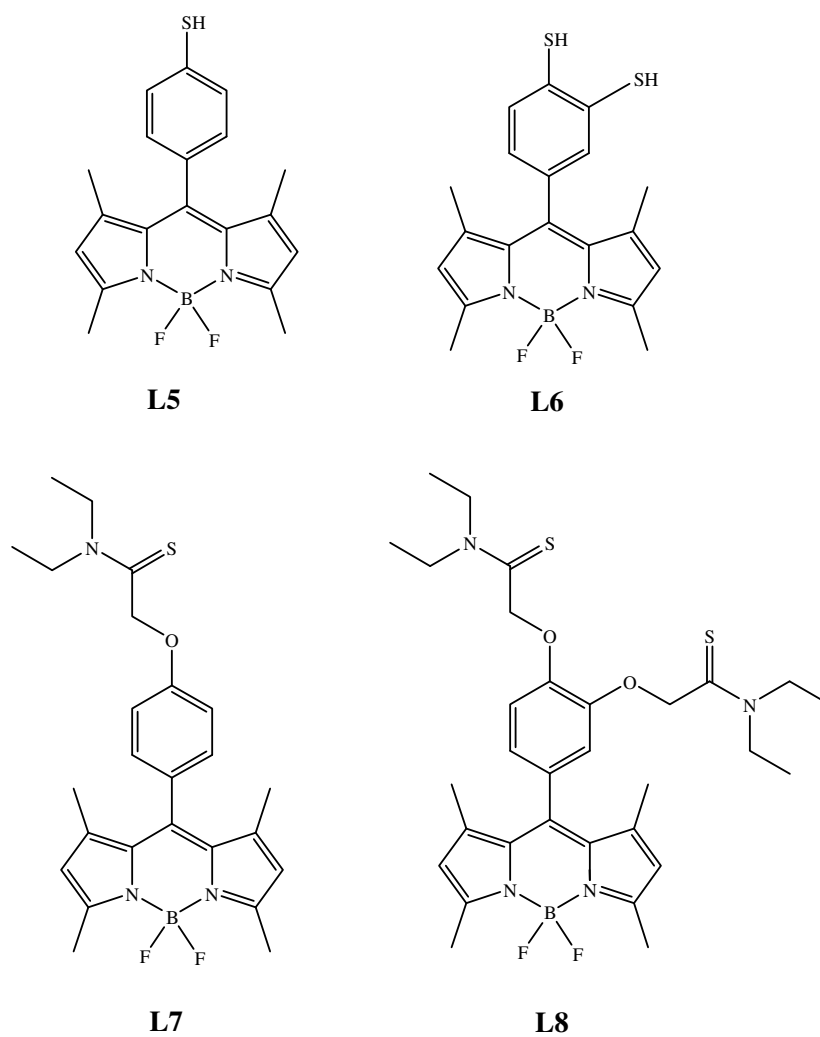
Figure 1.4 Target BODIPY-based chemosensors for calculation.

CHAPTER 2

THEORY AND LITERATURE REVIEWS

2.1 Supramolecular Chemistry

Supramolecular chemistry is a multi-disciplinary field. The concept and the term of supramolecular chemistry were introduced in 1978 as a development and generalization of earlier work. [17-19] The field of supramolecular chemistry has been defined in words 'Just as there is a field of *molecular chemistry* based on the covalent bond, there is a field of *supramolecular chemistry*, the chemistry of molecular assemblies and of the intermolecular bond' also as 'chemistry beyond the molecule' by Lehn (Figure 2.1). [20-21]
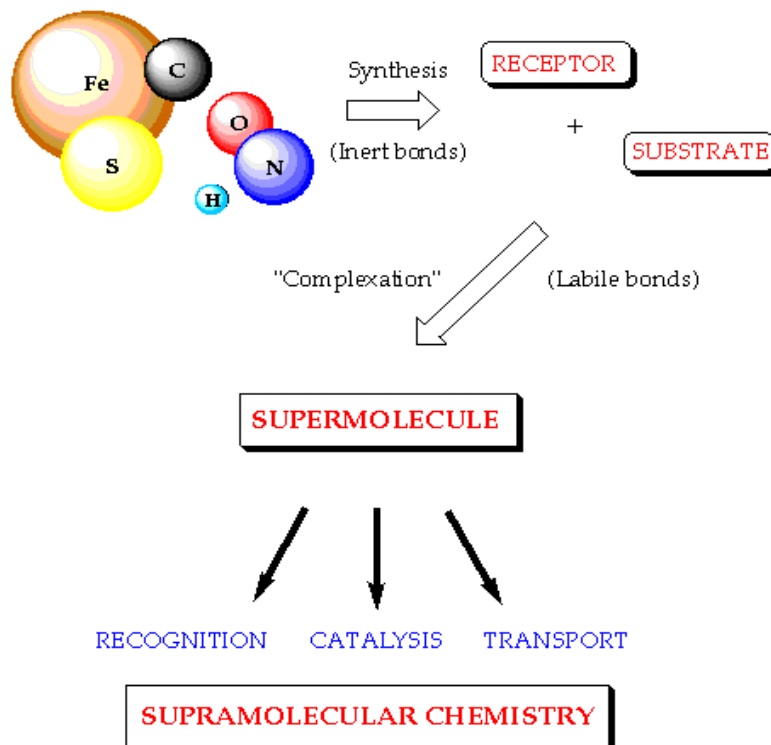
Figure 2.1 From molecular to supramolecular chemistry: molecules, supermolecules, molecular and supramolecular devices.

2.2 Molecular Recognition

2.2.1 Recognition, information, complementarity

Molecular recognition is a critical component of intermolecular processes, including enzyme-substrate recognition, receptor-ligand binding, molecular self-assembly, and chemical sensing. The design of new hosts and/or guests is essential for providing insight into the factors governing molecular recognition and for preparing new materials with desirable properties.

Molecular recognition is defined by the energy and the information involved in the binding and selection of guest(s) by a given receptor molecule; it may also involve a specific function. Here binding is not recognition, although it is often taken such. One may say that recognition is binding with a purpose, like receptors are ligands with a purpose. It implies a pattern recognition process through a structurally well-defined set of intermolecular interactions. Binding of ligand to guest forms a complex or supermolecule characterized by its thermodynamic and kinetic stability and selectivity, i.e., by the amount of energy and of information brought into operation.

Molecular recognition thus implies the (molecular) storage and (supra molecular) read out of molecular information. [22-23] The information is a key notion of supramolecular chemistry, in fact the most fundamental and the general one, that constitutes the common thread running through the whole field. Indeed, in this respect supramolecular chemistry can be considered as a chemical information science or molecular "informatics'' concerned with the molecular storage and the supramolecu-lar reading and processing of the information via the structural and temporal features of molecules and supermolecules. [24-25]

Basically, molecular recognition is defined by energy and information involved in the binding and selection of substrate(s) by a given receptor molecule containing a specific function. Sometimes, this idea is described as "*Lock and Key*" principle (Figure 2.2). The arrangement of binding sites in the host (lock) is complementary to the guest (key) both sterically (structurally) and electronically. [26]

High recognition by a receptor molecule consists in a large difference between the binding free energies of a given substrate and of the other substrates.
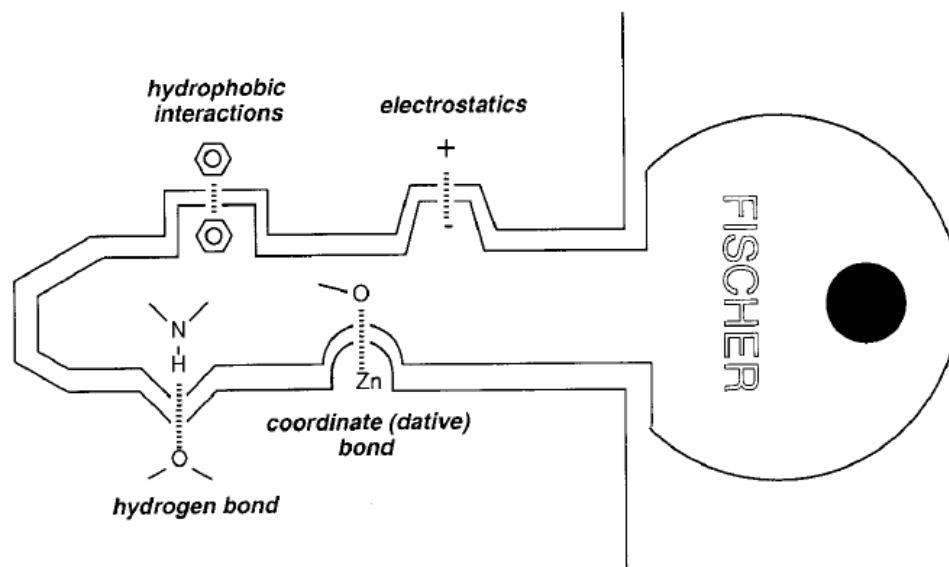
Figure 2.2 The lock and key principle: receptor sites in the host (lock) are

   complementary to the guest (key).

   It results in marked deviation from the statistical distribution. In order to achieve large differences in affinity several factors must be taken into account:

   a) steric (shape and size) complementarity between receptor and substrate

   b) interactional complementarity, i.e. the presence of complementary binding sites (electrostatic such as positive/negative, charge/dipole, dipole/dipole, hydrogen bond donor/acceptor, etc.) in the correct disposition on receptor and substrate so as to achieve complementary electronic and nuclear distribution (electrostatistic, H-bonding and van der Waals) maps

   c) large contact areas between receptor and substrate so as to contain

   d) multiple interaction sites, since non-covalent interactions are rather weak compared to covalent bonds

   e) strong overall binding; although high stability does in principle not necessarily imply high selectivity, this is usually the case; indeed, the differences in free energy of binding are likely to be larger when the binding is strong; high binding efficiency requires strong interaction; thus, in order to achieve efficient recognition,

both high stability and high selectivity, strong binding of receptor and substrate is required.

In addition, medium effects play an important role through the interaction of solvent molecules with receptor and substrate as well as with each other; thus the two partners should present geometrically matched hydrophobic/hydrophobic or hydrophilic/hydrophilic domains.

2.2.2 Non-covalent interactions

The glue used by supramolecular chemists to hold molecules together is non-covalent, and there are a number of such interactions that can be utilized. They include;

a) electrostatic interactions (ion/ion, ion/dipole and dipole/dipole);

b) hydrogen bonding;

c) π-π stacking interactions;

d) dispersion and induction forces (van der Waals forces);

e) hydrophobic or solvatophobic effects.

The bond energy of a typical single covalent bond is around 350 kJ/mol rising up to 942 kJ/mol for the very stable triple bond in N_2. The strengths of many of the non-covalent interactions used by supramolecular chemists are generally much weaker ranging from 2 kJ/mol for dispersion force, through to 20 kJ/mol for a hydrogen bond to 250 kJ/mol for ion/ion interaction. The power of supramolecular chemistry lies in the combination of a number of weak interactions, allowing strong
and selective recognition of specific guests to be achieved.

*Electrostatic interactions (*such as the ion/dipole interactions that operate
in valinomycin) are based on the Coulombic attraction between opposite charges
(Figure 2.3). Ion/ion interactions are non-directional, whilst for ion/dipole interactions the dipole must be suitably aligned for optimal binding efficiency. The high strength of electrostatic interactions has made them a prized tool amongst supramolecular chemists for achieving strong binding. There are many receptors for cations and anions which employ electrostatic interactions to hold the guest in place.

Arrays of hydrogen bonds, such as those employed in biological systems (i.e. the DNA double helix), have been utilized in receptors designed to coordinate neutral organic species such as barbiturates, short chain alcohols and amides, and also anions. [27] The directional nature of hydrogen bonds, combined with the precision with which the individual components can be built into molecular systems has made them especially attractive to molecular designers. This has facilitated the construction of complex architectures.
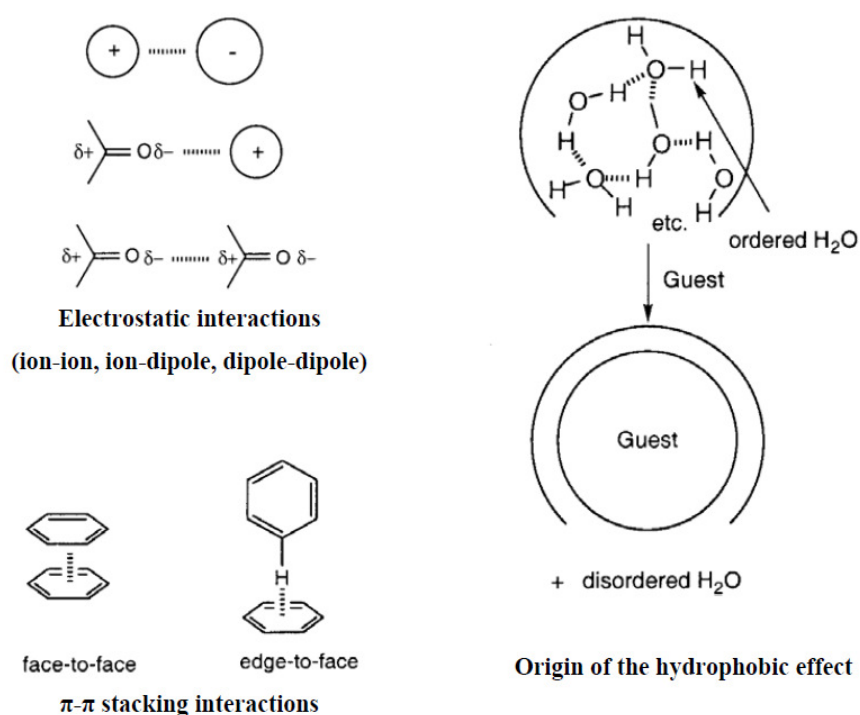
Figure 2.3 Some examples of Non-covalent interactions

The π-π stacking forces occur between systems containing aromatic rings in Figure 2.3. Attractive interactions can occur in either a "face-to-face'' or "edge to face'' manner (for example benzene crystallizes in a 'herring-bone' arrangement maximising edge-to-face contacts). Current theories suggest this attractive force is electrostatic in nature. Some very elegant receptors have been synthesized employing π-π interactions, including a receptor for benzoquinone. [28]

Dispersion forces (or induced dipole-induced dipole interactions) are attractive forces between molecules that occur when instantaneous dipoles in the

electron clouds around each molecule interact favourably. These van der Waals forces are believed to provide additional enthalpic stabilisation to the coordination of a hydrophobic guest into a hydrophobic cavity. They are, however, of a very general nature and so it is difficult to design receptors specifically to take full advantage of them. One such system may be a self-assembled 'tennis ball' that can encapsulate xenon atoms

*The hydrophobic effect (*Figure 2.3) is the specific driving force for the association of apolar binding partners in aqueous solution. Water molecules around the apolar surfaces of a hydrophobic cavity arrange themselves to form a structured array. With guest complexations the water molecules are released and become disordered. This results in a favourable increase in entropy. In addition, there is believed to be an enthalpic component to the hydrophobic effect. Receptors containing hydrophobic interior cavities designed to encapsulate organic guest molecules in aqueous solution include the cyclophanes and cyclodextrins.

*Classical coordination chemistry (*i.e. the coordination of metals by ligands donating two electrons to form a dative bond) although not strictly a non-covalent interaction is also widely used in supramolecular chemistry. The geometric requirements of metal ions, combined with the design of specific ligands have permitted the construction of complex and eye-catching molecular topologies catenanes and double and triple helices, and molecular grids.

Steric repulsion, this diminishes the strength of interactions as two molecules cannot occupy the same space. As may be expected from the lock and key analogy, however, it can play a very important role in determining the selectivity of a receptor species for a particular substrate and the stability of a specific complex.

2.3 Molecular Sensors

A receptor may be used as a sensor if it can report the presence of the guest by some physical means. Sensor should ideally be selective for a particular guest and not only report the presence of the guest molecule, but should also allow the chemist to monitor its concentration. This is important medically (for monitoring indicators of

physical function) and environmentally (monitoring pollutant levels). Two different strategies have been applied to sensor production. [29]

Firstly, the receptor can be used to create a modified material, for example an electrode. The receptor is incorporated into a polymer electrode, and this modified electrode can then show a selective response to the presence of the ion for which the receptor is selective, allowing the quantitative determination of ion concentrations in solution.

Alternatively, the sensing function can actually be incorporated at a molecular level. This is achieved by combining a binding site and a reporter group in one molecule. The reporter group is chosen to have electrochemical or spectroscopic properties that are altered by proximate host-guest interaction. This electrochemical or spectroscopic output can therefore be used to quantitatively detect specific guests.

2.3.1 Electrochemical sensors

Electrochemical sensors can be created by attachment of redox active group to a receptor. For such a sensor to useful, the receptor should be selective for guest of interest and the binding process must be coupled to the redox reaction; in other words the redox active center must 'feel the presence' of the bound guest. Many redox-active groups have been incorporated into this type molecular sensor; e.g. ferrocene, quinone and bipyridinum. So far, the coupling has been realized through one or a combination of the following pathways:

a) Direct coordinate bond formation between the redox center and the complexed guest [30]

b) Induced conformational perturbation of the redox center(s) caused by guest complexation [31]

c) Through-bond electrostatic communication.

A change in the redox properties of the receptor can be detected by an electrochemical technique such as cyclic voltametry (CV). Changes in the cyclic voltamogram can therefore be used to sense the presence of this guest.

2.3.2 Optical sensors

The most common type of optical sensor is fluorescent; there are also colorimetric, [32] and electron-transfer (ET) path-selective sensors, [33] the responses

in the last two examples are followed according to change in their absorbance. Fluorescence detection has three major advantages over other light-based investigation methods: high sensitivity, high speed, and safety. The point of safety refers to the fact that samples are not affected or destroyed in the process, and no hazardous by products are generated.

Fluorescence is the phenomenon in which absorption of light of a given wavelength by a fluorescent molecule is followed by the emission of light at longer wavelengths. The distribution of wavelength-dependent intensity that causes fluorescence is known as the fluorescence excitation spectrum, and the distribution of wavelength-dependent intensity of emitted energy is known as the fluorescence emission spectrum. [34]

Sensitivity is an important issue because the fluorescence signal is proportional to the concentration of the substance being investigated. Sensitivity of fluorescence arises from the differences between the excitation and emission wavelength. Relatively small changes in ion concentration in living cells can have significant physiological effects. Whereas absorbance measurements for colorimetric sensors can reliably determine concentrations only as low as several tenths of a micromolar, fluorescence techniques can accurately measure concentrations one million times smaller - pico- and even femtomolar. Using fluorescence, one can monitor very rapid changes in concentrations. Due to these advantages fluorescent sensors are especially attractive as they give a meaningful physical output which is easy to measure even at very low concentrations. They are, therefore, very sensitive and suitable for use in biological systems. But the biggest disadvantage of these fluorescent sensors, they mainly work in organic media, and in the aqueous media they don't show any responses. Recently, there is a strong demand in this area to synthesize water soluble derivatives of fluorescent sensors. Due to these limitations the number of commercial fluorescent sensors on the market is still relatively small.

2.4 Photophysics of Fluorescent Chemosensor

The principle of fluorescent chemosensors for specific analyte can be classified according to the nature of the photoinduced process such as photoinduced electron

transfer (PET), photoinduced charge transfer (PCT), fluorescence resonance energy transfer (FRET) and excimer formation (Figure 2.4). Photoinduced electron transfer chemosensors have been extensively studied. [35-36]

2.4.1 Photoinduced electron transfer

In photoinduced electron transfer, absorption of light by a molecule causes an electron to jump to another molecule or component of a composite system. Once the electron has jumped, a molecular radical ion pair is formed or in an organic/semicondu-

ctor nanostructure, an electron-hole pair is created. These ions or electron hole pairs have a finite lifetime after which they recombine (mostly geminate recombination) through radiative or nonradiative channels.
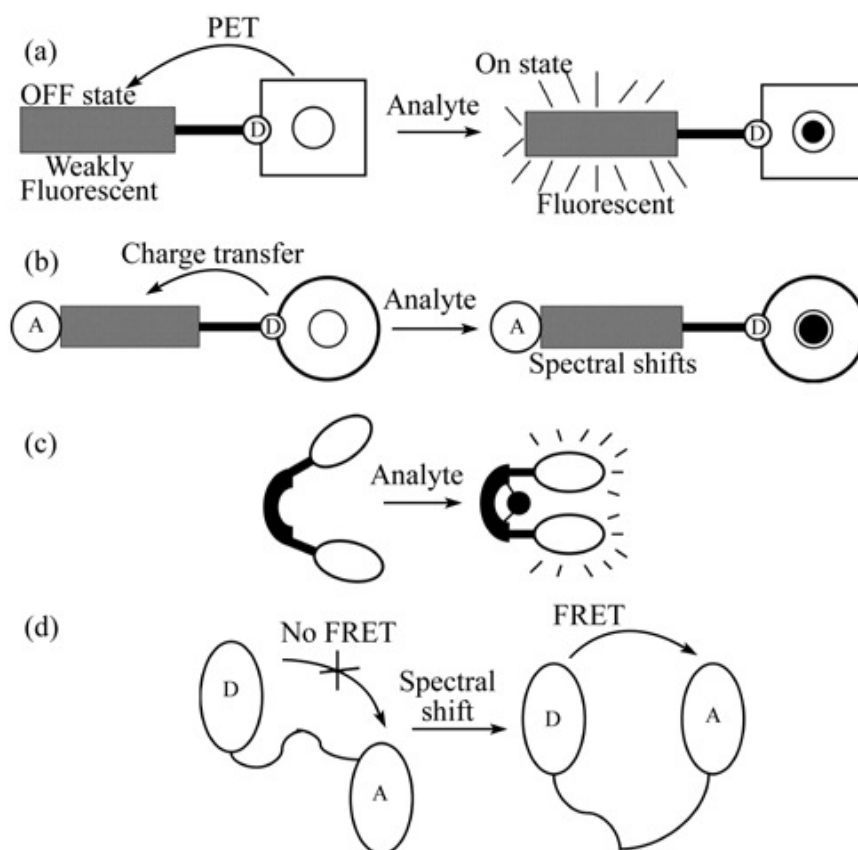
Figure 2.4 Principle of recognition by PET (a), PCT (b), excimer formation (c) and FRET systems (d).

This type of system consists of a fluorophore linked to a donor atom (usually an amino nitrogen). Upon excitating the fluorophore, an electron of the highest occupied molecular orbital (HOMO) is promoted to the lowest unoccupied molecular orbital (LUMO), which enables PET from the HOMO of the donor to the LUMO of the acceptor take place. Such a process provides a mechanism for nonradioactive deactivation of the excited state, causing a quenching effect of the fluorescence. [37-40]

Upon analyte binding, the redox potential of the donor is raised so that the relevant the HOMO becomes lower than that of the fluorophore. Consequently, PET is not possible anymore and the quenching process is suppressed. In the case of metal ion binding, the effect is called chelation-enhanced fluorescence (CHEF). [41-42]
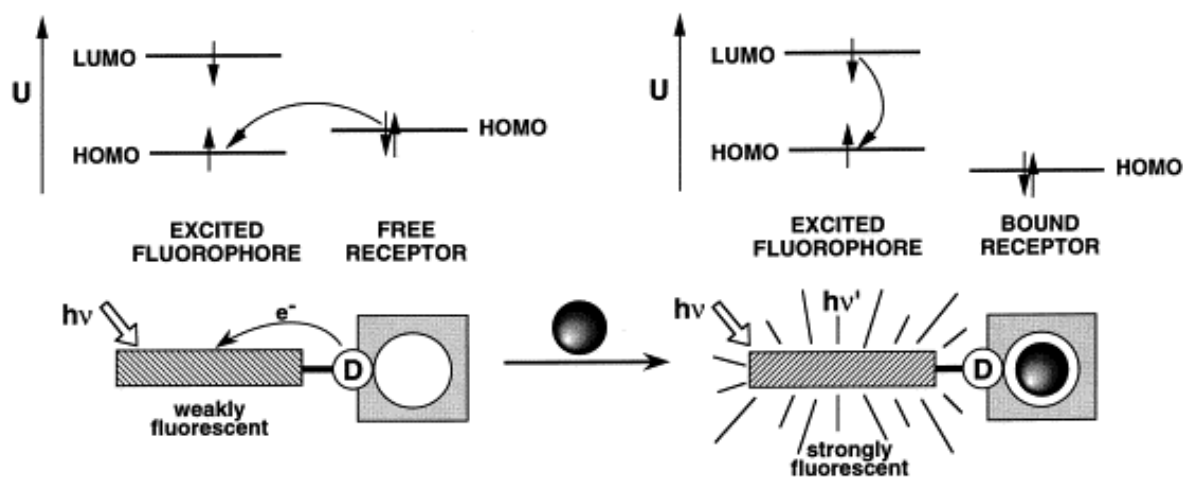
Figure 2.5 PET mechanism.

Many of the fluorescent chemosensors work with this principle. Selectivity for ions is achieved by the corrected choice of recognition moiety for the desired ion. A classical example is compound **10**. [43] The recognition moiety is not necessary to be crown ether. Cryptands like **8**, [44] podands **9**, [45] chelating [46] calixarene type receptors can also serve as ion binding sites.

The presented basic scheme is not only PET mechanism. With transition metals, electron transfer may occur from fluorescent chemosensor to the coordinated metal ion or vice versa. [47] Also in some instances, this results in quenching of the fluorescence by non-radioactive energy-transfer according to Dexter mechanism. PET

may sometimes occur from acceptor to donor. Then it is called oxidative PET as shown in Figure 2.6.
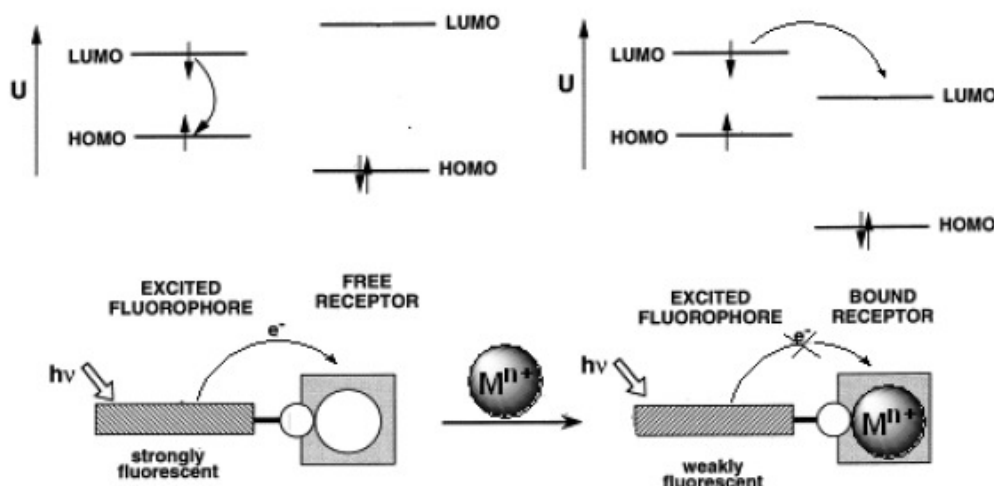
Figure 2.6 Oxidative PET mechanism.

In some instances, after the prevention of PET by metal binding, excitation energy is transferred from the fluorophore through ligand to another bound cation like Eu^{3+} or Tb^{3+}. This transfer is seen as the disappearance of emission signal from the fluorescent cations. [48]

2.4.2 Photoinduced charge transfer

When a fluorophore contains an electron-donating group (often an amino group) conjugated to an electron-withdrawing group, it undergoes intramolecular charge transfer from the donor to the acceptor during excitation by light. The consequent change in dipole moment results in a Stokes shift that depends on the microenvironment of the fluorophore. It can thus be anticipated that cations in close interaction with the donor or the acceptor moiety will change the photophysical properties of the fluorophore because the complexed cation affects the efficiency of intramolecular charge transfer. [49-50]

When a group (like an amino group) playing the role of an electron donor within the fluorophore interacts with a cation, the latter reduces the electron-donating character of this group; owing to the resulting reduction of conjugation, a blue shift of the absorption spectrum is expected together with a decrease of the extinction

coefficient. Conversely, a cation interacting with the acceptor group enhances the electron-withdrawing character of this group; the absorption spectrum is thus red-shifted and the molar absorption coefficient is increased. The fluorescence spectra are in principle shifted in the same direction as those of the absorption spectra. In addition to these shifts, changes in quantum yields and lifetimes are often observed. All these photophysical effects are obviously dependent on the charge and the size of the cation, and selectivity of these effects are expected.

Let us consider only the case where the dipole moment in the excited state is larger than that in the ground state. Then, when the cation interacts with the donor group, the excited state is more strongly destabilized by the cation than the ground state, and a blue shift of the absorption and emission spectra is expected (however the fluorescence spectrum undergoes only a slight blue shift in most cases). Conversely, when the cation interacts with the acceptor group, the excited state is more stabilized by the cation than the ground state, and this leads to a red shift of the absorption and emission spectra (Figure 2.7).
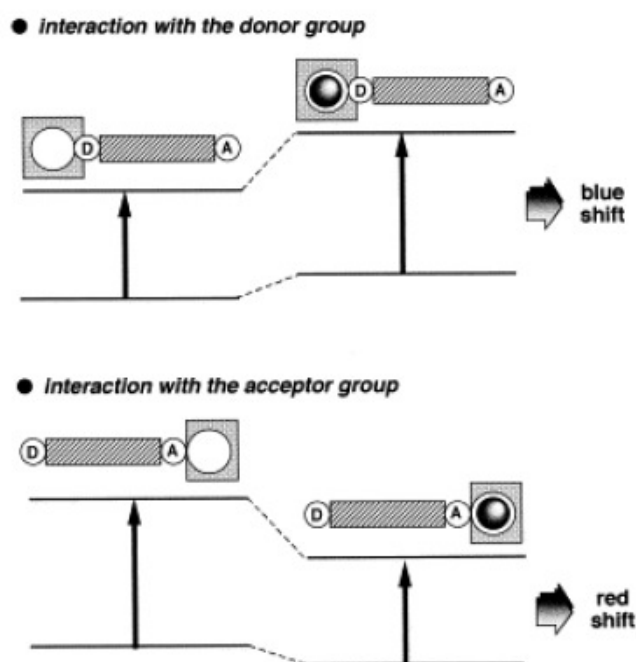
Figure 2.7 Spectral displacements of PCT sensors resulting from interaction of a bound cation with an electron-donating or electron-withdrawing group.

2.4.3 Fluorescence resonance energy transfer

Fluorescence resonance energy transfer arises from the interaction between a pair of dissimilar fluorophores, one of which acts as a donor of excited-state energy to the other (acceptor). This returns the donor to its electronic ground state, and emission may occur from the acceptor center. [51-52] Recently, more and more chemosensors were constructed based on FRET principle. [53-56]

2.4.4 Excimer-based chemosensors

Excimer-based chemosensors have become an active area of interest recently. Several fluorophores like pyrene, squaraine and anthracene can form excimer by weak interaction. [57] An excimer is a complex formed by the interaction of an excited fluorophore with another fluorophore in its ground state. Dual fluorescence is often observed with a monomer band and, at a longer wavelength, a broad band due to excimer formation. [58] The analyte binding may favor or hinder excimer formation, so the recognition can be monitored by the monomer: excimer fluorescence intensity ratio. [59-62]

2.5 Computational Chemistry [63-67]

A branch of chemistry that uses the results of theoretical chemistry incorporated into efficient computer programs to calculate the structures and properties of molecules is called computational chemistry (also called molecular modeling). Examples of such properties are energy and interaction energy, charge, dipole and higher multipole moment, vibrational frequencies, reactivity or other spectroscopic quantities. The main theoretical methods available belong to five board classes as described below.

Molecular mechanic simulations use the laws of classical physics to predict the structures and properties of molecules. Molecular mechanics is based on a model of a molecule as a collection of balls (atoms) held together by springs (bonds). The energy of a given collection of balls and springs i.e., of a given molecule; changing the geometry until the lowest energy is calculated by the normal spring lengths and the angles between them, and how much energy it takes to stretch and bend the springs. There are many different molecular mechanics methods. Each one is characterized by

its particular *force field*. Molecular mechanics calculations do not explicity treat the electrons in a molecular system. Instead, they perform computations based upon the interactions among the nuclei. Electronic effects are implicitly included in force fields through parametrization. This approximation makes molecular mechanics computations quite inexpensive computationally, and allows them to be used for very large systems containing many thousands of atoms.

Ab initio calculations (also called *ab initio* quantum mechanics: *ab initio* is from the Latin: "from the first principle") are based on the Schrödinger equation. This is one of the fundamental equations of modern physics and describes, among other things, how the electrons in molecule behave. The *ab initio* method solves the Schrödinger equation for a molecule and gives us the molecule's energy and wave function. The wave function is a mathematic function that can be used to calculate the electron distribution. The Schrödinger equation cannot be solved exactly for any molecule with more than one electron. Thus approximations are used.

Semiempirical (SE) calculations are, like *ab initio*, also based on the Schrödinger equation. Usually, the core electrons are not included in the calculation and only a minimal basis set is used. Also, some of the two-electron integrals are omitted. In order to correct for the errors introduced by omitting part of the calculation, the method is parameterized. Parameters to estimate the omitted values are obtained by fitting the results to experimental data or *ab initio* calculations. Often, these parameters replace some of the integrals that are excluded. The advantage of semi-empirical calculations is that they are much faster than *ab initio* calculations. The disadvantage of semi-empirical calculations is that the results can be erratic and fewer properties can be predicted reliably. Semi-empirical methods are parameterized to reproduce various results. Most often, geometry and energy (usually the heat of formation) are used. A few methods have been parameterized to reproduce a specific property, such as electronic spectra or NMR chemical shifts. Semi-empirical calculations can be used to compute properties other than those in the parameterization set. Many semi-empirical methods compute energies as heats of formation.

Density functional calculations (often called Density functional theory (DFT) calculations) are, like *ab initio* and SE calculations, based on the Schrödinger equation. However, unlike the other two methods, the DFT does not calculate a wave function,

but rather derives the electron distribution (electron density function) directly. A density functional is then used to obtain the energy for the electron density. A functional is a function of a function, in this case, the electron density.

Molecular dynamics (MD) is a simulation of the time-dependent behavior of a molecular system, such as vibrational motion. Thus one can simulate the motion of an enzyme as it changes shape on binding to the substrate, or the motion of a swarm of water molecules around a molecule of solute. This section provides an introduction of the theoretical method used in this study.

2.5.1 *Ab initio* methods

This is an approximate quantum mechanical calculation. The approximations are usually mathematical approximations, such as using a simpler functional form for a function or finding an approximate solution to a differential equation. In general, *ab initio* calculations give very good qualitative results and can yield increasingly accurate quantitative results as the molecules in question become smaller. The advantage of *ab initio* methods is that they eventually converge to the exact solution once all the approximations are made sufficiently small in magnitude. There are four sources of error in *ab initio* calculations; the Born-Oppenheimer approximation, the use of an incomplete basis set, incomplete correlation and the omission of relativistic effect. The disadvantage of *ab initio* methods is that they are expensive. These methods often take enormous amounts of computer CPU time, memory and disk space.

The most common type of *ab initio* calculation is called a Hartree-Fock calculation (abbreviated HF), in which the primary approximation is the central field approximation. This means that the Coulombic electron-electron repulsion is taken into account by integrating the repulsion term. This gives the average effect of the repulsion, but not the explicit repulsion interaction. This is a variational calculation, meaning that the approximate energies calculated are all equal to or greater than the exact energy. The energies are calculated in units called Hartrees (1 Hartree = 27.2116 eV). Because of the central field approximation, the energies from HF calculations are always greater than the exact energy and tend to a limiting value called the Hartree-Fock limit as the basis set is improved.

Hartree-Fock theory is very useful for providing initial, first-level predictions for many systems. It is also reasonable good at computing the structure and

vibrational frequencies of stable molecules and some transition states. As such, it is a good base-level of theory. However, its neglect of electron correlation makes it unsuitable for some purpose. For example, it is insufficient for accurate modeling of the energies of reactions and bond dissociation.

2.5.2 Density functional theory methods

Recently, a third class of electronic structure methods have come into wide use: density functional methods. These DFT methods are similar to *ab initio* methods in many ways. The DFT calculations require about the same amount of computation resources as Hartree-Fock theory. DFT methods are attractive because they include the effects of *electron correlation*- the fact that electrons in a molecular system react to one another's motion and attempt to keep out of one another's way-in their model.

The Hartree-Fock calculations consider this effect only in an average sense-each electron sees and reacts to an averaged electron density-while methods including electron correlation account for the instantaneous interactions of pairs of electrons with opposite spin. This approximation causes Hartree-Fock results to be less accurate for some types of systems. Thus, DFT methods can provide the benefits of some more expensive *ab initio* methods at essential Hartree-Fock cost.

The DFT methods compute electron correlation via general functionals of the electron density. The DFT functionals partition the electronic energy into several components which are computed separately: the kinetic energy, the electron-nuclear interaction, the Coulomb repulsion, and an exchange-correlation term accounting for the remainder of the electron-electron interaction (which is itself divided into separate exchange and correlation components in most actual DFT fomulations). A variety of functionals have been defined, generally distinguished by the way that they are exchange and correlation components:

a) Local exchange and correlation functionals involve only the value of the electron spin densities. Slater and X_α are well-known local change functionals, and the local spin density treatment of Vosko, Wilk and Nusair (VWN) is a widely-used local correlation functional.

b) Gradient-corrected functionals involve both the value of the electron spin densities and their gradients. Such functionals are also sometimes referred

to as non-local in the literature. A popular gradient-corrected exchange functional is one proposed by Becke in 1988; a widely-used gradient-corrected correlation functional is the LYP functional of Lee, Yang and Parr.

There are also several hybrid functionals, which define the exchange functional as a linear combination of Hartree-Fock, local and gradient-corrected exchange terms; this exchange functional is then combined with a local and/or gradient-corrected correlation functional. The best known of these hybrid functionals is Becke's three-parameter formulation; hybrid functionals based on it are available in GAUSSIAN program via the B3LYP.

2.5.3 Defining model chemistry

Model chemistry is characterized by the combination of theoretical procedure and basis set. Every calculation performed with Gaussian must specify the desired theoretical model chemistry in addition to specifying the molecular system to consider and which results to compute for it.

2.5.3.1 Method

The GAUSSIAN program contains a hierarchy of procedures corresponding to different level of theory. The most common used are listed in the following table 2.1:

Split valence basis set, the first way that a basis set can be made larger is to increase the number of basis functions per atom. Split valence basis set, such as 3- 21G and 6-31G, has two (or more) sizes of basis function for each valence orbital. Forexample, hydrogen and carbon are represented as: H: *1s, 1s′; C: 1s, 2s, 2s′, 2p_x, 2p_y, 2p_z, 2p_x′, 2p_y′, 2p_z′,* where the primed and unprimed orbitals differ in size.

Table 2.1 The most common used method in GAUSSIAN program

Key Word	Method	Availability
HF	Hartree-Fock self-consistent field	Through 2nd derivatives
B3LYP	Becke-style 3-parameter density functional theory (using the Lee-Yang-Parr correlation functional)	Through 2nd derivatives
MP2	2nd Order Mϕller-Plesset perturbation theory	Through 2nd derivatives
MP4	4th Order Mϕller-Plesset perturbation theory (including singles, doubles, triples and quadruples by default)	Energies only
QCISD(T)	Quadratic CI (single, doubles&triples)	Energies only

Polarized basis set, split valence basis set allows orbital to change size, but not to change shape. Polarized basis set removes this limitation by adding orbitals with angular momentum beyond what is required for the ground state to the description of each atom. For example, polarized basis set adds d functions to carbon atoms and *f* functions to transition metals, and some of them add *p* functions to hydrogen atoms.

Diffuse function, a large-size version of s- and p-type functions. They allow orbitals to occupy in a larger region of space. Basis set with diffuse function is important for systems where electrons are relatively far from the nucleus: molecules with lone pairs, anions and other systems with significant negative charge, system in their excited states, systems with low ionization potentials, descriptions of absolute acidities, and so on.

2.5.3.2 Basis set

A basis set is a mathematical representation of the molecular orbitals within a molecule. The basis set can be interpreted as restricting each electron to a particular region of space. Larger basis set impose fewer constraints on electrons and more accurately approximate exact molecular orbitals.

Minimal basis set, minimal basis set contains the minimum number of basis functions needed for each atom, as in these examples: H: *1s*; C: *1s, 2s, 2p$_x$, 2p$_y$, 2p$_z$*. Minimal basis set uses fixed-size atomic-type orbitals. The STO-3G basis set is a minimal basis set. It uses three Gaussian primitives per basis function, which accounts for the "3G" in its name. "STO" stands for "Slater-type orbitals," and the STO-3G basis set approximates Slater orbitals with GAUSSIAN functions.

Table 2.2 The most commonly-used basis sets

Basis Set [Applicable Atoms]	Description	Basis 1st row atoms	Function hydrogen atoms	Default function types*
STO-3G [H-Xe]	Minimal basis set (stripped down in the interest of performance): use for more qualitative results on very large systems when cannot afford even 3-21G	5	1	**6D**
3-21G [H-Xe]	Split valence: 2 sets of functions in the valence region provide a more accurate representation of orbitals. Use for very large molecules for which 6-31G(d) is too expensive	9	2	**6D**
6-31G(d) or 6-31G* [H-Cl]	Adds polarization functions to heavy atoms: use for most jobs on up to medium/large sized systems. (This basis set uses the 6-component type d functions)	15	2	**6D 7F**

Table 2.2 (continued)

Basis Set [Applicable Atoms]	Description	Basis 1st row atoms	Function hydrogen atoms	Default function types*
6-31+G(d) [H-Cl]	Adds diffuse functions: important for systems with lone pairs, anions, exited states	19	2	**6D 7F**
6-31G(d,p) or 6-31G** [H-Cl]	Adds polarization functions to the hydrogens as well: use when the hydrogen are the site of interest (for example, bond energies) and for final, accurate energy calculations	15	5	**6D 7F**
6-31+G(d,p) [H-Cl]	Adds *p* functions to hydrogens as well: use when the 6-31G(d,p) and diffuse functions are used	19	5	**6D 7F**
6-311+G(d,p) [H-Br]	Triple zeta: adds extra valence functions (3 sizes of *s* and *p* functions) to 6-31+G(d) Diffuse functions can also be added to the hydrogen atoms via a second +	22	6	**5D 7F**
6-311+G(2d,p) [H-Br]	Puts 2 *d* functions on heavy atoms (plus diffuse functions), and 1 *p* function on hydrogens	27	6	**5D 7F**
6-311+G(2df,2p) [H-Br]	Puts 2 *d* functions and 1 f function on heavy atoms(plus diffuse function),and 2 *p* functions on the hydrogen atoms	34	9	**5D 7F**
6-311++G(3df,2pd) [H-Br]	Puts 3 *d* functions and 1 f function on heavy atoms, and 2*p* functions and 1 *d* function on hydrogens, as well as diffuse functions on both	39	15	**5D 7F**

*6D denotes Cartesian, 6-component d functions, 5D and 7F denote "pure" 5-component *d* functions and 7-component *f* functions, respectively

      High angular momentum basis set even larger basis set is now practical for many systems. Such basis set adds multiple polarization functions per atom to the triple zeta basis set. For example, the 6-31G(2d) basis set adds two *d* functions per heavy atom instead of just one, while the 6-311++G(3df,3pd) basis set contains three sets of valence region functions, diffuse functions on both heavy atoms and hydrogens, and multiple polarization function: 3 *d* functions and 1 *f* function on heavy atoms and 3 *p* functions and 1 *d* function on hydrogen atoms. Such basis set is useful for describing the interaction between electrons in electron correlation methods; they are not generally needed for Hartree-Fock calculations. The following table summarizes the most commonly-used basis sets.

2.6 BODIPY Chemistry

2.6.1 General properties of BODIPY Dyes

      The boron-dipyrromethne (hereafter referred to as BODIPYs) are a class of fluorescent dyes that are finding an increasing number of applications in both the material and optical imaging fields. BODIPYs have a sharp fluorescence profile, high degree of photostability and can have fluorescent quantum yields approaching unity, depending on the attached substituents.
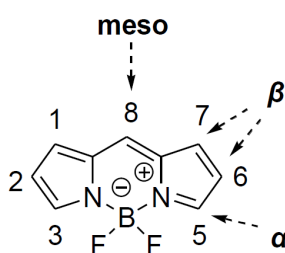
Figure 2.8 Basic BODIPY core structure.

The BODIPYs and their dipyrrin precursors have been recently reviewed [68-70] with emphasis placed on their syntheses, reactions and applications as fluorescent chemo-sensors. These reviews outlined the relatively straightforward synthetic routes to the BODIPY fluorophore (Figure 2.8), as well as a variety of reliable reactions that can be carried out to produce a shift in the absorption and emission wavelengths. BODIPYs have been used to detect metal cations, [71-79] anions, [80-83] reactive oxygen species [84] and even changes in viscosity [85] by alterations in either the fluorescence intensity or wavelength. Marked changes in the fluorescence intensity as a means of detection are more common and occured because of an ON/OFF switching of photo induced electron transfer, generally between the BODIPY core and an 8-phenyl substituent. More recently, BODIPY derivatives have been functionalized with groups promoting singlet oxygen generation (e.g., iodide groups), allowing their used as photodynamic therapy agents, an application more commonly associated with porphyrins and phthalocyanines. [86-90]

2.6.2 BODIPY synthesis

Given the role found by BODIPY dyes, many methods for their synthesis have been described. The construction of the basic procedure of the BODIPY core usually starts from a simple pyrrole condensation with a highly electrophilic carbonyl compound, e.g. aldehyde, acid anhydride and acyl chloride. Due to the instability of an unsubstituted dipyrromethene intermediate, which can undergo rapid polymerization or porphyrin formation; most routes involve 2-substituted pyrroles. With this in mind, Burgess and collaborators [68] have described the three major routes of BODIPY synthesis: from pyrroles and acid chlorides, from pyrroles and aldehydes, and from ketopyrroles. These are described below.

2.6.2.1 The major route of BODIPY synthesis from pyrroles and acid chlorides

This method of formation involves the condensation of acyl chlorides with pyrroles to give the dipyrrin core of dipyrromethenes, and then subsequent reaction of this with boron trifluoride etherate (BF$_3$.OEt$_2$) in the presence of triethylamine (Et$_3$N) to afford the BODIPY core. The first method used to synthesis a BODIPY derivative followed such a strategy. [68] This process was undertaken in a one-pot, two-step procedure to give the products in 18-86% overall yield (Scheme 2.1). [91]
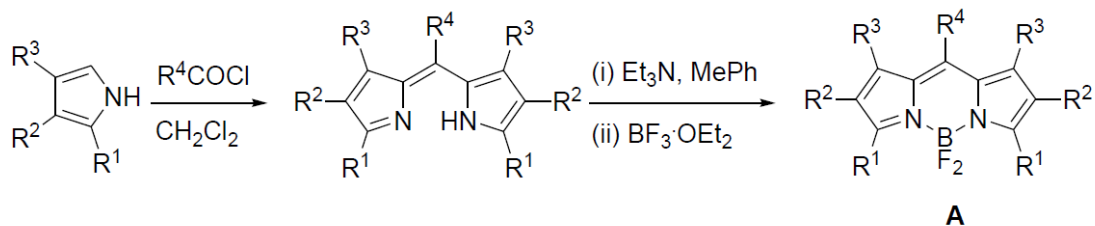
Scheme 2.1 Synthesis of symmetric BODIPY dyes from acyl chloride derivatives.

The advantage of this method is in the formation of the dipyrromethene in a single process. However, conversions are not always complete and this can complicate purification. One example of this method is a report by Burgess *et al.* describing the synthesis of BODIPYs from acyl chloride derivatives. Intermediate dipyrromethenes **2** were obtained from pyrroles **1** on reaction with 4-iodobenzoyl chloride in 1,2-dichloroethane. After purification via flash chromatography, the compounds **2** were treated with Et$_3$N and methyl phenol before adding BF$_3$.OEt$_2$. The reaction mixture was then heated at 80°C for 20 min. The final BODIPYs **3** were isolated following chromatography on alumina (Scheme 2.2). [92]

1a 1-Naph	**2a** 28%	**3a** 90%
1b 4-MeOC$_6$H$_4$	**2b** 87%	**3b** 99%
1c 4-FC$_6$H$_4$	**2c** 82%	**3c** 99%
1d 2-MeOC$_6$H$_4$	**2d** 65%	**3d** 94%
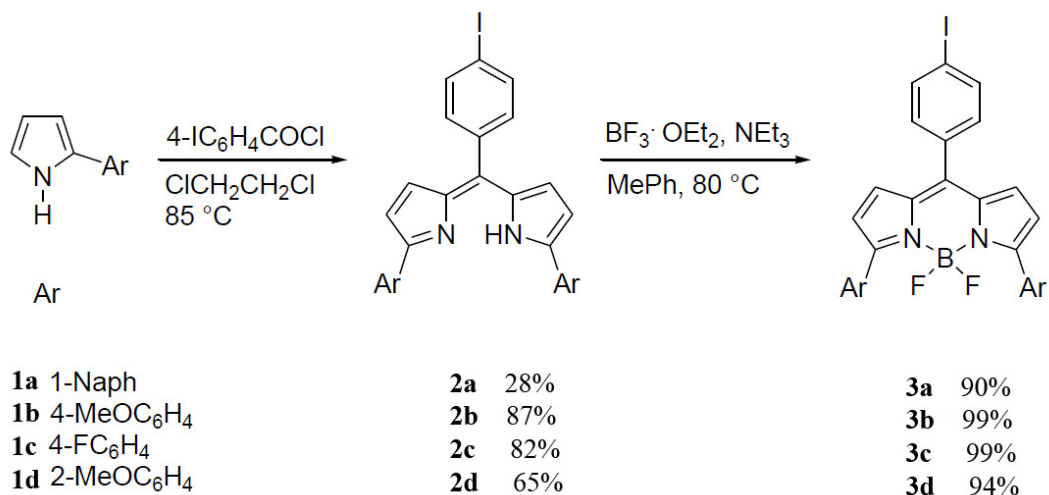
Scheme 2.2 Synthesis of symmetric F-BODIPY dyes.

2.6.2.2 The major route of BODIPY synthesis from pyrroles and aldehydes

The second method of formation of BODIPYs involves the condensation of aromatic aldehydes with pyrroles to give, after oxidation, the dipyrromethene intermediates. Reaction of the dipyrromethene precursors with BF$_3$.OEt$_2$ in the presence of a tertiary amine then forms the BODIPYs. Several groups have performed this pathway in a one-pot process. Due to instability of the required unsubstituted dipyrromethene precursors, the condensation usually needs an electron rich substituent, either on the pyrrole R1 or aldehyde R4 position. As stated above, the distinction of this method is the requirement for the oxidation of the first formed dipyrromethanes **B**. In most examples, 2,3-dichloro-5,6-dicyano-*p*-benzoquinine (DDQ) was used as the oxidizing agent. [93-95] The overall yield of this reaction varied from 18-43% depending on the substrate (Scheme 2.3). [96-98]
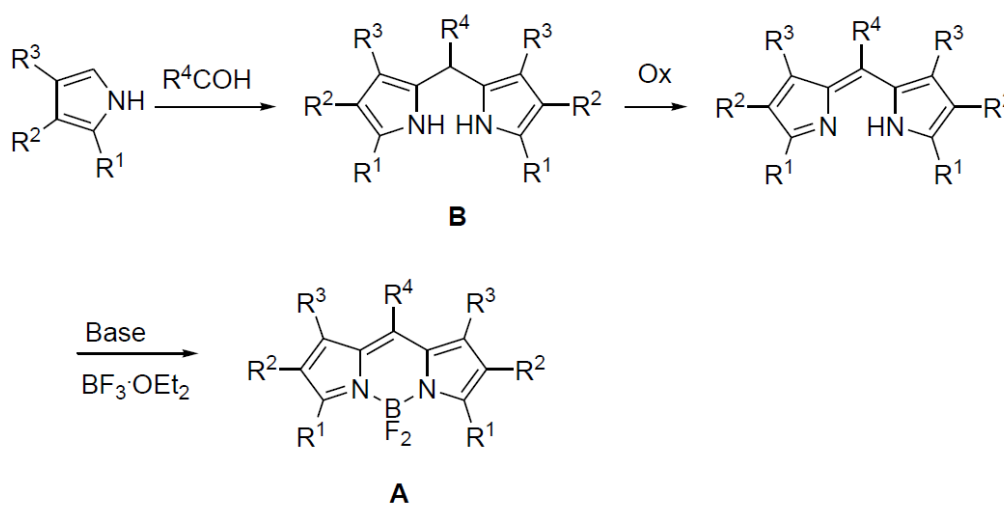
Scheme 2.3 Synthesis of symmetric F-Bodipy dyes from aldehyde derivatives.

This strategy of condensation of pyrroles with benzaldehyde derivatives is direct and convenient. However, the need for the oxidation means that one more step is required before complexation with boron component. Despite this, many reports have used pyrroles and aldehydes as the starting material, than follow the alternative approach from acid chlorides. For example, Gossauer and co-workers [94] have been synthesised BODIPY fluorophores from aldehydes with chiral substituents at the α-positions (Scheme 2.4).
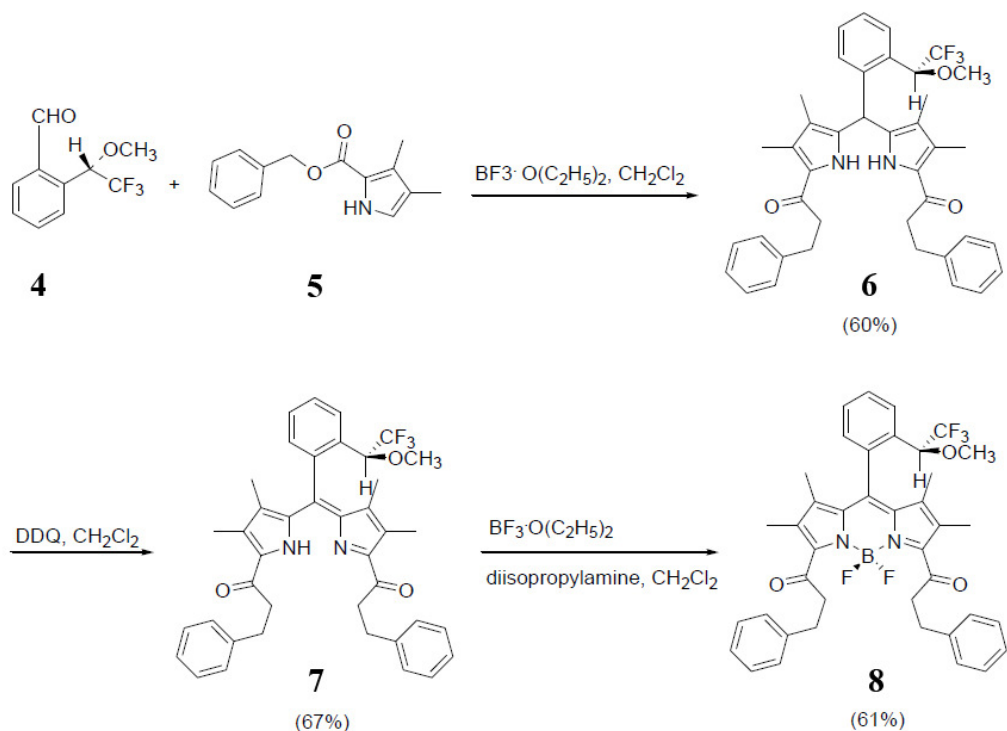
Scheme 2.4 Synthesis of BODIPYs from aldehydes.

2.6.2.3 The major route of BODIPY synthesis from ketopyrroles

In the previous two methods using acid chlorides or aldehydes, condensation with pyrrole occurs to form symmetrically substituted BODIPY dyes. However, asymmetrically substitute BODIPY dyes cannot be prepared by these routes. Generation of asymmetric BODIPYs can be achieved through condensation of ketopyrrole with a second pyrrole molecule to give the intermediate dipyrromethene followed by reaction with $BF_3.OEt_2$ and base (Scheme 2.5). [68]

The main advantage of this method is in its application to incorporate diverse substituents on the pyrrole rings. However, isolation of the unstable dipyrromethene hydrochloride salt intermediates is difficult. Overall, although this method needs one more step to isolate the ketopyrrole intermediates, the final yields are still high.
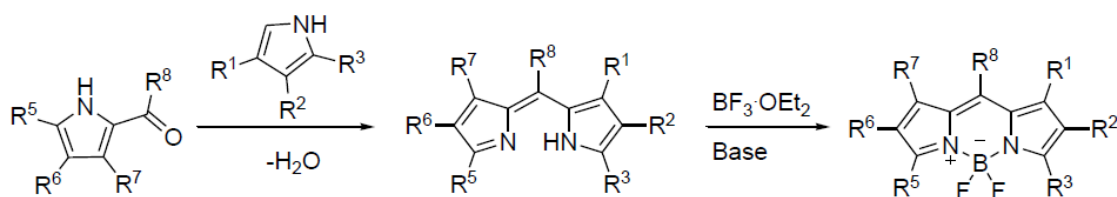
Scheme 2.5 Synthesis BODIPYs from ketopyrroles.

In Schemes 2.6 and 2.7 give examples of BODIPY synthesis from ketopyrroles relevant to this project. Work by Tahtaoui *et al*. had shown that the synthesis of BODIPY **13** could be achieved in a three-step process. [99] Firstly, 2-ketopyrrole **11** was prepared through the reaction of 4-iodobenzoyl chloride **10** with the magnesium salt of pyrrole **9** made by deprotonation with a Grignard reagent. In the second step, the hydrochloride salt of the dipyrromethene **12** is produced from the condensation of pyrrole **9** and ketopyrrole **11** using phosphoryl chloride as the dehydrating agent. Dipyrromethene **12** can be converted directly to the target material **13** after complexation with $BF_3.OEt_2$ in the presence of Et_3N (Scheme 2.6).

Similarly, unsymmetrical substituted BODIPY **15** was also prepared by this method (Scheme 2.7). [68]
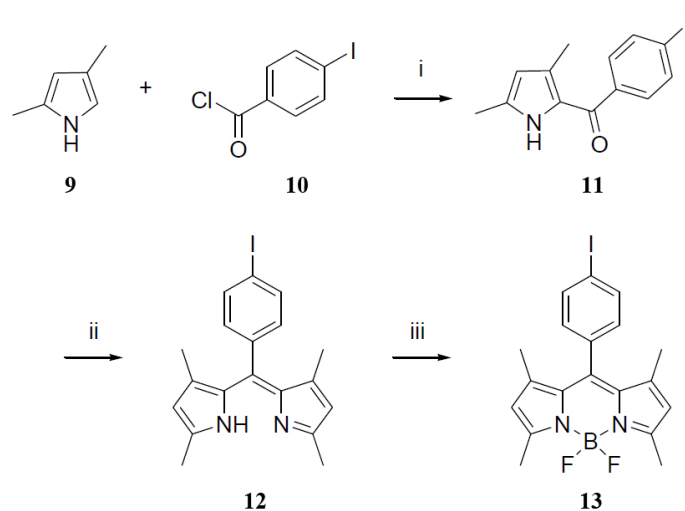
(i) CH_3MgBr, ether, 81%; (ii) $POCl_3$, CH_2Cl_2/pentane, 0°C, 46%;
(iii) $BF_3.OEt_2$, NEt_3, toluene, 80%.

Scheme 2.6 Synthesis of symmetrical BODIPY from ketopyrrole.
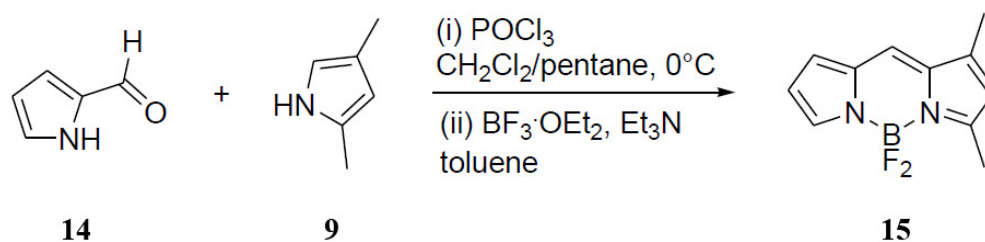
Scheme 2.7 Synthesis of unsymmetrical BODIPY from ketopyrrole.

2.7 Recent Publication BODIPY Based Cation Sensors

The development of efficient sensors that operate by fluorescence modulation is of great interest in analytical chemistry and for the clinical, medical and environmental sciences. [100] The key feature of all such applications is that the trapping of an analyte at some pre-designed site, such as a cavity inside a macrocycle or a hydrophobic patch, causes a pronounced change in the fluorescence properties of the sensor. Recognition of the analyte in this manner can increase or decrease fluorescence but, in general, a better analytical procedure is when the presence of the analyte causes the appearance of fluorescence. In many cases, improved sensitivity can be obtained when the sensing event perturbs a charge-transfer excited state or interrupts intramolecular electron transfer. [101] Daub and Rurack [102] were the first to show the high potential for BODIPY dyes in this field, and their original research has been followed by countless examples of BODIPY-based fluorescent molecular sensors.

The preferred strategy for using fluorescent dyes to monitor cations employs a functionalized macrocycle to trap the target ion, with the selectivity being set by the size and coordination sphere offered by the macrocycle. To switch off an intramolecular charge transfer process, upon substrate recognition, it is normal practice to incorporate a suitable nitrogen donor group into the macrocyclic structure but sufficiently close to the BODIPY core to facilitate light induced electron transfer.

In the past decade, fluorescent probes for Zn^{2+} have attracted a great deal of attention and many probes have been proposed based on numerous fluorophores. Di (2-picolyl)-amine is the most widely used ionophore for Zn^{2+}. Sensors for the detection and

imaging of Zn^{2+}, especially in biological systems, have been extensively reviewed. [103-107] A recent review describes the tools and tactics for the optical detection of Hg^{2+}. [108] Another recent review paper deals with the chemistry and biology of zinc, iron and copper in neurobiology. [109]

The ratiometric BODIPY-linked azacrown ether sensor **16** with high selectivity for potassium over other alkali ions in MeCN is the first example of a probe synthesized using SNAr of 3,5-dichloro BODIPY (Figure. 2.8). [110] A large conformational change of the sensor upon K^+ binding (K_d of the 1 : 1 complex K^+–**16** equals 0.5 mM) was invoked to explain the blue shifts in absorption and emission. Later research [111] confirmed these findings and showed that some alkaline-earth metal ions (Ca^{2+}) and HTM ions (Pb^{2+}, Hg^{2+}) also produced comparable spectral hypsochromic shifts and increases of quantum yield Φ.

The BODIPY derivative **17** with an aza-15-benzocrown-5 chelator is a Na^+-sensitive indicator. [112] The selectivity for Na^+ over K^+ is less than 2. The fluorescence emission intensity increased ca. 7-fold upon Na^+ binding and ca. 3-fold upon K^+ binding.

16
CH₃CN
apo: λ_{abs} 529 nm, λ_{em} 565 nm, Φ 0.006
+ K⁺: λ_{abs} 505 nm, λ_{em} 520 nm, Φ 0.04, K_d 5 x 10^{-4} M

17
MOPS buffer (pH 7.0)
apo: λ_{ex} 498 nm, λ_{em} 510 nm
$K_d(Na^+)$ 100 mM, $K_d(K^+)$ 170 mM
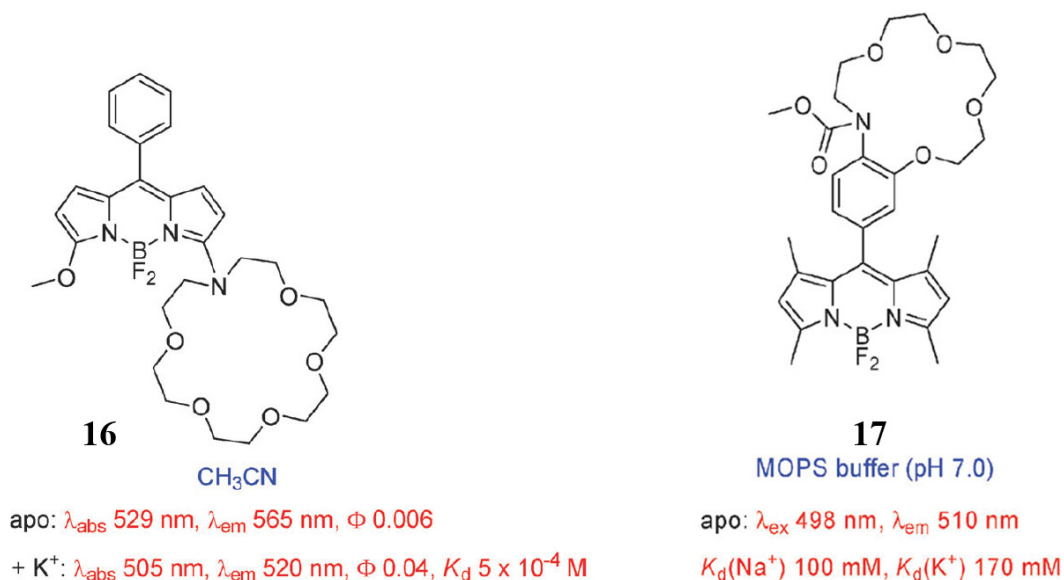
Figure 2.9 Fluorescent chemosensors for Na^+ and K^+.

In solvents more polar than hexane, BODIPY sensor **18** having a 13-phenyl-1,4,7,10-tetraoxa-13-azacyclopentadecane chelator shows dual emission from the

locally excited (LE) and intramolecular charge transfer (ICT) state, both fluorescence quantum yields being low. [113-114] In acetonitrile solution, only emission from the LE state of **18** was observed (Φ 0.0002). Crowned compound **18** forms 1 : 1 complexes with alkali (Li$^+$, Na$^+$) and alkaline-earth (Mg^{2+}, Ca^{2+}, Sr^{2+}, Ba^{2+}) metal ions, the latter being the stronger (K_d measured for the cation complexes of 50 are in the order Na$^+$ > Li$^+$ > Mg^{2+} > Ba^{2+} > Sr^{2+} > Ca^{2+}). Coordination of the cation to the nitrogen of the aza crown leads to cationdependent enhancement of the LE fluorescence quantum yield and cation-independent slight (2–3 nm) red shifts of labs and lem. The stability of the 1 : 1 complex between Na$^+$ and **18** is solvent dependent: K_d of Na$^+$–**18** equals 6 mM in acetonitrile and 23 mM in methanol.

The same aza-15-crown-5 chelator as **18** is attached via a styryl linker to the 3-position of the BODIPY core to produce compound **19**. [115] Apo **19** in acetonitrile solution has a low fluorescence quantum yield which was attributed to the ICT character of the excited state. Also this sensor was not selective because it forms 1 : 1 complexes with several alkali (Li$^+$, Na$^+$), alkaline-earth (Mg^{2+}, Ca^{2+}, Ba^{2+}) and transition (Zn^{2+}) metal ions and protons, producing large blue shifts and significant cation-induced fluorescence amplifications. The stability of the metal-ion complexes with **19** decreases in the order: Ba^{2+} > Li$^+$ > Na$^+$ $\approx$ Zn^{2+} > Ca^{2+} > Mg^{2+} (Figure. 2.9).

18

CH$_3$CN

apo: λ_{abs} 496 nm, λ_{em} 505 nm, Φ 0.0002

K_d(Ca^{2+}) 1.7 x 10^{-4} M, K_d(Na$^+$) 6.3 x 10^{-3} M

19

CH$_3$CN

apo: λ_{abs} 608 nm, λ_{em} 723 nm, Φ 0.08

pK_a 0.09, K_d(Li$^+$) 9 x 10^{-4} M, K_d(Na$^+$) 4.4 x 10^{-3} M, K_d(Mg^{2+}) 7 x 10^{-2} M

K_d(Ca^{2+}) 1 x 10^{-2} M, K_d(Ba^{2+}) 5 x 10^{-4} M, K_d(Zn^{2+}) 5 x 10^{-3} M
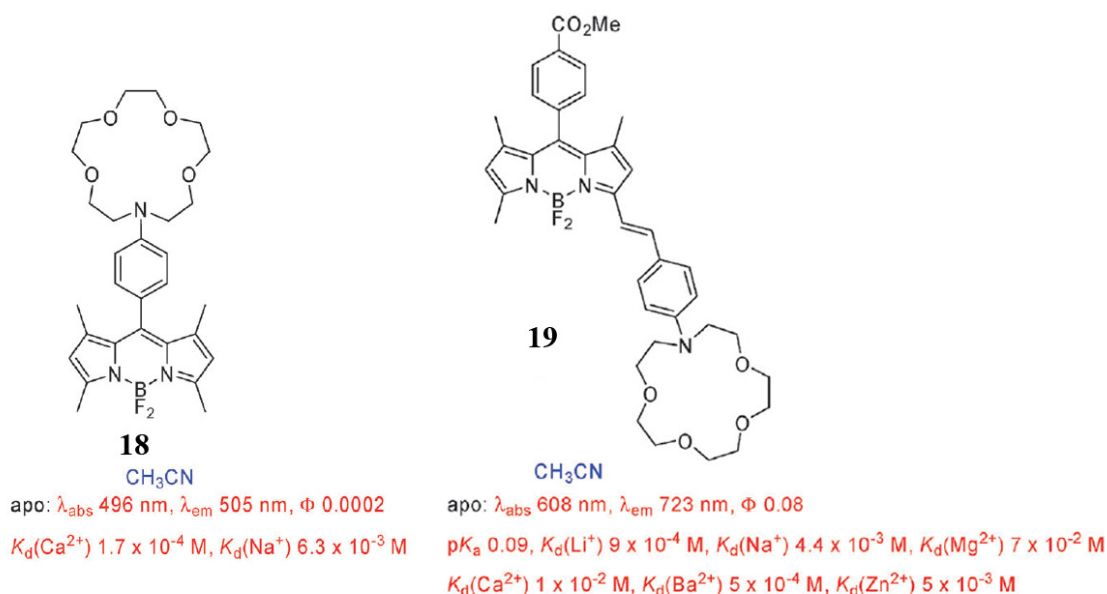
Figure 2.10 Sensors with aza-15-crown-5 chelator at different locations.

Two 'off–on' indicators with *o*-aminophenol-*N,N,O*-triacetic acid (APTRA) meso-APTRA substituents as low-affinity chelators for calcium but with different groups (methyl in **20a** versus *p*-anisyl in **20b**) at the 3,5-positions have very similar dissociation constants of the 1 : 1 33–Ca^{2+} complexes and quantum yields. [116] The absorption and fluorescence emission spectra of **20b** are red-shifted by 65 and 100 nm, respectively, compared to those of **20a**. Reductive PET from APTRA to BODIPY is shut down upon Ca^{2+} complex formation so that a large fluorescence enhancement is observed without any spectral shifts (Figure. 2.18).

Compound **21** has a selective fluorescence turn-on response to Ni^{2+} compared to other biologically relevant metal ions in water (Na^{+}, K^{+}, Mg^{2+}, Ca^{2+}, Mn^{2+}, Fe^{2+}, Co^{2+}, Cu^{2+}, Zn^{2+}). [117] Addition of 50 equiv. of Ni^{2+} switches off PET and triggers ca. 25-fold fluorescence turn-on with no shifts of labs and lem compared to the apo probe. Confocal microscopy shows that **21** can respond to changes in Ni^{2+} levels within live cells (Figure. 2.18).

20
R = Me
R = 4-methoxyphenyl

MOPS buffer (pH 7.2)

20a λ_{ex} 505 nm, λ_{em} 525nm,
   Φ(apo) 0.004, Φ(Ca^{2+}) 0.14, K_d(Ca^{2+}) 96 µM

20b λ_{ex} 570 nm, λ_{em} 625nm,
   Φ(apo) 0.003, Φ(Ca^{2+}) 0.13, K_d(Ca^{2+}) 103 µM

21
HEPES buffer (pH 7.1)
apo: λ_{abs} 495 nm, λ_{em} 507 nm, Φ 0.002
+ Ni^{2+}: K_d 193 µM, Φ 0.055
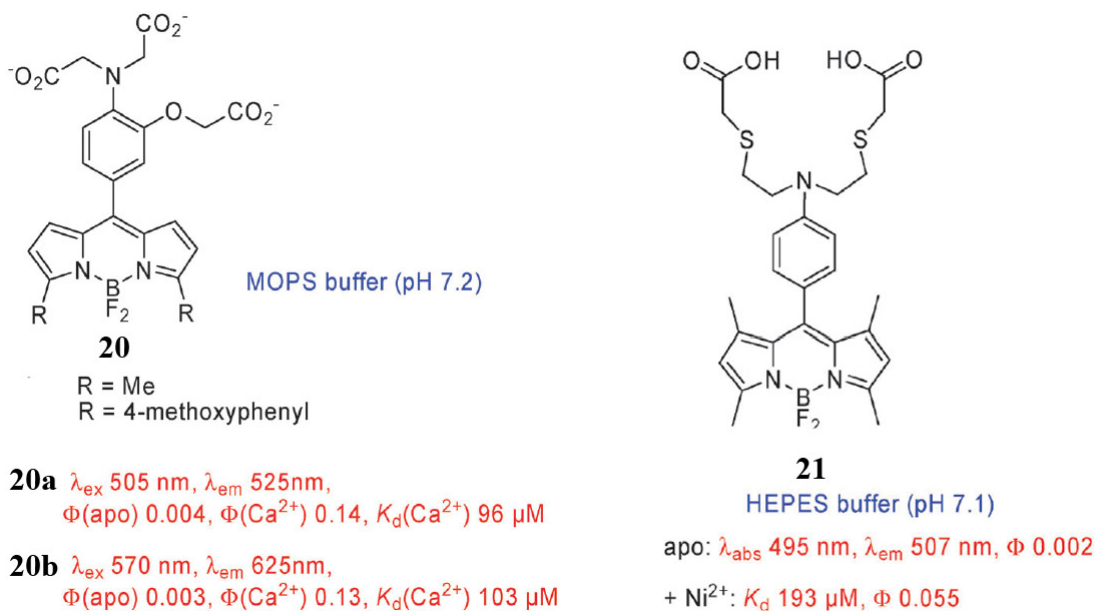
Figure 2.11 Metal ion sensing dyes **20** and **21**.

A highly selective PET fluorescent sensor **22** for Hg^{2+} containing a BODIPY fluorophore and a NS_2O_2 pentachelating receptor has been presented by Jianjun and co-worker. [118] (Figure 2.11) Sensor **22** displays high selectivity and large fluorescence enhancement for Hg^{2+}, and its fluorescence emission is pH-independent under a large physiological pH range, which indicates that it has potential applications for biological toxicities. Furthermore, **22**Hg1 also displays response to some anions such as Cl^-, Br^-, CO_3^{2-}, SCN^- and CH_3COO^-, which is attributed to the significant coordinating ability of these anions to Hg^{2+}.
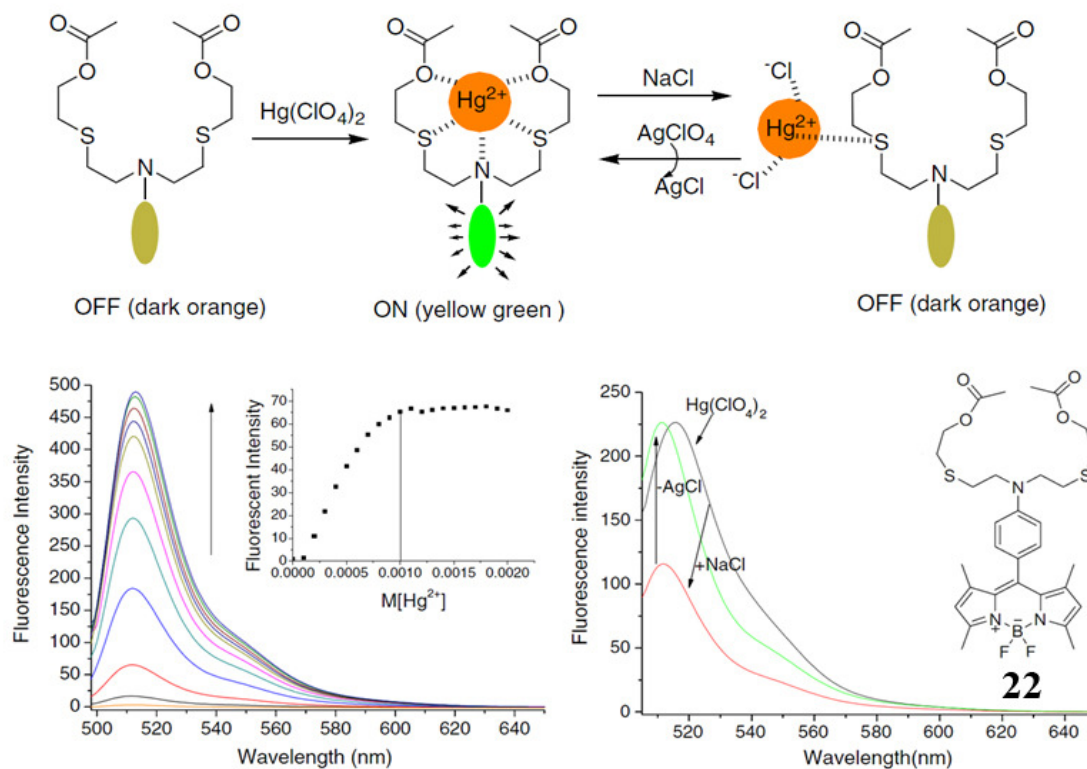
Figure 2.12 Fluorescence response of **22** (1 μM) to different concentrations of Hg^{2+} (a) Changes of Fluorescence-Switching by addition of salts in water–ethanol Solution (b)

A boron-dipyrromethene (BODIPY)-based fluorescence probe with a *N,N'*-(pyridine-2, 6-diylbis(methylene))- dianiline substituent (**23**) has been prepared by condensation of 2,6-pyridinedicarboxaldehyde with 8-(4-amino)- 4,4-difluoro-1,3,5,7-tetramethyl-4-bora-3a,4a-diaza-*s*-indacene and reduction by NaBH$_4$. [119] The sensing properties of compound **23** toward various metal ions are investigated via fluorometric titration in methanol, which show highly selective fluorescent turn-on response in the presence of Hg^{2+} over the other metal ions, such as Li$^+$, Na$^+$, K$^+$, Ca^{2+}, Mg^{2+}, Pb^{2+}, Fe^{2+}, Co^{2+}, Ni^{2+}, Cu^{2+}, Zn^{2+}, Cd^{2+}, Ag$^+$, and Mn^{2+}. Computational approach has been carried out to investigate the mechanism why compound **23** provides different fluorescent signal for Hg^{2+} and other ions. Theoretic calculations of the energy levels show that the quenching of the bright green fluorescence of boradiazaindacene fluorophore is due to the reductive PET from the aniline subunit to the excited state of BODIPY fluorophore. In metal complexes, the frontier molecular orbital energy levels changes greatly. Binding of Zn^{2+} or Cd^{2+} ion leads to significant decreasing of both the HOMO and LUMO energy levels of the receptor, thus inhibit the reductive PET process, whereas an oxidative PET from the excited state fluorophore to the receptor occurs, vice versa, which also quenches the fluorescence. However, for **23**-Hg^{2+} complex, both the reductive and oxidative PETs are prohibited; therefore, strong fluorescence emission from the fluorophore can be observed experimentally. The agreement of the experimental results and theoretic calculations suggests that our calculation method can be applicable as guidance for the design of new chemosensors for other metal ions.
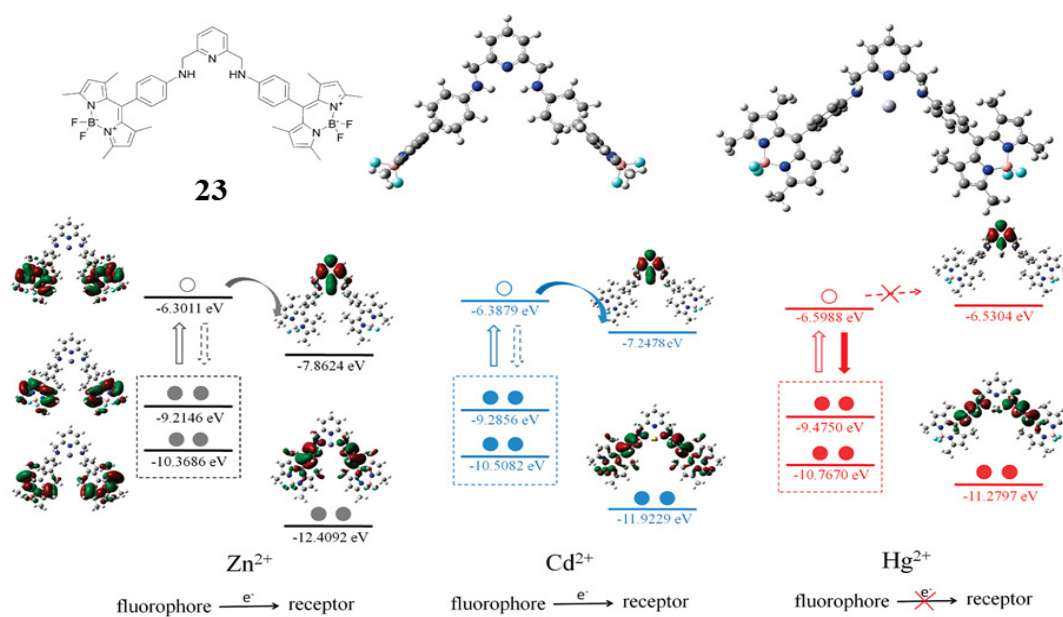
Figure 2.13 Frontier orbital energy diagrams and electron-transfer paths in
23 and after attachment of Zn^{2+} ion .

CHAPTER 3

METHODOLOGY

3.1 Analytical Measurement

Nuclear Magnetic Resonance (NMR) spectra were recorded on Varian 400 MHz NMR spectrometers. Ligands were dissolved in deuterated dimethylsulfoxide (DMSO-d_6) and deuterated chloroform-d (CDCl$_3$). Electrospray mass spectra were determinutesed on a Micromass Platform quadrupole mass analyser (HP1050) with an electrospray ion source using acetonitrile as solvent. UV-Vis complexation spectra were measured by a Perkin Elmer Lambda25 spectrophotometer at 25 ℃. Fluorescent complexation spectra were recorded by Perkin Elmer SL50B fluorescence spectrophotometer.

3.2 Materials

Unless otherwise specified, the solvents and all materials were reagent grades purchased from Fluka, BHD, Aldrich, Carlo Erba, Merck or J.T. Baker and were used without further purification. Commercial grade solvents such as acetone, dichloromethane, hexane, methanol and ethylacetate were purified by distillation before using. Acetonitrile and dichloromethane for set up the reaction were dried over calcium hydride and freshly distilled under nitrogen atmosphere prior to use.

Column chromatographies were carried out on silica gel (Kieselgel 60, 0.063-0.200 nm, Merck). Thin layer chromatography (TLC) was performed on silica gel plates (Kieselgel 60, F$_{254}$, 1 mm, Merck). Compounds on TLC plates were detected by the UV-light. All manipulations were carried out under nitrogen atmosphere.

The synthesized compounds were characterized by ^{1}H-NMR, ^{13}C-NMR spectroscopies and mass spectrometry.

3.3 Synthesis

It is our interest to synthesize cation sensors by combining receptor units with signaling units. The most common modes of signal transduction typically involve electrochemical or optical changes in the sensor incurred by association of cations with the receptors. Of particular interest in this regard is "colorimetric cation sensors" species that would allow the so-called "naked-eye" detection of cations without resort to any instrument.

This research is aimed at the synthesis of cation sensors containing organic dyes giving optical signal. Phenyl hydroxyl *N,N* diethyl acetamine moieties are used for cation receptors because they can interact with cationic species effectively by electrostatic interaction. BODIPY-based sensing units are directly linked to the receptor units that were designed to have various distances for different cations. The synthetic pathways are shown in Schemes 3.1-3.3.
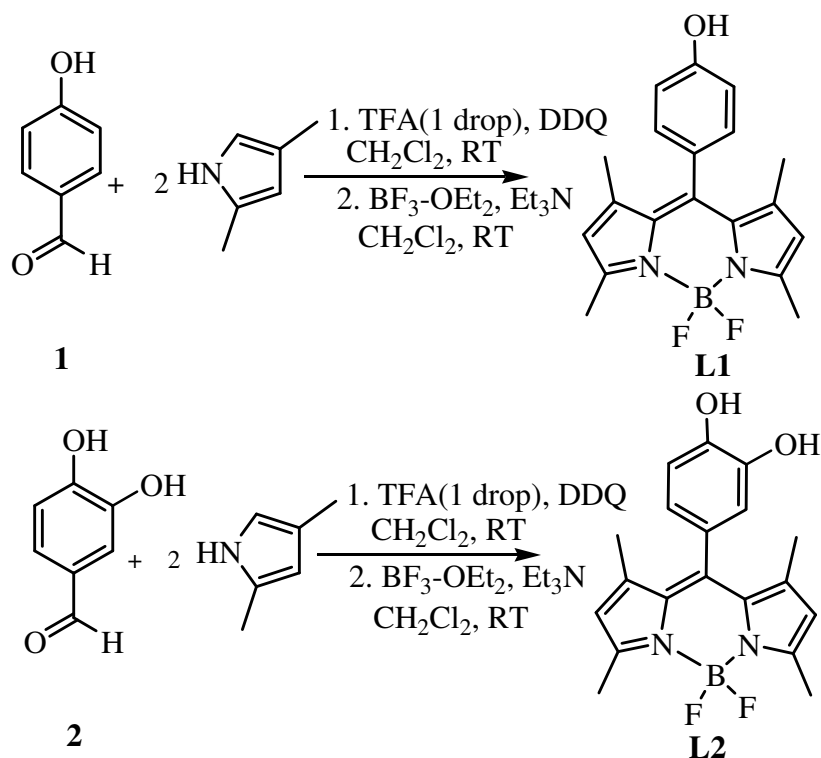
Scheme 3.1 Synthesis of BODIPY-based chemosensors **L1** and **L2**.
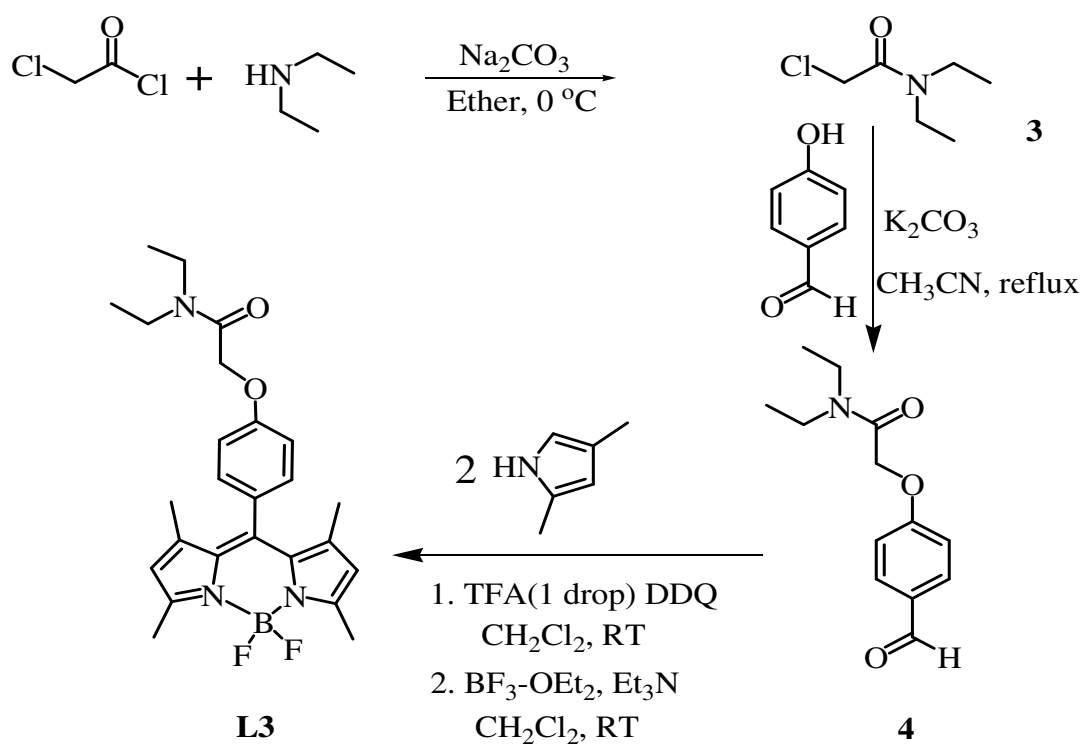
Scheme 3.2 Synthesis of BODIPY-based chemosensor **L3**.
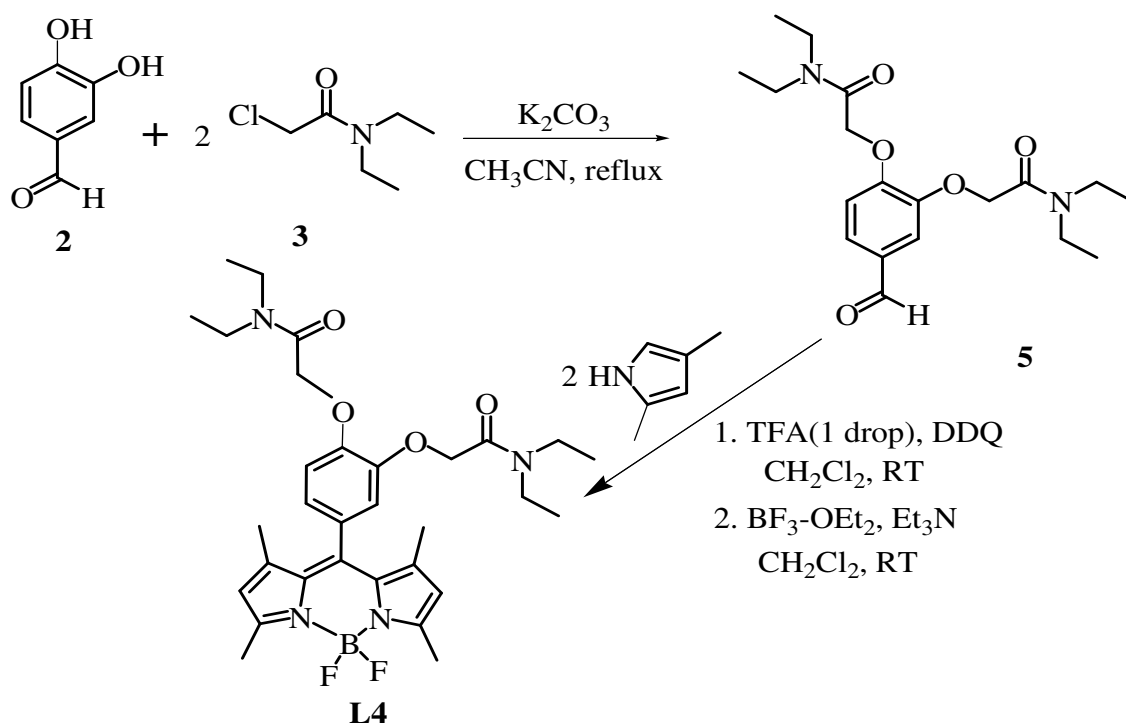
Scheme 3.3 Synthesis of BODIPY-based chemosensor **L4**.

3.3.1 Preparation of 8-(4-hydroxyphenyl)-1,3,5,7-tetramethyl- BODIPY, L1

1   **L1**
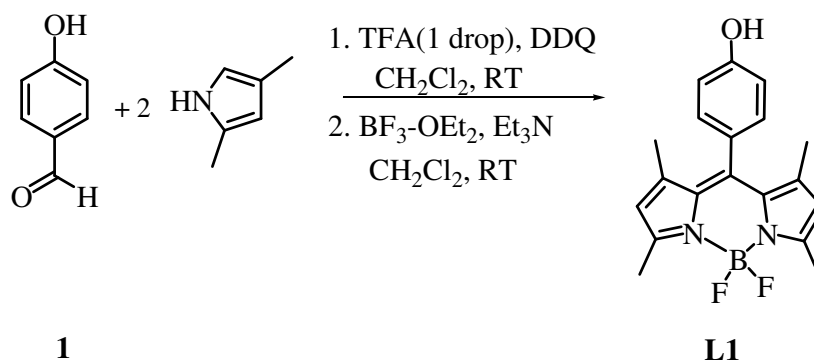
The 4-hydroxybenzaldehyde, **1** (127 mg, 0.104 mmol) and 2,4-dimethylpyr-role (0.21 ml, 0.204 mmol) were dissolved in anhydrous methylene chloride (CH_2Cl_2, 150 ml) under nitrogen (N_2) atmosphere. Then one drop of trifluoroacetic acid (TFA) was added into the solution, and the solution was stirred for 1 h at room temperature. A solution of 2,3-dichloro-5,6-dicyano-1,4-benzoquinone (DDQ, 250 mg, 2.16 mmol) in CH_2Cl_2 was added with syringe, and the reaction was continued for another 2 h. Then triethylamine (Et_3N, 2 ml) was added followed by trifluoride etherate (BF_3-OEt_2, 4 ml) during 30 min and stirred overnight. After concentrated in vacuum, the residue was purified by column chromatography (silica, CH_2Cl_2/MeOH, 10/1, v/v) the desired product **L1** was obtained as greened-red solid (129 mg, 37% yield).

Characterization data for **L1**

^{1}H-NMR spectrum (400 MHz, CDCl$_3$-d_6, ppm): δ 1.44 (s, 6H, CH_3-pyrrole), 2.55 (s, 6H,CH_3-pyrrole), 5.19 (s, 1H,HO-phenol), 5.98 (s, 2H, H-pyrrole), 6.94 (d, 2H *J*=8.4 Hz, ArH), 7.12 (d, 2H *J*=8.4 Hz, ArH)

^{13}C-NMR spectrum (400 MHz, DMSO-d_6, ppm): δ 14.1, 14.7, 38.5, 39.2 (4C, C-methyl), 39.5, 39.5, 39.6, 40.2, (4C, C-pyrrole), 116.9, 121.4, (2C, C-ArH) 124.1, 129.3, 131.3, 142.7, 154.7, 158.5 (2C-pyrrole)

MALDI-TOF MS (m/z): 340.2 (100) calcd: 341.0

3.3.2 Preparation of 8-(3,4-dihydroxyphenyl)-1,3,5,7-tetramethyl-BODIPY, L2

2   **L2**
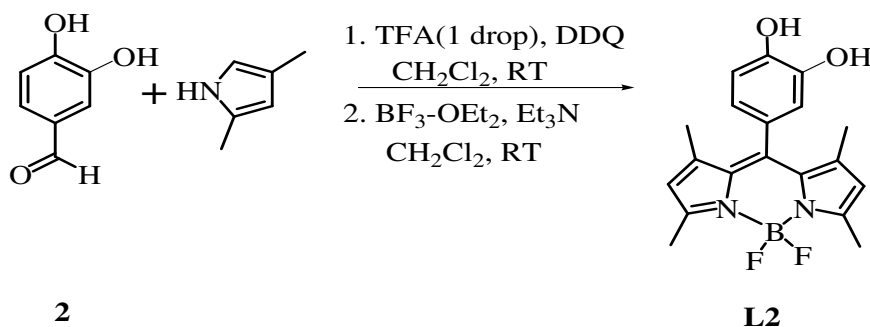
The 3,4-dihydroxybenzaldehyde, **2** (319mg, 1 mmol) and 2,4-dimethylpyrrole (0.26 ml, 2 mmol) were dissolved in anhydrous CH_2Cl_2 (150 ml) under N_2 atmosphere. Then one drop of TFA was added into the solution, and the solution was stirred for 15 min at room temperature. A solution of DDQ (360 mg, 2.16 mmol) in CH_2Cl_2 was added with syringe, and the reaction was continued for another 2 h. Then Et_3N (2 ml) was added followed by BF_3-OEt_2 (4 ml) during 30 min and stirred overnight. After concentrated in vacuum, the residue was purified by column chromatography (silica, CH_2Cl_2/MeOH, 10/5, v/v), the desired product **L2** was obtained as dark red solid (136 mg, 36 % yield).

Characterization data for **L2**

^{1}H-NMR spectrum (400 MHz, CDCl$_3$-d_6, ppm): δ 1.49 (s, 6H, CH$_3$-pyrrole), 2.53 (s, 6H, CH$_3$-pyrrole), 5.96 (s, 2H, H-pyrrole), 6.65 (d, 1H J=8.4 Hz, C$_6$H$_5$), 6.74 (s, 1H, ArH), 6.96 (d, 1H, J=8.0 Hz, ArH)

^{13}C-NMR spectrum (400 MHz, DMSO-d_6, ppm): δ 13.7, 14.1, 21.6, 28.2, (4C-methyl), 28.5, 33.7 (2C, C-pyrrole), 114.5, 116.2, 118.3, 120.7, (5C, C-ArH) 124.5, 131.3, 142.3, 146.5, 146.7, 154.0 (8C, C-pyrrole)

MALDI-TOF MS (m/z) : 356.2 (100) [M+Cl]⁻, calcd: 357.2.

3.3.3 Preparation of 2-chloro-*N,N*-diethylacetamide, 3
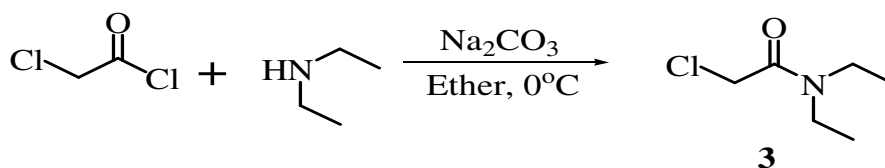
To a suspension of diethylamine (11.43 ml, 110 mmol), Na_2CO_3 (10.60 g) and ether (100 ml) at -10°C were added chloroacetyl chloride (7.95 ml, 100 mmol). The reaction mixture was maintained below room temperature during the addition. The mixture was stirred for 45 min. The solid was removed by filtration, and the filtrate was concentrated resulting in a residue. The residue was dissolved in CH_2Cl_2, extracted with 1 N HCl followed by dilute Na_2CO_3 and dried over solid sodium sulfate which resulted in an aqueous and organic layer. Concentration of the organic layer afforded a light yellow liquid. The residue was purified by distillation (60-70°C, 2 mm Hg) to provide 8.18 g of light yellow oil. The NMR spectrum of this light yellow liquid was consistent with the desired product and indicated that the compound was > 95% pure.

Characterization data for **3**

^{1}H-NMR spectrum (400 MHz, $CDCl_3$-d_6, ppm): δ 1.13 (t, 3H, *J*=14 Hz, CH_3-amide), δ 1.23 (t, 3H, *J*= 14.4 Hz, CH_3-amide)

3.3.4 Preparation of *N,N*-diethyl-2-(4-ormylphenoxy) acetamide, 4
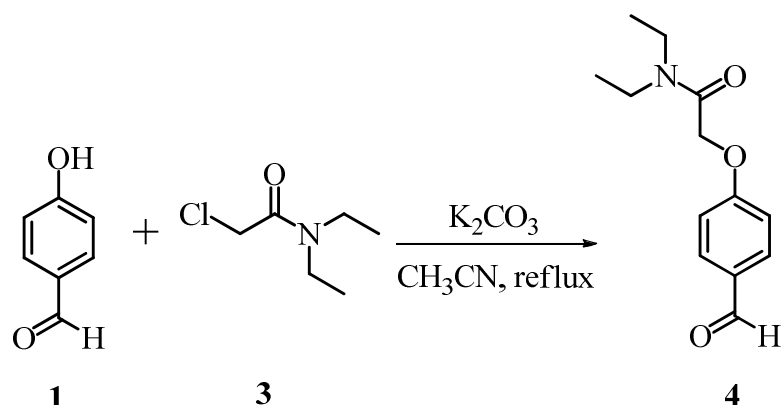
A suspension of 4-hydroxybenzaldehyde, **1** (492 mg, 4 mmol), potassium carbonate (K_2CO_3 0.76 g) and 2-chloro-*N,N*-diethylacetamide, **3** (0.3 ml, 2 mol) in

CH₃CN 50 ml was refluxed overnight. The solid was removed by filtration. Subsequently, the filtrate was concentrated under reduced pressure resulting in a residue. The residue was dissolved in CH_2Cl_2 (100 ml), washed with 0.5 M HCl (100 ml), followed by water (200 ml). After dried with sodium sulfate (Na_2SO_4), the solvent was removed under reduced pressure. The crude product was purified by column chromatography (silica, CH_2Cl_2/MeOH, 0 - 5 %, v/v), the desired product **4** (856 g) was obtained as the yellow oil in 90% yield.

Characterization data for **4**

^{1}H-NMR spectrum (400 MHz, CDCl₃-d_6, ppm): δ 1.13 (t, 3H, *J*=14 Hz, CH₃-amide), δ 1.22 (t, 3H, *J*=6.8 Hz, CH₃-CH₂N), 3.36 (q, 4H, CH₃-CH₂N), 4.80 (s, 2H, CH₂-OCO), 7.05 (d, 2H *J*=8.4 Hz, ArH), 7.83 (d, 2H *J*=9.4 Hz, ArH), 9.89 (s, 1H, H_CHO)

3.3.5 Preparation of 8-(4-(2-(diethylamino)-2-oxoethoxy)phenyl)-1,3,5,7-tetramethyl- BODIPY, L3

4   **L3**
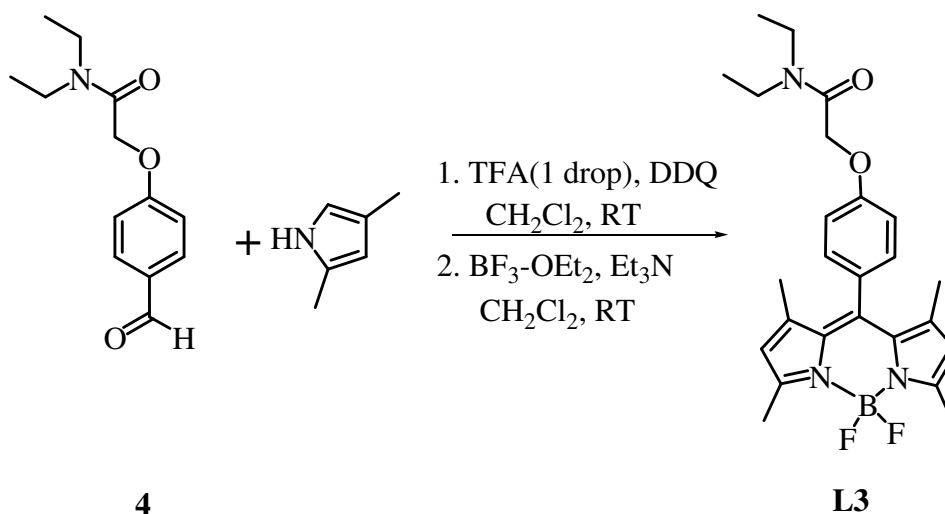
The 4-dihydroxybenzaldehyde, **4** (504 mg, 2 mmol) and 2,4-dimethylprrole(0.42 ml, 4 mmol) were dissolved in anhydrous CH_2Cl_2 (160 ml) under N₂ atmosphere. Then one drop of TFA was added into the solution, and the solution was stirred for 15 min at room temperature. A solution of DDQ (454 mg, 2 mmol) in CH_2Cl_2 was added with syringe, and the reaction was continued for another 2 h. Then Et₃N (2 ml) was added followed by BF₃-OEt₂ (4 ml) during 30 min and stirred overnight. After concentrated in vacuo, the residue was purified by column chromatography (silica,

CH₂Cl₂/MeOH, 10/2, v/v) the desired product **L3** was obtained as brown solid (314 mg, 33% yield).

Characterization data for **L3**

^{1}H-NMR spectrum (400 MHz, CDCl₃-d_6, ppm): δ 1.12 (t, 3H, J=14 Hz, CH₃-amide), δ 1.21 (t, 3H, J= 14 Hz, CH₃-amide), δ 1.41 (s, 6H, CH₃-pyrrole), 2.55 (s, 6H,CH₃-pyrrole), 3.42 (q, 4H, CH₂-CH₂N), 4.75 (s, 2H, OCH₂CO), 5.97 (s, 2H,H-pyrrole), 7.06 (d, 2H J=8.8 Hz, ArH), 7.17 (d, 2H J=8.4 Hz, ArH)

^{13}C-NMR spectrum (400 MHz, DMSO-d_6, ppm): δ 12.6 (2C, CH₃-CH₂N), 14.6 (2C, CH₃-pyrrole), 40.4, 41.8 (2C, CH₂- CH₂N), 67.3 (C, CH₂OCO), 115.7, 121.3, 129.5 (5C, C-ArH) 131.6, 141.2, 142.6, 155.0, 158.4, 166.7 (8C, C-pyrrole)

MALDI-TOF MS (m/z) : 452.8 (100) calcd: 453.2

3.3.6 Preparation of 2,2'-((4-formyl-1,2-phenylene)bis(oxy))bis (*N,N*-diethylacetamide), 5
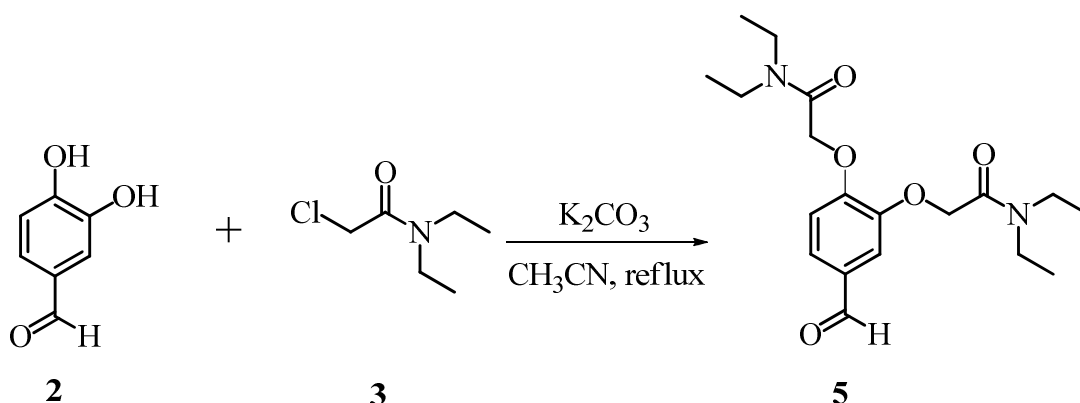
A suspension of 3,4-dihydroxybenzaldehyde, **2** (748 mg, 5 mmol), K₂CO₃ (3.255 g) and 2-chloro-*N,N*-diethylacetamide, **3** (2.8 ml, 20 mmol) in CH₃CN 50 ml was refluxed overnight. The solid was removed by filtration. Subsequently, the filtrate was concentrated under reduced pressure resulting in a residue. The residue was dissolved in CH₂Cl₂ (100 ml), washed with 0.5 M HCl (100 ml), followed by water (200 ml). After dried with Na₂SO₄, the solvent was removed under reduced pressure. The crude product was purified by column chromatography (silica, CH₂Cl₂/MeOH, 0 - 5%, v/v), the desired product **5** (1.39 g) was obtained as the yellow oil in 70% yield.

Characterization data for **5**

^{1}H-NMR spectrum (400 MHz, CDCl$_3$-d_6, ppm): δ 1.11 (t, 6H, J=13.2 Hz, CH$_3$- CH$_2$N), δ 1.16 (t, 6H, J=14.4 Hz, CH$_3$- CH$_2$N), 3.34 (q, 8H, CH$_2$-CH$_2$N), 4.82 (s, 2H, CH$_2$-OCO), 4.88 (s, 2H, OCH$_2$CO), 7.04 (d, 1H, J=8.4 Hz ArH), 7.40 (s, 1H, ArH), 7.45 (d, 1H, J=8.4 Hz, ArH), 9.82 (s, 1H, H_CHO)

3.3.7 Preparation of 8-(3,4-bis(2-(diethylamino)-2-oxoethoxy)phenyl)-1,3,5,7-tetramethyl- BODIPY, L4

5   **L4**
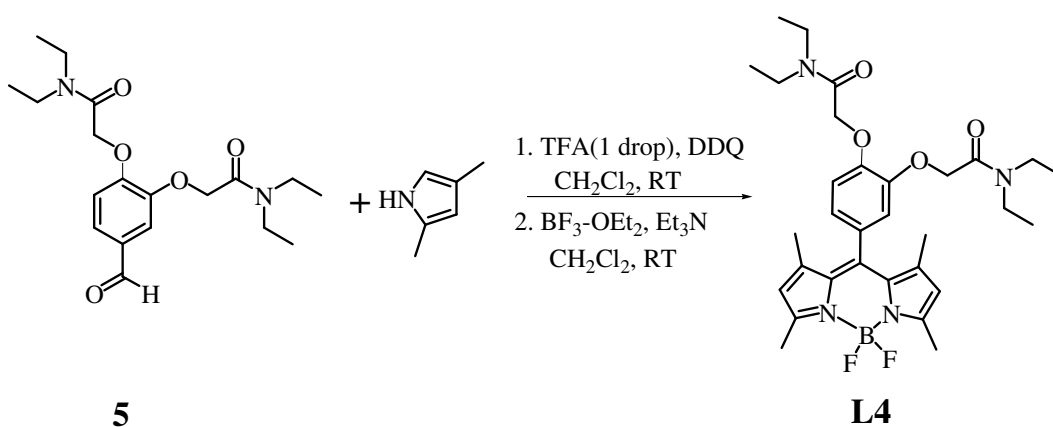
The 2,2'-((4-formyl-1,2-phenylene)bis(oxy))bis(*N,N*-diethylacetamide), **5** (728 mg, 2 mmol) and 2,4-dimethylpyrrole (0.42 ml, 4 mmol) were dissolved in anhydrous CH$_2$Cl$_2$ (160 ml) under N$_2$ atmosphere. Then one drop of TFA was added into the solution, and the solution was stirred for 5 h at room temperature. A solution of DDQ (360 mg, 2.16 mmol) in CH$_2$Cl$_2$ was added with syringe, and the reaction was continued for another 4 h. Then Et$_3$N (2 ml) was added followed by BF$_3$-OEt$_2$ (4 ml) during 30 min and stirred overnight. After concentrated in vacuo, the residue was purified by column chromatography (silica, CH$_2$Cl$_2$/MeOH, 10/5, v/v) the desired product **L4** (291 mg) was obtained as brown solid in 25 % yield.

Characterization data for **L4**

^{1}H-NMR spectrum (400 MHz, CDCl$_3$-d_6, ppm): δ 1.07 (t, 6H, J=15.2 Hz, CH$_3$-amide), δ 1.19 (t, 6H, J=13.6 Hz, CH$_3$-amide), 1.45 (s, 6H, CH$_3$-pyrrole), 2.54 (s, 6H,CH$_3$-pyrrole), 3.32 (q, 8H, CH$_2$-amide), 4.74 (s, 2H, OCH$_2$CO), 4.83 (s, 2H, OCH$_2$

CO), 5.97 (s, 2H, H-pyrrole), 6.78 (s, 1H, ArH), 7.1 (s, 1H, ArH), 7.08 (d, 1H, J=8.0 Hz, ArH)

^{13}C-NMR spectrum (400 MHz, DMSO-d_6, ppm): δ 12.6, 13.9 (4C, CH$_3$-amide), 14.3, 29.4 (4C, CH$_3$-pyrrole), 40.3,41.5, 41.8, (4C, CH$_2$-amide), 67.9, 68.6 (2C, CH$_2$OCO), 114.0, 115.4, 121.2, 121.6, 128.8, (5C, C-ArH) 131.6, 141.2, 142.9, 148.4, 149.1, 154.9, 166.3, 166.6 (8C, C-pyrrole)

MALDI-TOF MS (m/z): 582.3 (100) calcd: 582.3

3.4 Complexation studies

The absorption spectra of BODIPY-based chemosensors and excesses equivalent of some cations were recorded from 400 - 900 nm at ambient temperature. The fluorescence behavior of synthetic receptors and their excesses cation complexation was also investigated.

3.5 Computational Methods

Structures of BODIPY-based chemosensors and theirs complexes with cation guest i.e., Na$^+$, Ag$^+$, Al^{3+} and Cu^{2+} have been optimized by using the DFT method. Association model of 1 : 1 complex of cation with receptor was selected as most plausible structure for this kind of receptors. The DFT calculation has been performed using the Becke's three-parameter exchange functional with the Lee–Yang–Parr correlation functional (B3LYP). All calculations have been performed using the MO computation at the B3LYP/LanL2DZ level of theory. The HOMO and LUMO energy gaps were also investigated at the same level of theory.

Thermodynamic property changes (ΔX) i.e., total energy (ΔE), enthalpy (ΔH) and Gibbs free energy (ΔG) changes, of complexation can be expressed as follows:

$$\Delta X = X \text{ (receptor/cation) - } [X \text{ (receptor) } + X \text{ (cation)}] \tag{1}$$

Where X (receptor/cation), X (receptor) and X (cation) are the thermodynamic properties of the receptor/cation complex, free receptor and cation, respectively.

In addition, natural bond orbital (NBO) analysis implemented in GAUSSIAN 03 program is applied through a series of intermolecular interactions under the above system to evaluate the NBO charges. All calculations were performed with the GAUSSIAN 03 program. The molecular graphics of all related species were generated with the MOLEKEL 4.3 program.

CHAPTER 4

RESULTS AND DISCUSSION

4.1 Synthesis of BODIPY-Based Receptor Containing Hydroxyl Group

      The synthesis of cation sensors which combine receptor units with signaling units is interesting. The most common mode of signal transduction typically is optical changes in the sensor incurred by association of cations with the receptors. Hydroxyl moieties are used for cation receptors because they can interact with cationic species effectively by ion/dipole interaction.

      4.1.1 Synthesis and characterization of receptor, L1
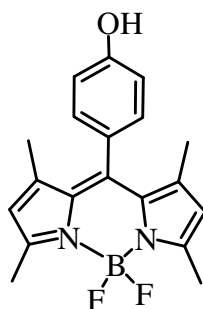
L1

      Receptor **L1** was obtained by coupling reaction of 4-hydroxybenz aldehyde and 2,4-dimethylpyrrole in anhydrous CH_2Cl_2 at room temperature under nitrogen atmosphere. The receptor **L1** was obtained as a greened red solid in 37% yield. ^{1}H-NMR spectrum of receptor **L1** in $CDCl_3$-d_6 showed aldehydric proton at 9.76 ppm and NH proton at 5.00 ppm disappears. The protons of phenol and pyrrole were shown at around 6.94 - 7.12 and at 5.98 ppm, respectively.

4.1.2 Synthesis and characterization of receptor L2
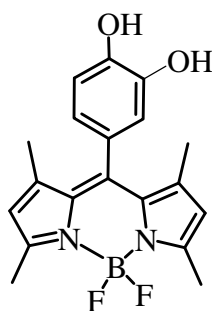
L2

Receptor **L2** was obtained by coupling reaction of 3,4-dihydroxybenz aldehyde and 2,4-dimethylpyrrole in anhydrous CH_2Cl_2 at room temperature under argon atmosphere. The receptor **L2** was obtained as a red solid in 36% yield. ^{1}H-NMR spectrum of receptor **L2** in CDCl$_3$-d_6 shows aldehydric proton at 9.76 ppm and NH proton at 5.00 ppm disappears. The protons of phenol are shown around at 6.98, 6.74 and 6.50 ppm. The protons of pyrrole are shown at around 5.96 ppm.

4.2 Synthesis of BODIPY-Based Receptor Containing Amide Group

4.2.1 Synthesis and characterization of receptor L3

a) Preparation of 2-chloro-*N,N*-diethylacetamide, 3
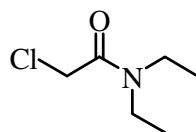
3

Compound **3** was synthesized by the reaction between diethylamine and chloroacetyl chloride in the presence of sodium carbonate and ether at 0°C. The compound **3** was obtained as light yellow oil in 78% yield. ^{1}H-NMR spectrum of compound **3** in DMSO-d_6 shows CH$_3$ and CH$_2$ protons in amide at 1.13 and 3.38 ppm, respectively. The protons of CH$_2$ near chlorine atom are shown at around 4.10 ppm.

b) Preparation of *N,N*-diethyl-2-(4-formylphenoxy)acetamide, 4
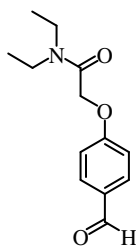
4

Compound **4** was synthesized by the reaction between 4-hydroxybenz-aldehyde and 2-chloro-*N,N*-diethylacetamide, **3** in the presence of potassium carbonate and acetonitrile. The compound **4** was obtained as a pale yellow oil in 90% yield. ^{1}H-NMR spectrum of compound **4** in DMSO-d_6 shows CH$_3$ and CH$_2$ protons in amide at 1.13 and 3.38 ppm, respectively. The protons of phenyl proton and aldehyde are shown at around 7.05 – 7.85 and 9.88 ppm, respectively.

c) Synthesis and characterization of receptor L3
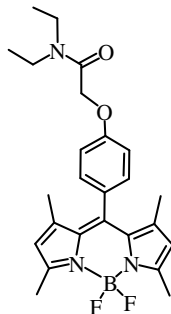
L3

Receptor **L3** was obtained by coupling reaction of *N,N*-diethyl-2-(4-formylphenoxy)acetamide and 2,4-dimethylpyrrole in the presence of trifluoroacetic acid and anhydrous methylene chloride at room temperature under argon atmosphere. The receptor **L3** was obtained as a brown solid in 33% yield. ^{1}H-NMR spectrum of receptor **L3** in CDCl$_3$-d_6 shows CH$_3$ and CH$_2$ protons in amide at 1.12 and 3.42 ppm, respectively. The protons of phenyl group and CH$_2$CO are shown at around 7.06 – 7.19 and 4.75 ppm, respectively and CH$_3$ protons in pyrrole are at 1.41 and 2.55 ppm.

4.2.2 Synthesis and characterization of receptor L4

a) Preparation of 2,2'-((4-formyl-1,2-phenylene)bis(oxy))bis(*N,N*-diethyacetamide), 5
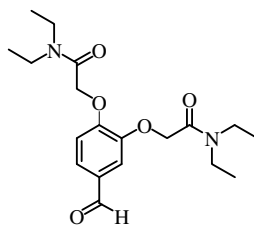
5

Compound **5** was synthesized by the reaction between 3,4-dihydroxy benzaldehyde and 2-chloro-*N,N*-diethylacetamide, **3** in the presence of potassium carbonate and acetonitrile. The compound **5** was obtained as a yellow oil in 70% yield. ^{1}H-NMR spectrum of compound **5** in DMSO-d_6 shows CH_3 and CH_2 protons in amide at around 1.11 – 1.27 and 3.14 - 3.47 ppm, respectively. The protons of phenyl group and aldehyde are shown at around 7.04 – 7.48 and 9.82 ppm, respectively.

b) Synthesis and characterization of receptor L4
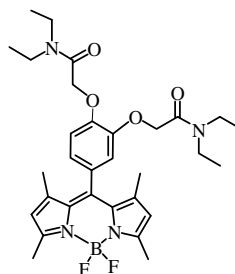
L4

Receptor **L4** was obtained by coupling reaction of compound **5** and 2,4-dimethylpyrrole in the presence of TFA and anhydrous CH_2Cl_2 at room temperature under argon atmosphere. The receptor **L4** was obtained as a brown solid in 25% yield. ^{1}H-NMR spectrum of receptor **L4** in CDCl$_3$-d_6 shows CH_3 and CH_2 protons in amide at around 1.07-1.24 and 3.32-3.47 ppm, respectively. The protons of phenyl group are shown at around 6.78-7.10 ppm, and CH_2CO were shown at around 4.74 and 4.83 ppm and CH_3 protons in pyrrole are shown 1.45 and 2.54 ppm.

4.3 The Complexation Studies of Synthetic Compounds with Various Cations by Using UV-Vis and Fluorescent Spectroscopy

Compounds **L1** and **L2** contain hydroxyl units and compounds **L3** and **L4** contain amide units for binding cations. This research is aimed to compare the binding ability of synthetic compounds toward cations. Because of their importance in environmental and biological systems, representative cations such as Na^+, K^+, Ca^{2+}, Al^{3+}, Ge^{4+} ions especially Pb^{2+} ion which is poison and transition cations such as Cr^{3+}, Co^{2+}, Ni^{2+}, Cu^{2+}, Zn^{2+}, Ag^+, Cd^{2+}, Hg^{2+} and Fe^{2+} were chosen for studies. Cation binding studies of all compounds were carried out by UV-vis spectroscopy.

4.3.1 The complexation studies of L1 with cations by using UV-vis and fluorescent spectroscopies

Firstly, to evaluate the complexation ability of the receptor **L1** to cations, UV-vis spectroscopy experiments of the receptor **L1** were carried out in dry methanol solution using excess standard salt solution of 15 cations. The UV-vis spectra of **L1** in the presence and absence of cations are presented in Figure 4.1. The addition of Cu^{2+}, Ag^+ and Al^{3+} to **L1** solution made the hypochromic shift absorption spectra compared with absorption spectra of **L1**, which is ascribed to the formation of cationic complex.

Secondly, the fluorescence spectroscopy experiments of the receptor **L1** were carried out in dry MeOH solution using excess standard salt solution of 15 cations. The fluorescent spectra of **L1** in the presence and absence of cations are presented in Figure 4.2. The addition of Cu^{2+} and Cr^{3+} to **L1** solution made the hypochromic shift emission spectra compared with emission spectra of **L1** especially Al^{3+}, which is ascribed to the formation of cationic complex. The ion-dipole interaction between cation and the electron donor of receptor increases the electron density and decreases the size of cation. This increase in charge density results in the reduction of absorption. [120] The addition of other cations induces a slightly change because of the configuration of the receptor **L1** is not matching with cations. [121]

Figure 4.1 UV-vis spectrum changes of receptor **L1** upon addition of various cations.

Conditions: **L1** (1.0×10^{-5} M) and cation salts (50 equiv.) in dry MeOH.

Figure 4.2 Fluorescent spectrum changes of receptor **L1** upon addition of various cations.

Conditions: **L1** (1.0×10^{-5} M) and cation salts (50 equiv.) in dry MeOH.

4.3.2 The complexation studies of L2 with cations by using UV-vis and fluorescent spectroscopies

Firstly, to evaluate the complexation ability of the receptor **L2** to cations, the UV-vis spectroscopy experiments of the receptor **L2** were carried out in dry MeOH solution using excess standard salt solution of 15 cations. The UV-vis spectra of **L2** in the presence and absence of cations are presented in Figure 4.3. Upon the addition of Al^{3+} to **L2** solution made the hypochromic shift absorption spectra compared with absorption spectra of **L2** , which is ascribed to the formation of cationic complex with 2 hydroxyl groups. The ion-dipole interaction between cation and the electron donor of receptor increases the electron density and decreases the size of cation. This increase in charge density results in the reduction of absorption. [120] The addition of other cations induces a slightly decreased change except for Hg^{2+} because of the configuration of the receptor **L2** is not matching with cations. [121]

Secondly, to evaluate again the complexation ability of the receptor **L2** to cations, the fluorescence spectroscopy experiments of the receptor **L2** were carried out in dry methanol solution using excess standard salt solution of Na^+, K^+, Ca^{2+}, Pb^{2+}, Al^{3+}, Ge^{4+}, Cr^{3+}, Fe^{2+}, Co^{2+}, Ni^{2+}, Cu^{2+}, Zn^{2+}, Ag^+, Cd^{2+} and Hg^{2+}. The fluorescent spectra of **L2** in the presence and absence of cations are presented in Figure 4.4. Upon the addition of Ge^{4+}, Cr^{3+} and Al^{3+} to **L2** solution made the decrease emission spectra compared with emission spectra of **L2** especially Al^{3+}, which is ascribed to the formation of cationic complex. The ion-dipole interaction between cation and the electron donor of receptor increases the electron density and decreases the size of cation. This decrease in size of cation and increase in electron density of cation result in the reduction of fluorescence intensity. [120] The addition of other cations such as Na^+, K^+, Ca^{2+}, Pb^{2+}, Fe^{2+}, Co^{2+}, Ni^{2+}, Cu^{2+}, Zn^{2+}, Cd^{2+}, Ag^+ and Hg^{2+} induces a slightly changes because of the configuration of the receptor **L2** is not matching with cations. [121]

Figure 4.3 UV-vis spectrum changes of receptor **L2** upon addition of various cations. Conditions: **L2** (1.0×10^{-5} M) and cation salts (50 equiv.) in dry MeOH.
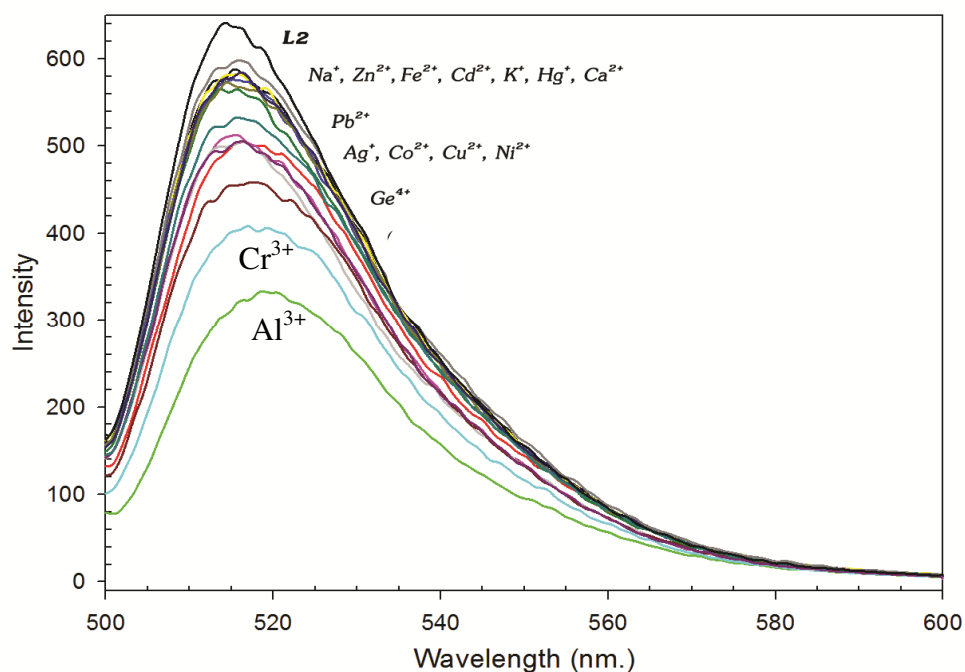
Figure 4.4 Fluorescent spectrum changes of receptor **L2** upon addition of various cations. Conditions: **L2** (1.0×10^{-5} M) and cation salts (50 equiv.) in dry MeOH.

4.3.3 The complexation studies of L3 with cations by using UV-vis and fluorescent spectroscopies

Firstly, to evaluate the complexation ability of the receptor **L3** to cations, the UV-vis spectroscopy experiments of the receptor **L3** were carried out in dry methanol solution using excess standard salt solution of Na^+, K^+, Ca^{2+}, Pb^{2+}, Al^{3+}, Ge^{4+}, Cr^{3+}, Fe^{2+}, Co^{2+}, Ni^{2+}, Cu^{2+}, Zn^{2+}, Ag^+, Cd^{2+} and Hg^{2+}. The UV-vis spectra of **L3** in the presence and absence of cations are presented in Figure 4.5. Upon the addition of Al^{3+} and Cu^{2+} to **L3** solution made the decrease absorption spectra compared with absorption spectra of **L3** , which is ascribed to the formation of cationic complex with 1 amide group. The ion-dipole interaction between cation and the electron donor of receptor increases the electron density and decreases the size of cation. This increase in charge density results in the reduction of absorption. [120] The addition of other cations such as Na^+, K^+, Ca^{2+}, Pb^{2+}, Ge^{4+}, Cr^{3+}, Fe^{2+}, Co^{2+}, Ni^{2+}, Zn^{2+}, Ag^+, Cd^{2+} and Hg^{2+} induces a slightly decreased change because of the configuration of the receptor **L3** is not matching with cations. [121] Conditions: **L3** (6.5×10^{-5} M) and cation salts (50 equiv.) in dry MeOH.

Secondly, to evaluate again the complexation ability of the receptor **L3** to cations, the fluorescence spectroscopy experiments of the receptor **L3** were carried out in dry methanol solution using excess standard salt solution of Na^+, K^+, Ca^{2+}, Pb^{2+}, Al^{3+}, Ge^{4+}, Cr^{3+}, Fe^{2+}, Co^{2+}, Ni^{2+}, Cu^{2+}, Zn^{2+}, Ag^+, Cd^{2+} and Hg^{2+}. The fluorescent spectra of **L3** in the presence and absence of cations are presented in Figure 4.6. The addition of all cations induces a slightly change because of the configuration of the receptor **L3** is not matching with cations, [121] but upon the addition of Cr^{3+} and Al^{3+} to **L3** solution made the decrease emission spectra compared with emission spectra of **L3.**
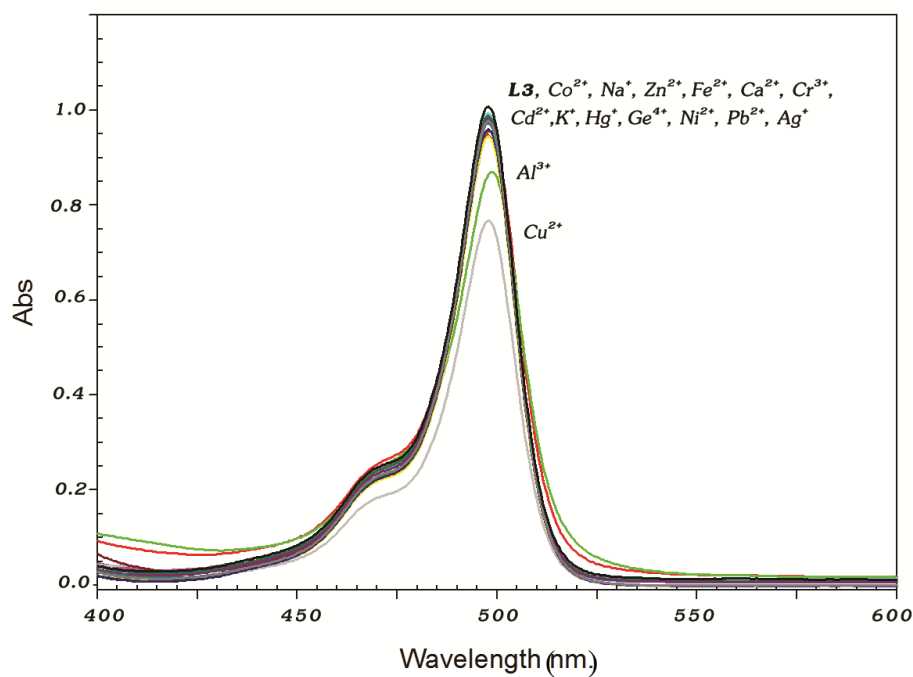
Figure 4.5 UV-vis spectrum changes of receptor **L3** upon addition of various cations.
Conditions: **L3** (6.5×10^{-5} M) and cation salts (50 equiv.) in dry MeOH.
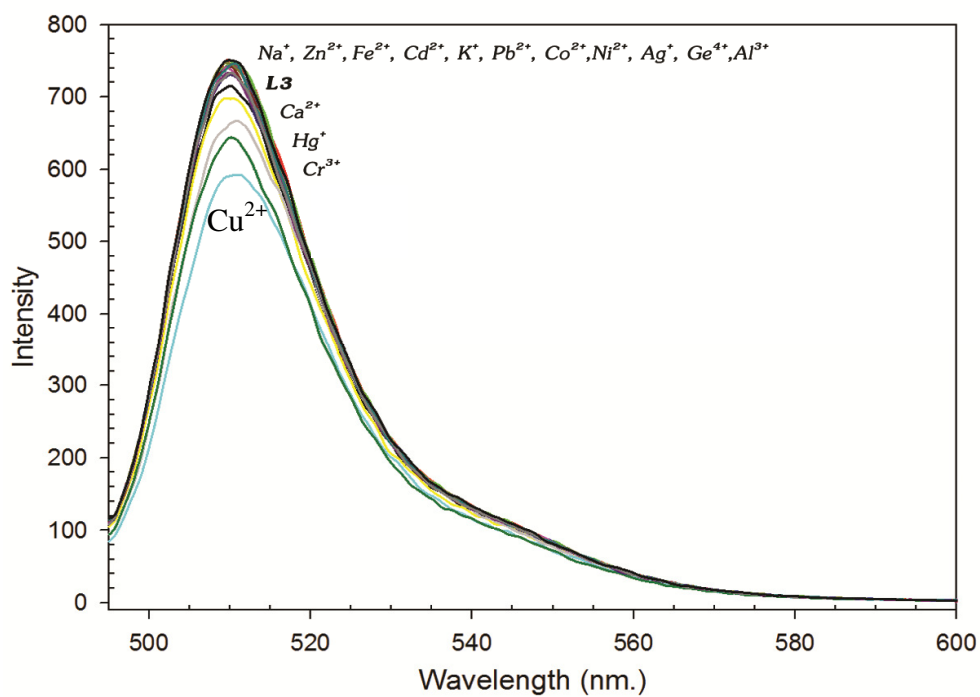
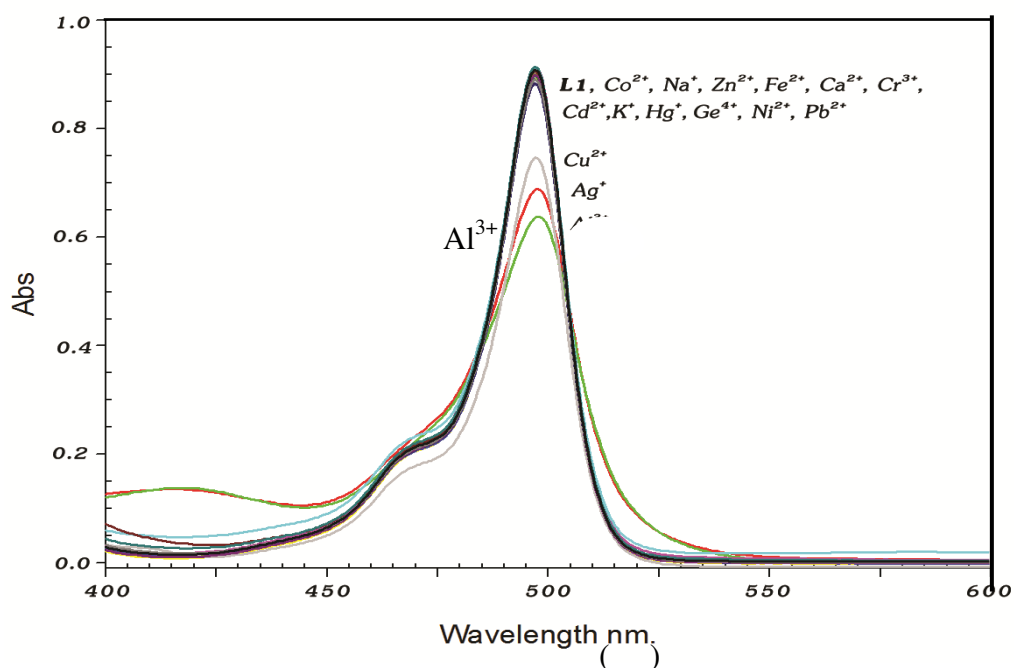**Figure 4.6** Fluorescent spectrum changes of receptor **L3** upon addition of various cations.
Conditions: **L3** (1.0×10^{-5} M) and cation salts (50 equiv.) in dry MeOH.

4.3.4 The complexation studies of L4 with cations by using UV-vis and fluorescent spectroscopies

Firstly, to evaluate the complexation ability of the receptor **L4** to cations, the UV-vis spectroscopy experiments of the receptor **L4** were carried out in dry methanol solution using excess standard salt solution of Na^+, K^+, Ca^{2+}, Pb^{2+}, Al^{3+}, Ge^{4+}, Cr^{3+}, Fe^{2+}, Co^{2+}, Ni^{2+}, Cu^{2+}, Zn^{2+}, Ag^+, Cd^{2+} and Hg^{2+}. The UV-vis spectra of **L4** in the presence and absence of cations are presented in Figure 4.7. Upon the addition of Cu^{2+} to **L4** solution made the decrease absorption spectra compared with absorption spectra of **L4**, which is ascribed to the formation of cationic complex with 2 amide groups. The ion-dipole interaction between cation and the electron donor in two amide groups of receptor strongly increases. This increase in ion-dipole interaction results in the reduction of absorption. [120] The addition of other cations such as Na^+, K^+, Ca^{2+}, Pb^{2+}, Al^{3+}, Ge^{4+}, Cr^{3+}, Fe^{2+}, Co^{2+}, Ni^{2+}, Zn^{2+}, Ag^+, Cd^{2+} and Hg^{2+} induces a slightly decreased change because of the configuration of the receptor **L4** is not matching with cations. [121]

Secondly, to evaluate again the complexation ability of the receptor **L4** to cations, the fluorescence spectroscopy experiments of the receptor **L4** were carried out in dry methanol solution using excess standard salt solution of Na^+, K^+, Ca^{2+}, Pb^{2+}, Al^{3+}, Ge^{4+}, Cr^{3+}, Fe^{2+}, Co^{2+}, Ni^{2+}, Cu^{2+}, Zn^{2+}, Ag^+, Cd^{2+} and Hg^{2+}. The fluorescent spectra of **L4** in the presence and absence of cations are presented in Figure 4.8. Upon the addition of Cu^{2+} of and to **L4** solution made the decrease emission spectra compared with emission spectra of **L4** , which is ascribed to the formation of cationic complex. The ion-dipole interaction between cation and the electron donor in two amide groups of receptor increases the interaction which results in the reduction of fluorescent intensity. [120] The addition of other cations such as Na^+, K^+, Ca^{2+}, Pb^{2+}, Al^{3+}, Ge^{4+}, Cr^{3+}, Fe^{2+}, Co^{2+}, Ni^{2+}, Zn^{2+}, Cd^{2+}, Ag^+ and Hg^{2+} induces a slightly changes because of the configuration of the receptor **L4** is not matching with cations. [120]
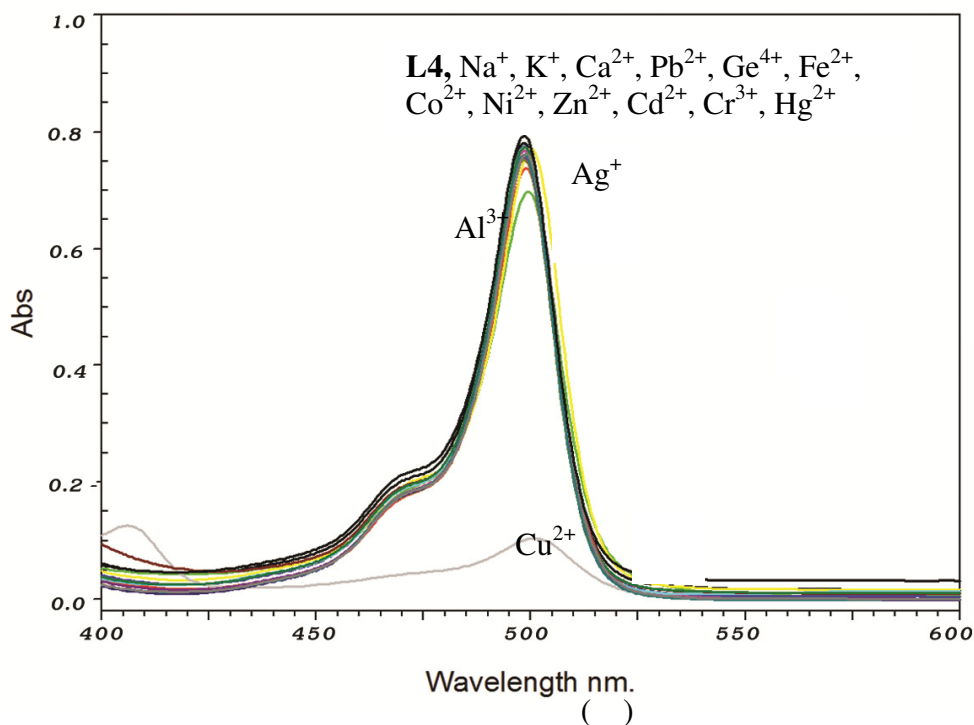
Figure 4.7 UV-vis spectrum changes of receptor **L4** upon addition of various cations.

Conditions: **L4** (1.0×10^{-5} M) and cation salts (50 equiv.) in dry MeOH.
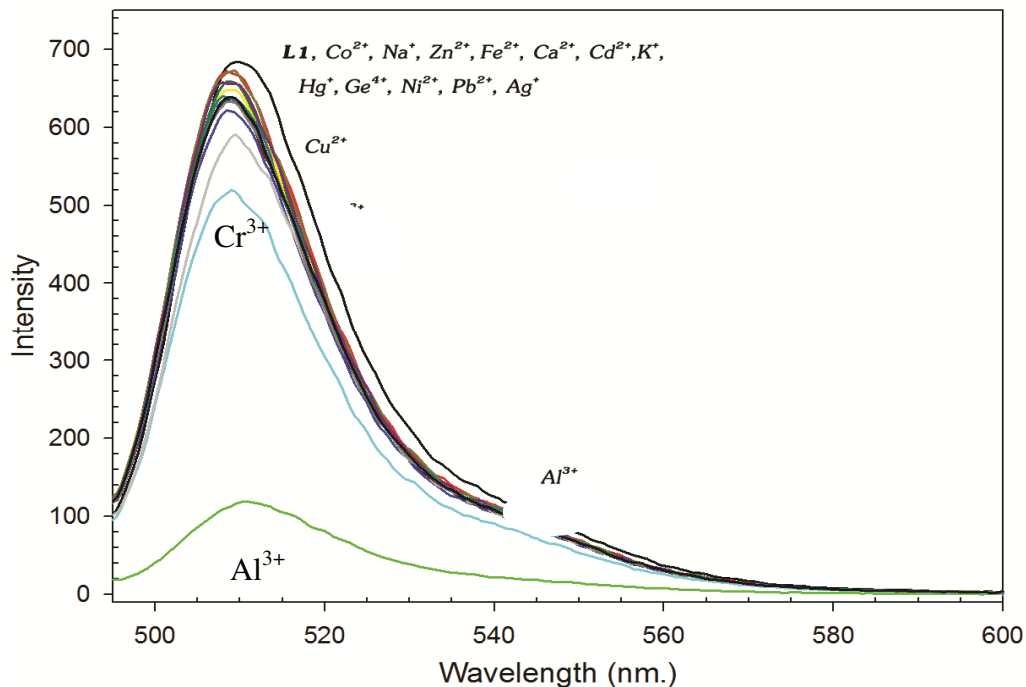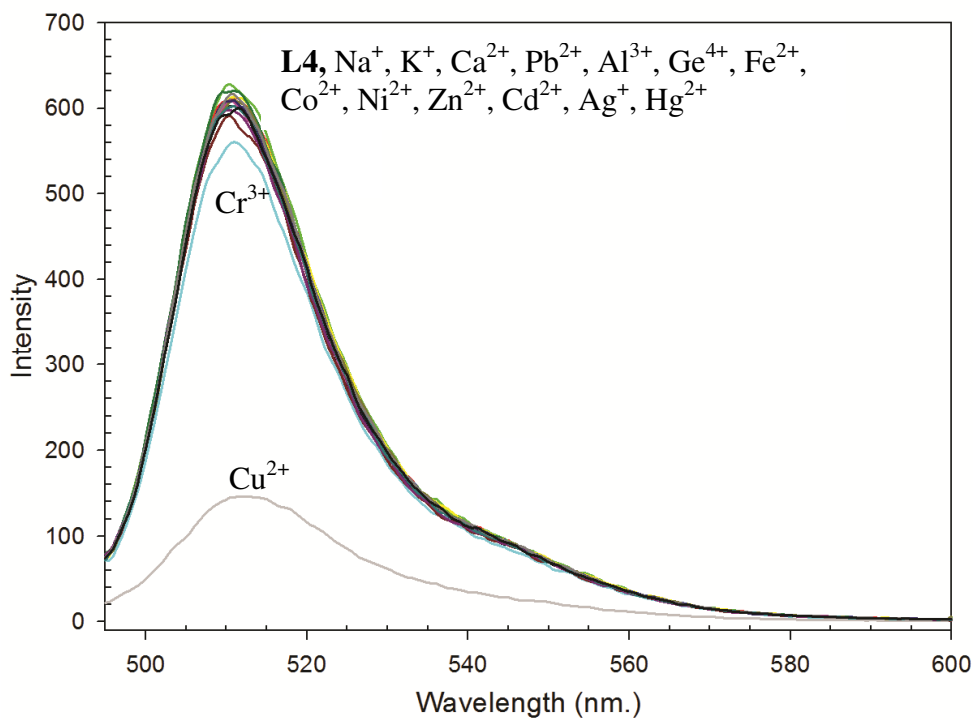

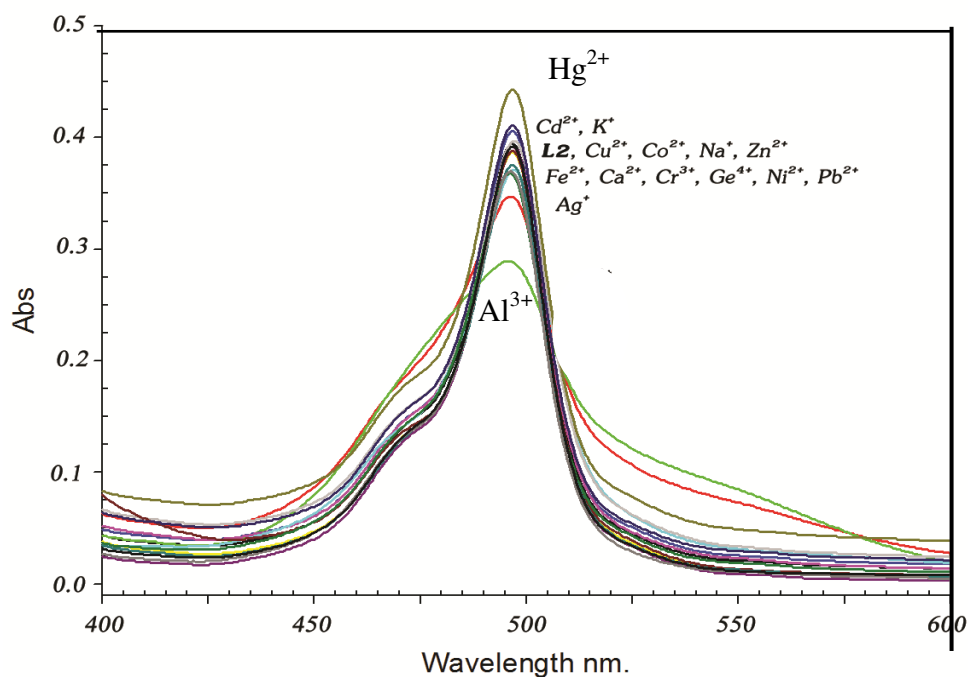**Figure 4.8** Fluorescent spectrum changes of receptor **L4** upon addition of various cations.

Conditions: **L4** (6.5×10^{-5} M) and Cation salts (50 equiv.) in dry MeOH.

From the spectra of **L1, L2, L3** and **L4** with various cations in Figure 4.1 – 4.8, the results are concluded in Table 4.1. The cations (Na^+, Ag^+, Al^{3+} and Cu^{2+} ions) were chosen to investigate their geometries and electronic structure of receptors and their complexes by computational studies using the DFT method. The reason of the high selectivity of Al^{3+} and Cu^{2+} is related to the configuration of the receptors matching with the cations, whereas Ag^+ induces a slightly interaction and Na^+ is not related to the configuration of the receptors. This is also confirmed by the geometry optimized structure according to the DFT using the B3LYP/LanL2DZ level.

Table 4.1 Conclusion of interaction between receptors **L1, L2, L3** and **L4** with cations

Condition	UV-vis spectroscopy				Fluorescence spectroscopy			
	L1	**L2**	**L3**	**L4**	**L1**	**L2**	**L3**	**L4**
High selectivity	Al^{3+} Ag^+ Cu^{2+}	Al^{3+}	Cu^{2+}	Cu^{2+}	Al^{3+}	Al^{3+}, Cr^{3+} Ge^{4+}	Cu^{2+}	Cu^{2+}
Medium selectivity	non	Ag^+ Hg^{2+}	Al^{3+}	Ag^+	Cr^{3+} Cu^{2+}	Ag^+, Co^{2+} Cu^{2+}, Ni^{2+} Pb^{2+}	Cr^{3+} Hg^{2+}	Cr^{3+}
Low selectivity	Na^+ K^+, Ca^{2+} Pb^{2+} Ge^{4+} Cr^{3+} Fe^{2+} Co^{2+} Ni^{2+} Zn^{2+} Cd^{2+} Hg^{2+}	Na^+ K^+ Ca^{2+} Pb^{2+} Ge^{4+} Cr^{3+} Fe^{2+} Co^{2+} Ni^{2+} Cu^{2+} Zn^{2+} Cd^{2+}	Na^+ K^+ Ca^{2+} Pb^{2+} Ge^{4+} Cr^{3+} Fe^{2+} Co^{2+} Ni^{2+} Zn^{2+} Ag^+ Cd^{2+} Hg^{2+}	Na^+ K^+ Ca^{2+} Pb^{2+} Ge^{4+} Cr^{3+} Fe^{2+} Co^{2+} Ni^{2+} Cu^{2+} Zn^{2+} Cd^{2+} Hg^{2+}	Na^+ K^+ Ca^{2+} Pb^{2+} Ge^{4+} Fe^{2+} Co^{2+} Ni^{2+} Zn^{2+} Ag^+ Cd^{2+} Hg^{2+}	Na^+ K^+, Ca^{2+} Fe^{2+} Zn^{2+}, Cd^{2+} Hg^{2+}	Na^+ K^+ Ca^{2+} Pb^{2+} Al^{3+} Ge^{4+} Fe^{2+} Co^{2+} Ni^{2+} Zn^{2+} Ag^+ Cd^{2+}	Na^+ K^+ Ca^{2+} Pb^{2+} Al^{3+} Ge^{4+} Fe^{2+} Co^{2+} Ni^{2+} Zn^{2+} Ag^+ Cd^{2+} Hg^{2+}

4.4 Computational Study

To investigate their geometry and electronic structure of complexes, computational studies were performed on receptors and their complexes, which divided into two parts. In the first part, the complexation properties including geometrical structures, complexation energies and electronic properties of BODIPY-based chemosensors **L1**, **L2**, **L3**, **L4** which had oxygen atoms as donor atoms and their complexes with cations, i.e., Na^+, Ag^+, Al^{3+} and Cu^{2+} ions have been studied using the DFT method.

In the second part, geometrical structures, complexation energies and electronic properties of BODIPY-based chemosensors **L5**, **L6**, **L7**, **L8** which had sulphur atoms as donor atoms and their complexes with cations, i.e., Na^+, Ag^+, Al^{3+} and Cu^{2+} ions were also studied using the DFT method.

4.4.1 Computational study of BODIPY-based chemosensors L1, L2, L3, L4 which had oxygen atoms as donor atoms and their complexes with cations

The aim of this topic is to predict the molecular properties of BODIPY-based chemosensors containing hydroxyl moieties or amide moieties as cation binding sites receptors. Different amount and different functional group of binding sites which are directly linked to BODIPY were designed to have various distances for different cations including; 8-(4-hydroxyphenyl)-1,3,5,7-tetramethyl-BODIPY, (**L1**), 8-(3,4-dihydroxyphenyl)- 1,3,5,7-tetramethyl-BODIPY, (**L2**), 8-(4-(2-(diethylamino)-2-oxoethoxy)phenyl)- 1,3,5,7-tetramethyl-BODIPY, (**L3**) and 8-(3,4-bis(2-(diethyl amino)-2-oxoethoxy)phenyl)- 1,3,5,7-tetramethyl- BODIPY, (**L4**) .

The DFT has been employed to optimize the structures of the receptors **L1**, **L4** and their complexes with cations Na^+, Ag^+, Al^{3+} and Cu^{2+} ions. The LanL2DZ basis set was used for all complexation studies. A 1 : 1 association of the receptor and cation which was plausible in dilute solutions was selected as model studied. The single-point energy was obtained at the same level used for the geometry optimizations which also provided zero point vibrational energy (ZPVE) correction to the energy (ΔE_{ZPE}), standard enthalpy (ΔH) and Gibbs free energy changes (ΔG) of the reactions.

The chemical and optimized structures of the receptors **L1**, **L2**, **L3** and **L4** are shown in Figure 4.9. The DFT optimized structures of cations complexed with the receptors **L1**, **L2**, **L3** and **L4**, their selected geometrical parameters and Gibbs free energy changes (Δ*G*) are shown in Figures 4.10, 4.11, 4.12 and 4.13, respectively.

2D **3D**
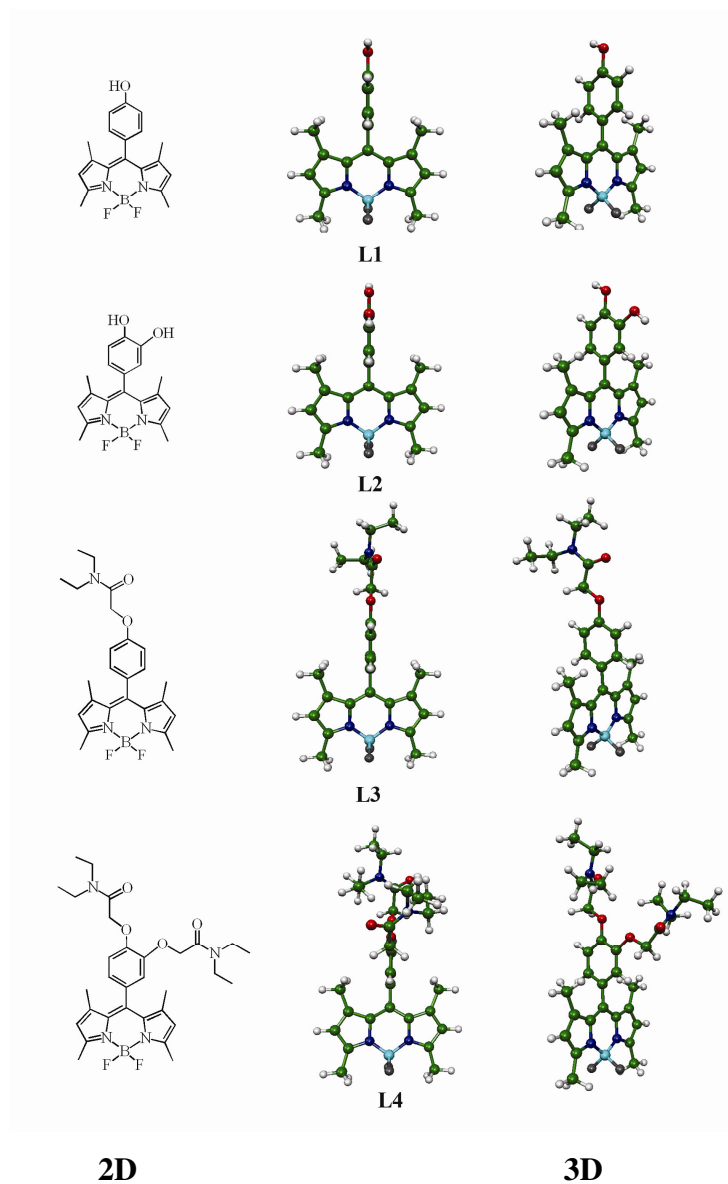
Figure 4.9 The chemical and optimized structures of the receptors **L1, L2, L3** and **L4**.
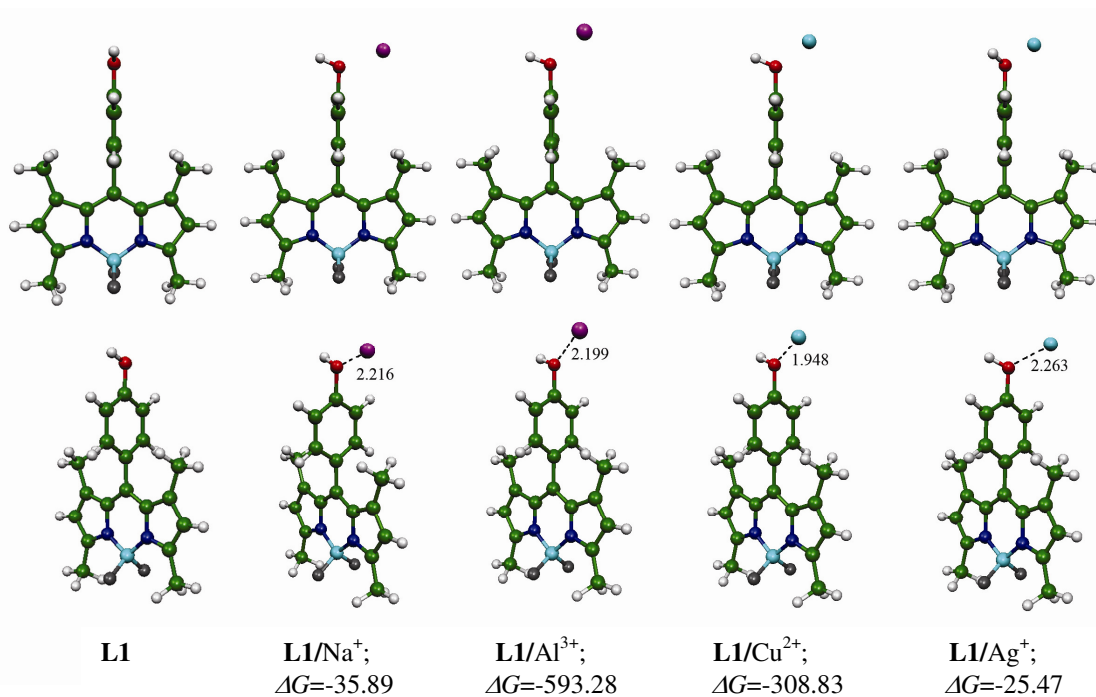
Figure 4.10 The optimized structures of the receptor **L1** and its complexes with cations, the binding free energies are in kcal/mol and the bond distances are in Å.
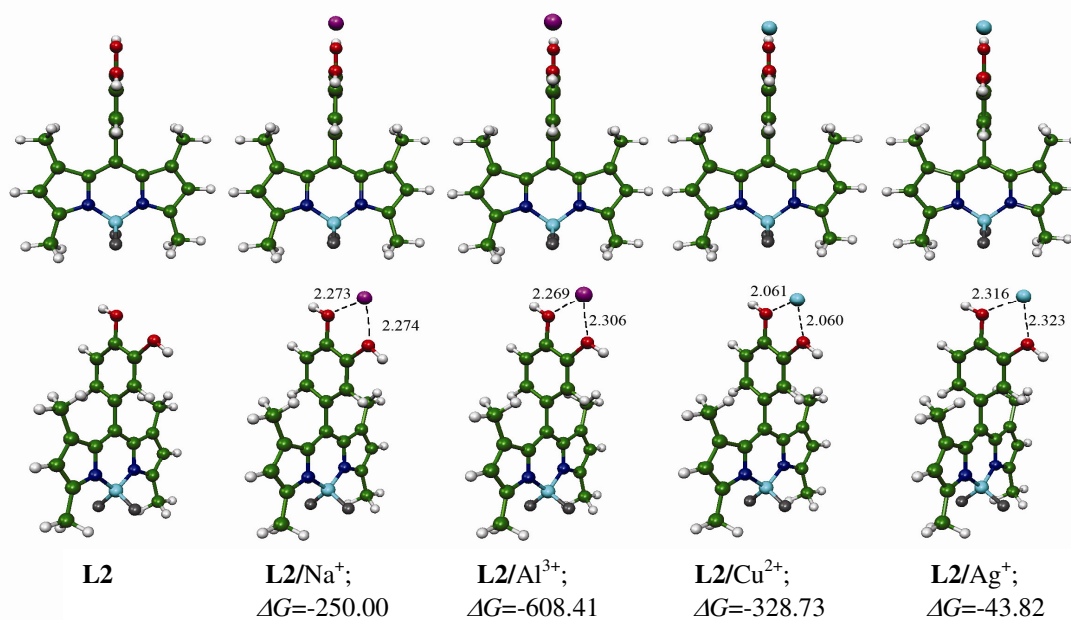
Figure 4.11 The optimized structures of the receptor **L2** and its complexes with cations, the binding free energies are in kcal/mol and the bond distances are in Å.
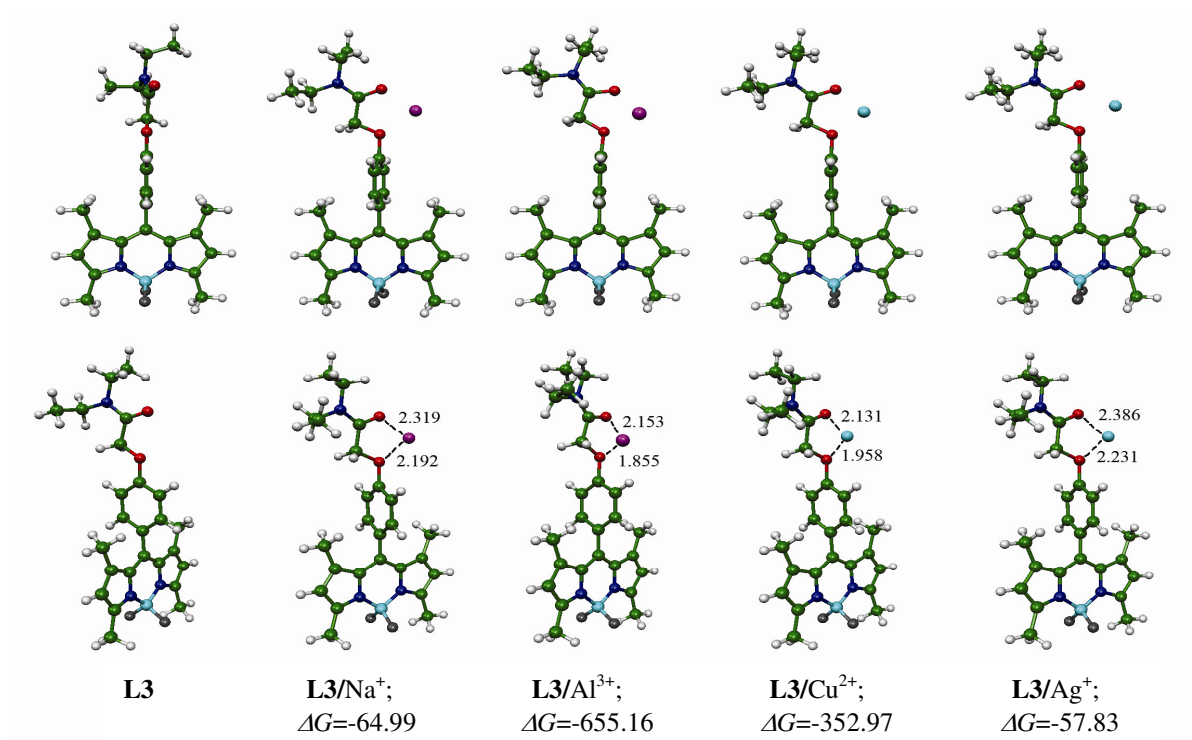
Figure 4.12 The optimized structures of the receptor **L3** and its complexes with cations, the binding free energies are in kcal/mol and the bond distances are in Å.
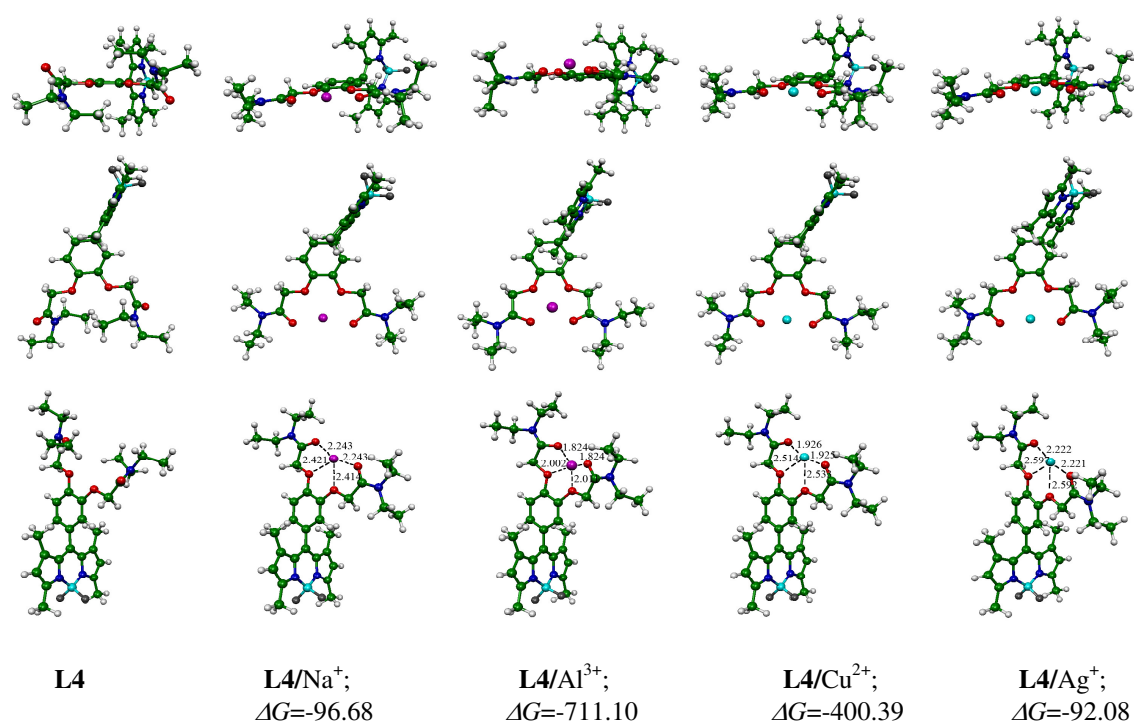
Figure 4.13 The optimized structures of the receptor **L4** and its complexes with cations, the binding free energies are in kcal/mol and the bond distances are in Å.

The results confirm that the receptors **L1**, **L2**, **L3** and **L4** form stable complexes with Al^{3+} ion through a large number of ion-dipole interactions. The cationic guests are found to locate on the receptors. For the complexes between the receptors **L2** and **L3** and cations occur via two bonds, whereas the complexes of receptors **L1** and **L4** and cations occur via one bond and four bonds, respectively.

The binding energy, enthalpy and Gibbs free energy changes of complexation between receptors **L1, L2, L3, L4** and various cations computed using the DFT method are presented in Tables 4.2 and 4.3. The plot of Gibbs free energy changes and charge transfers between receptor and cation of complexes are displayed in Figures 4.14 and 4.15, respectively. When considering the binding energy, enthalpy and Gibbs free energy changes of all complexations, the negative values of changes indicate that the complexations are thermodynamically favorable. For aluminium cations, the results show that aluminium complexes with receptors **L1, L2, L3** and **L4** are the most stable complexes because the Gibbs free energy changes are the most negative values (ΔG of **L1**/Al^{3+} = -593.28, **L2**/Al^{3+}= -608.41, **L3**/Al^{3+} = -655.16 and **L4**/Al^{3+} =-711.10 kcal/mol). Whereas copper ion complexes with receptors **L1, L2, L3** and **L4** are the less stable complexes because the Gibbs free energy changes are the more negative values of changes (ΔG of **L1**/Cu^{2+} = -308.83, **L2**/Cu^{2+} = -328.73, **L3**/Cu^{2+} = -352.97 and **L4**/Cu^{2+} = -352.97 kcal/mol). As found in the previous reports, the higher charge transfers between cation and receptor are the stronger binding interaction then the Al complexes, the highest in charge transfers, are the most stable complexes, except for **L3**. Whereas the copper complexes, the higher in charge transfers, are the more stable complexes, except for **L3**. It should be noted here that the results correspond to the experiment.

The HOMO (E_{HOMO}), LUMO (E_{LUMO}), the frontier molecular orbital energy gap (E_{gap}), chemical hardness (η), electronic chemical potential (μ) and Mulliken electronegativity (χ) of receptors, **L1**, **L2**, **L3** and **L4** and their cation complexes are tabulated in Table 4.4. For all free receptors the energy level HOMO goes from -0.240 eV for receptor **L3** to -0.210 eV for receptor **L1**. For the LUMO level of all free receptors in which the energy is decreasing from -0.100 eV for receptor **L1** to -0.208 eV for receptor **L3**. The energy gaps of all cation complexes are different and range between 0.012-0.104, 0.015-0.125, 0.012-0.107 and 0.012-0.107 eV for receptors **L1**, **L2**, **L3** and **L4**, respectively. The energy gaps of complexes are not much different from their

corresponding free receptors except for the Al complexes and Ag complexes with receptors **L1** and **L2** and the copper complexes with receptors **L3** and **L4** .

Table 4.2 The binding energy (ΔE), enthalpy (ΔH) and Gibbs free energy (ΔG) changes of complexations between receptors **L1**, **L2** and cations

Cations	ΔE^{a}		ΔH^{a}		ΔG^{a}	
	L1	L2	L1	L2	L1	L2
Na^+	-23.65	-253.63	-23.77	-268.63	-35.89	-250.00
Al^{3+}	-580.46	-596.90	-580.27	-597.04	-593.28	-608.41
Cu^{2+}	-315.55	-336.67	-315.64	-337.05	-308.83	-328.73
Ag^+	-32.06	-51.41	-32.03	-51.67	-25.47	-43.82

[a] In kcal/mol.

Table 4.3 The binding energy (ΔE), enthalpy (ΔH) and Gibbs free energy (ΔG) changes of complexations between receptors **L3**, **L4** and cations

Cations	ΔE^{a}		ΔH^{a}		ΔG^{a}	
	L3	L4	L3	L4	L3	L4
Na^+	-54.50	-86.94	-54.89	-87.47	-64.99	-96.68
Al^{3+}	-644.84	-703.04	-645.20	-704.71	-655.16	-711.10
Cu^{2+}	-361.13	-408.22	-361.38	-408.46	-352.97	-400.39
Ag^+	-66.18	-101.03	-66.44	-101.34	-57.83	-92.08

[a] In kcal/mol.

The charge-transfer nature of the electronic transitions of receptors and its cation is better illustrated by the drawings of molecular orbitals. The frontier orbital shapes of the receptors **L1**, **L2**, **L3**, **L4** and their complexes with cations presented over isosurface value of 0.05 au are displayed in Figures 4.16, 4.17, 4.18 and 4.19, respectively.
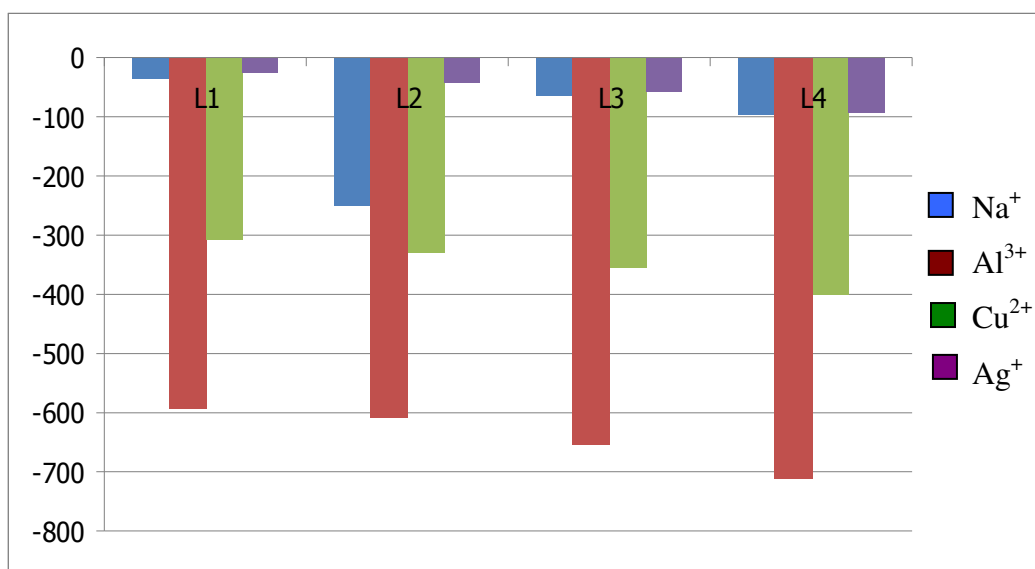
Figure 4.14 Gibbs free energy changes in kcal/mol of the receptor **L1, L2, L3** and **L4** complexes with cations.
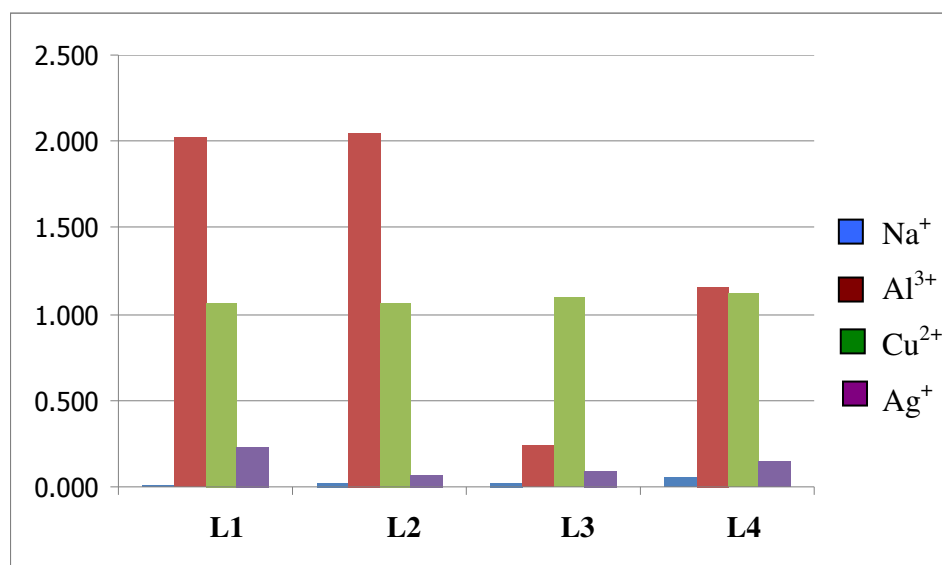
Figure 4.15 The charge transfers in e⁻ between the receptors **L1, L2, L3** and **L4** complexes with cations.

The HOMO density and the LUMO density of all free receptors are located at the same position which is at the pyrrole unit. As consideration of the most stable complexes of Al^{3+} (**L2**/Al^{3+}**, L3**/Al^{3+}**, L4**/Al^{3+}**)**, each of LUMO of complexes is located at the oxygen of hydroxyl groups, except for **L1**/Al^{3+}. Each of HOMO densities of complexes is somewhat analogous to densities of free receptors except for **L1**/Al^{3+}.

Table 4.4 The computed orbital energies and frontier molecular orbital energy gap of the receptors **L1, L2, L3, L4** and their complexes with anions

Receptor/cation	E_{LUMO}[a]	E_{HOMO}[a]	E_{gap}[a]	η[b]	μ[c]	χ[d]
L1	-0.100	-0.210	0.110	0.055	-0.155	0.155
L1/Na$^+$	-0.179	-0.283	0.104	0.052	-0.231	0.231
L1/Al^{3+-}	-0.550	-0.604	0.054	0.027	-0.577	0.577
L1/Cu^{2+}	-0.362	-0.454	0.092	0.046	-0.408	0.408
L1/Ag$^+$	-0.284	-0.296	0.012	0.006	-0.290	0.290
L2	-0.102	-0.211	0.109	0.055	-0.157	0.157
L2/Na$^+$	-0.178	-0.284	0.106	0.053	-0.231	0.231
L2/Al^{3+}	-0.554	-0.569	0.015	0.007	-0.562	0.562
L2/Cu^{2+}	-0.333	-0.459	0.126	0.063	-0.396	0.396
L2/Ag$^+$	-0.272	-0.287	0.015	0.007	-0.280	0.280
L3	-0.208	-0.240	0.110	0.055	-0.153	0.153
L3/Na$^+$	-0.169	-0.276	0.034	0.017	-0.259	0.259
L3/Al^{3+-}	-0.516	-0.528	0.107	0.054	-0.223	0.223
L3/Cu^{2+}	-0.318	-0.444	0.012	0.006	-0.522	0.522
L3/Ag$^+$	-0.242	-0.276	0.126	0.063	-0.381	0.381
L4	-0.103	-0.213	0.110	0.055	-0.158	0.158
L4/Na$^+$	-0.169	-0.276	0.107	0.054	-0.222	0.222
L4/Al^{3+-}	-0.440	-0.452	0.107	0.054	-0.223	0.223
L4/Cu^{2+}	-0.308	-0.392	0.012	0.006	-0.446	0.446
L4/Ag$^+$	-0.168	-0.275	0.084	0.042	-0.350	0.350

[a] In eV.

[b] Chemical hardness, $\eta = E_{gap}/2$.

[c] Electronic chemical potential, $\mu = (E_{HOMO}+E_{LUMO})/2$.

[d] The Mulliken electronegativity, $\chi = -(E_{HOMO}+E_{LUMO})/2$.
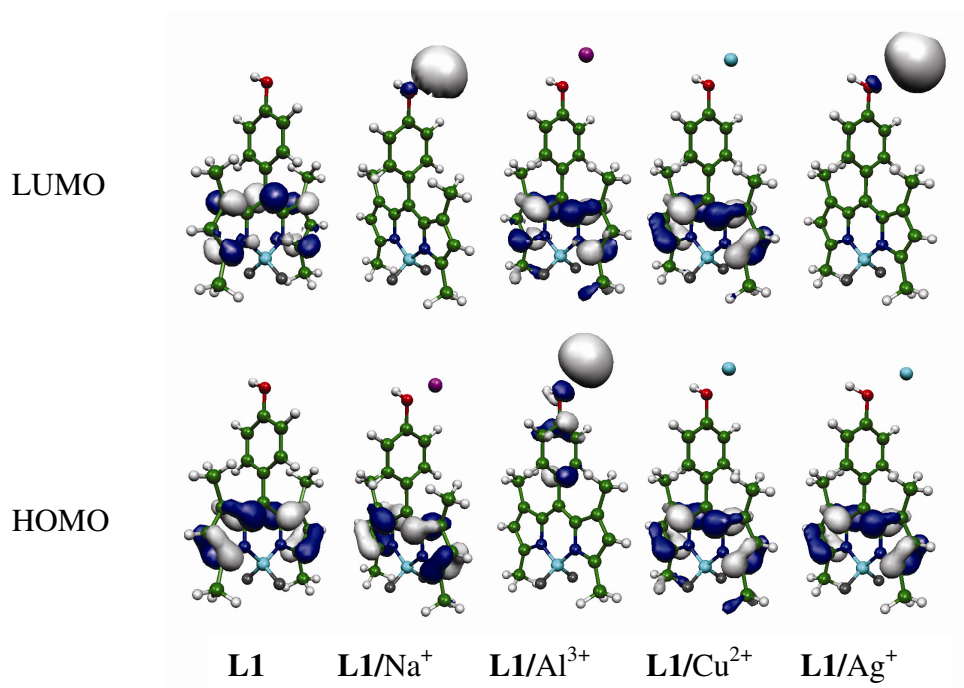
Figure 4.16 Plots of the LUMO (Top) and HOMO (Bottom) orbitals of the free forms of
receptor **L1** and its complexes with cationic guests at iso-surface value of
0.05 au.
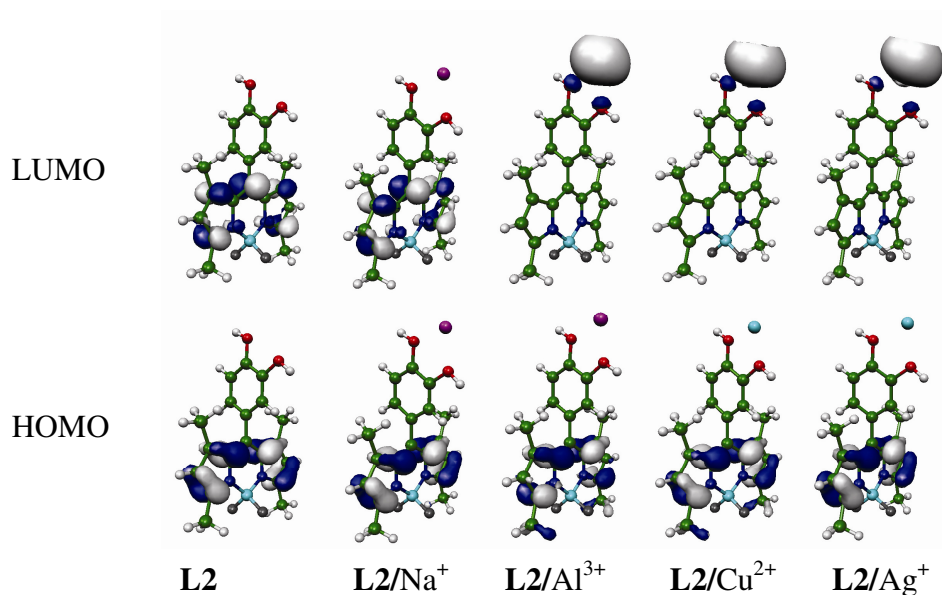
Figure 4.17 Plots of the LUMO (Top) and HOMO (Bottom) orbitals of the free forms of
receptor **L2** and its complexes with cationic guests at iso-surface value of
0.05 au.

Mahasarakham University
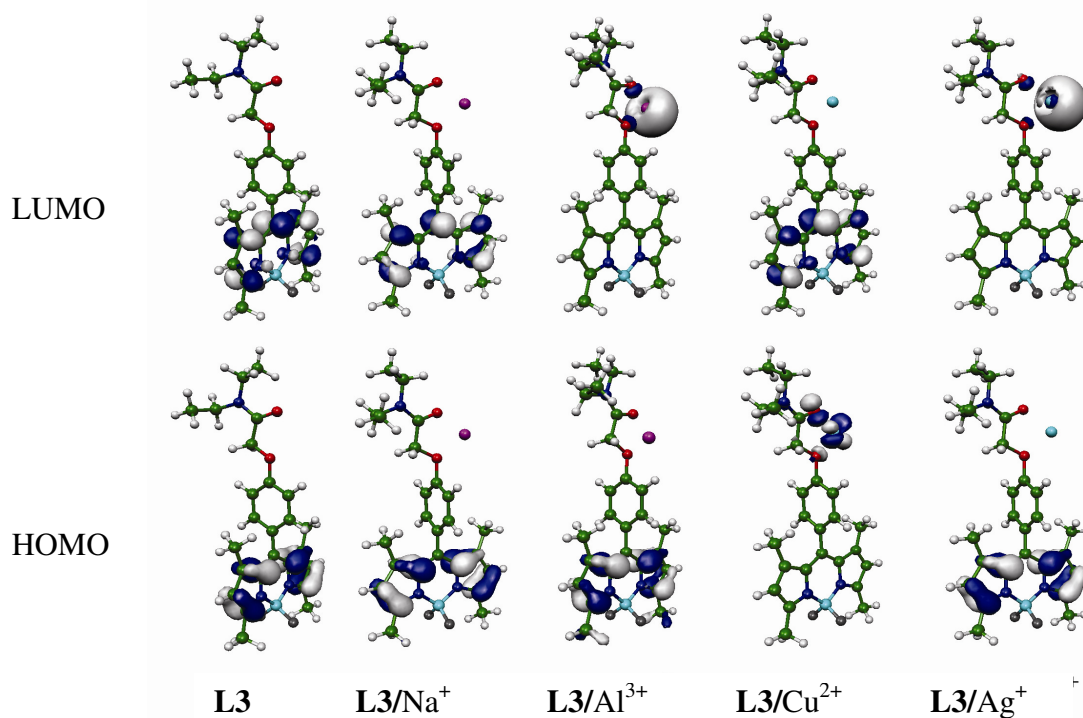
Figure 4.18 Plots of the LUMO (Top) and HOMO (Bottom) orbitals of the free forms of
receptor **L3** and its complexes with cationic guests at iso-surface value of
0.05 au.
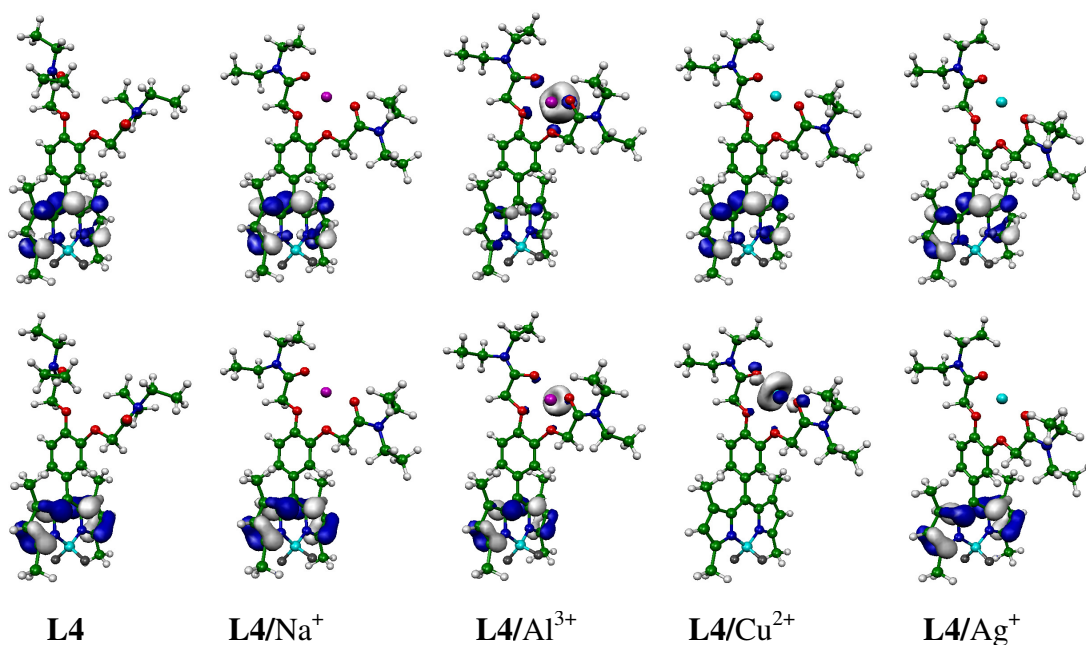
Figure 4.19 Plots of the LUMO (Top) and HOMO (Bottom) orbitals of the free forms of
receptor **L4** and its complexes with cationic guests at iso-surface value of
0.05 au.

4.4.2 Computational study of BODIPY-based chemosensors L5, L6, L7, L8 which had sulphur atoms as donor atoms and their complexes with cations

The recognition of cations by BODIPY-based thiohydroxyl receptors and thioamide receptors has been investigated by the DFT method and show that Al^{3+} is the most selective ion for forming complexes with all receptors. In this part, different amount and different functional group of binding sites which are directly linked to BODIPY were designed to have various distances for different cations including; 8-(4-thiohydroxyphenyl)-1,3,5,7-tetramethyl- BODIPY, (**L5**), 8-(3,4-dithiohydroxyphenyl)-1,3,5,7-tetramethyl- BODIPY, (**L6**), 8-(4-(2-(diethylthioamino)-2-oxoethoxy)phenyl)-1,3,5,7-tetramethyl-BODIPY, (**L7**), and 8-(3,4-bis(2-(diethylthioamino)- 1,3,5,7-tetra methyl- BODIPY, (**L8**). The theoretical studies to gain clearer information i.e., geometrical structure, binding energy, molecular orbital and charge transfer, on the origin of molecular recognition affinity have never been considered. Then the density functional theory has been employed to optimize the structures of receptors **L5**, **L6**, **L7**, **L8** and their complexes with cations i.e., Na^+, Ag^+, Al^{3+} and Cu^{2+} ions. A 1:1 association of the receptor and cation which is plausible in dilute solutions has been selected as model studied. The LanL2DZ basis set was used for all complexation studies. Geometrical structures of the receptors and their cation complexes have been computed by full geometrical optimization without any constrains. Figure 4.14 displays the chemical and the DFT optimized geometries of receptors **L5**, **L6**, **L7** and **L8**. The chemical and optimized structures of the receptors **L5**, **L6**, **L7** and **L8** are shown in

Figure 4.20. The DFT optimized structures of cations complexed with the receptors **L5**, **L6**, **L7** and **L8**, their selected geometrical parameters and ΔG are shown in Figures 4.22, 4.23, 4.24 and 4.25, respectively. The results confirm that the receptors **L5**, **L6**, **L7** and **L8** form stable complexes with Al^{3+} ion through a large number of ion/dipole interactions.
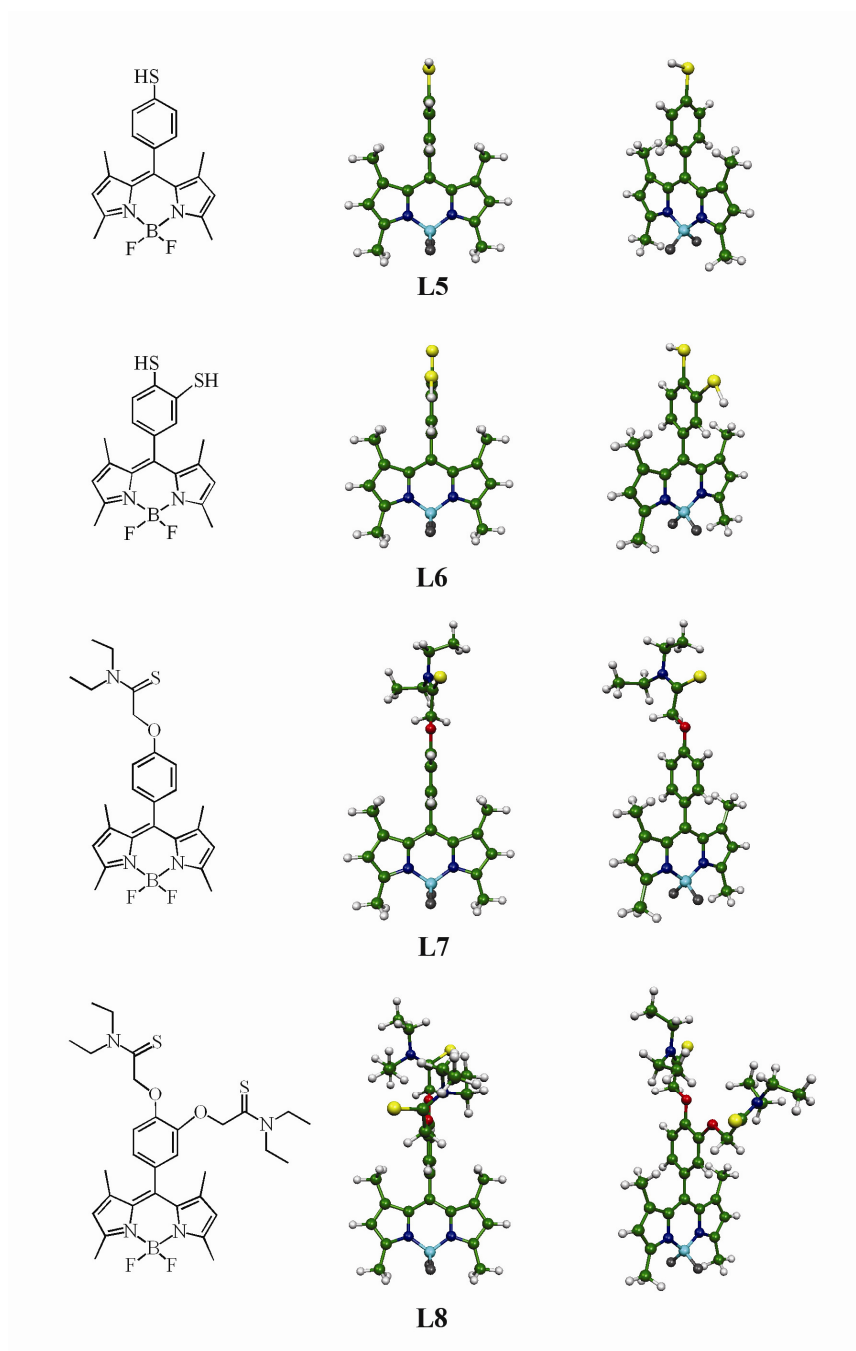
Figure 4.20 The chemical and optimized structures of the receptors **L5, L6, L7** and **L8**.

The cationic guests are found to locate on the receptors. For the complexes between the receptors **L6** and **L7** and cations occur via two bonds, whereas the complexes of receptors **L5** and **L8** and cations occur via one bond and four bonds, respectively. Except for **L5**/Al^{3+} and **L8**/Cu^{2+}, geometrical optimizations were not convergent .
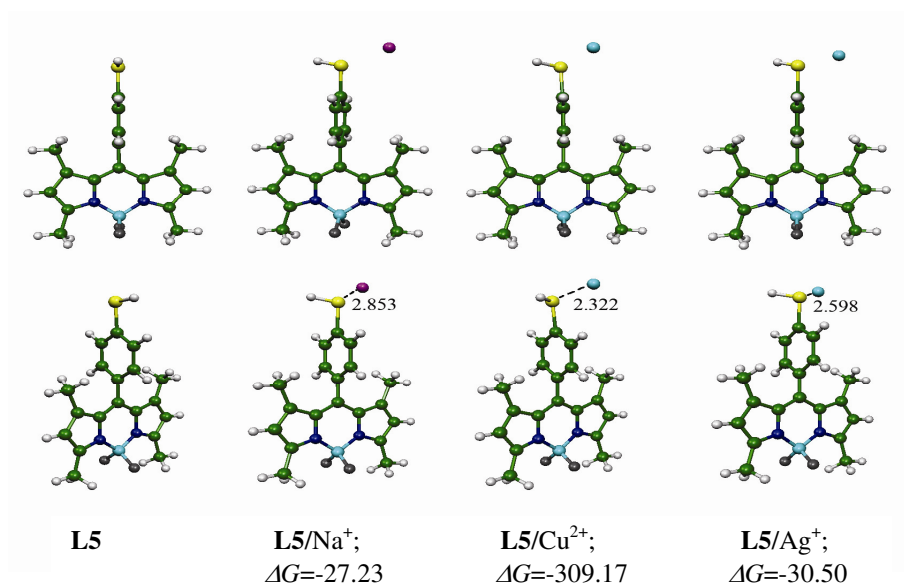
Figure 4.21 The optimized structures of the receptor **L5** and its complexes with cations, the binding free energies are in kcal/mol and the bond distances are in Å.
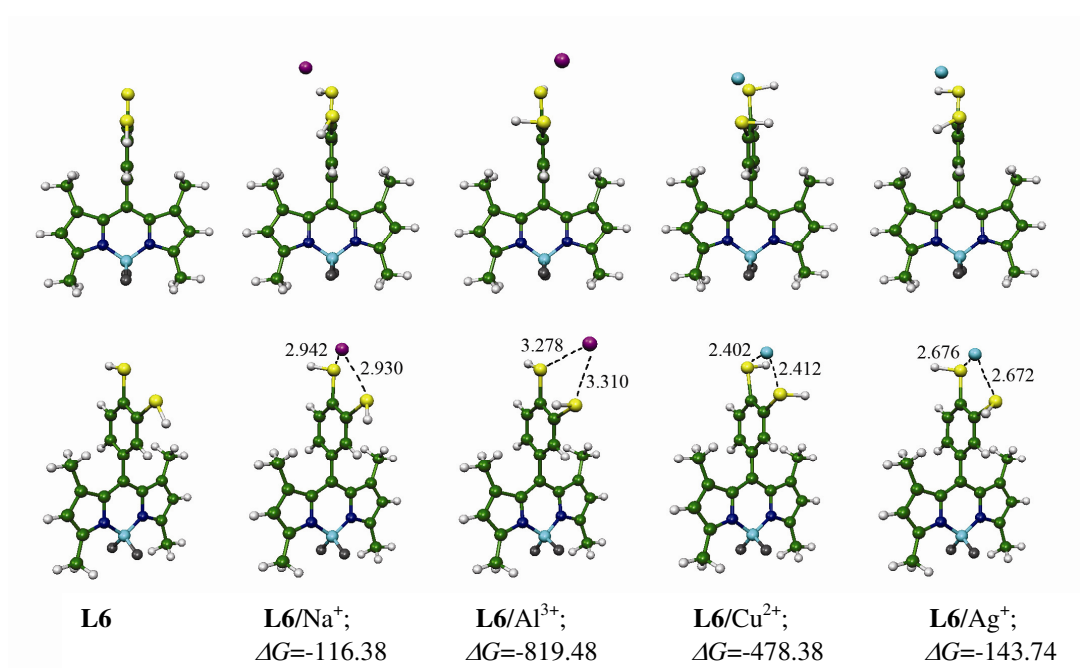
Figure 4.22 The optimized structures of the receptor **L6** and its complexes with cations, the binding free energies are in kcal/mol and the bond distances are in Å.
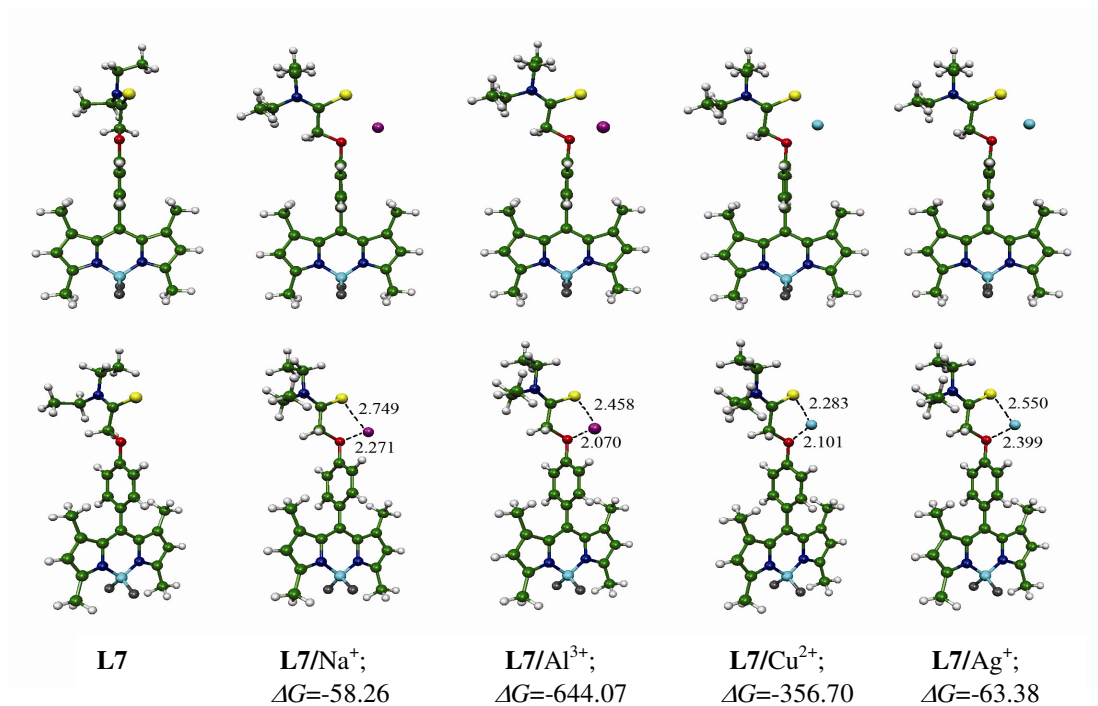
Figure 4.23 The optimized structures of the receptor **L7** complexes with cations, the binding free energies are in kcal/mol and the bond distances are in Å.
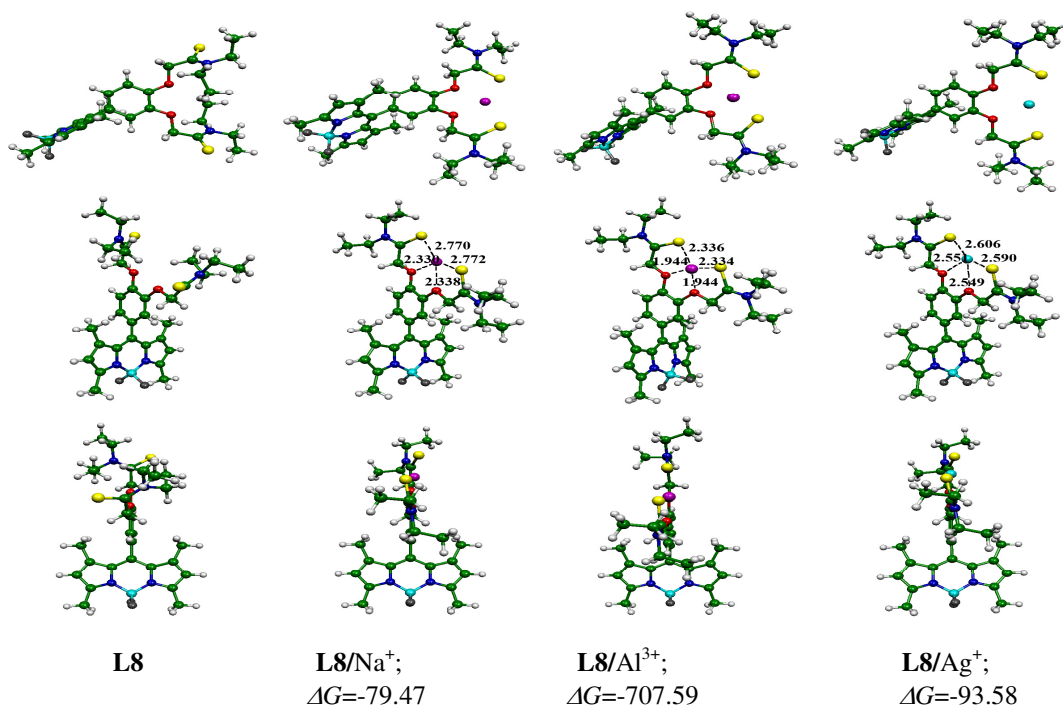
Figure 4.24 The optimized structures of the receptor **L8** and its complexes with cations, the binding free energies are in kcal/mol and the bond distances are in Å.

The binding energy, enthalpy and Gibbs free energy changes of complexation between receptors **L5**, **L6**, **L7, L8** and various cations computed using the DFT method are presented in Tables 4.5 and 4.6.

Table 4.5 The binding energy (ΔE), enthalpy (ΔH) and Gibbs free energy (ΔG) changes of complexations between receptors **L5**, **L6** and cations

Cations	ΔE^{a}		ΔH^{a}		ΔG^{a}	
	L5	**L6**	**L5**	**L6**	**L5**	**L6**
Na^+	-15.13	-23.10	-15.25	-22.89	-27.23	-34.78
Al^{3+}	-[b]	-580.64	-[b]	-580.08	-[b]	-593.47
Cu^{2+}	-316.20	-330.01	-316.46	-330.12	-309.17	-322.58
Ag^+	-37.25	-47.65	-37.43	-47.62	-30.50	-40.65

[a] In kcal/mol.   [b] Unconvergence complexes.

Table 4.6 The binding energy (ΔE), enthalpy (ΔH) and Gibbs free energy (ΔG) changes of complexations between receptors **L7**, **L8** and cations

Cations	ΔE^{a}		ΔH^{a}		ΔG^{a}	
	L7	**L8**	**L7**	**L8**	**L7**	**L8**
Na^+	-47.78	-68.66	-48.09	-69.08	-58.26	-79.47
Al^{3+}	-633.53	-697.63	-633.72	-698.46	-644.07	-707.59
Cu^{2+}	-365.18	-[b]	-365.41	-[b]	-356.76	-[b]
Ag^+	-71.21	-101.43	-71.37	-101.58	-63.38	-93.58

[a] In kcal/mol.   [b] Unconvergence complexes.

The plot of ΔG and charge transfers between receptor and cation of complexes are displayed in Figures 4.26 and 4.27, respectively. When considering the binding energy, enthalpy and Gibbs free energy changes of all complexations, the negative values of changes indicate that the complexations are thermodynamically favorable. For Al cations, the results show that Al complexes with receptors **L5, L6, L7** and **L8** are the most stable complexes because the Gibbs free energy changes are the

most negative values (ΔG of **L6**/Al^{3+}= -819.48, **L7**/Al^{3+} = -644.07 and **L8**/Al^{3+} = -707.59 kcal/mol). Whereas Cu ion complexes with receptors **L5, L6, L7** and **L8** are the less stable complexes because the Gibbs free energy changes are the least negative values (ΔG of **L5**/Cu^{2+} = -309.17, **L6**/Cu^{2+} = -478.38 and **L7**/Cu^{2+} = -356.70 kcal/mol). As found in the previous reports, the higher charge transfer between cation and receptor are the stronger binding interaction then the Al complexes, the highest in charge transfers, are the most stable complexes. Whereas the Cu complexes, the highest in charge transfers, are the least stable complexes.
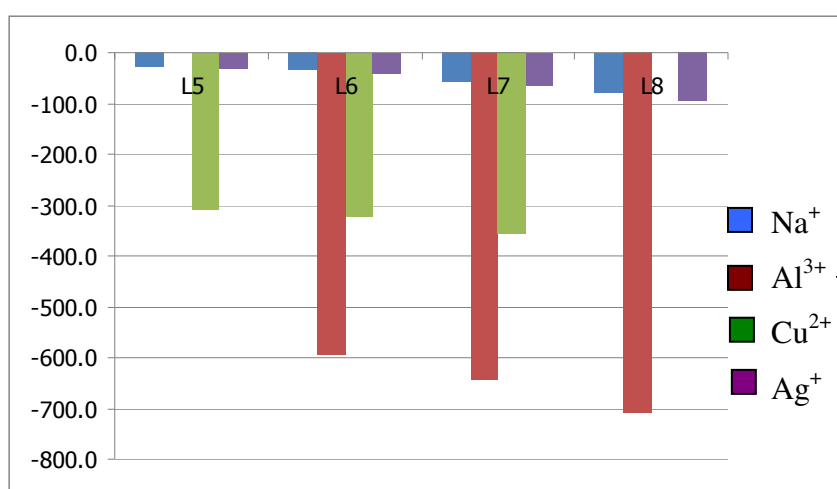
Figure 4.25 Gibbs free energy changes in kcal/mol of the receptors **L5, L6, L7** and **L8** complexes with cations.
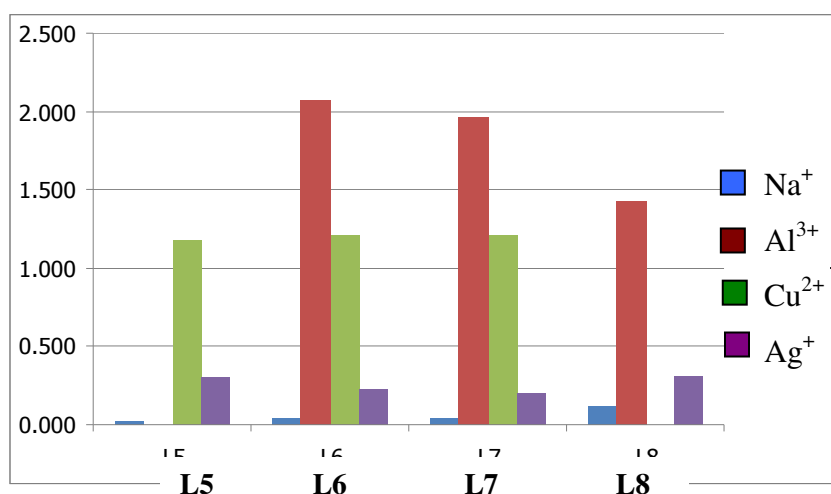
Figure 4.26 The charge transfers in e between the receptors **L5, L6, L7** and **L8** complexes with cations.

The energies of HOMO (E_{HOMO}), LUMO (E_{LUMO}), the frontier molecular orbital energy gap (E_{gap}), chemical hardness (η), electronic chemical potential (μ) and Mulliken electronegativity (χ) of receptors **L5, L6, L7** and **L8** and their cation complexes are tabulated in Table 4.7. For all free receptors, the energy level HOMO goes from -0.214 eV for receptor **L6** to -0.203 eV for receptor **L7**. For the LUMO level of all free receptors in which the energy is decreasing from -0.104 eV for receptor **L6** to -0.098 eV for receptor **L7**. The energy gaps of all cation complexes are different and range between 0.013-0.101, 0.025-0.126, 0.012-0.114 and 0.014-0.108 eV for receptors **L5, L6, L7** and **L8**, respectively. The energy gaps of complexes are not much different from their corresponding free receptors except for the Al complexes with receptors **L5, L6, L7** and **L8**.

The charge-transfer nature of the electronic transitions of receptors and cations is better illustrated by drawings of molecular orbitals. The frontier orbital shapes of the receptors **L5, L6, L7** and **L8** and their complexes with anions presented over isosurface value of 0.05 au are displayed in Figures 4.28, 4.29, 4.30 and 4.31, respectively. The LUMOs of all free receptors are located at the same position which is at the pyrrole unit. The HOMOs of free receptors **L5** and **L6** are located at the same position which is at the pyrrole unit, whereas the HOMOs of free receptors **L7** and **L8** are located at the same position which is at the thioamide unit.

As consideration of the most stable complexes of aluminium ion (**L6**/Al^{3+} and **L7**/Al^{3+}), each of HOMO of complexes is located at the sulphur, except to **L8**/Al^{3+}. Each of LUMO of complexes is somewhat analogous to densities of free receptors (**L6**/Al^{3+} and **L7**/Al^{3+}) except for **L8**/Al^{3+}.

Table 4.7 The computed orbital energies and frontier molecular orbital energy gap of the receptors **L5, L6, L7** and **L8** and their complexes with cations

Receptor/cation	E_{LUMO}[a]	E_{HOMO}[a]	E_{gap}[a]	η[b]	μ[c]	χ[d]
L5	-0.102	-0.211	0.109	0.055	-0.157	0.157
L5/Na$^+$	-0.190	-0.278	0.088	0.044	-0.234	0.234
L5/Al^{3+}	-	-	-	-	-	-
L5/Cu^{2+}	-0.353	-0.454	0.101	0.051	-0.404	0.404
L5/Ag$^+$	-0.280	-0.293	0.013	0.006	-0.287	0.287
L6	-0.104	-0.214	0.110	0.055	-0.159	0.159
L6/Na$^+$	-0.181	-0.283	0.102	0.051	-0.232	0.232
L6/Al^{3+}	-0.538	-0.563	0.025	0.013	-0.551	0.551
L6/Cu^{2+}	-0.334	-0.460	0.029	0.015	-0.276	0.276
L6/Ag$^+$	-0.261	-0.290	0.126	0.063	-0.397	0.397
L7	-0.098	-0.203	0.105	0.053	-0.151	0.151
L7/Na$^+$	-0.172	-0.279	0.107	0.054	-0.226	0.226
L7/Al^{3+}	-0.511	-0.523	0.012	0.006	-0.517	0.517
L7/Cu^{2+}	-0.319	-0.433	0.114	0.057	-0.376	0.376
L7/Ag$^+$	-0.227	-0.277	0.050	0.025	-0.252	0.252
L8	-0.103	-0.210	0.107	0.054	-0.157	0.157
L8/Na$^+$	-0.173	-0.281	0.108	0.054	-0.227	0.227
L8/Al^{3+}	-0.420	-0.434	0.014	0.007	-0.427	0.427
L8/Cu^{2+}	-[e]	-[e]	-[e]	-[e]	-[e]	-[e]
L8/Ag$^+$	-0.170	-0.278	0.108	0.054	-0.224	0.224

[a] In eV.

[b] Chemical hardness, $\eta = E_{gap}/2$.

[c] Electronic chemical potential, $\mu = (E_{HOMO} + E_{LUMO})/2$.

[d] The Mulliken electronegativity, $\chi = -(E_{HOMO} + E_{LUMO})/2$.

[e] Unconvergence complexes.
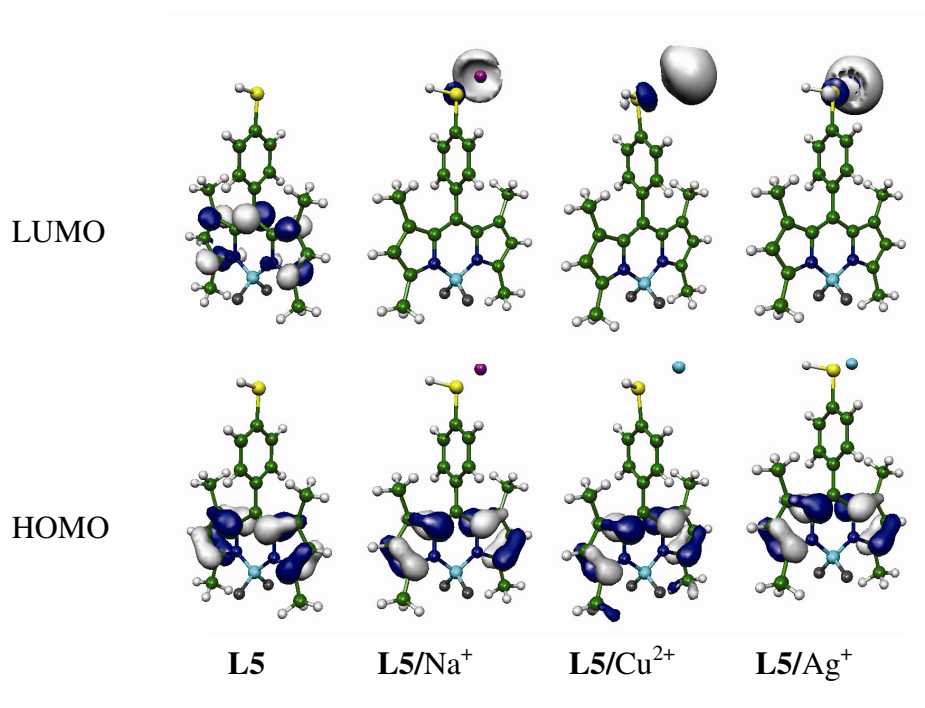
Figure 4.27 Plots of the LUMO (Top) and HOMO (Bottom) orbitals of the free forms of
receptor **L5** and its complexes with cationic guests at iso-surface value of
0.05 au.
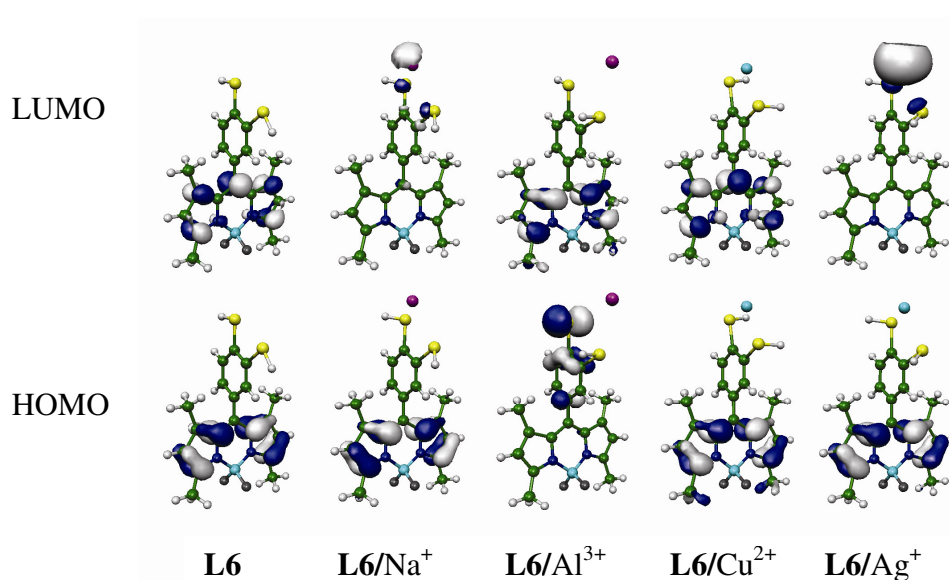
Figure 4.28 Plots of the (Top) and HOMO (Bottom) orbitals of the free forms of receptor
L6 and its complexes with cationic guests at iso-surface value of 0.05 au.
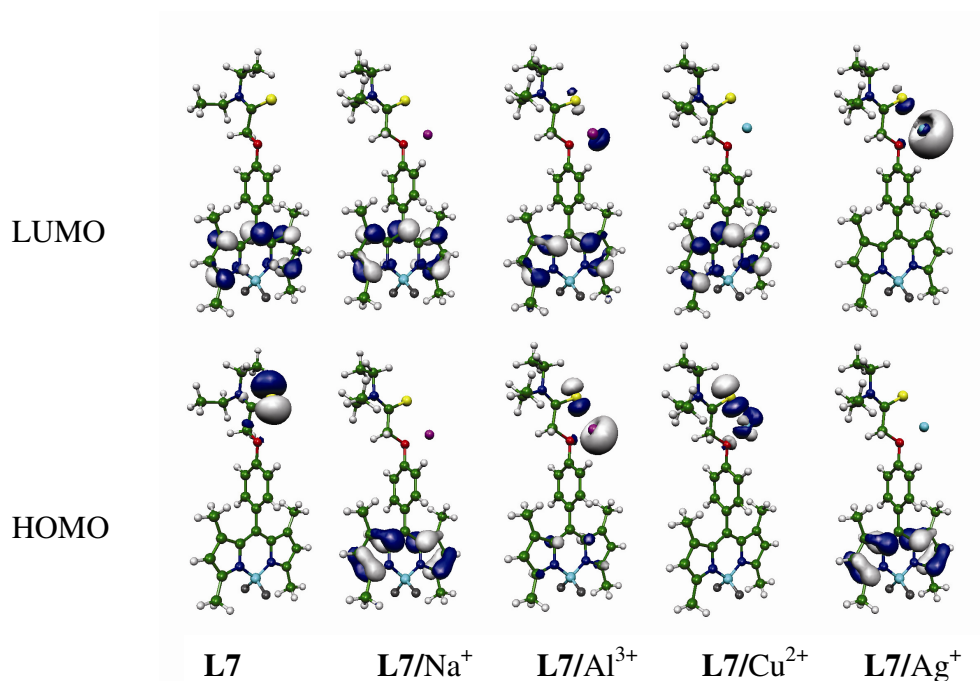
Figure 4.29 Plots of the (Top) and HOMO (Bottom) orbitals of the free forms of receptor
L7 and its complexes with cationic guests at iso-surface value of 0.05 au.
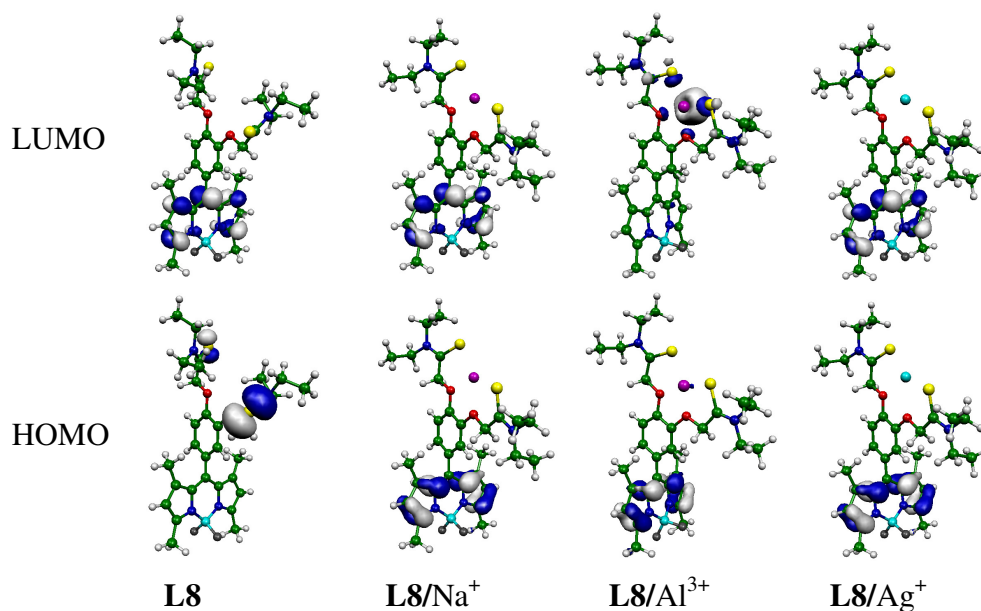
Figure 4.30 Plots of the (Top) and HOMO (Bottom) orbitals of the free forms of receptor
L8 and its complexes with cationic guests at iso-surface value of 0.05 au.

CHAPTER 5

CONCLUSION

The BODIPY-based receptors **L1** and **L2** containing hydroxyl units and **L3** and **L4** containing amide units for cation recognition were synthesized and studied the binding abilities with Na^+, K^+, Ca^{2+}, Pb^{2+}, Al^{3+}, Ge^{4+}, Cr^{3+}, Fe^{2+}, Co^{2+}, Ni^{2+}, Cu^{2+}, Zn^{2+}, Ag^+, Cd^{2+} and Hg^{2+} ions by using UV-vis and fluorescent spectroscopies. The UV-vis spectroscopy shows the decreasing of maxima absorption intensity when successive addition of Al^{3+} ion in methanol solution of all receptors except for receptor **L4.** For receptors **L4**, the maxima absorption intensity decreases when addition of Cu^{2+} ion. The fluorescent spectroscopy shows the decreasing of maxima emission intensity when successive addition of Al^{3+} ion in methanol solution of receptors **L2** and **L3**. For receptors **L1** and **L4**, the maxima emission intensity decreases when addition of Cu^{2+} ion.

The complexations between receptors and cations were carried out using the B3LYP/DFT method. The LandL2DZ basis set was used for all complexation studies. All calculations were performed with the GAUSSIAN 03 program.

Complexation of BODIPY-based receptors **L1**, **L2**, **L3** and **L4** containing oxygen donor atom with Na^+, Ag^+, Al^{3+} and Cu^{2+} ions have been studied by using the DFT calculation. The results show that the receptors establish a large number of ion/dipole interactions with cations. The binding abilities of receptors **L1**, **L2**, **L3** and **L4** with cations are in the same decreasing order: $Al^{3+} > Cu^{2+} > Na^+ > Ag^+$.

Complexation of BODIPY-based receptors **L5**, **L6**, **L7** and **L8** containing sulphur donor atom with Na^+, Ag^+, Al^{3+} and Cu^{2+} ions have been studied by using the DFT calculation. The results show that the receptors establish a large number of ion/dipole interactions with cations. The binding abilities of receptors **L5**, **L6**, **L7** and **L8** with cations are in the same decreasing order: $Al^{3+} > Cu^{2+} > Ag^+ > Na^+$.

REFERENCES

REFERENCES

[1] Demchenko AP. "Introduction to fluorescence sensing". Netherlands: s.n.; **2009**.

[2] Ueno T, Urano Y, Setsukinai K, Takakusa H, Kojima H, Kikuchi K, Ohkubo K, Fukuzumi S, Nagano T. "Rational principles for modulating fluorescence properties of fluorescein". *J. Am. Chem. Soc.,* **2004**, 126, 14079-14085.

[3] French PMW, Taylor JR. "The passive modelocking of the continuous wave rhodamine B dye laser". *Opt. Commun,* **1986**, 58, 53-55.

[4] Mahmood T, Paul A, Ladame S. "Synthesis and spectroscopic and DNA-binding properties of fluorogenic acridine-containing cyanine dyes". *J. Org. Chem.* **2010**, 75, 204-207.

[5] Li L, Ruzgas T, Gaigalas AK. "Fluorescence from Alexa 488 fluorophore immobilized on a modified gold electrode*". Langmuir*, **1999**, 15, 6358-6363.

[6] Bonasera V, Alberti S, Sacchetti A. "Protocol for high-sensitivity/long linear-range spectrofluorimetric DNA quantification using ethidium bromide". *BioTechniques,* **2007**, 43, 173-174.

[7] Treibs A, Kreuzer FH. "Difluoroboryl complexes of di- and tripyrrylmethenes". *Justus Liebigs Ann. Chem.*, **1968**, 718, 208-223.

[8] Wang W, Fan J, Gao X, Wang B, Sun S, Peng X. "Design and development of a new pyrromethene dye with improved photostability and lasing efficiency: theoretical rationalization of photophysical and photochemical properties". *J. Org. Chem.,* **2009,** 74, 7675-7683.

[9] Ohsaki Y, Shinohara Y, Suzuki M, Fujimoto T. "A pitfall in using BODIPY dyes to label lipid droplets for fluorescence microscopy". *Histochem. Cell Biol.,* **2010**; 130: 477-480.

[10] Marmé N, Knemeyer JP, Sauer M, Wolfrum J. "Inter- and intramolecular fluorescence quenching of organic dyes by tryptophan". *Bioconjugate Chem.,* **2003**, 14, 1133-1139.

[11] Faulds K, McKenzie F, Smith W, Graham D. "Quantitative simultaneous multianalyte detection of DNA by dual-wavelength surface-enhanced resonance raman scattering". *Angew. Chem.,* **2007**, 19, 1861-1863.

[12] García-Moreno I, Costela A, Campo L, Sastre R, Amat-Guerri F, Liras M, López Arbeloa F, Bañuelos Prieto J, López Arbeloa I. "8-phenyl-substituted dipyrromethene BF_2 complexes as highly efficient and photostable laser dyes". *J. Phys. Chem.,* **2004**, 108, 3315-3323.

[13] Liras M, Prieto JB, Pintado-Sierra M, Arbeloa FL, García-Moreno I, Costela A, Infantes L, Sastre R, Amat-Guerri F. "Synthesis, photophysical properties and laser behavior of 3-amino and 3-acetamido BODIPY dyes". *Org. Lett.,* **2007**, 9, 4183-4186.

[14] Chen X, Lenhert S, Hirtz M, Lu N, Fuchs H, Chi L. "Langmuir-blodgett patterning: a way to build mesoscopic structure on the surface from bottom-up". *Acc. Chem. Res.,* **2007**, 40, 393-401.

[15] Golvkova TA, Kozlov DV, Neckers DC. "Synthesis and properties of novel fluorescent switches". *J. Org. Chem.,* **2005**, 70, 5545-5549.

[16] Turfan B, Akkaya EU. "Modulation of boradiazaindacene emission by cation-mediated oxidative PET". *Org. Lett.,* **2002**, 4, 2857-2859.

[17] Lehn J-M. "Supramolecular chemistry: concepts and cerspectives, VCH". Weinheim: s.n.; **1995**.

[18] Beer PD, Gale PA, Smith DK. "Supramolecular chemistry". New York: Oxford University Press; **1999**.

[19] Jeffrey GA. "An Introduction to hydrogen bonding". New York: Oxford University Press; **1997**.

[20] Arduini A, Secchi A, Pochini A. "Recognition of amides by new rigid Calix". *J.Org.Chem.,* **2000**, 65, 9085-9091.

[21] Bodenant B, Weil T, Businelli-Pourcel M, Fages F, Barbe B, Pianet I, Laguerre M. "Synthesis and solution structure analysis of a bispyrenyl bishydroxamate calix[4]arene-based receptor, a fluorescent chemosensor for Cu^{2+} and Ni^{2+} metal ions". *J. Org. Chem.*, **1999**, 64, 7034-7039.

[22] Czarnik AW. "Chemosensors of ion and molecule recognition: recent applications to pyrophosphate and to dopamine sensing". *ACS Symposium Series, Interfacial Design and Chemical Sensing* **1997**, 561, 314-323.

[23] Czarnik AW, Deseverge JP. "NATO ASI Series, series C; mathematical and physical sceinces". s.l.: Kluwer Academic Publishers; **1997**.

[24] Lehn JM. "Supramolecular chemistry - Scope and perspectives. Molecules, supermolecules, and molecular devices". *Angew. Chem. Int. Ed. Engl.,* **1988**, 27, 89-112.

[25] Lehn JM. "Perspectives in supramolecular chemistry - From molecular recognition towards molecular information processing and self-organization". *Angew.Chem. Int. Ed. Engl*., **1990**, 29, 1304-1319.

[26] Beer PD, Gale PA, Smith DK. "Supramolecular chemistry". New York: Oxford University Press Inc.; **1999**.

[27] Braga D, Grepioni F, Novoa JJ. "Inter-anion O-H⁻···O⁻ hydrogen bond like interactions: the breakdown of the strength-length analogy". *Chem. Commun*., **1998**, 25, 1959-1960.

[28] Kim E-I, Paliwal S, Wilcox CS. "Measurements of molecular electrostatic field effects in edge-to-face aromatic interactions and CH-π interactions with implications for protein folding and molecular recognition". *J. Am. Chem. Soc*., **1998**, 120, 11192-11193.

[29] De Silva AP, Gunaratne HQN, Gunnlaugsson T, Huxley AJM, Rademacher JT, Rice TE. "Chemosensors for ion and molecule recognition". *Mathematical and Physical Sceinces,* **1997**, 492, 143-147.

[30] Beer Paul D, Chen Z, Drew Michael GB, Gale P A. "Metal, ammonium and alkyl ammonium cation recognition by a novel calix[4]arene-diquinone crown ether". *J. Chem. Soc. Chem. Comm.,* **1994**, 19, 2207-2208.

[31] Beer Paul D, Chen Z, Grieve A, Haggitt J. "A new bipyridinium bis benzo crown ether ligand whose redox properties are dependent upon complexed cation induced conformational switching effects". *J. Chem. Soc. Chem. Comm.*, **1994**, 20, 2413-2414.

[32] Black CB, Andrioletti B, Try AC, Ruiperez C, Sesler JL. "Cation". *J. Am. Chem. Soc.*, **1999**, 121, 10438-10439.

[33] Shiratori H, Ohno T, Nozaki K, Osuka A. "Change of electron-transfer path-selectivity in a triad by F⁻-coordination at a boronate-ester bridge". *Chem. Commun*., **1999**, 21, 2181 - 2182.

[34] Lehn JM. Supramolecular Photochemistry, Ed. Balzani, V.NATO ASI Series, Series C". *Mathematical and Physical Sceinces*, **1997**, 214, 29.

[35] Desvergne J, Czarnik A W. "Chemosensors of ion and molecule recognition, NATO ASI series". Dordrecht: Kluwer; **1997**.

[36] Bryan AJ, de Silva AP, de Silva SA, Rupasinghe RADD, Sandanayake KRAS. "Photo-induced electron transfer as a general design logic for fluorescent molecular sensors for cations". *Biosensors*, **1989**, 4, 169-179.

[37] Martinez-Manez R, Sancenon F. "Fluorogenic and Chromogenic Chemosensors and Reagents for Anions". *Chem. Rev*., **2003**, 103, 4419-4476.

[38] Aoki I, Sakaki T, Shinkai S. "Fluorescence reading-out of the molecular-recognition process". *J. Chem. Soc. Chem. Commun.*, **1992**, 18, 1341-1345.

[39] Ji HF, Dabestani R, Brown GM, Sachleben RA. "A new highly selective calix[4]crown-6 fluorescent caesium probe". *Chem.Commun*. **2000**, 10, 833-834.

[40] Ji HF, Brown GM, Dabestani R. "Calix[4]arene-based Cs^+ selective optical sensor". *Chem. Commun*., **1999**, 9, 609-610.

[41] Kim JS, Shon OJ, Rim JA, Kim SK, Yoon J. "Pyrene-armed calix[4]aza-crowns as new fluorescent ionophores: "molecular taekowndo" process via fluorescence change". *J. Org. Chem*., **2002**, 67, 2348-2351.

[42] Kim JS, Noh KH, Lee SH, Kim SK, Kim SK, Yoon J. "Molecular taekwondo. 2. a new calix[4]azacrown bearing two different binding sites as a new fluorescent Ionophore". *J. Org. Chem*., **2003**, 68, 597-600.

[43] de Silva AP, de Silva SA. "Fluorescent signalling crown ethers; 'switching on' of fluorescence by alkali metal ion recognition and binding in situ*". J. Chem. Soc. Chem. Commun*., **1986**, 13, 1709-1710.

[44] de Silva AP, Gunaratne HQN, Sandanayake KRAS. "A new benzo-annelated cryptand and a derivative with alkali cation-sensitive fluorescence". *Tetrahedron Lett*., **1990**, 3, 5193-5196.

[45] Fabbrizzi L, Lichelli M, Pallavicini P, Perotti A, Sacchi D. "An Anthracene-Based Fluorescent Sensor for Transition Metal Ions". *Angew. Chem. Int. Ed. Engl*. **1994**, 33, 1975-1977.

[46] de Silva AP, Gunaratne HQN, Maguire GEM. "'Off-on' fluorescent sensors for physiological levels of magnesium ions based on photoinduced electron transfer (PET), which also behave as photoionic OR logic gates". *J. Chem. Soc. Chem. Commun*., **1994**, 17, 1213-1214.

[47] Gilat SL, Adronov A, Frĕchet JMJ. "Light harvesting and energy transfer in novel convergently constructed dendrimers". *Angew. Chem. Int. Ed*., **1999**, 38, 1422-1427.

[48] Turfan B, Akkaya EU. "Modulation of boradiazaindacene emission by cation-mediated oxidative PET". *Org. Lett*., **2002**, 4, 2857-2859.

[49] Valeur B, Bourson J, Pouget J. "American Chemical Society". Washington, DC: s.n.; **1993**.

[50] Valeur B, Badaoui F, Bardez E, Bourson J, Boutin P, Chatelain I, Devol B. Larrey JP Lefèvre, Soulet In A, Desvergne J-P, Czarnik AW. "Chemosensors of ion and molecule recognition, NATO ASI series". Kluwer: Dordrecht; **1997**.

[51] Lakowicz JR. "Principles of fluorescence spectroscopy". New York: Plenum Publishers Corp; **1999**.

[52] Stryer L, Haugland RP. "Energy transfer: A Spectroscopic ruler". *Natl. Acad. Sci. USA*., **1967**, 58, 719-726.

[53] Jin T. "Membrane transport of neurotransmitter acetylcholine and related compounds across a phospholipid bilayer by a calix[6]arene ester". *Chem. Commun*., **1999**, 20, 2129-2130.

[54] Arduini M, Felluga F, Mancin F, Rossi P, Tecilla P, Tonellato U, valentinuzzib N. "Aluminium fluorescence detection with a FRET amplified chemosensor". *Chem. Commun*., **2003,** 13, 1606-1607.

[55] Ono A, Togashi H. "Highly selective oligonucleotide-based sensor for mercury(II) in aqueous solutions". *Angew. Chem. Int. Ed*., **2004**, 43, 4300-4302.

[56] Cao HS, Heagy MD. "Fluorescent chemosensors for carbohydrates: a decade's worth of bright spies for saccharides in review". *J. Fluor.,* **2004**, 14, 569-584.

[57] Birks JB. "Photophysics of Aromatic molecules". New York: JohnWiley; **1970**.

[58] Winnik FM. "Photophysics of preassociated pyrenes in aqueous polymer solutions and in other organized media". *Chem. Rev*., **1993**, 93, 587-614.

[59] Yang JS, Lin CS, Hwang CY. "Cu^{2+}-Induced Blue Shift of the Pyrene Excimer Emission: A New Signal Transduction Mode of Pyrene Probes". *Org. Lett.,* **2001**, 3, 889-892.

[60] Liao JH, Chen CT, Fang JM. "A Novel phosphate chemosensor utilizing anion-induced fluorescence change". *Org. Lett.,* **2002**, 4, 561-564.

[61] Kim SK, Lee SH, Lee JY, Lee JY, Bartsch RA, Kim JS. "An Excimer-based, binuclear, On-Off switchable calix[4]crown chemosensor". *J. Am. Chem. Soc.*, **2004**, 126, 16499-16506.

[62] Choi JK, Kim SH, Yoon JY, Lee KH, Bartsch RA, Kim JS. "A PCT-based, pyrene-armed calix[4]crown fluoroionophore". *J. Org. Chem.*, **2006**, 71, 8011-8015.

[63] Clark T. "A handbook of computational chemistry". New York: Wiley; **1985**.

[64] Cramer CJ. "Essentials of computational chemistry". s.l.: John Wiley & Sons; **2002**.

[65] Jensen F. "Introduction to computational chemistry". s.l.: John Wiley & Sons; **1999**.

[66] Young D. "Computational chemistry: A practical guide for applying techniques to real world problems". s.l.: John Wiley & Sons; **2001**.

[67] Foresman J, Frisch A. "Exploring chemistry with electronic structure methods". s.l.: Gaussian, Inc.; **1996**.

[68] Loudet A, Burgess K. "BODIPY Dyes and their derivatives: Syntheses and Spectroscopic Properties". *Chem. Rev.*, **2007**, 107, 4891-4932.

[69] Wood TE, Thompson A. "Advances in the chemistry of dipyrrins and their complexes". *Chem. Rev.*, **2007**, 107, 1831-1861.

[70] Ulrich G, Ziessel R, Harriman A. "The Chemistry of fluorescent bodipy dyes: versatility unsurpassed". *Angew. Chem. Int. Ed.*, **2008**, 47, 1184-1201.

[71] Jiang JL, Lu H, Shen Z. "Synthesis, spectroscopic properties and Hg^{2+} recognition based on a boron dipyrromethene dye (BODIPY)". *Chinese J. Inorg. Chem.*, **2010**, 26, 1105-1108.

[72] Atilgan S, Ozdemir T, Akkaya EU. "A Sensitive and Selective Ratiometric Near IR Fluorescent Probe for Zinc Ions Based on the Distyryl−Bodipy Fluorophore". *Org. Lett.*, **2008**, 10, 4065-4067.

[73] Lu H, Xiong L, Liu H, Yu M, Shen Z, Li F, You X. "A highly selective and sensitive fluorescent turn-on sensor for Hg^{2+} and its application in live cell imaging". *Org. Biomol. Chem.*, **2009**, 7, 2554-2558.

[74] Kim, H. J.; Kim, J. S. "Bodipy appended cone-calix[4]arene: selective fluorescence changes upon Ca^{2+} binding" *Tetrahedron Lett.*, **2006**, 47, 7051-7055.

[75] Koutaka H, Kosuge JI, Fukasaku N, Hirano T, Kikuchi K, Urano Y, Kojima H, Nagano T. "A Novel fluorescent probe for zinc ion based on boron dipyrromethene (BODIPY) chromophore". *Chem. Pharm. Bull*., **2004**, 52, 700-703.

[76] Wang D, Shiraishi Y, Hirai T. "A distyryl BODIPY derivative as a fluorescent probe for selective detection of chromium(III)". *Tetrahedron Lett*., **2010**, 51, 2545-2549.

[77] Lu H, Zhang S, Liu H, Wang Y, Shen Z, Liu C, You X. "Experimentation and theoretic calculation of a BODIPY sensor based on photoinduced electron transfer for ions detection". *J. Phys. Chem. A*., **2009**, 113, 14081-14086.

[78] Du J, Fan J, Peng X, Li H, Wang J, Sun S. "Highly selective and anions controlled fluorescent sensor for Hg^{2+} in aqueous environment". *J. Fluoresc.*, **2008**, 18, 919-924.

[79] Tian M, Peng X, Fan J, Wu Y. "Progress on boron dipyrromethene fluorophore based on fluorescence cations probes". *Chin. J. Anal. Chem*., **2006**, 34, S283-S288.

[80] Rao MR, Mobin SM, Ravikanth M. "Boron-dipyrromethene based specific chemodosimeter for fluoride ion". *Tetrahedron,* **2010**, 66, 1728-1734.

[81] Coskun A, Akkaya EU. "Difluorobora-s-diazaindacene dyes as highly selective dosimetric reagents for fluoride anions". *Tetrahedron Lett*., **2004**, 45, 4947-4949.

[82] Fan J, Guo K, Peng X, Du J, Wang J, Sun S, Li H. "A Hg^{2+} fluorescent chemosensor without interference from anions and Hg^{2+}-imaging in living cells". *Sens.Actuators B*., **2009**, 142, 191-196.

[83] Shiraishi Y, Maehara H, Sugii T, Wang D, Hirai T. "A BODIPY-indole conjugate as a colorimetric and fluorometric probe for selective fluoride anion detection". *Tetrahedron Lett*., **2009**, 50, 4293-4296.

[84] Saito R, Ohno A, Ito E. "Synthesis of boradiazaindacene-imidazopyrazinone conjugate as lipophilic and yellow-chemiluminescent chemosensor for superoxide radical anion". *Tetrahedron*, **2010**, 66, 583-590.

[85] Alamiry MAH, Benniston AC, Copley G, Elliott KJ, Harriman A, Stewart B, Zhi YG. "A Molecular Rotor Based on an Unhindered Boron Dipyrromethene (Bodipy) Dye". *Chem. Mater*., **2008**, 20, 4024-4032.

[86] Yogo T, Urano Y, Ishitsuka Y, Maniwa F, Nagano T. "Highly efficient and photostable photosensitizer based on BODIPY chromophore". *J. Am. Chem. Soc.*, **2005**, 127, 12162-12163.

[87] Lim SH, Thivierge C, Nowak-Sliwinska P, Han J, Van Den Bergh H, Wagniares G, Burgess K, Lee HB. "Synthesis and in vitro photodynamic activities of pegylated distyryl boron dipyrromethene derivatives". *J. Med. Chem.*, **2010**, 53, 2865-2874.

[88] Erbas S, Gorgulu A, Kocakusakogullari M, Akkaya EU. "Non-covalent functionalized SWNTs as delivery agents for novel Bodipy-based potential PDT sensitizers". *Chem. Commun.*, **2009**, 15, 4956-4958.

[89] Adarsh N, Avirah RR, Ramaiah D. "Tuning photosensitized singlet oxygen generation efficiency of novel Aza-BODIPY dyes". *Org. Lett.*, **2010**, 12, 5720-5723.

[90] Ozlem S, Akkaya EU. "Thinking outside the silicon box: molecular AND logic as an additional layer of selectivity in singlet oxygen generation for photodynamic therapy". *J. Am. Chem. Soc.*, **2009**, 131, 48-49.

[91] Ziessel R, Bonardi L, Retailleau P, Ulrich G. "Dipyrromethene dyes as fluorescent probes". *J. Org. Chem.*, **2006**, 71, 3093-3102.

[92] Treibs A, Kreuzer FH. "Difluorboryl-komplexe von di- und tripyrrylmethenen". *Liebigs Ann. Chem.*, **1968**, 718, 203.

[93] Gossauer A, Nydegger F, Kiss T, Sleziak R, Stoeckli-Evans H. "Synthesis, chiroptical properties, and solid-state structure determination of two new chiral dipyrrin difluoroboryl chelates". *J. Am. Chem. Soc.*, **2004**, 126, 1772-1780.

[94] Gabe Y, Urano Y, Kikuchi K, Kojima H, Nagano T. "Highly sensitive fluorescence probes for nitric oxide based on boron dipyrromethene chromophore-rational design of potentially useful bioimaging fluorescence probe". *J. Am. Chem. Soc.*, **2004**, 126, 3357-3367.

[95] Zhang X, Xiao Y, Qian X. "Highly efficient energy transfer in the light harvesting system composed of three kinds of boron−dipyrromethene derivatives". *Org. Lett.*, **2008**, 10, 29-32.

[96] Li L, Nguyen B, Burgess K. "Functionalization of the 4,4-difluoro-4-bora-3a, 4a-diaza-s-indacene (BODIPY) core". *Bioorg. Med. Chem. Lett.*, **2008**, 18, 3112-3116.

[97] Cakmak Y, Akkaya EU. "Phenylethynyl-BODIPY oligomers: bright dyes and fluorescent building blocks". *Org. Lett.*, **2009**, 11, 85-88.

[98] Liu JY, Yeung HS, Xu W, Li X, Ng DKP. "Syntheses of the P-Methylase substrates of the bialaphos biosynthetic pathway". *Org. Lett.*, **2008**, 10, 5521-5524.

[99] Tahtaoui C, Thomas C, Rohmer F, Klotz P, Duportail G, Mely Y, Bonnet D, Hibert M. "Convenient method to access new 4,4-dialkoxy- and 4,4-diaryloxy-diaza-s-indacene dyes: synthesis and spectroscopic evaluation". *J. Org. Chem.,* **2007**, 72, 269-272.

[100] de Silva AP, Gunaratne HQN, Gunnlaugsson T, Huxley AJM, Mc Coy CP, Rademacher JT, Rice TE. "Signaling recognition events with fluorescent sensors and switches". *Chem. Rev.*, **1997**, 97, 1515-1566.

[101] Rurack K, Resch-Genger U. "Rigidization, preorientation and electronic decoupling-the 'magic triangle' for the design of highly efficient fluorescent sensors and switches". *Chem. Soc. Rev.*, **2002**, 31, 116-127.

[102] Kollmannsberger M, Rurack K, Resch-Genger U, Daub J. "Ultrafast charge transfer in amino-substituted boron dipyrromethene dyes and its inhibition by cation complexation: A new design concept for highly sensitive fluorescent probes". *J. Phys. Chem. A.*, **1998**, 102, 10211-10220.

[103] Jiang P, Guo Z. "Fluorescent detection of zinc in biological systems: recent development on the design of chemosensors and biosensors". *Coord. Chem. Rev.*, **2004**, 248, 205-229.

[104] Kikuchi K, Komatsu K, Nagano T. "Zinc sensing for cellular application". *Curr. Opin. Chem. Biol.*, **2004**, 8, 182-191.

[105] Lim NC, Freake HC, Bruckner C. "Illuminating Zinc in Biological Systems". *Chem.-Eur.J.*, **2005**, 11, 38-49.

[106] Carol P, Sreejith S, Ajayaghosh A. "Ratiometric and near-infrared molecular probes for the detection and imaging of zinc ions". *Chem.-Asian J.*, **2007**, 2, 338-348.

[107] Xu DR. "Fluorescent chemosensors for Zn^{2+}". *Chem. Soc. Rev.,* **2010**, 39, 1996-2006.

[108] Nolan EM, Lippard SJ. "Tools and tactics for the optical detection of mercuric ion". *Chem. Rev*., **2008**, 108, 3443-3480.

[109] Que EL, Domaille DW, Chang CJ. "Metals in Neurobiology: Probing Their Chemistry and Biology with Molecular Imaging". *Chem. Rev*., **2008**, 108, 1517-1549.

[110] Baruah M, Qin W, Vallee RAL, Beljonne D, Rohand T, Dehaen W, Boens N. "A Highly potassium-selective ratiometric fluorescent indicator based on BODIPY azacrown ether excitable with visible light". *Org. Lett*., **2005**, 7, 4377-4380.

[111] Moczar I, Huszthy O, Maidics Z, Kadar M, Toth K. "Synthesis and optical characterization of novel enantiopure BODIPY linked azacrown ethers as potential fluorescent chemosensors". *Tetrahedron*, **2009**, 65, 8250-8258.

[112] Martin VV, Rothe A, Gee KR. "Fluorescent metal ion indicators based on benzoannelated crown systems: a green fluorescent indicator for intracellular sodium ions". *Bioorg. Med. Chem. Lett*., **2005**, 15, 1851-1855.

[113] Rurack K, Sczepan M, Spieles M, Resch-Genger U, Rettig W. "Correlations between complex stability and charge distribution in the ground state for Ca^{2+} and Na^+ complexes of charge transfer chromo- and fluoroionophores". *Chem. Phys. Lett.,* **2000**, 320, 87-94.

[114] Kollmannsberger M, Rurack K, Resch-Ginger U, Daub J. "Ultrafast charge transfer in amino-substituted boron dipyrromethene dyes and its inhibition by cation complexation: A new design concept for highly sensitive fluorescent probes". *J. Phys. Chem. A.,* **1998**, 102, 10211-10220.

[115] Qin W, Baruah M, Sliwa M, Van der Auweraer M, De Borggraeve WM, Beljonne D, Van Averbeke B, Boens N. "Ratiometric, fluorescent BODIPY dye with aza crown ether functionality: Synthesis, solvatochromism, and metal ion complex formation". *J. Phys. Chem. A*., **2008**, 112, 6104-6114.

[116] Basaric N, Baruah M, Qin W, Metten B, Smet M, Dehaen W, Boens N. "Synthesis and spectroscopic characterisation of BODIPY® based fluorescent off-on indicators with low affinity for calcium". *Org. Biomol. Chem.*, **2005**, 3, 2755-2761.

[117] Dodani SC, He Q, Chang CJ. "A Turn-On Fluorescent Sensor for Detecting Nickel in Living Cells". *J. Am. Chem. Soc.*, **2009**, 131, 18020-18021.

[118] Du J, Fan J, Peng X, Li H, Wang J, Sun S. "Highly selective and anions controlled fluorescent sensor for Hg^{2+} in aqueous environment". *J. Fluoresc.* **2008**, 18, 919-924.

[119] Lu H, Zhang SS, Liu HZ, Wang YW, Shen S, Liu C GL, You XZ. "Experimentation and theoretic calculation of a BODIPY sensor based on photoinduced electron transfer for ions detection". *J. Phys. Chem. A.,* **2009**, 113, 14081-14086.

[120] Piyaauksornsak S, Tangthongkul T, Wanbayor R, Wanno B, Ruangpornvisuti V. Molecular structures of 8,8′-dithioureido-2,2′-binaphthalene derivatives and their anions recognition: an ONIOM investigation". *Struct. Chem.*, **2009**, 20, 767-780.

[121] Munk VP, Cham ST, Fenton RR, Hocking RK, Hambley TW. "Insights into the van der Waals radius of low-spin Ni^{2+} from molecular mechanics studies and the crystal structures of [Ni(cis-cyclohexane-1,3-diamine)$_2$]Cl$_2$,[Ni{R) 5,5,7-trimethyl-1,4-diazacycloheptane}$_2$]Cl$_2$.H$_2$O and [Ni(5,7-dimethyl-1,4-diazacycloheptane)$_2$](ClO$_4$)$_2$.Synthesis of 5,7-dimethyl-1,4-diazacycloheptane and an improved synthesis of cis-cyclohexane-1,3-diamine". *Aust. J. Chem.*, **2002**, 55, 523-529.

APPENDICES

APPENDIX A
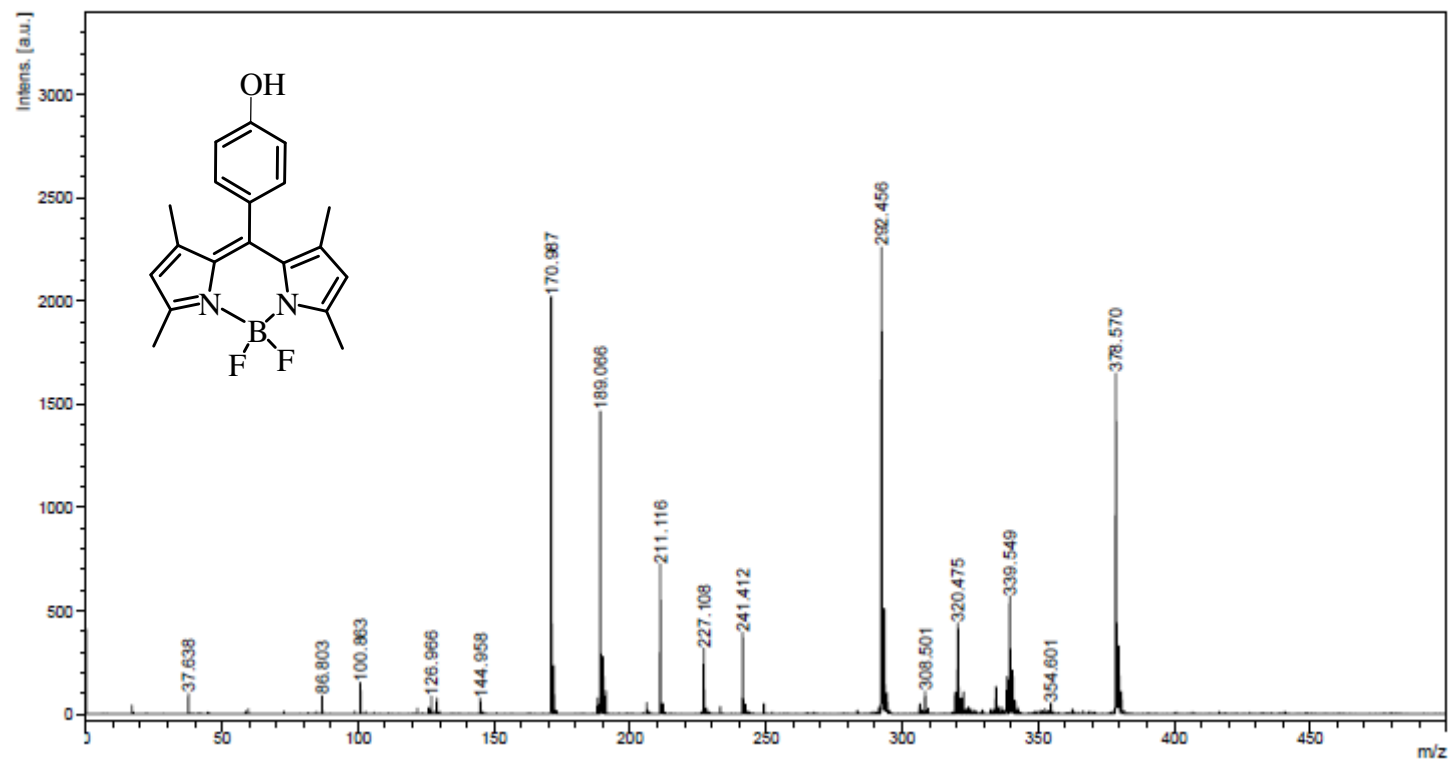
Figure A1 Mass spectrum of **L1**.
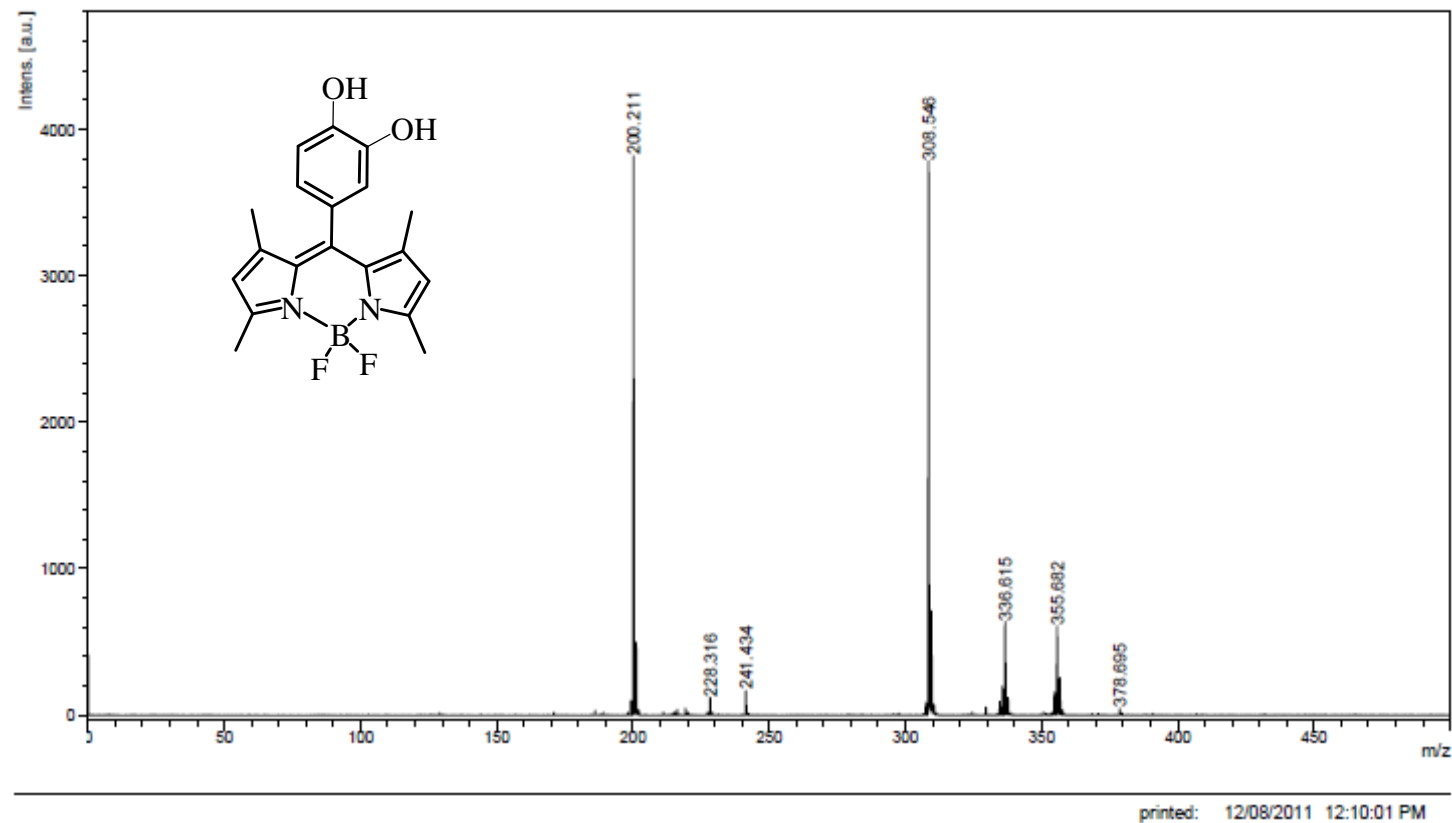
Figure A2 Mass spectrum of **L2**.

Comment 1   L3
Comment 2

Figure A3 Mass spectrum of **L3**.
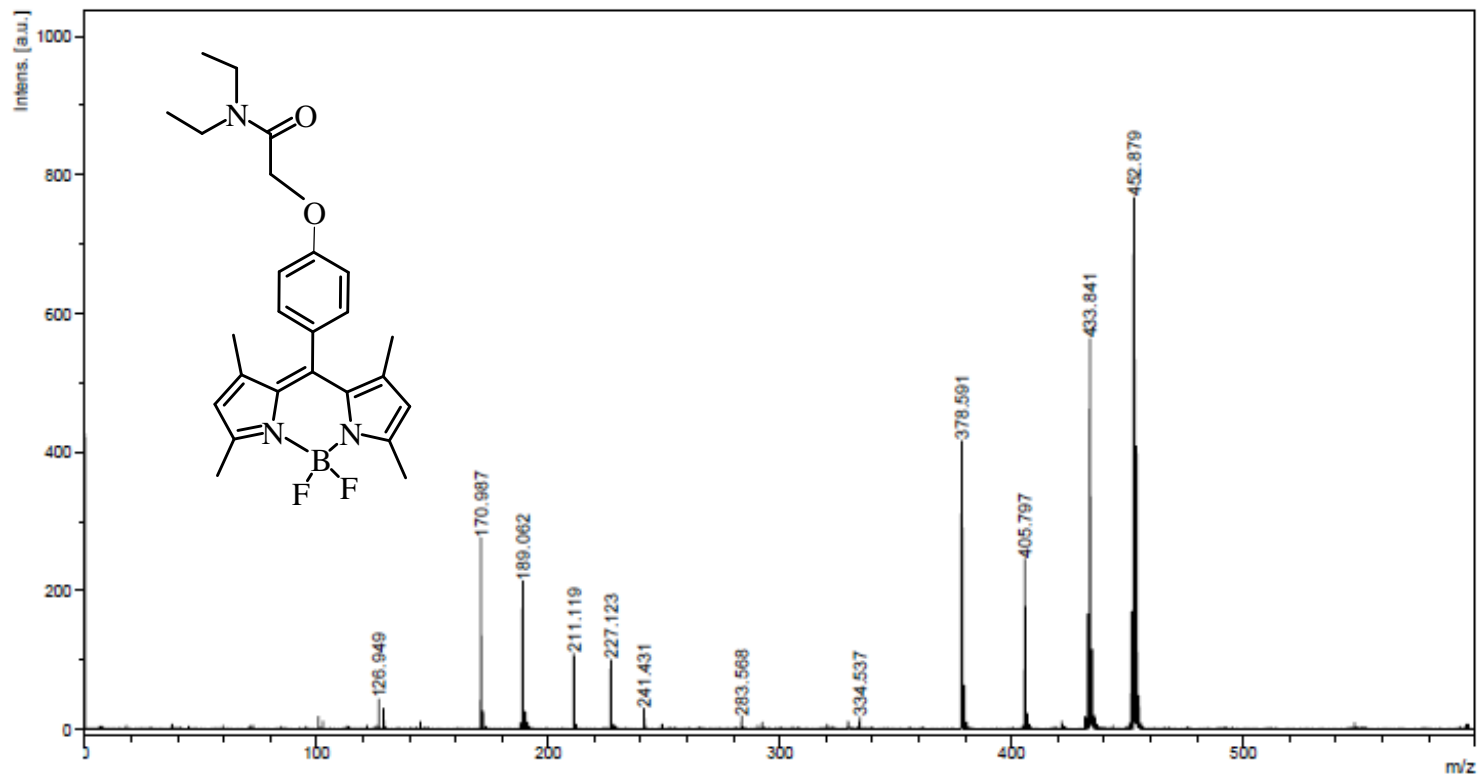
printed: 12/08/2011 12:11:12 PM

Comment 1   L4
Comment 2

Figure A4 Mass spectrum of **L**4.
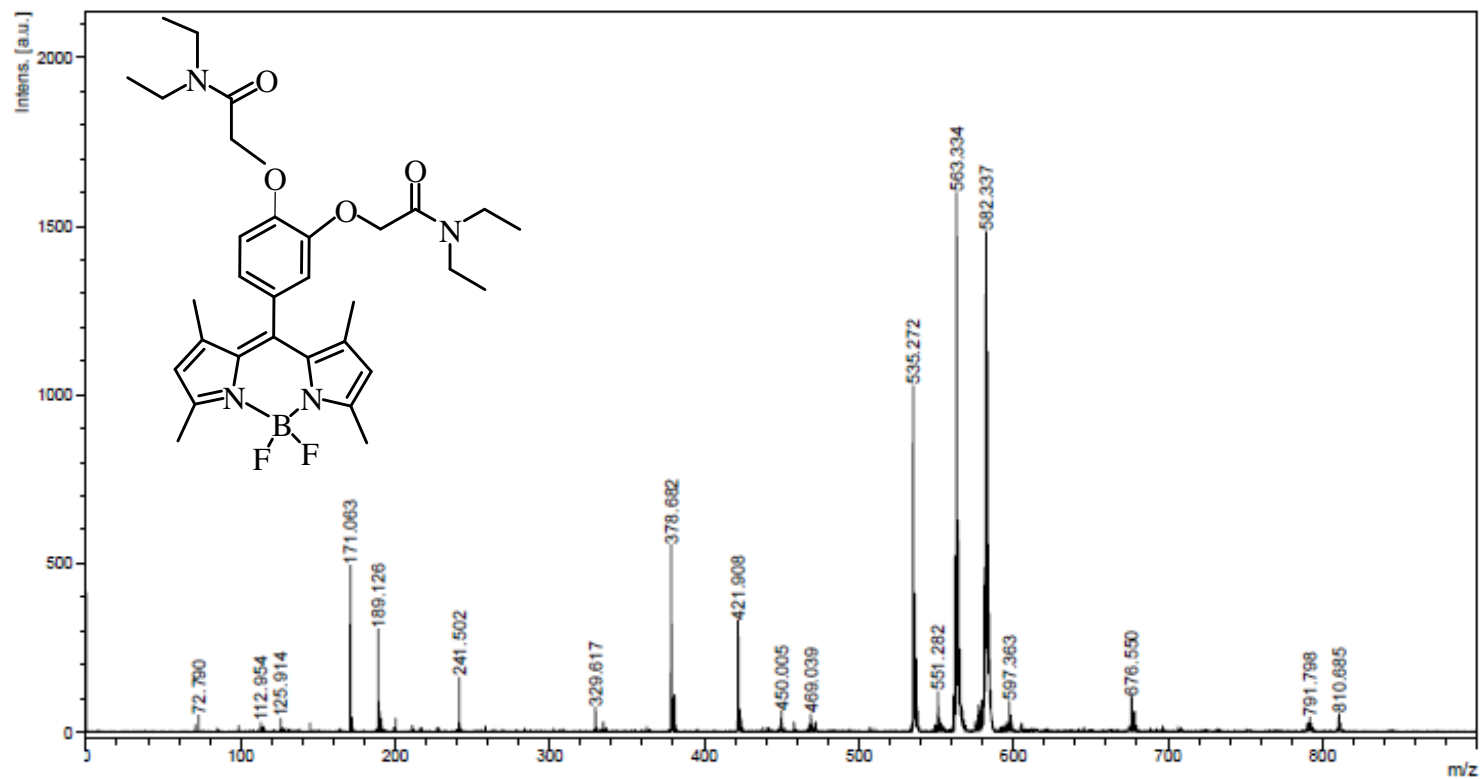
printed: 12/08/2011 12:13:51 PM

Mahasarakham University
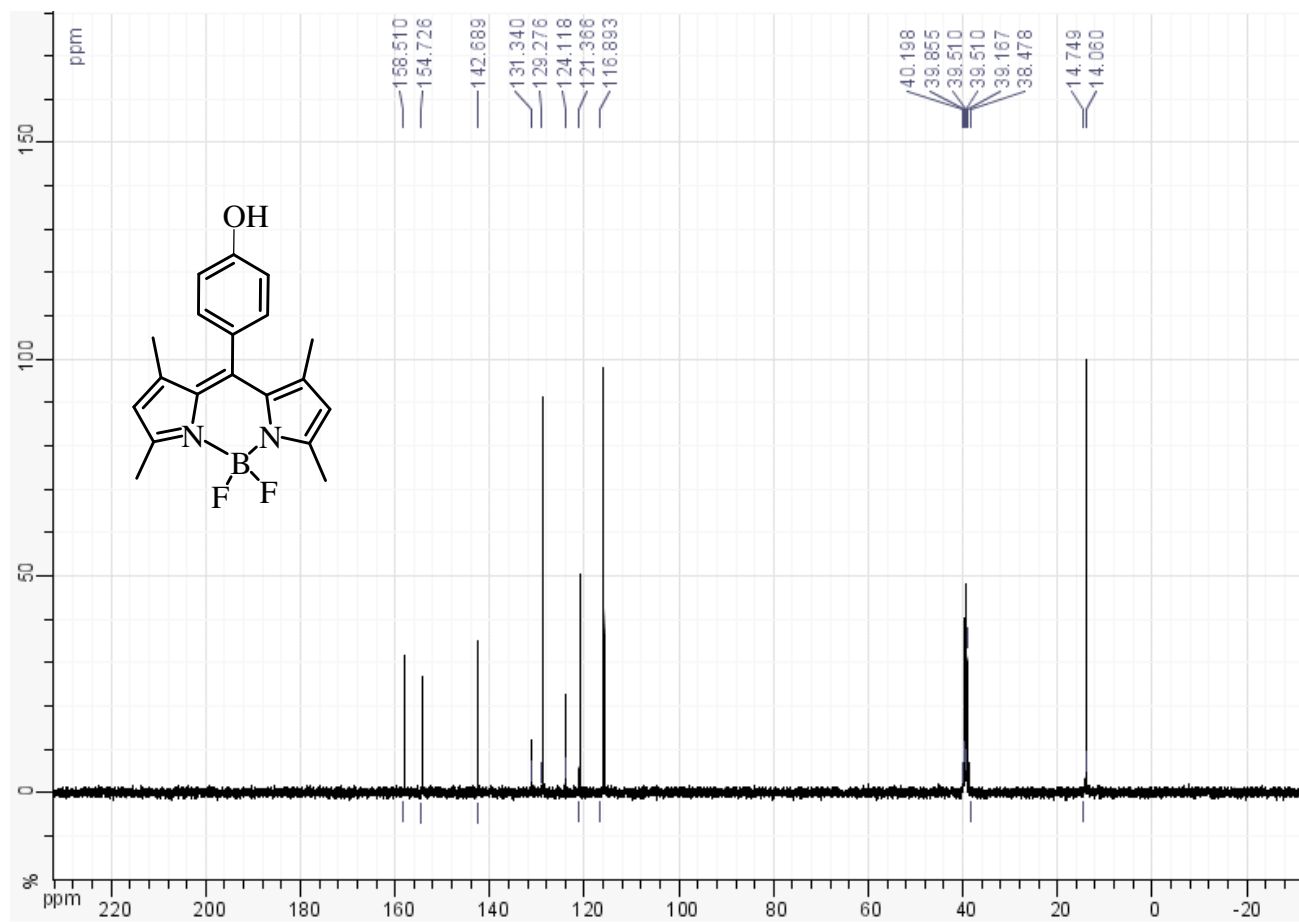
Figure A5 ^{13}C-NMR spectrum of **L1** in DMSO-d_6 with 400 MHz.
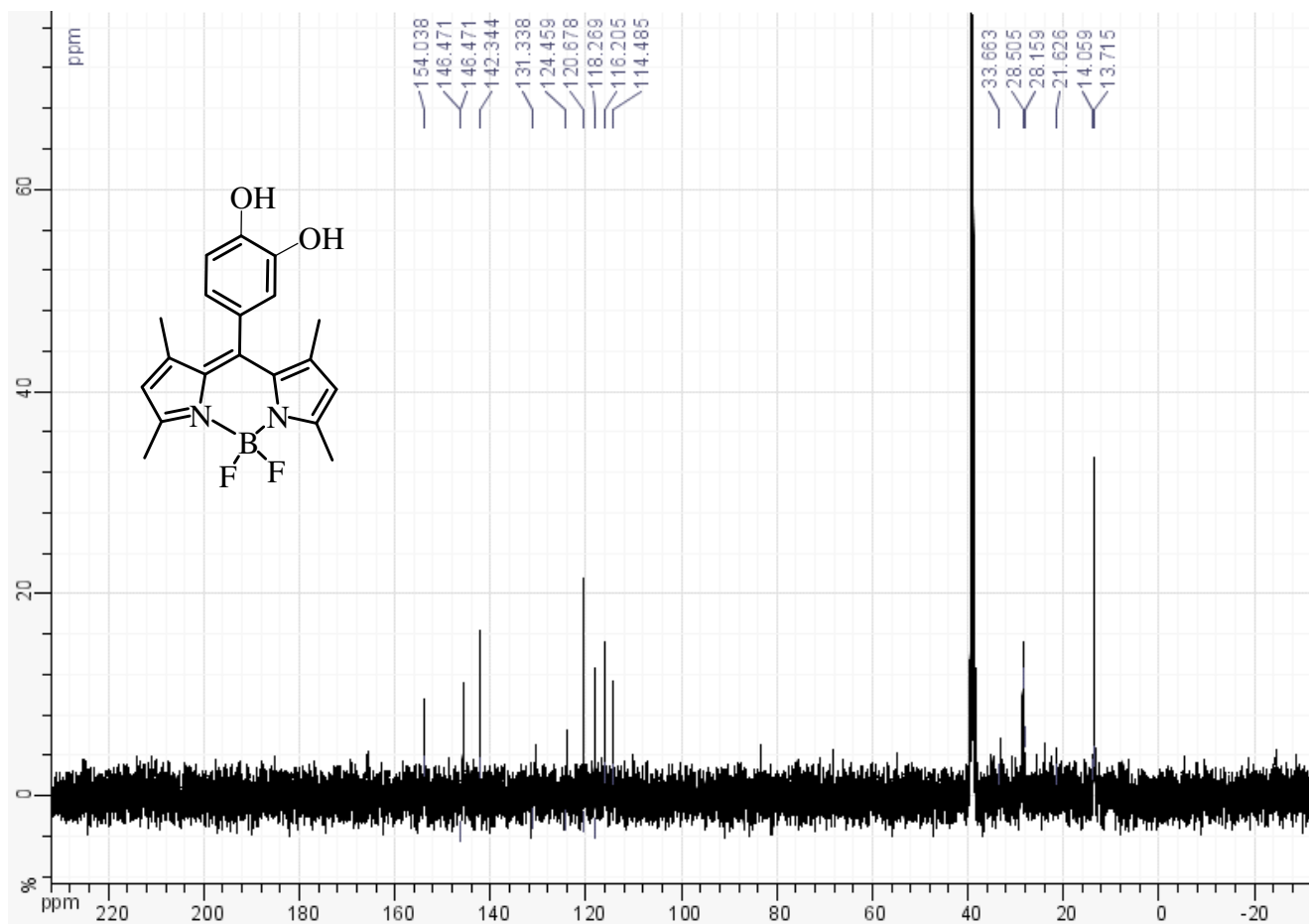
Figure A6 ^{13}C-NMR spectrum of **L2** in DMSO-d_6 with 400 MHz.
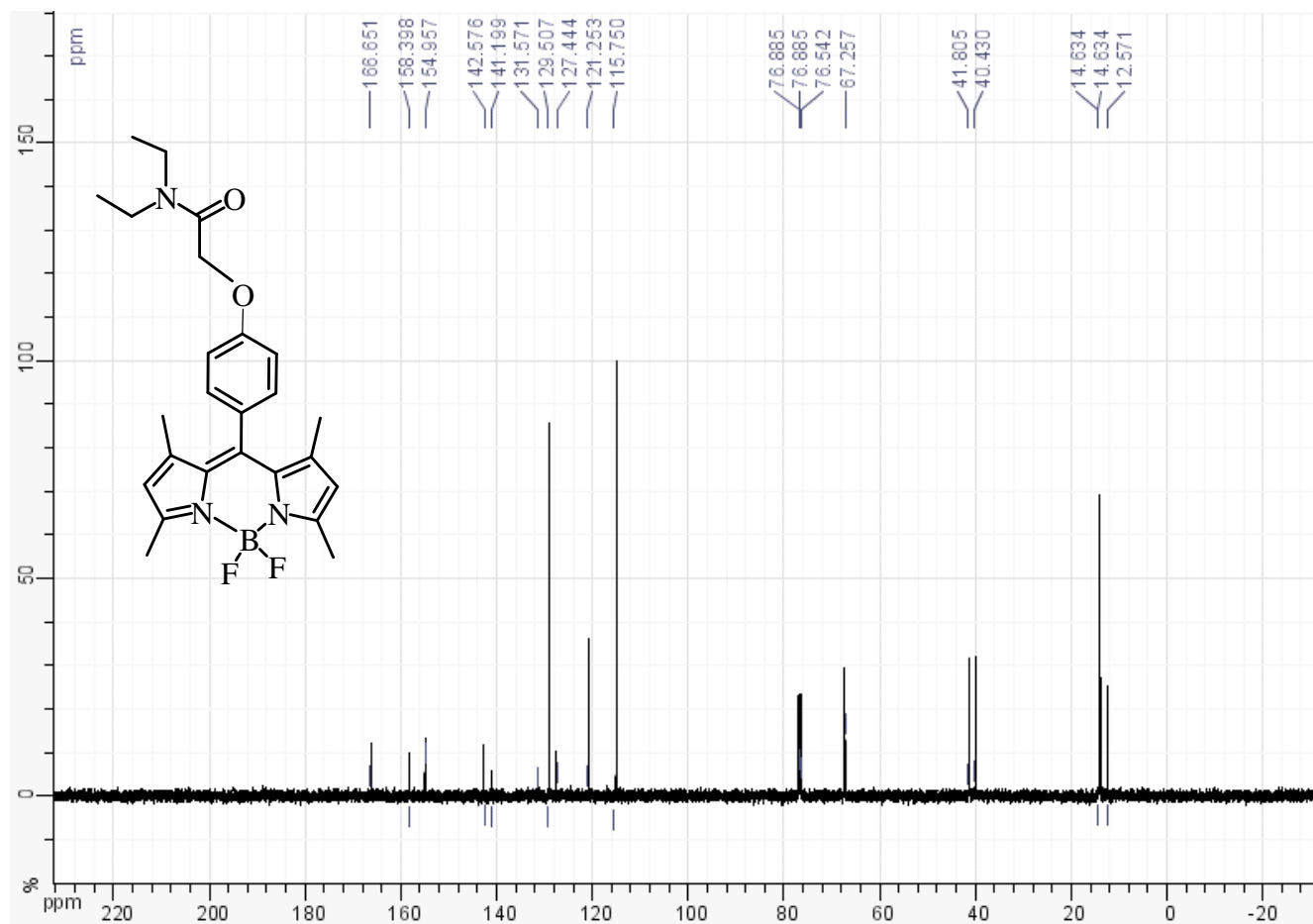
Figure A7 ^{13}C-NMR spectrum of **L3** in DMSO-d_6 with 400 MHz.
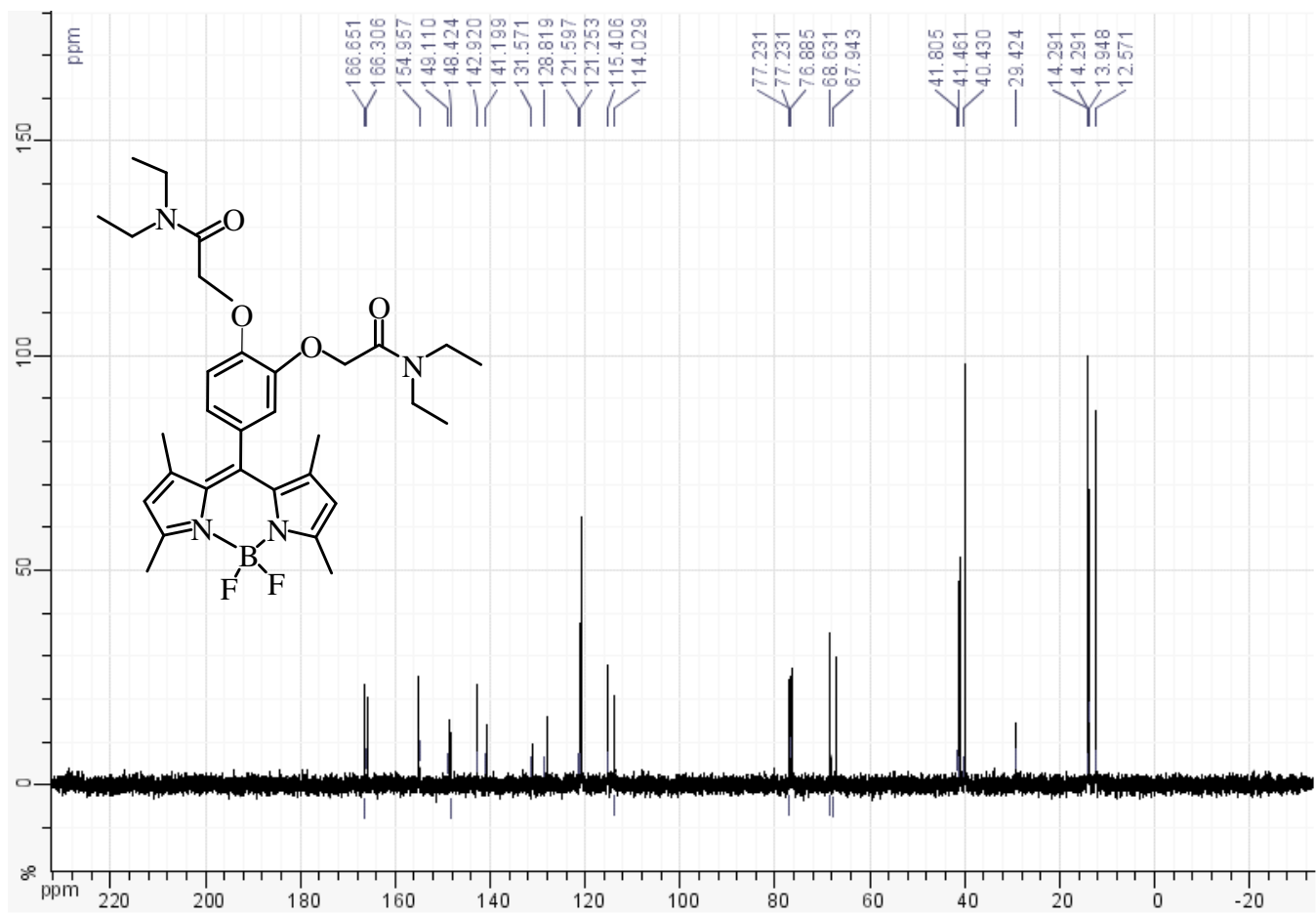
Figure A8 ^{13}C-NMR spectrum of **L4** in DMSO-d_6 with 400 MHz.
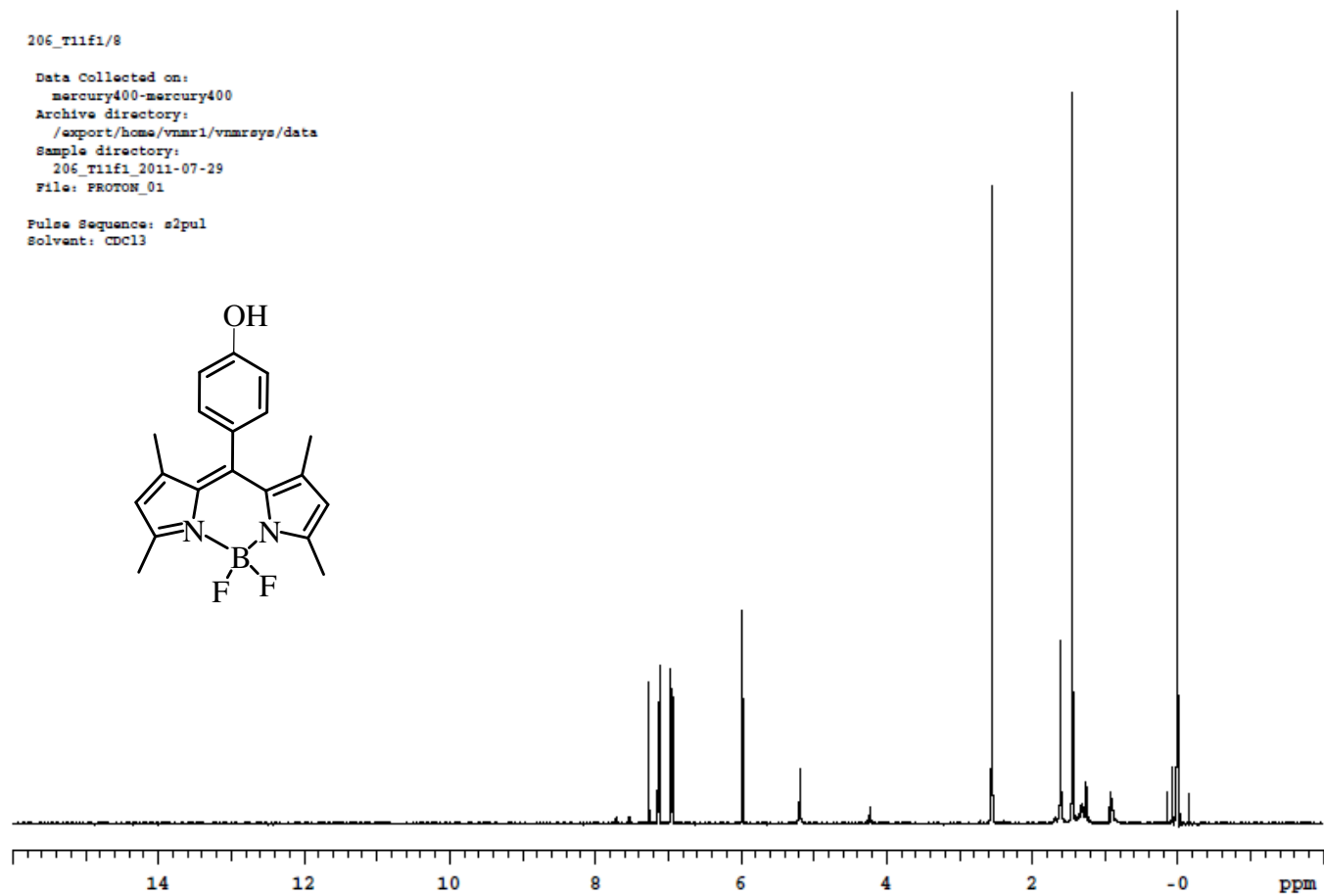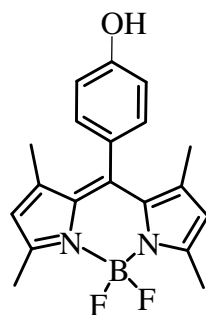
Figure A9 ^{1}H-NMR spectrum of **L1** in CDCl$_3$ with 400 MHz.
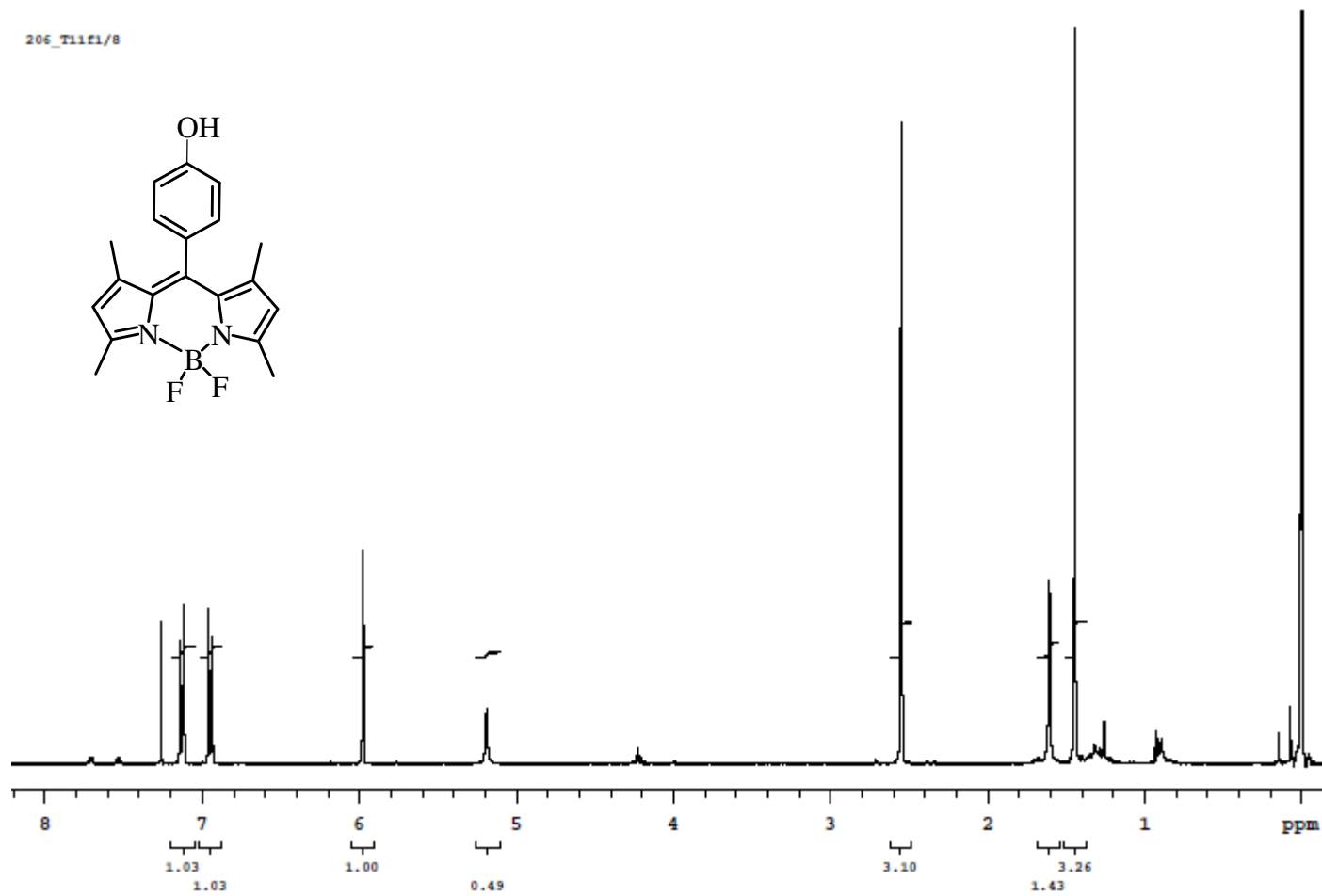
Figure A10 ^{1}H-NMR spectrum of **L1** in CDCl$_3$ with 400 MHz.
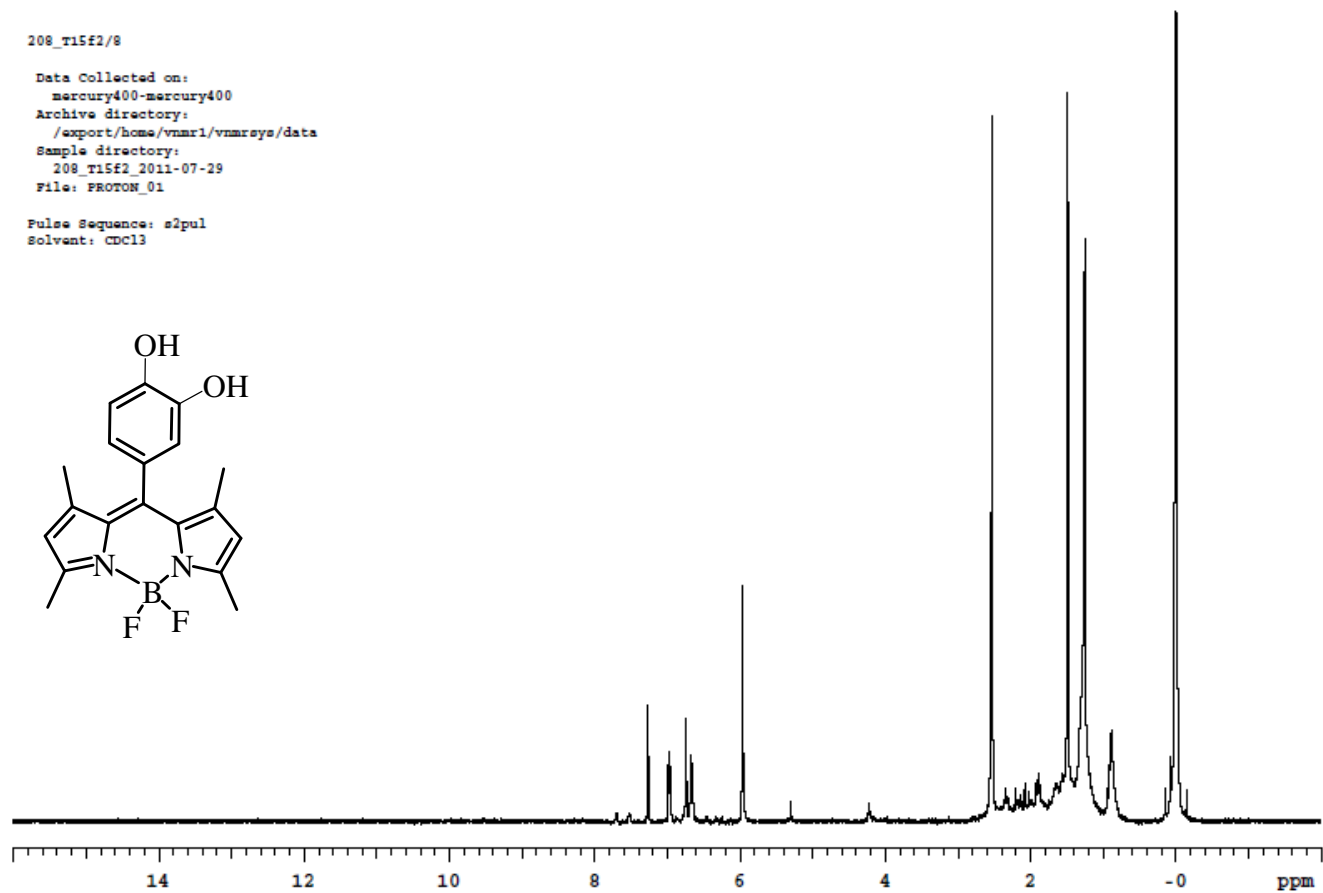
Figure A11 ^{1}H-NMR spectrum of **L**2 in CDCl$_3$ with 400 MHz.
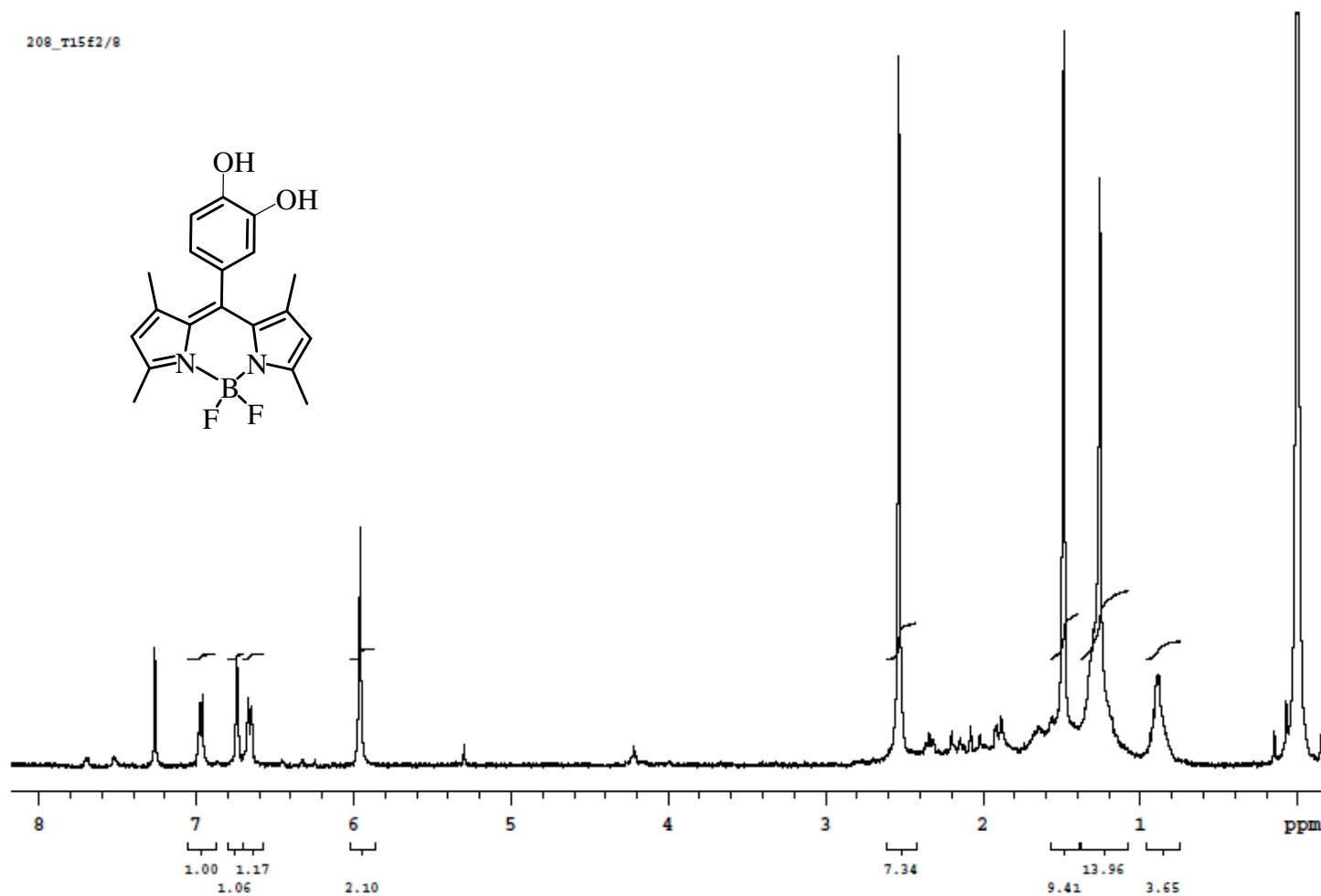
Figure A12 ^{1}H-NMR spectrum of **L2** in CDCl$_3$ with 400 MHz.
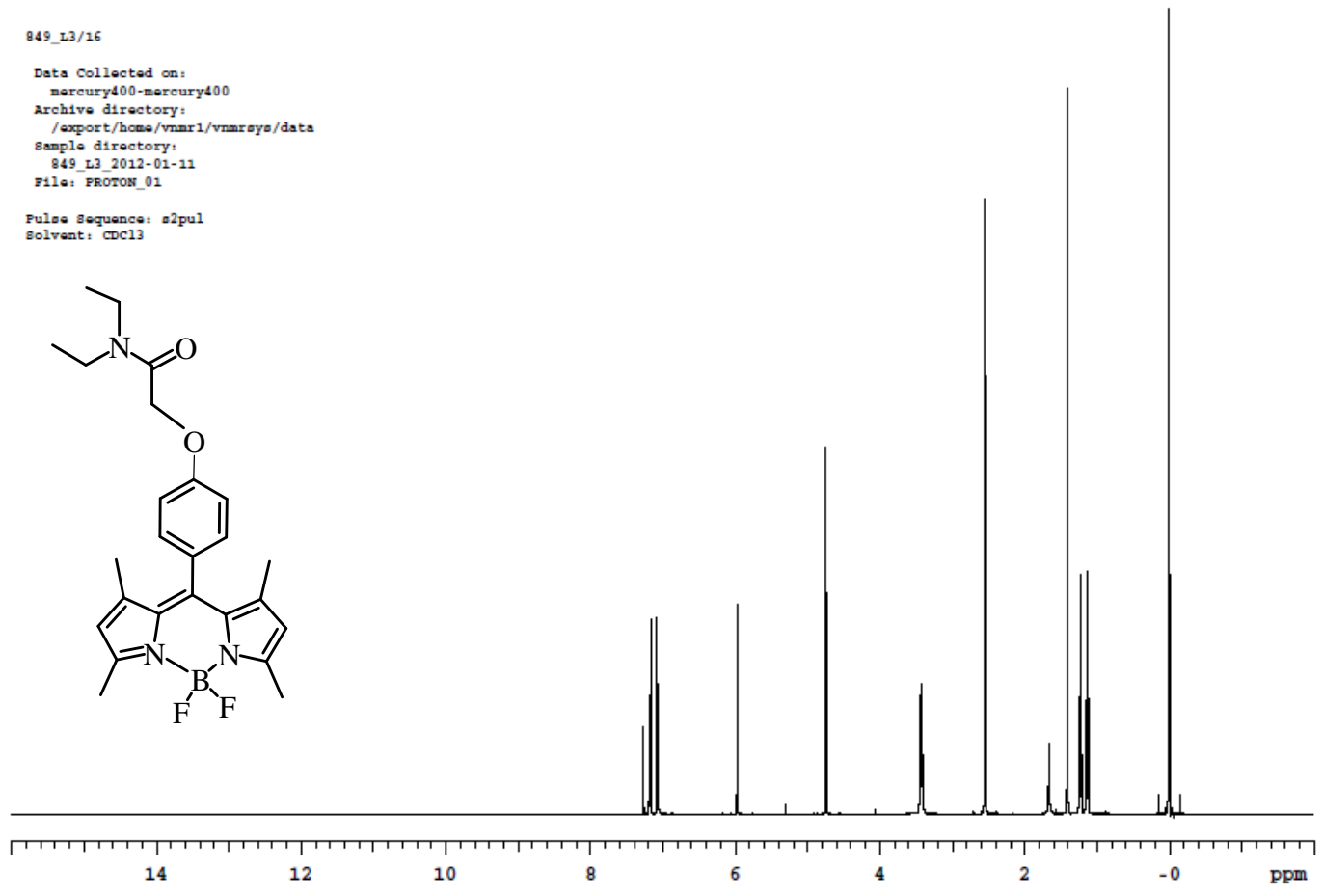
Figure A13 ^{1}H-NMR spectrum of **L**3 in CDCl$_3$ with 400 MHz.
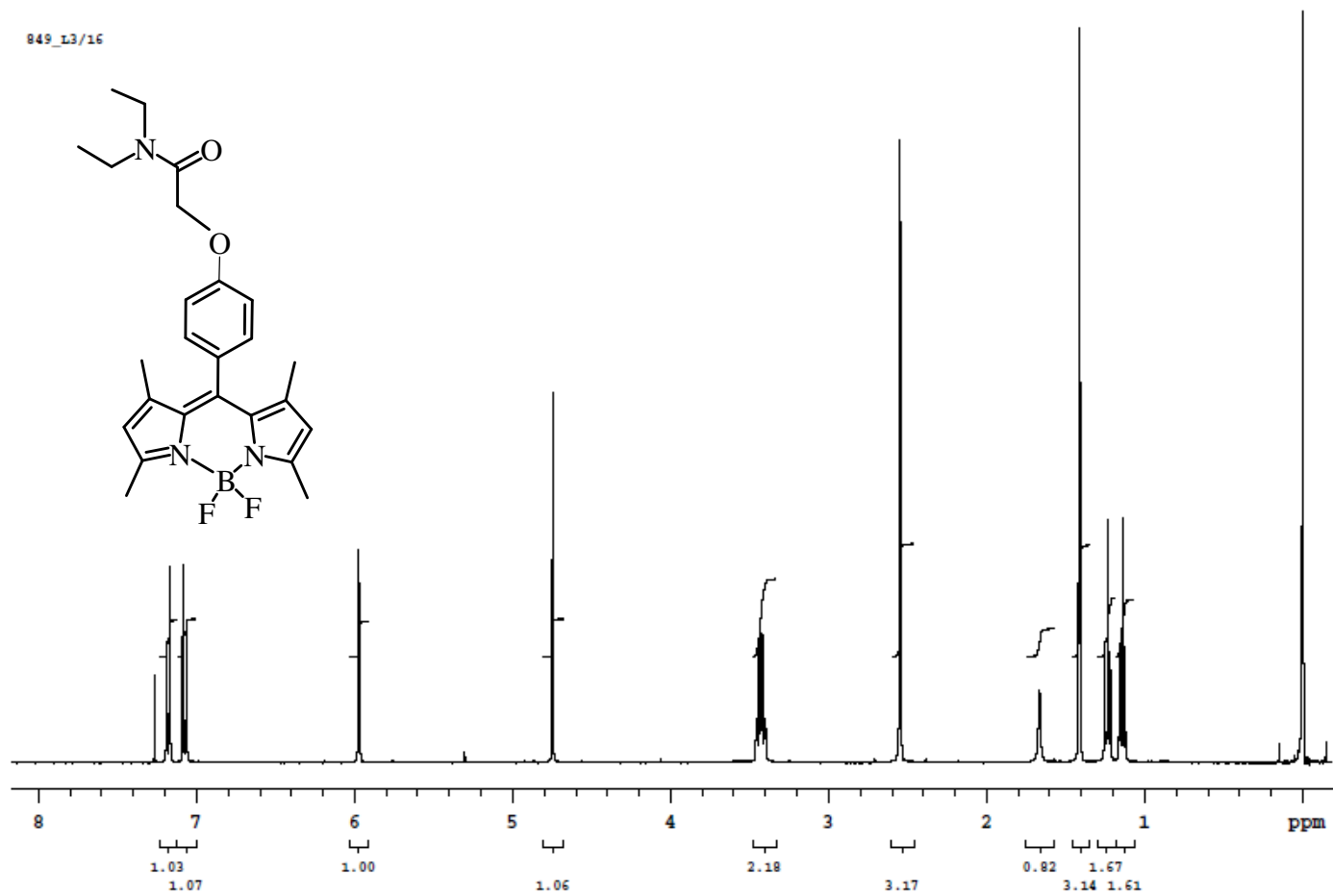
Figure A14 ^{1}H-NMR spectrum of **L3** in CDCl$_3$ with 400 MHz.
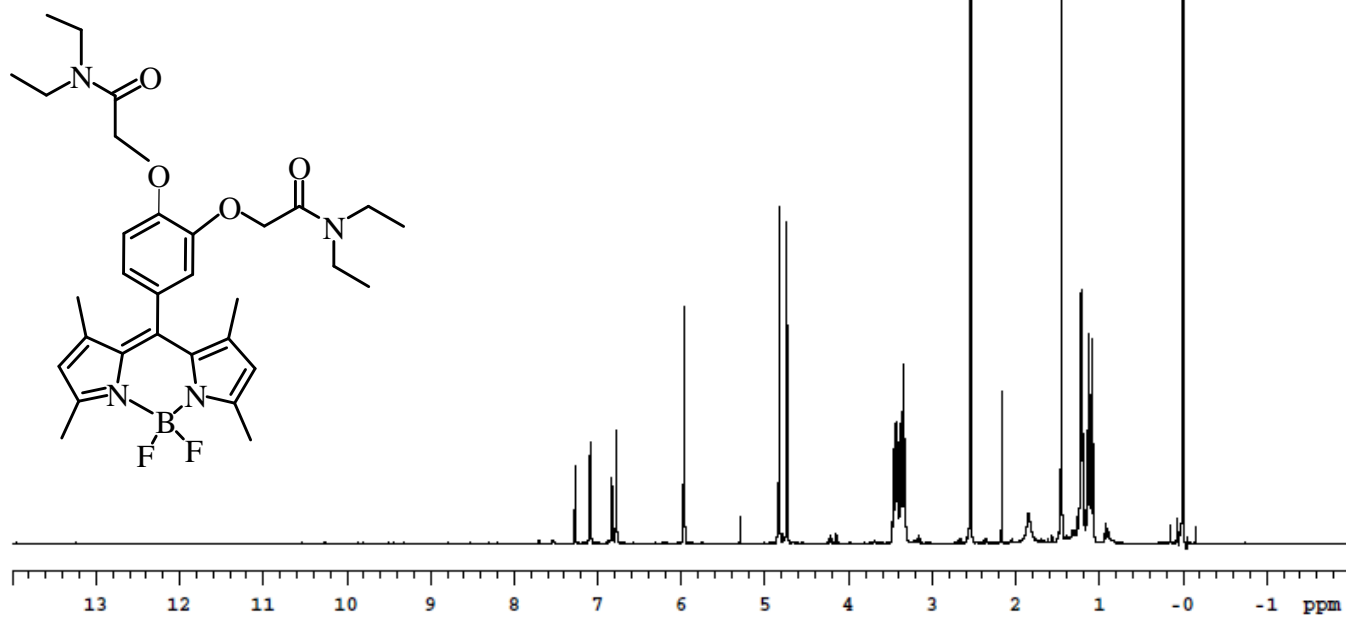
Figure A15 ^{1}H-NMR spectrum of **L**4 in CDCl₃ with 400 MHz.
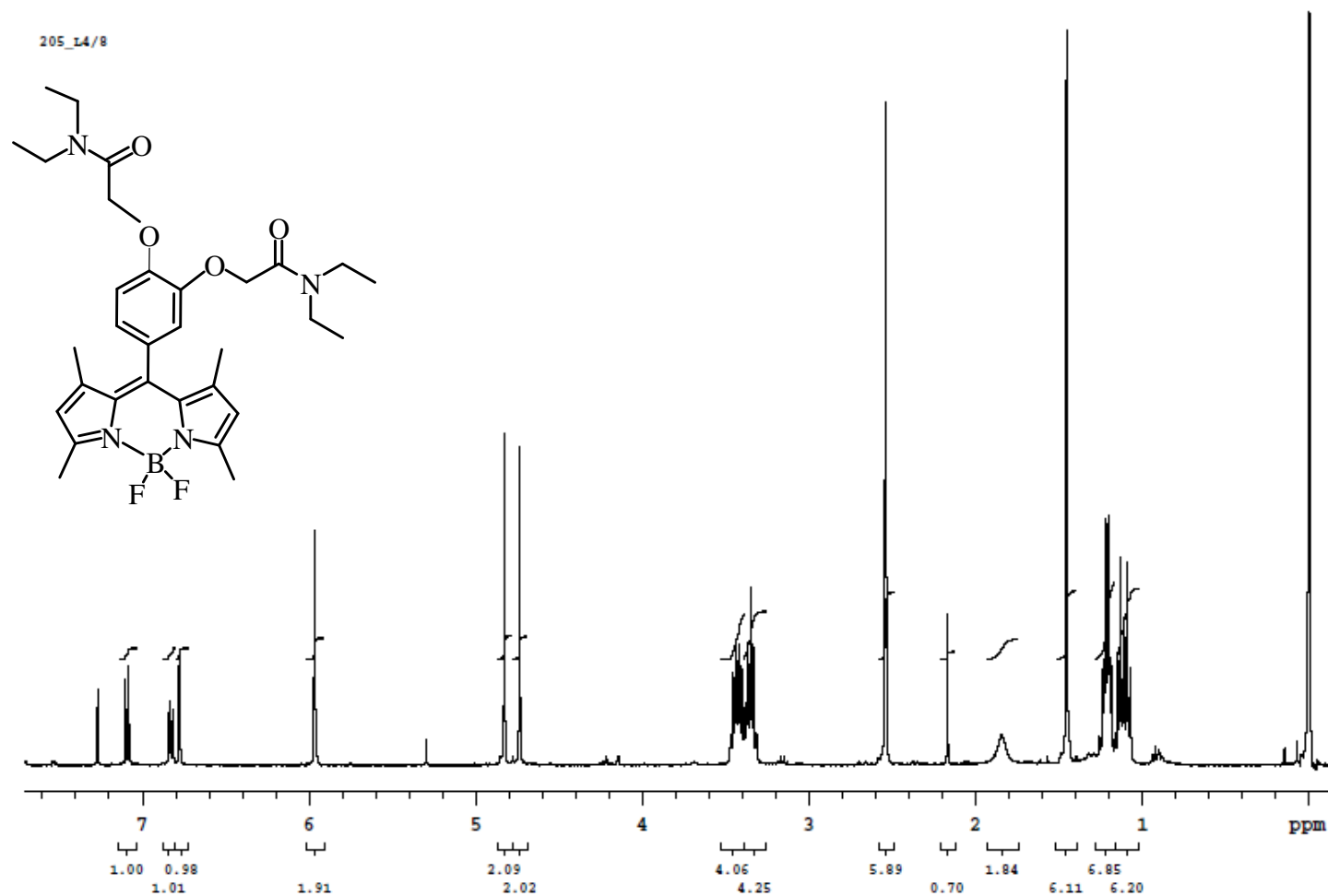
Figure A16 ^{1}H-NMR spectrum of **L4** in CDCl$_3$ with 400 MHz.
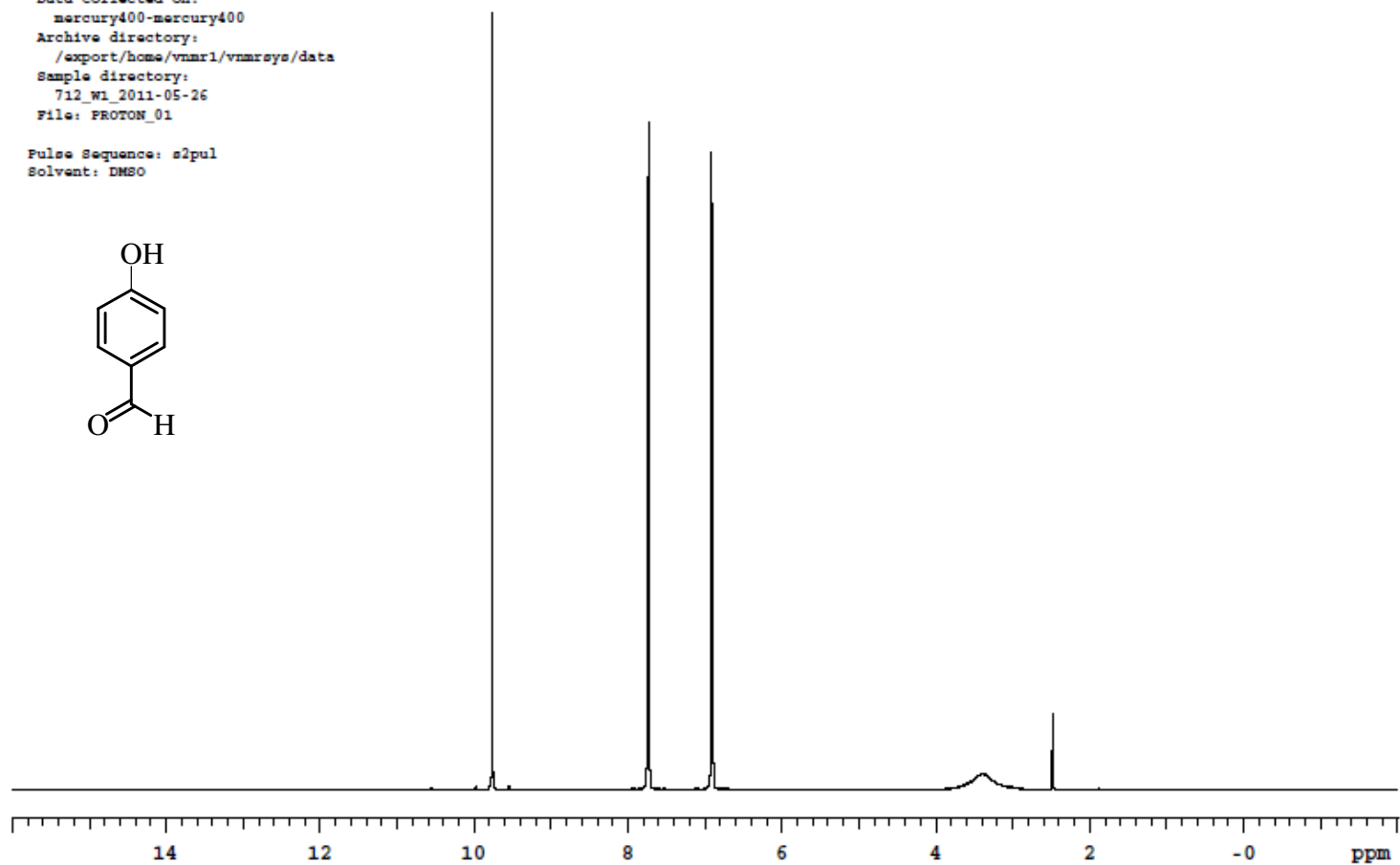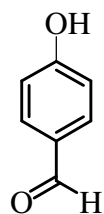
Figure A17 ^{1}H-NMR spectrum of compound **1** in DMSO-d_6 with 400 MHz.
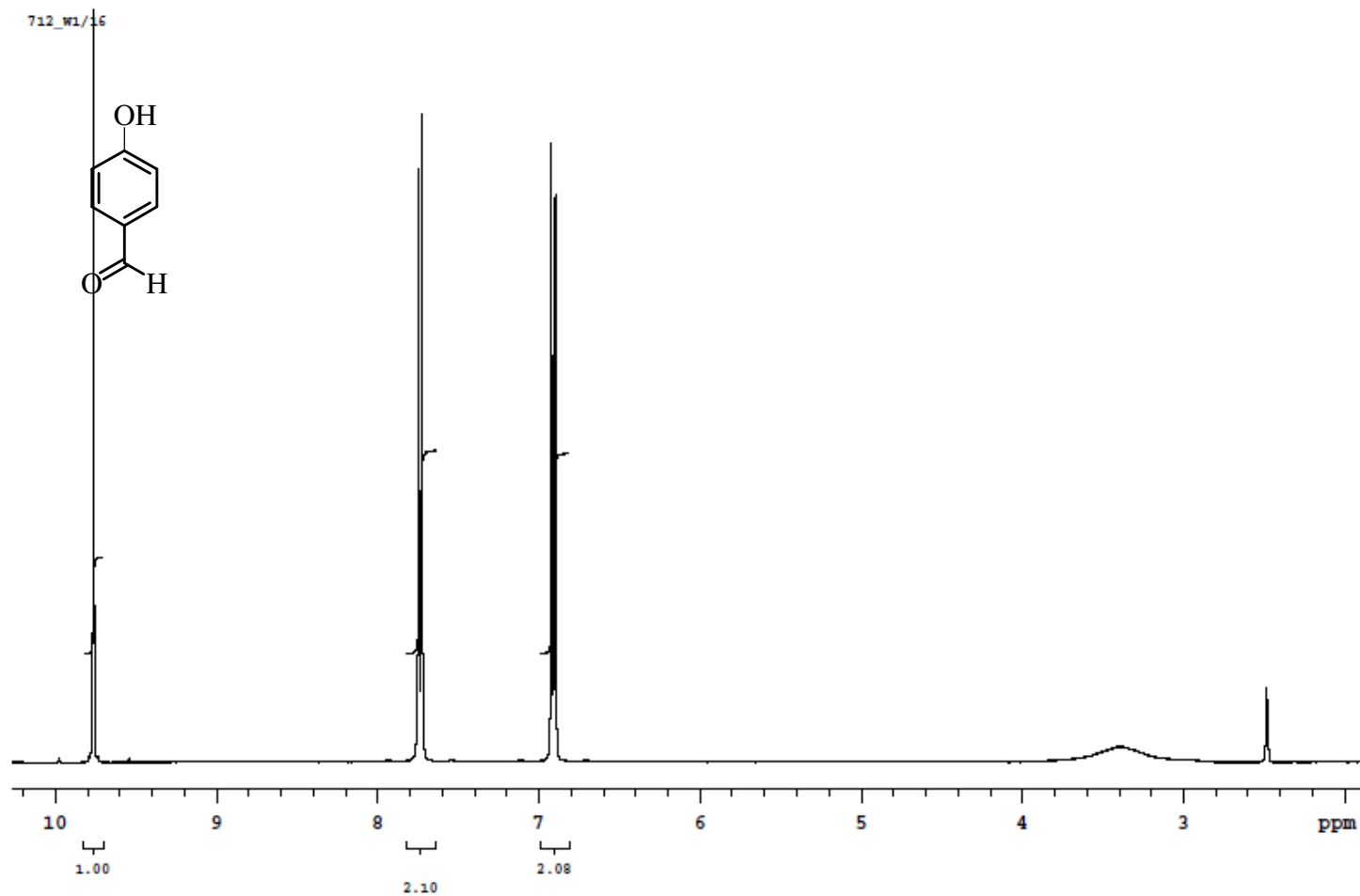
Figure A18 ^{1}H-NMR spectrum of compound **1** in DMSO-d_6 with 400 MHz.
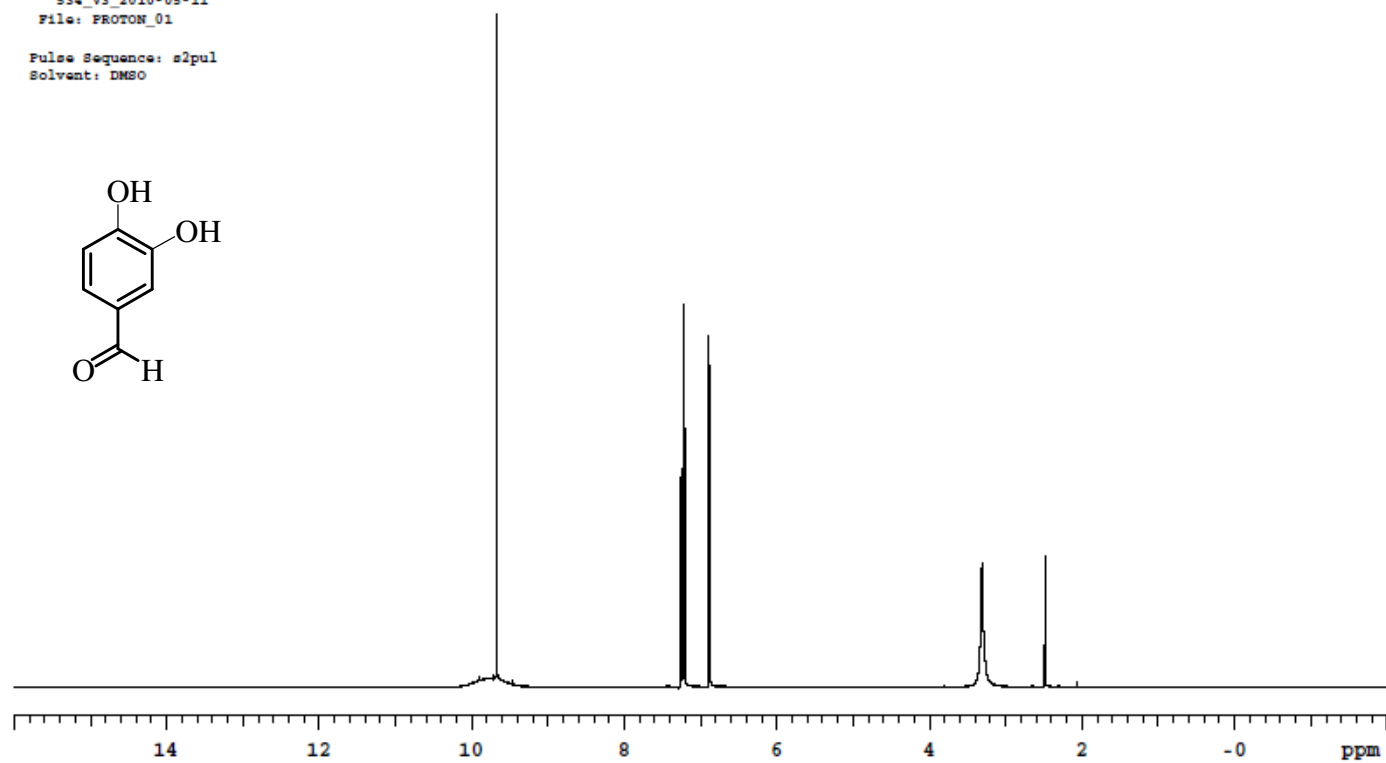
Figure A19 ^{1}H-NMR spectrum of compound **2** in DMSO-d_6 with 400 MHz.
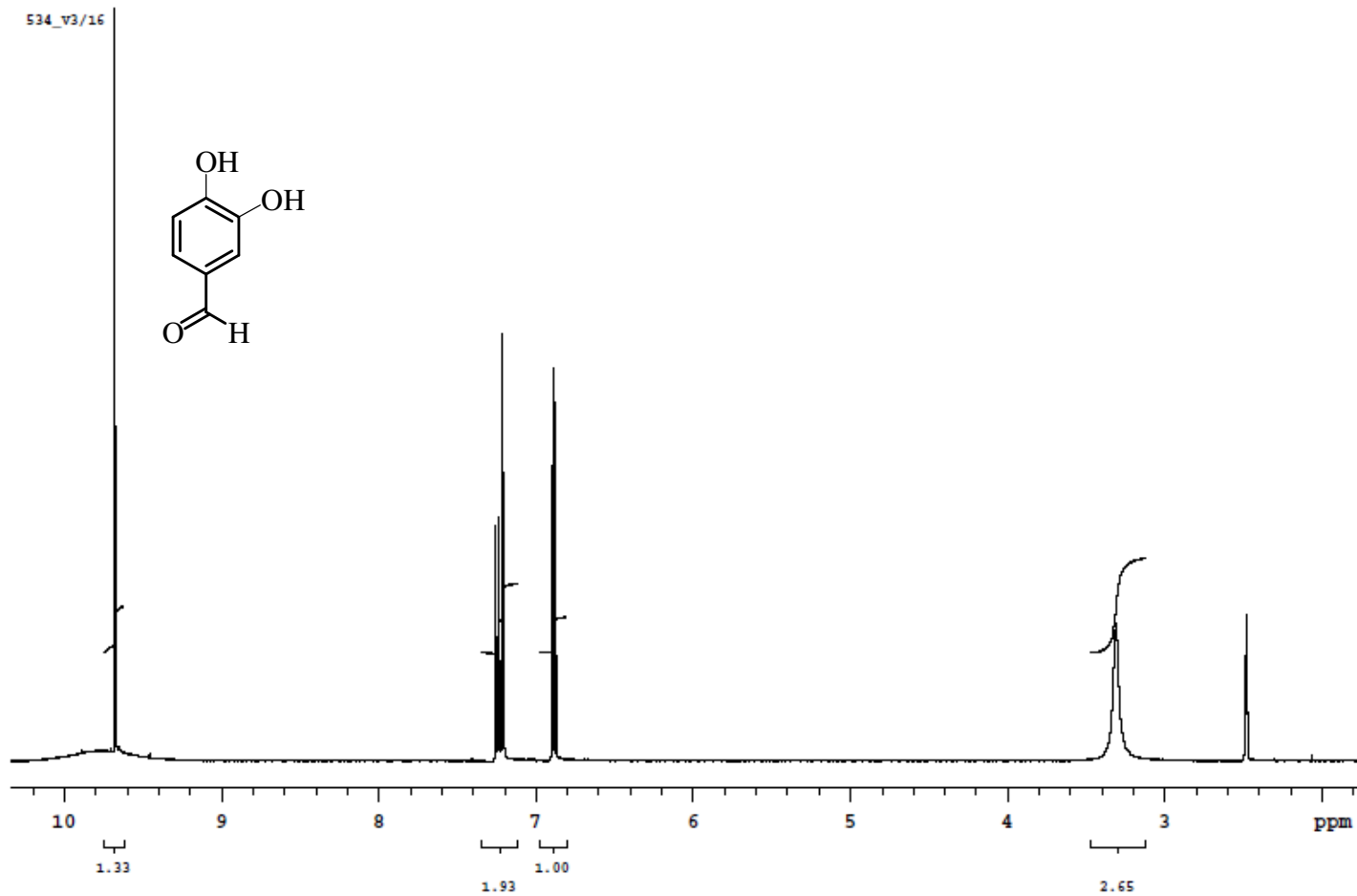
Figure A20 ^{1}H-NMR spectrum of compound **2** in DMSO-d_6 with 400 MHz.

Figure A21 ^{1}H-NMR spectrum of compound **3** in CDCl$_3$ with 400 MHz.

JJ1

Data Collected on:
  mercury400-mercury400
Archive directory:
  /export/home/cpuser/vnmrsys/data
Sample directory:
  sm002_2018-07-03
File: PROTON_01

Pulse Sequence: s2pul
Solvent: CDCl3

Temp. 0.0 C / 273.1 K

Relax. delay 1.000 sec
Pulse 45.0 degrees
Acq. time 1.995 sec
Width 6389.8 Hz
8 repetitions
OBSERVE   H1, 399.8626601 MHz
DATA PROCESSING
FT size 32768
Total time 0 min

| 13 | 12 | 11 | 10 | 9 | 8 | 7 | 6 | 5 | 4 | 3 | 2 | 1 | -0 | -1 | ppm |

0.09   0.85 -0.01   15.75   0.01   41.65
    1.00 0.03 3.56   28.26   1.16   7.64
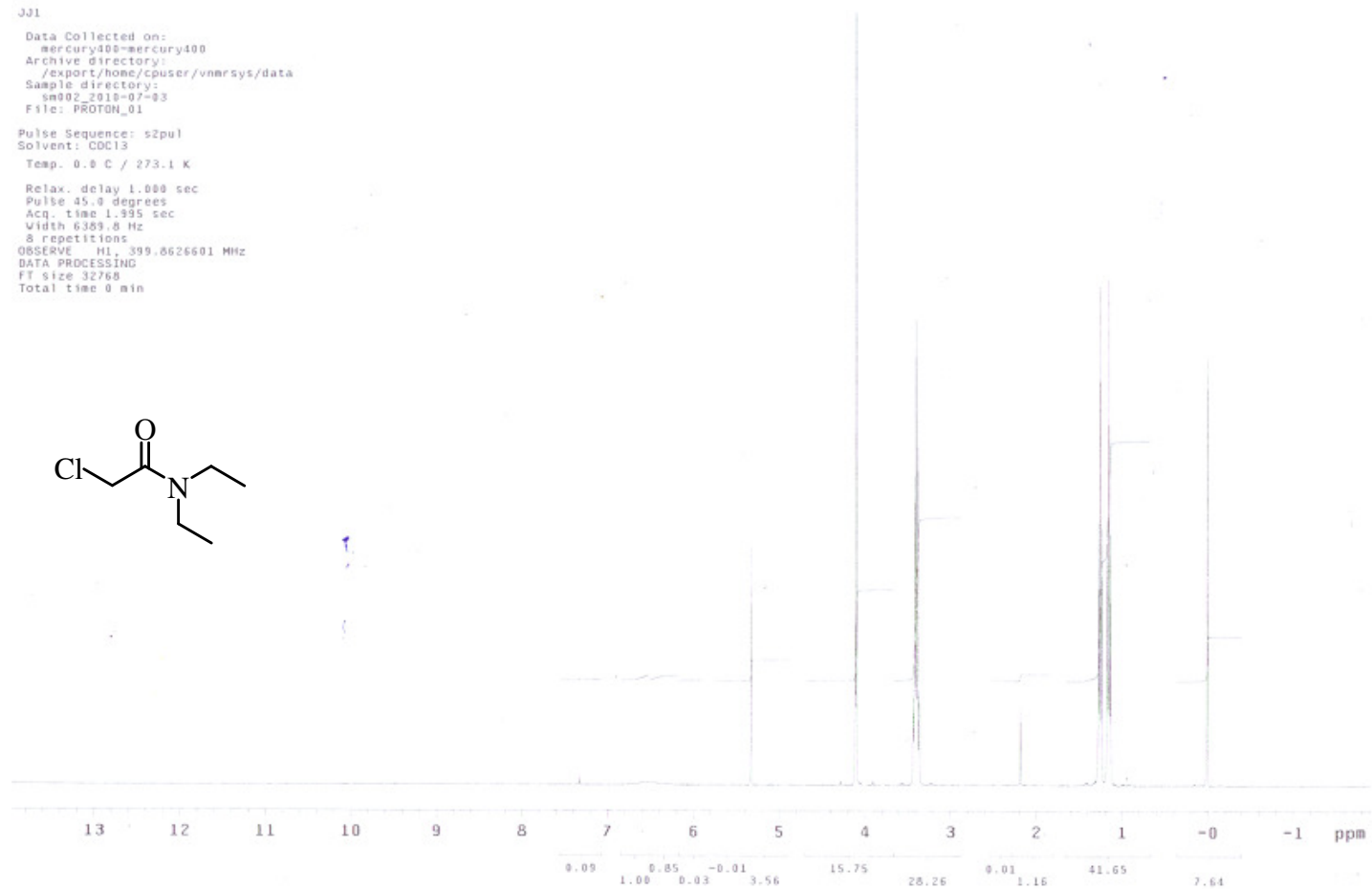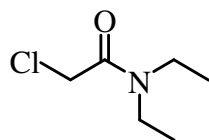
Figure A22 ^{1}H-NMR spectrum of compound **3** in CDCl$_3$ with 400 MHz.

Data Collected on:
mercury400-mercury400
Archive directory:
/export/home/cpuser/vnmrsys/data
Sample directory:
sm005_2010-07-03
File: PROTON_01

Pulse Sequence: s2pul
Solvent: CDCl3

Relax. delay 1.000 sec
Pulse 45.0 degrees
Acq. time 1.995 sec
Width 6389.8 Hz
8 repetitions
OBSERVE   H1, 399.8626597 MHz
DATA PROCESSING
FT size 32768
Total time 0 min
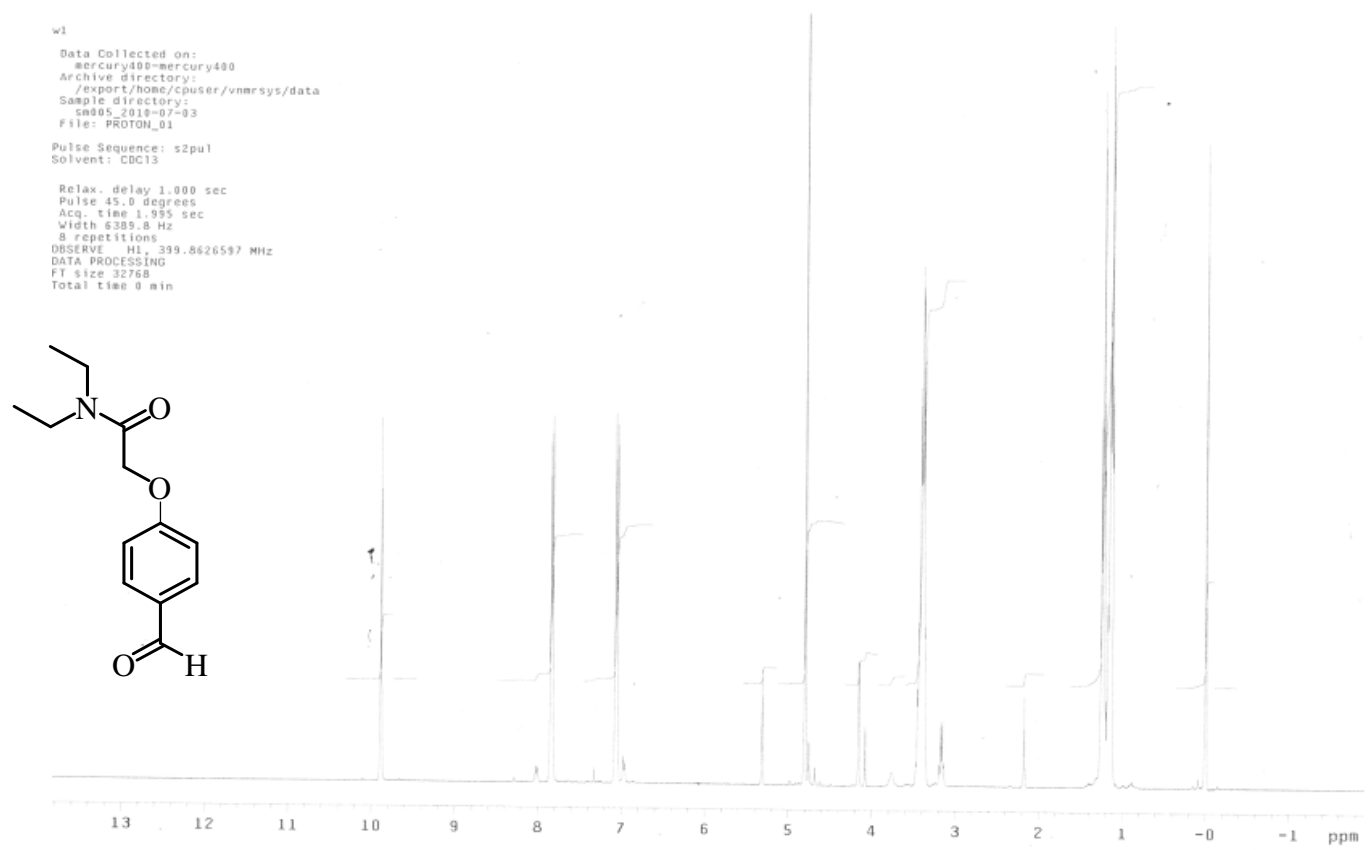
Figure A23 ^{1}H-NMR spectrum of compound 4 in CDCl$_3$ with 400 MHz.

Data Collected on:
 mercury400-mercury400
Archive directory:
 /export/home/cpuser/vnmrsys/data
Sample directory:
 sm005_2010-07-03
File: PROTON_01

Pulse Sequence: s2pul
Solvent: CDCl3

Temp. 0.0 C / 273.1 K

Relax. delay 1.000 sec
Pulse 45.0 degrees
Acq. time 1.995 sec
Width 6389.8 Hz
8 repetitions
OBSERVE   H1, 399.8626597 MHz
DATA PROCESSING
FT size 32768
Total time 0 min
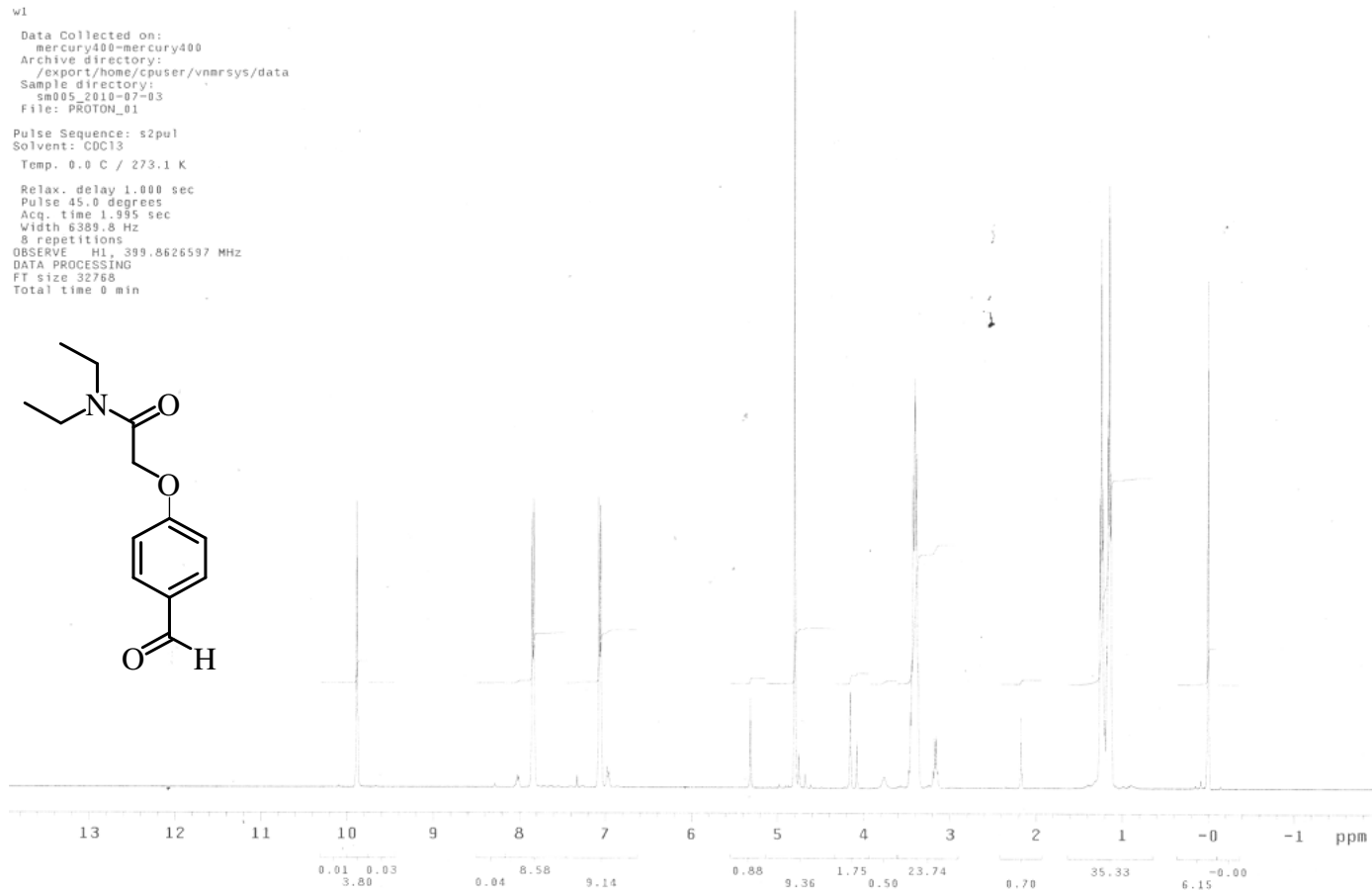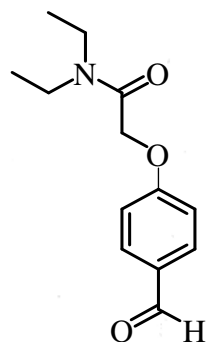
Figure A24 ^{1}H-NMR spectrum of compound **4** in CDCl$_3$ with 400 MHz.

Mahasarakham University
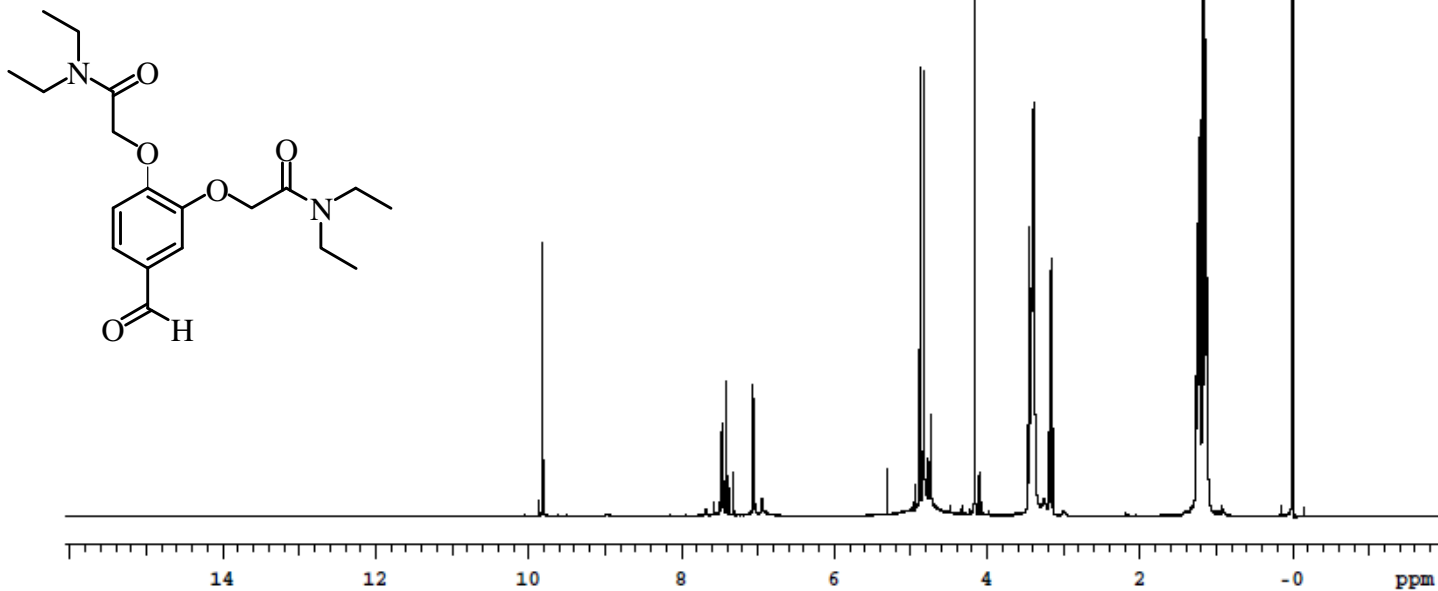
Figure A25 ^{1}H-NMR spectrum of compound **5** in CDCl$_3$ with 400 MHz.
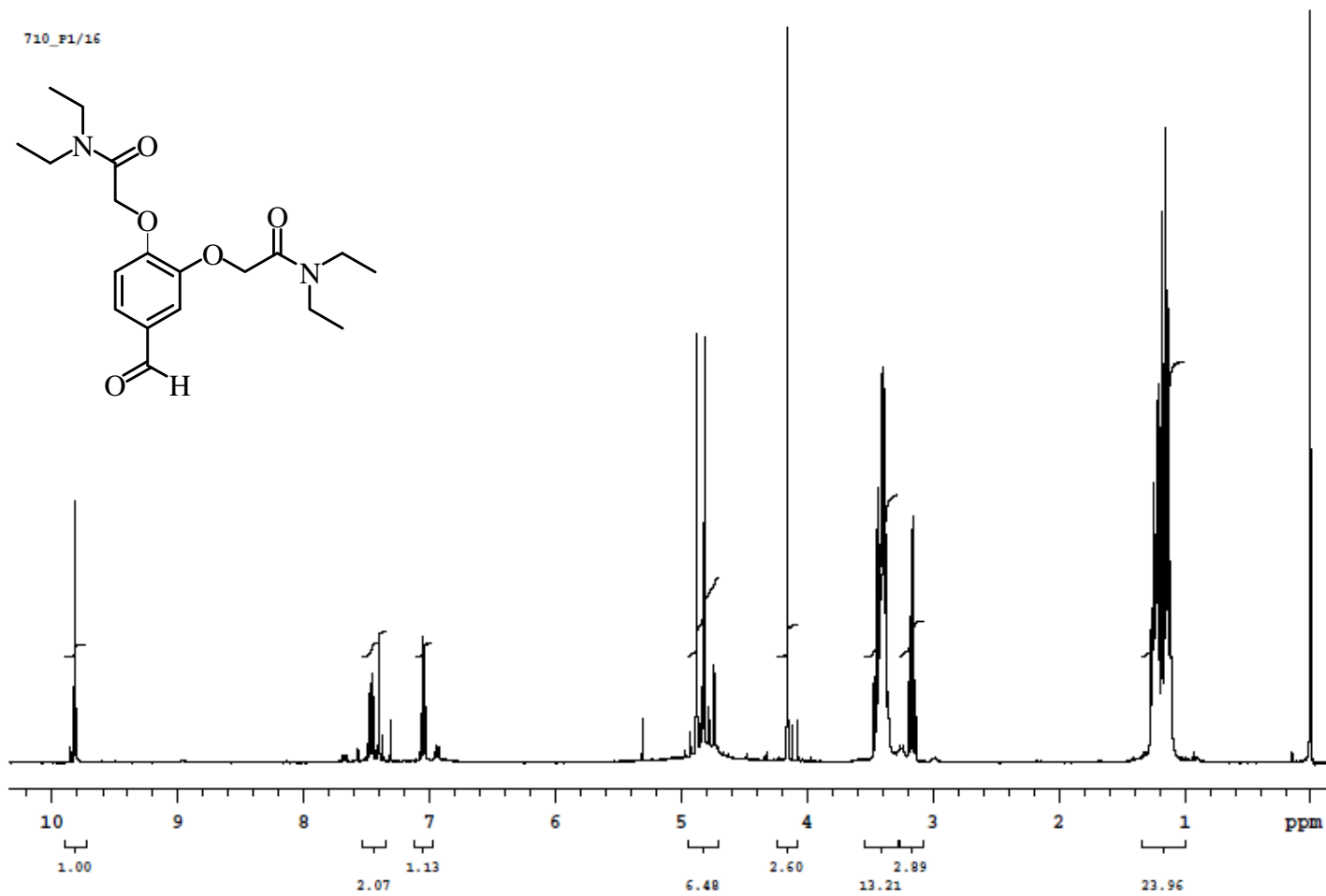
Figure A26 ^{1}H-NMR spectrum of compound **5** in CDCl$_3$ with 400 MHz.
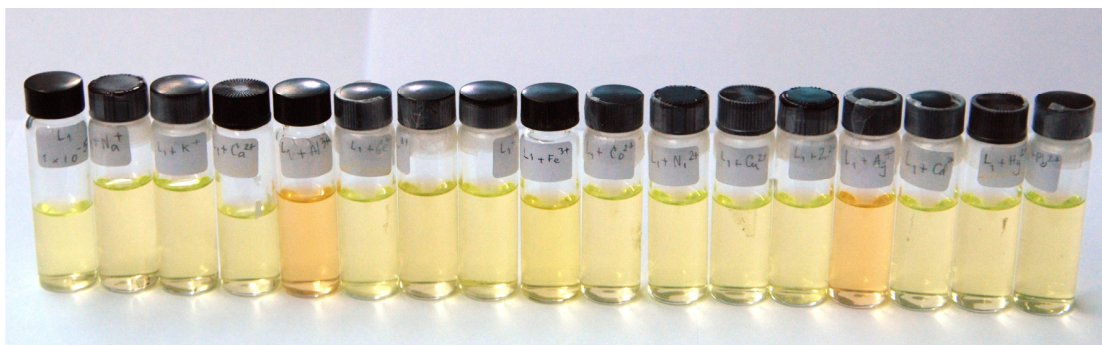
Figure A27 The color change of **L1** upon addition of 1.0×10^{-5} M different metal ions.

Figure A28 The color change of **L2** upon addition of 1.0×10^{-5} M different metal ions.
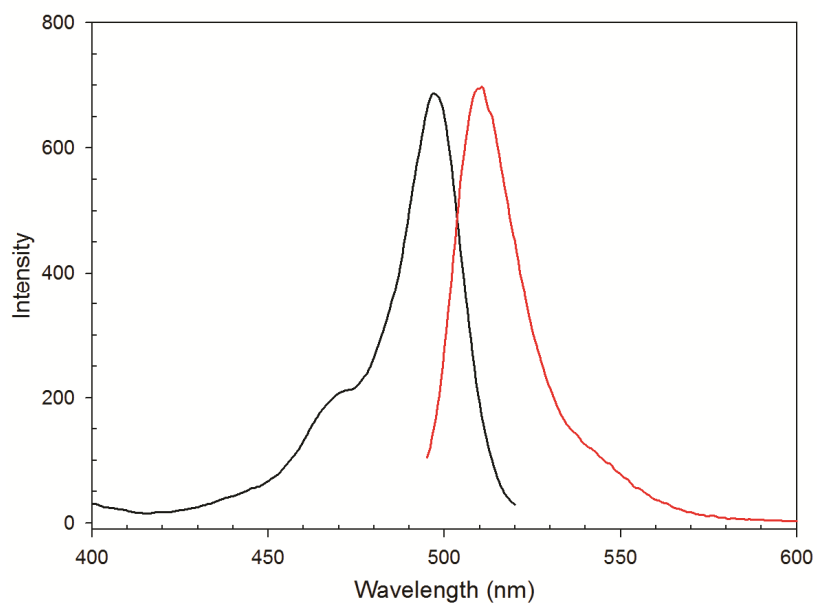
Figure A29 Absorption (black curve) and fluorescence (red curve) spectra recorded for receptor **L1** in MeOH at room temperature. The excitation wavelength was 450 nm.
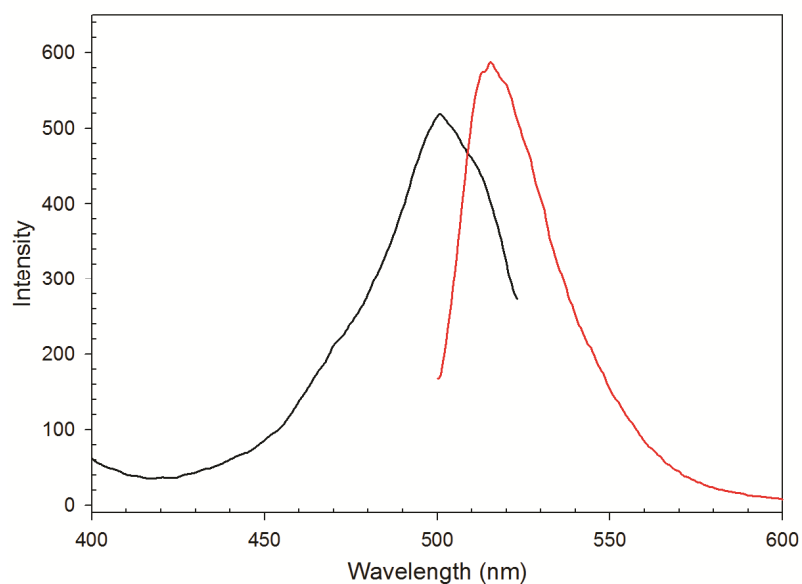
Figure A30 Absorption (black curve) and fluorescence (red curve) spectra recorded for receptor **L2** in MeOH at room temperature. The excitation wavelength was 450 nm.
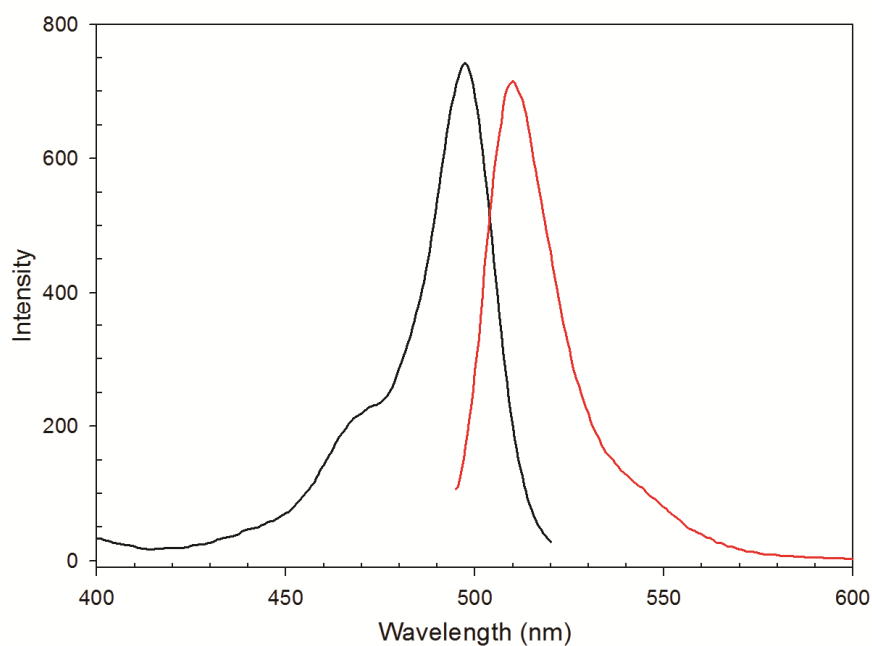
Figure A31 Absorption (black curve) and fluorescence (red curve) spectra recorded for
receptor **L3** in MeOH at room temperature. The excitation wavelength
was 450 nm.
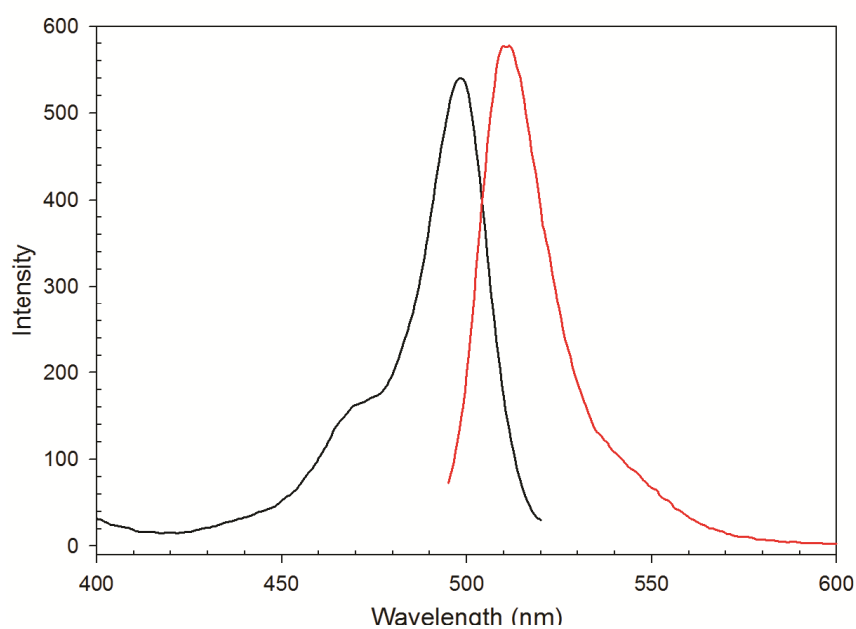
Figure A32 Absorption (black curve) and fluorescence (red curve) spectra recorded for
receptor **L4** in MeOH at room temperature. The excitation wavelength
was 450 nm.

APPENDIX B
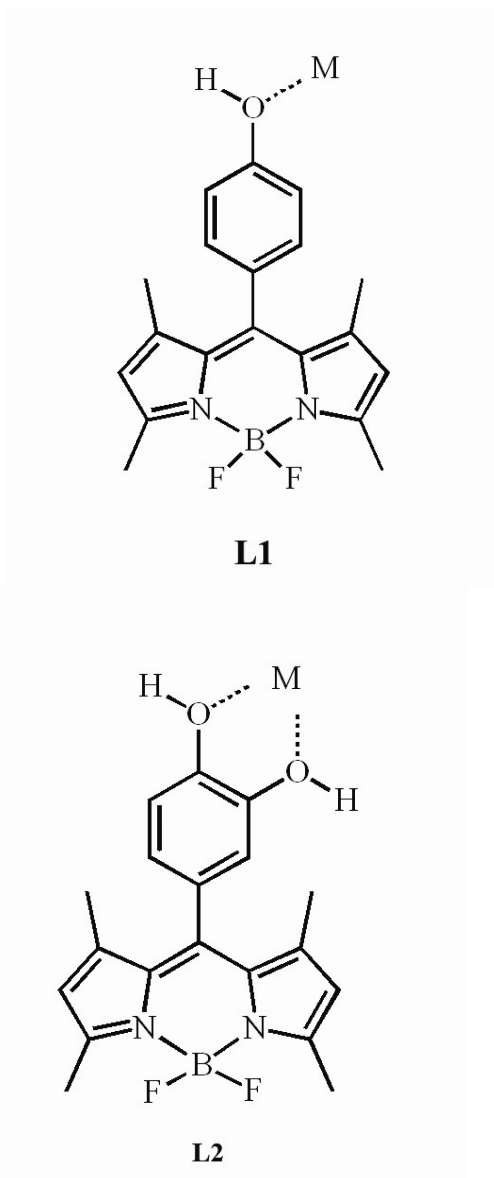
Figure B1 Proposed binding modes of receptors **L1**and **L2** complexes with cation.
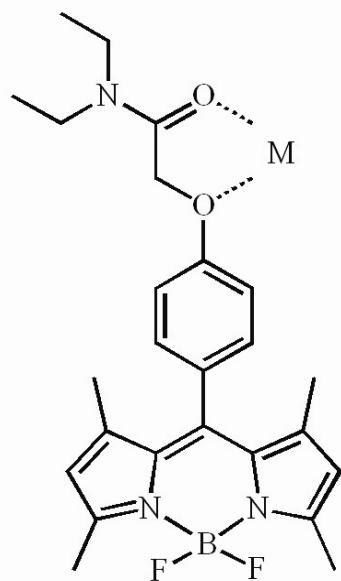
L3
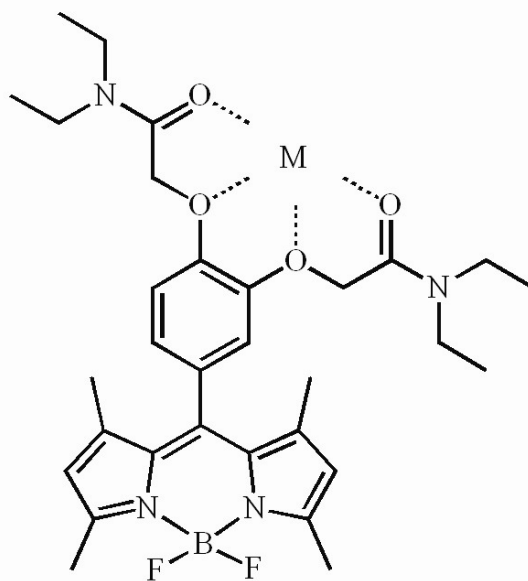
L4

Figure B2 Proposed binding modes of receptors **L3**and **L4** complexes with cation.
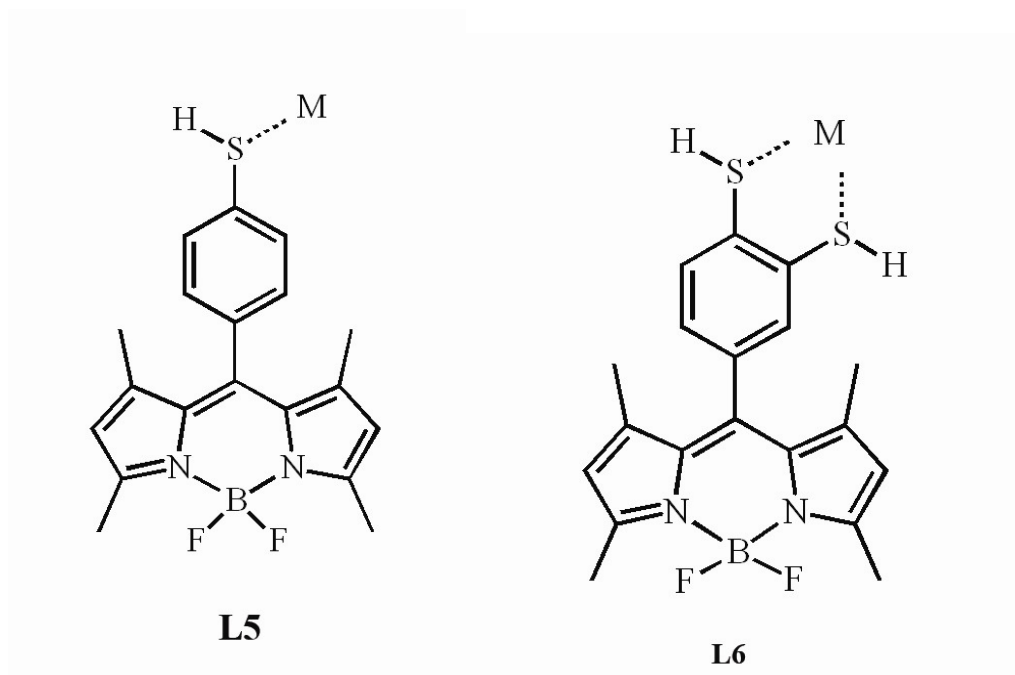
Figure B3 Proposed binding modes of receptors **L5** and **L6** complexes with cation.
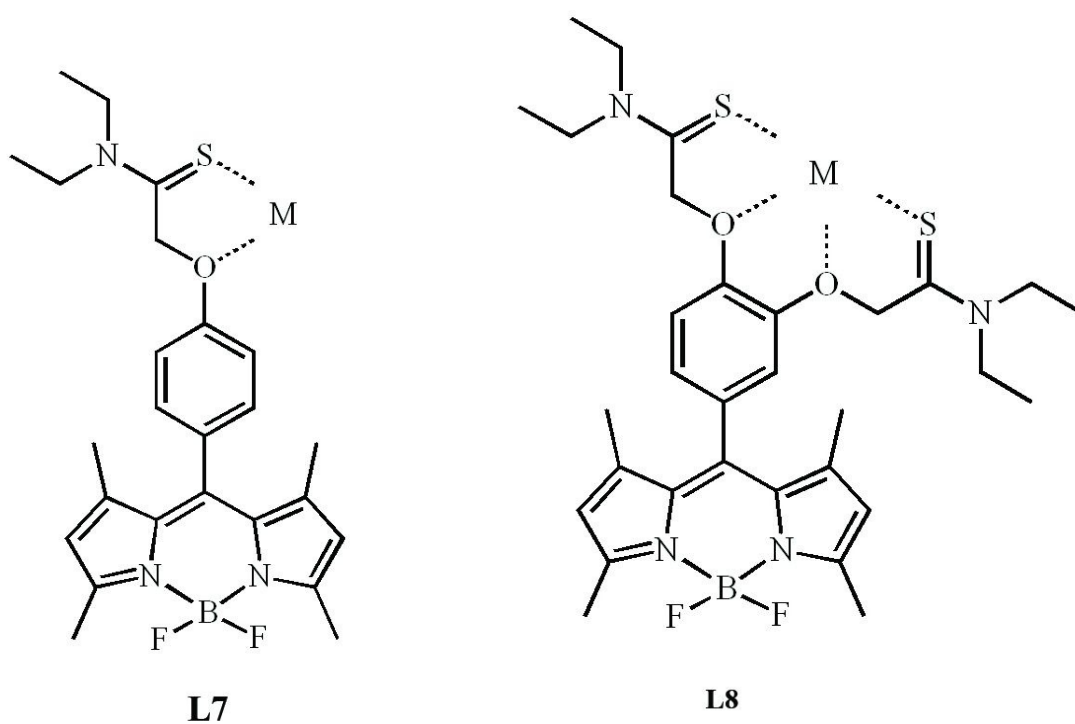
Figure B4 Proposed binding modes of receptors **L7** and **L8** complexes with cation.
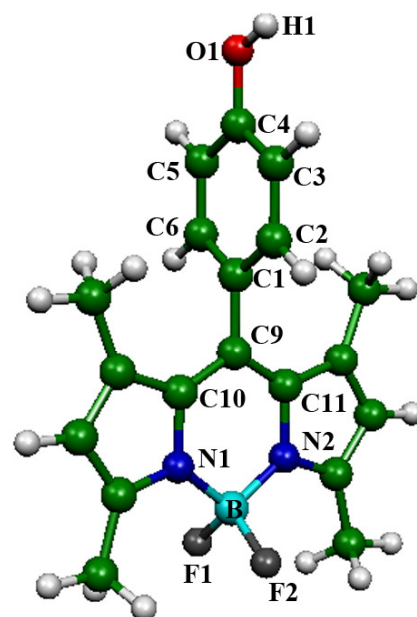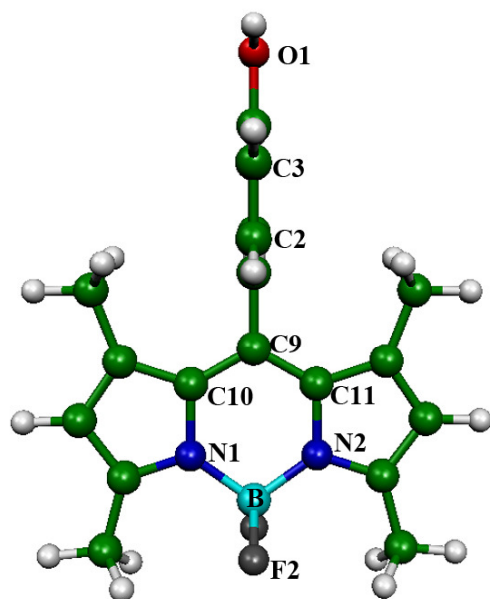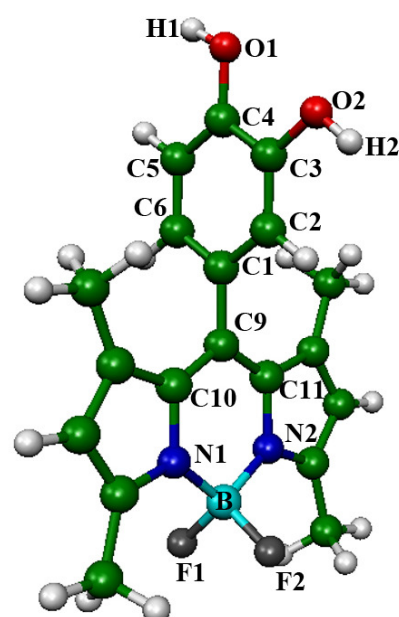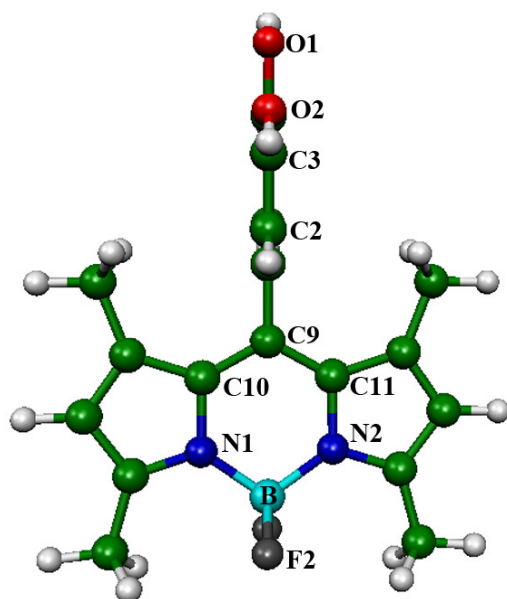
Figure B5 Atomic labeling of receptors **L1** and **L2**.

L3
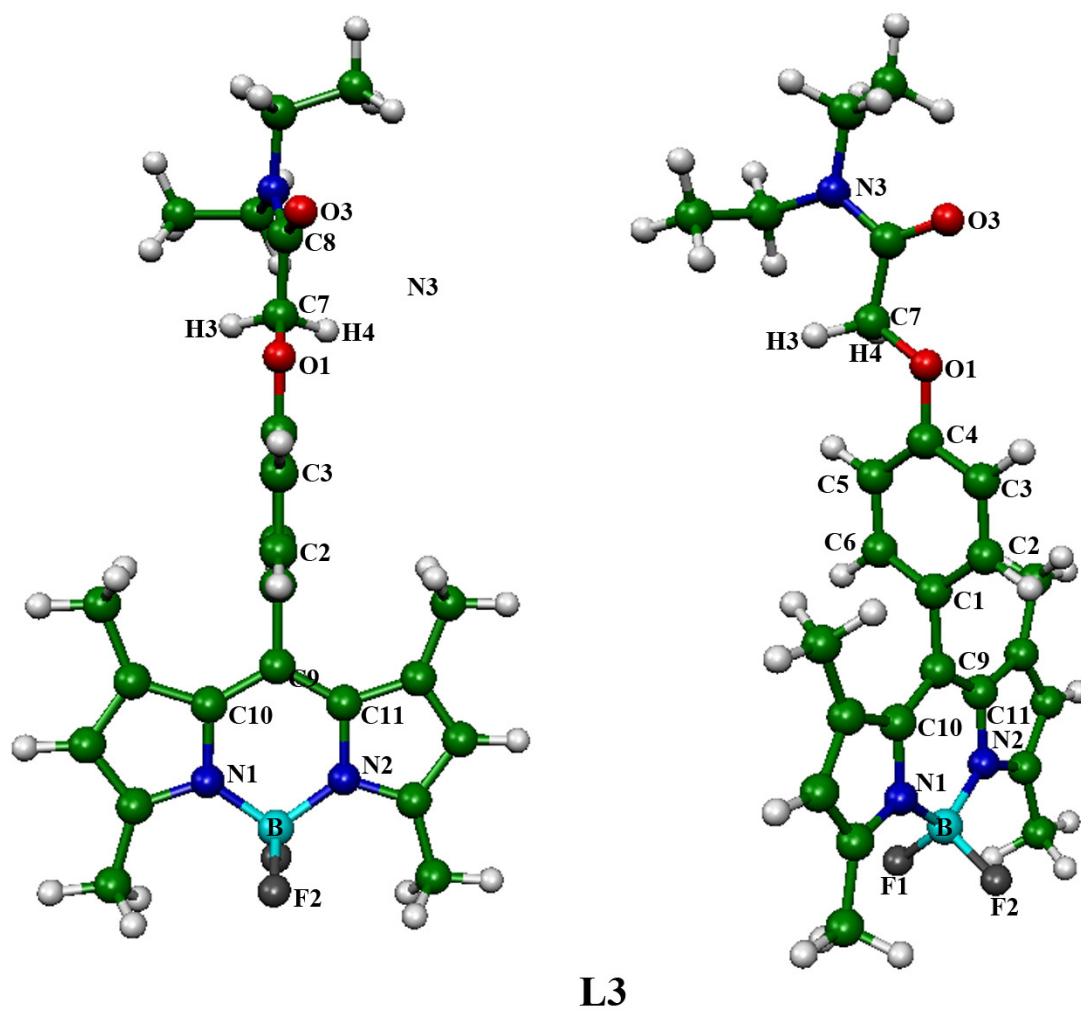
Figure B6 Atomic labeling of receptor **L3.**
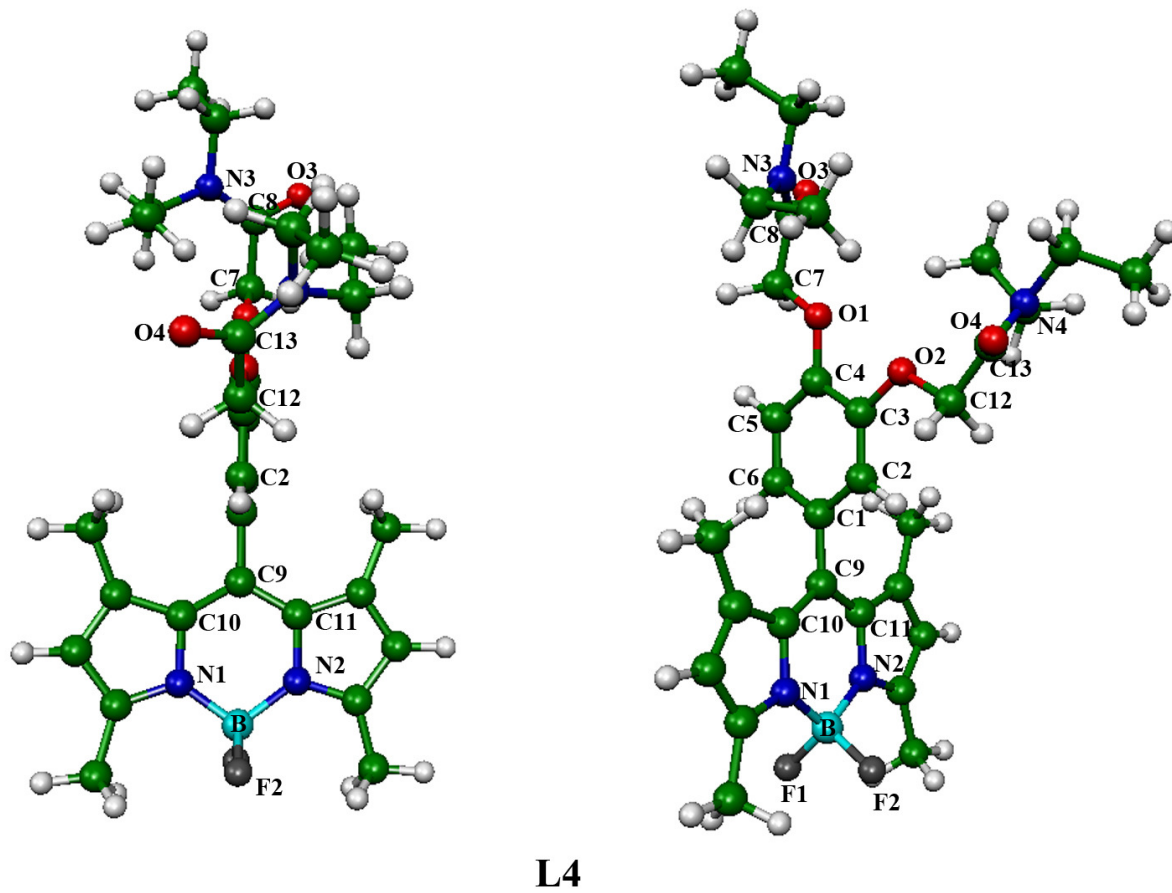
Figure B7 Atomic labeling of receptor **L4.**

L5

L6
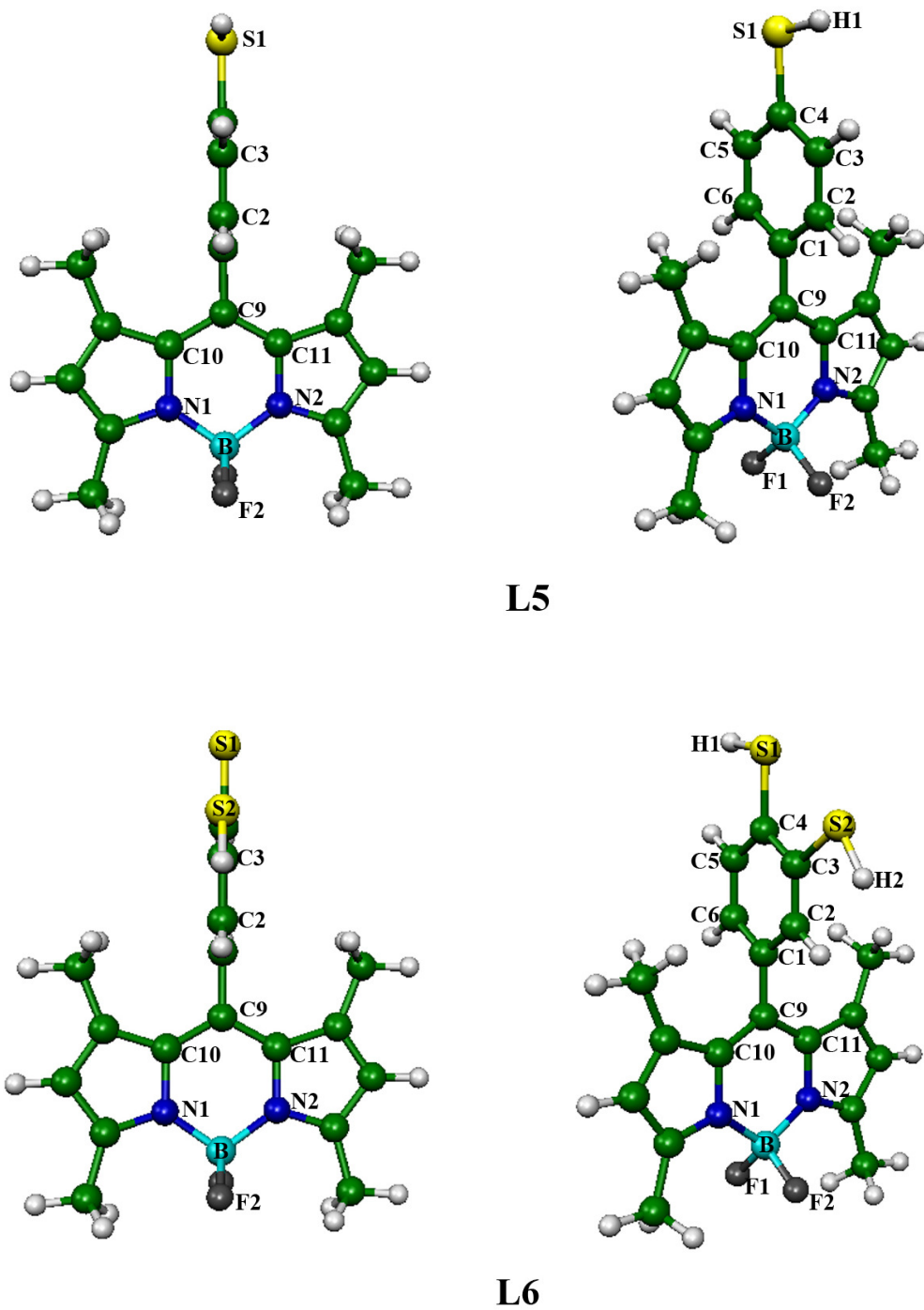
Figure B8 Atomic labeling of receptors **L5 and L6**.
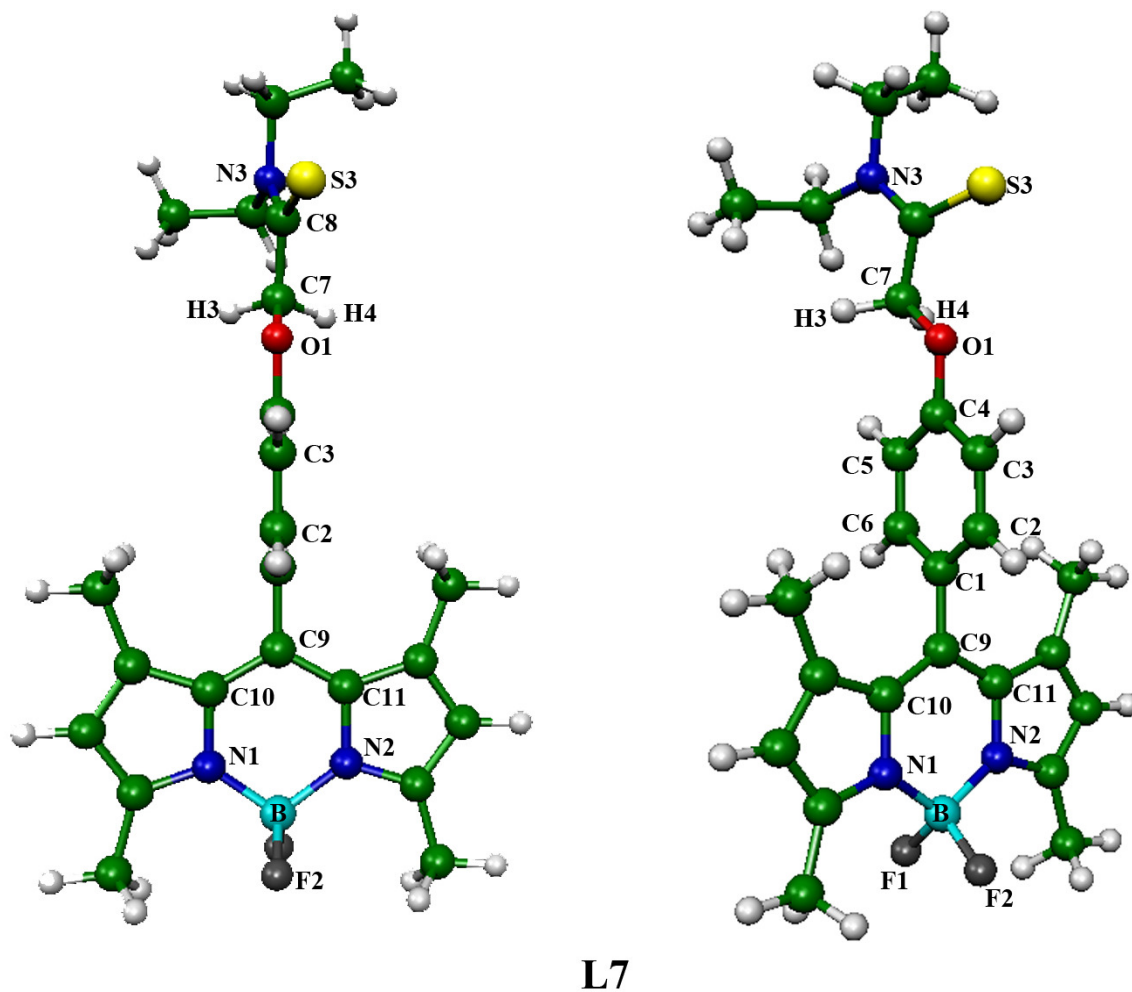
L7

Figure B9 Atomic labeling of receptor **L7.**

L8
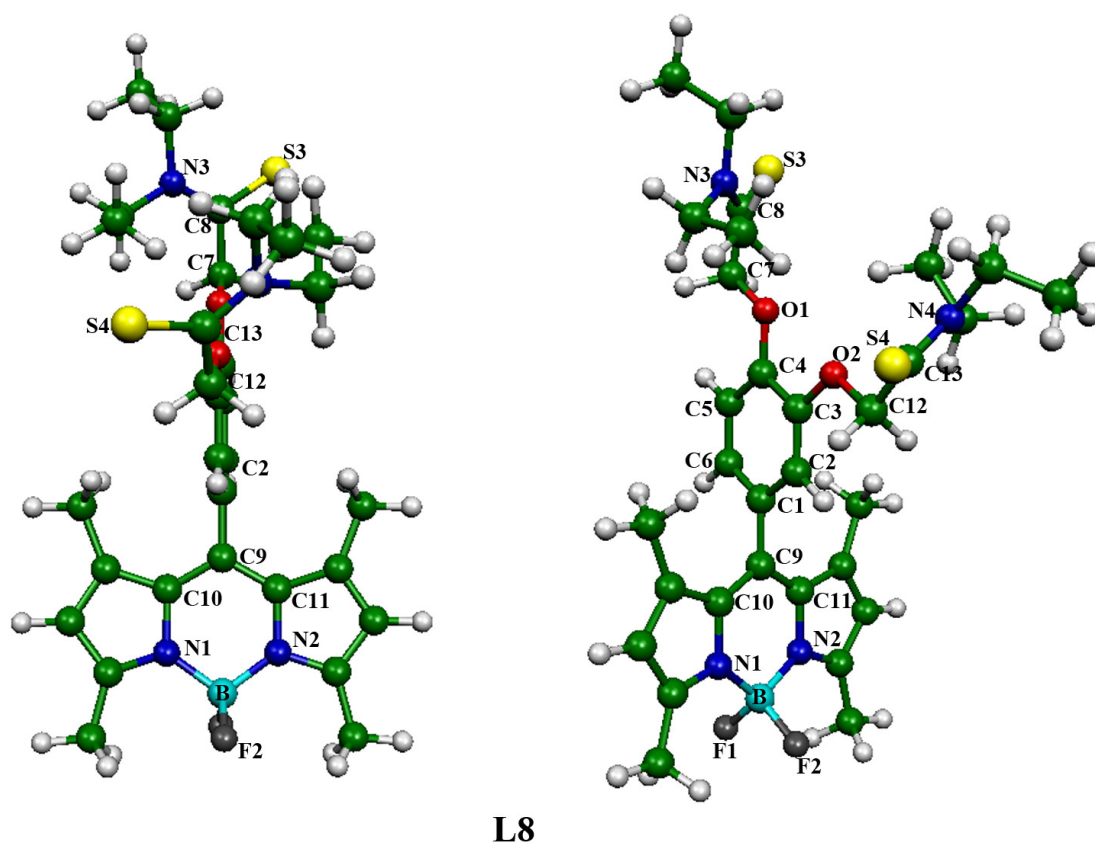
Figure B10 Atomic labeling of receptor **L8**.

Table B1 Geometrical data for the structure of receptor **L1** and its complexes with various cationic guests obtained by using DFT calculation.

Parameter	L1	L1/Na$^+$	L1/Al^{3+}	L1/Cu^{2+}	L1/Ag$^+$
Distances (Å)					
C3-C4	1.408	1.403	1.403	1.400	1.400
C4-O1	1.399	1.453	1.458	1.460	1.443
C4-C5	1.409	1.403	1.403	1.400	1.401
O1-M	-	2.216	2.199	1.948	2.263
O1-H1	0.979	0.979	0.987	0.981	0.979
N1-B	1.534	1.538	1.558	1.547	1.539
N2-B	1.534	1.538	1.559	1.547	1.539
B-F1	1.449	1.443	1.412	1.426	1.440
B-F2	1.449	1.443	1.412	1.426	1.441
Angles (°)					
H1-O1-C4	112.4	111.8	111.5	112.5	112.8
M-O1-H1	-	135.9	117.1	120.5	123.2
M-O1-C4	-	112.3	131.5	127.0	123.3
O1-C4-C3	116.8	118.9	118.9	118.6	120.1
O1-C4-C5	122.9	118.9	118.9	118.6	117.6
C2-C1-C9	120.6	120.4	120.2	120.2	120.5
C6-C1-C9	120.6	120.4	120.2	120.2	120.3
C1-C9-C10	119.7	119.5	121.2	120.2	119.5
C1-C9-C11	119.7	119.2	121.5	120.3	119.6
N1-B-N2	108.3	108.1	105.2	106.7	107.9
N1-B-F1	110.3	110.2	109.8	109.9	110.1
N1-B-F2	110.3	110.2	109.7	109.9	110.1
N2-B-F1	110.3	110.1	109.8	109.9	110.1
N2-B-F2	110.3	110.1	109.8	109.9	110.1
F1-B-F2	107.3	108.2	112.3	110.4	108.5
Dihedral angles (°)					
H1-O1-C4-C3	180.0	-91.2	-89.4	-89.6	132.7
H1-O1-C4-C5	0.0	91.4	90.5	90.1	143.1

Table B1 (continued)

Parameter	L1	L1/Na$^+$	L1/Al^{3+}	L1/Cu^{2+}	L1/Ag$^+$
Dihedral angles (°)					
M-O1-C4-C5	-	-88.6	-89.5	-90.0	-45.9
C2-C1-C9-C10	90.0	90.1	89.8	89.8	89.0
C2-C1-C9-C11	-90.0	-89.9	-90.2	-90.2	-91.5
C6-C1-C9-C10	-90.0	-90.0	-89.7	-89.8	-90.6
C6-C1-C9-C11	90.0	90.0	90.3	90.2	88.9

Table B2 Geometrical data for the structure of receptor **L2** and its complexes with various cationic guests obtained by using DFT calculation.

Parameter	L2	L2/Na$^+$	L2/Al^{3+}	L2/Cu^{2+}	L2/Ag$^+$
Distances (Å)					
C3-C4	1.417	1.404	1.407	1.407	1.404
C3-O2	1.394	1.424	1.414	1.419	1.424
C4-O1	1.394	1.424	1.413	1.417	1.423
C4-C5	1.405	1.401	1.398	1.398	1.400
O1-M	-	2.273	2.269	2.061	2.316
O2-M	-	2.274	2.306	2.060	2.322
O1-H1	0.979	0.978	0.984	0.979	0.978
O2-H2	0.980	0.978	0.983	0.979	0.978
N1-B	1.534	1.538	1.559	1.548	1.538
N2-B	1.534	1.538	1.559	1.548	1.538
B-F1	1.449	1.441	1.411	1.425	1.441
B-F2	1.449	1.445	1.412	1.427	1.444
Angles (°)					
H1-O1-C4	111.8	111.1	115.1	114.7	112.9
H2-O2-C3	111.9	111.2	116.0	114.9	112.9
M-O1-H1	-	133.0	116.0	131.6	130.73
M-O1-C4	-	115.9	122.5	113.7	116.4
M-O2-H2	-	132.9	122.7	131.3	130.8
M-O2-C3	-	115.9	121.3	113.8	116.3
O1-M-O2	-	73.4	68.0	80.3	72.0
O1-C4-C3	117.3	117.5	114.4	116.3	117.75
O1-C4-C5	123.4	122.6	125.0	123.5	122.2
O2-C3-C2	123.1	117.4	125.24	123.3	121.9
O2-C3-C4	117.2	122.2	113.8	116.0	117.6
C2-C1-C9	119.8	119.6	120.2	120.0	120.1
C6-C1-C9	121.1	121.3	119.9	120.5	120.8
C1-C9-C10	119.7	119.3	121.3	120.2	119.3
C1-C9-C11	119.7	119.3	121.3	120.2	119.3
N1-B-N2	108.3	108.1	105.1	106.7	108.1
N1-B-F1	110.3	110.2	109.8	110.0	110.2
N1-B-F2	110.3	110.0	109.7	109.9	110.0
N2-B-F1	110.3	110.2	109.8	110.0	110.2
N2-B-F2	110.3	110.0	109.7	109.9	110.0
F1-B-F2	107.3	108.2	112.4	110.5	108.3
Dihedral angles (°)					
H1-O1-C4-C3	179.9	-180.0	180.0	180.0	-179.4
H1-O1-C4-C5		0.0	0.0	0.0	0.7
H2-O2-C3-C2		0.0	0.0		

Table B2 (continued)

Parameter	L2	L2/Na$^+$	L2/Al^{3+}	L2/Cu^{2+}	L2/Ag$^+$
Dihedral angles (°)					
H2-O2-C3-C4	-180.0	180.0	180.0	-180.0	179.4
M-O1-C4-C3	-	0.0	0.0	0.0	1.1
M-O1-C4-C5	-	-180.0	-180.0	180.0	-178.8
M-O2-C3-C2	-	180.0	180.0	-180.0	179.0
M-O2-C3-C4	-	0.0	0.0	0.0	-0.9
C2-C1-C9-C10	89.6	89.5	90.7	90.1	91.3
C2-C1-C9-C11	-89.7	-89.5	-90.6	-90.1	-88.9
C6-C1-C9-C10	-90.4	-90.5	-89.3	-89.9	-88.8
C6-C1-C9-C11	90.3	90.5	89.4	-90.1	91.1

Table B3 Geometrical data for the structure of receptor **L3** and its complexes with various cationic guests obtained by using DFT calculation.

Parameter	L3	L3/Na$^+$	L3/Al^{3+}	L3/Cu^{2+}	L3/Ag$^+$
Distances (Å)					
C3-C4	1.411	1.403	1.403	1.404	1.402
C4-O1	1.395	1.438	1.449	1.434	1.441
C4-C5	1.411	1.404	1.403	1.404	1.403
O1-M	-	2.319	2.153	2.131	2.386
O3-M	-	2.192	1.855	1.958	2.231
C7-C8	1.542	1.540	1.535	1.542	1.539
C7-O1	1.445	1.471	1.499	1.481	1.467
C8-O3	1.254	1.279	1.323	1.292	1.287
C8-N3	1.383	1.351	1.313	1.337	1.346
N1-B	1.534	1.537	1.554	1.547	1.537
N2-B	1.534	1.537	1.554	1.547	1.538
B-F1	1.450	1.444	1.417	1.427	1.444
B-F2	1.449	1.444	1.417	1.427	1.444
Angles (°)					
M-O1-C4	-	127.8	126.4	131.4	129.1
M-O1-C7	-	117.9	115.9	112.6	116.3
M-O3-C8	-	123.6	128.2	119.2	122.0
O1-M-O3	-	71.3	76.2	80.7	71.4
O1-C4-C3	115.0	119.1	119.0	119.1	118.9
O1-C4-C5	125.0	119.3	118.9	119.2	119.2
O1-C7-C8	107.8	107.9	104.8	108.0	109.3
O3-C8-C7	122.0	119.1	114.8	119.3	120.7
O3-C8-N3	122.3	122.6	121.9	121.5	121.0
C2-C1-C9	120.7	120.4	120.6	120.3	120.4
C6-C1-C9	120.6	120.4	119.9	120.3	120.4
C1-C9-C10	119.7	119.4	121.1	120.4	119.3
C1-C9-C11	119.8	119.5	120.7	120.3	119.6
N1-B-N2	108.3	108.1	105.7	106.7	108.1
N1-B-F1	110.3	110.1	109.8	110.0	110.2
N1-B-F2	110.3	110.1	109.9	109.9	110.1
N2-B-F1	110.3	110.1	109.8	109.9	110.2
N2-B-F2	110.4	110.2	109.8	110.0	110.2
F1-B-F2	107.3	108.1	111.7	110.3	108.1
Dihedral angles (°)					
M-O1-C4-C3	-	90.0	89.9	91.3	91.4
M-O1-C4-C5	-	-87.8	-85.9	-85.5	-86.9
M-O1-C7-C8	-	-4.1	-1.7	-3.9	-4.8
M-O3-C8-C7	-	-4.0	-1.4	87.6	-4.9

Table B3 (continued)

Parameter	L3	L3/Na$^+$	L3/Al^{3+}	L3/Cu^{2+}	L3/Ag$^+$
M-O3-C8-N3	-	176.4	178.8	176.8	175.8
O1-C7-C8-O3	-	5.1	1.9	5.0	6.3
C2-C1-C9-C10	91.1	91.0	90.5	91.0	-89.8
C2-C1-C9-C11	-89.2	-89.1	-90.6	-89.1	90.2
C6-C1-C9-C10	-88.8	-89.0	-90.6	-89.1	-89.7
C6-C1-C9-C11	90.9	90.9	88.4	90.4	90.3

Table B4 Geometrical data for the structure of receptor **L4** and its complexes with various cationic guests obtained by using DFT calculation.

Parameter	L4	L4/Na$^+$	L4/Al^{3+}	L4/Cu^{2+}	L4/Ag$^+$
Distances (Å)					
N1-B	1.534	1.537	1.546	1.546	1.537
N2-B	1.534	1.537	1.548	1.545	1.537
B-F1	1.449	1.441	1.422	1.427	1.441
B-F2	1.449	1.447	1.433	1.431	1.448
C3-C4	1.424	1.418	1.405	1.424	1.419
C3-O2	1.395	1.407	1.440	1.391	1.404
C4-O1	1.395	1.407	1.439	1.389	1.404
C4-C5	1.404	1.401	1.392	1.400	1.402
O1-M	-	2.421	2.002	2.514	2.597
O2-M	-	2.414	2.011	2.533	2.592
O3-M	-	2.243	1.824	1.925	2.222
O4-M	-	2.243	1.824	1.926	2.221
C7-C8	1.532	1.542	1.539	1.541	1.541
C7-O1	1.395	1.454	1.489	1.451	1.446
C8-O3	1.266	1.273	1.330	1.284	1.279
C8-N3	1.372	1.356	1.310	1.343	1.352
C12-C13	1.532	1.542	1.540	1.542	1.541
C12-O2	1.464	1.355	1.489	1.449	1.448
C13-O4	1.265	1.273	1.329	1.283	1.279
C13-N4	1.372	1.355	1.310	1.343	1.352
Angles (°)					
M-O1-C4	-	121.6	119.2	125.8	123.8
M-O1-C7	-	119.8	117.6	112.6	116.6
M-O2-C3	-	121.8	119.1	125.2	123.9
M-O2-C12	-	119.7	117.4	112.5	116.5
M-O3-C8	-	126.0	123.8	132.3	128.6
M-O4-C13	-	125.8	123.8	133.0	128.5
O1-M-O2	-	65.8	76.3	60.9	61.0
O1-M-O3	-	67.8	79.5	69.7	66.2
O2-M-O4	-	68.0	79.4	69.2	66.3
O3-M-O4	-	158.4	108.3	160.3	166.5
O1-C4-C3	115.9	115.4	112.0	114.2	115.6
O1-C4-C5	124.7	125.0	126.8	126.0	124.8
O1-C7-C8	109.1	106.7	103.3	105.3	107.2
O2-C3-C2	124.5	124.6	126.6	125.9	124.4
O2-C3-C5	115.7	115.4	111.8	113.9	115.7
O2-C12-C13	109.1	106.8	103.4	105.3	107.3

Table B4(continued)

Parameter	L4	L4/Na$^+$	L4/Al^{3+}	L4/Cu^{2+}	L4/Ag$^+$
Angles (°)					
O3-C8-C7	118.3	119.6	114.7	119.9	121.2
O3-C8-N3	122.5	122.7	121.3	121.1	122.1
O4-C13-C12	118.4	119.6	119.9	121.3	114.8
O4-C13-N4	122.5	122.7	121.2	121.1	122.0
C2-C1-C9	119.7	118.7	119.6	118.8	119.1
C6-C1-C9	120.9	122.0	120.7	122.0	121.1
C1-C9-C10	119.8	119.4	120.3	119.4	119.7
C1-C9-C11	119.6	119.5	120.3	119.5	119.4
N1-B-N2	108.3	108.2	106.8	108.2	107.0
N1-B-F1	110.4	110.3	110.1	110.3	110.3
N1-B-F2	110.3	110.0	109.8	110.0	109.5
N2-B-F1	110.3	110.3	110.1	110.3	110.2
N2-B-F2	110.3	110.0	109.9	110.0	109.4
F1-B-F2	107.3	108.0	110.1	108.0	110.5
Dihedral angles (°)					
M-O1-C4-C3	-	0.730	1.130	0.871	9.924
M-O1-C4-C5	-	-179.497	-179.243	-179.472	-167.870
M-O1-C7-C8	-	-2.348	-2.413	-2.781	-7.915
M-O2-C3-C2	-	-179.733	-179.486	-179.440	168.004
M-O2-C3-C4	-	0.470	1.124	0.897	-9.020
M-O2-C12-C13	-	-2.065	-3.301	-2.837	5.633
M-O3-C8-C7	-	-4.290	-4.756	-5.298	6.612
M-O3-C8-N3	-	175.986	175.732	175.192	-172.807
M-O4-C13-C12	-	-3.484	-3.311	-3.853	-9.660
M-O4-C13-N4	-	176.795	177.023	176.529	169.815
O1-C7-C8-O3	122.653	4.037	4.452	4.920	1.452
O1-C4-C3-O2	-0.871	-0.748	-1.354	-1.089	-0.508
O2-C12-C13-O4	121.990	3.390	4.133	4.178	1.643
C2-C1-C9-C10	87.882	88.840	90.554	88.895	90.414
C2-C1-C9-C11	-92.051	-89.006	-89.645	-89.154	-89.330
C6-C1-C9-C10	-92.527	-91.169	-89.723	-91.117	-90.117
C6-C1-C9-C11	87.540	90.985	90.211	90.835	90.140

Table B5 Geometrical data for the structure of receptor **L5** and its complexes with various cationic guests obtained by using DFT calculation.

Parameter	L5	L5/Na$^+$	L5/Cu^{2+}	L5/Ag$^+$
Distances (Å)				
C3-C4	1.410	1.405	1.404	1.404
C4-S1	1.842	1.86863	1.881	1.875
C4-C5	1.409	1.406	1.405	1.405
S1-M	-	2.853	2.322	2.598
S1-H1	1.376	1.375	1.378	1.378
N1-B	1.534	1.538	1.547	1.539
N2-B	1.534	1.538	1.548	1.539
B-F1	1.449	1.444	1.425	1.442
B-F2	1.449	1.443	1.426	1.441
Angles (°)				
H1-S1-C4	97.2	100.5	99.9	99.6
M-S1-H1	-	119.6	103.4	102.1
M-S1-C4	-	115.1	112.8	107.1
S1-C4-C3	117.5	117.7	122.7	116.3
S1-C4-C5	123.0	121.1	115.5	121.9
C2-C1-C9	120.7	120.6	120.3	120.7
C6-C1-C9	120.6	120.2	120.3	120.1
C1-C9-C10	119.7	119.5	120.1	119.5
C1-C9-C11	119.7	119.3	120.4	119.4
N1-B-N2	108.3	108.1	106.7	108.0
N1-B-F1	110.3	110.1	109.9	110.1
N1-B-F2	110.3	110.2	110.0	110.2
N2-B-F1	110.3	110.1	110.0	110.1
N2-B-F2	110.3	110.2	109.8	110.1
F1-B-F2	107.3	108.1	110.4	108.4
Dihedral angles (°)				
H1-S1-C4-C3	0.005	-110.900	-58.114	-131.341
H1-S1-C4-C5	-179.992	69.798	120.439	48.845
M-S1-C4-C3	-	119.122	51.048	89.668
M-S1-C4-C5	-	-60.181	-130.398	-91.426
C2-C1-C9-C10	89.937	91.693	87.786	89.668
C2-C1-C9-C11	-89.984	-88.620	-183.970	-91.426
C6-C1-C9-C10	89.937	-88.161	-91.663	-90.364
C6-C1-C9-C11	-89.984	91.527	88.244	88.542

Table B6 Geometrical data for the structure of receptor **L6** and its complexes with various cationic guests obtained by using DFT calculation.

Parameter	L6	L6/Na$^+$	L6/Al^{3+}	L6/Cu^{2+}	L6/Ag$^+$
Distances (Å)					
C3-C4	1.415	1.408	1.415	1.413	1.410
C3-S2	1.843	1.858	1.866	1.880	1.874
C4-S1	1.843	1.858	1.829	1.878	1.872
C4-C5	1.409	1.408	1.416	1.408	1.410
S1-M	-	2.942	3.278	2.402	2.676
S2-M	-	2.930	3.310	2.412	2.672
S1-H1	1.376	1.373	1.375	1.381	1.379
S2-H2	1.376	1.373	1.381	1.381	1.378
N1-B	1.534	1.538	1.559	1.548	1.539
N2-B	1.534	1.538	1.558	1.548	1.539
B-F1	1.448	1.442	1.413	1.425	1.441
B-F2	1.449	1.445	1.414	1.426	1.443
Angles (°)					
H1-S1-C4	96.1	98.1	99.4	98.5	97.5
H2-S2-C3	96.2	98.2	98.1	98.6	97.6
M-S1-H1	-	118.8	132.7	102.9	104.7
M-S1-C4	-	107.4	117.5	97.7	100.6
M-S2-H2	-	121.1	103.7	102.2	105.6
M-S2-C3	-	107.8	115.0	97.6	100.7
S1-M-S2	-	68.2	59.9	95.1	81.9
S1-C4-C3	119.2	120.6	118.9	124.9	124.1
S1-C4-C5	121.7	119.9	121.8	115.7	116.6
S2-C3-C2	121.4	119.6	117.8	115.5	116.2
S2-C3-C4	119.1	120.3	121.9	124.5	123.8

Table B6 (continued)

Parameter	L6	L6/Na$^+$	L6/Al^{3+}	L6/Cu^{2+}	L6/Ag$^+$
Angles (°)					
C2-C1-C9	119.9	119.8	119.1	120.2	119.9
C6-C1-C9	121.1	121.3	121.8	120.7	121.3
C1-C9-C10	119.6	119.4	121.1	120.1	119.3
C1-C9-C11	119.6	119.3	121.1	120.3	119.2
N1-B-N2	108.3	108.1	105.3	106.7	108.1
N1-B-F1	107.3	110.2	109.8	110.0	110.2
N1-B-F2	110.3	110.0	109.7	109.9	110.0
N2-B-F1	110.3	110.2	109.8	109.9	110.2
N2-B-F2	110.3	110.1	109.8	109.9	110.1
F1-B-F2	107.3	108.2	112.2	110.5	108.3
Dihedral angles (°)					
H1-S1-C4-C3	-179.3	-153.1	174.0	100.5	-127.8
H1-S1-C4-C5	0.8	29.6	-8.0	-83.9	55.7
H2-S2-C3-C2	0.8	-26.4	-90.4	84.9	-54.4
H2-S2-C3-C4	-179.3	156.4	92.8	-99.4	129.2
M-S1-C4-C3	-	-29.5	24.5	-3.9	-21.2
M-S1-C4-C5	-	153.2	-157.5	171.7	162.2
M-S2-C3-C2	-	-152.8	160.3	-171.5	-162.0
M-S2-C3-C4	-	29.9	-16.4	4.2	21.7
C2-C1-C9-C10	89.7	94.1	89.9	87.13	94.9
C2-C1-C9-C11	-89.8	-85.2	-85.5	-93.4	-84.7
C6-C1-C9-C10	-90.3	-86.5	-90.3	-91.6	-86.2
C6-C1-C9-C11	90.3	94.2	94.4	87.9	94.2

Table B7 Geometrical data for the structure of receptor **L7** complexes with various cationic guests obtained by using DFT calculation.

Parameter	L7	L7/Na$^+$	L7/Al^{3+}	L7/Cu^{2+}	L7/Ag$^+$
Distances (Å)					
C3-C4	1.411	1.404	1.404	1.403	1.403
C4-O1	1.395	1.441	1.436	1.441	1.462
C4-C5	1.411	1.404	1.404	1.403	1.402
S1-M	-	2.271	2.101	2.399	2.070
S3-M	-	2.749	2.283	2.550	2.458
C7-C8	1.534	1.532	1.536	1.532	1.529
C7-O1	1.445	1.470	1.479	1.460	1.500
C8-S3	1.715	1.746	1.771	1.765	1.792
C8-N3	1.370	1.347	1.336	1.340	1.320
N1-B	1.534	1.538	1.547	1.538	1.553
N2-B	1.534	1.538	1.547	1.538	1.553
B-F1	1.450	1.443	1.427	1.444	1.418
B-F2	1.449	1.443	1.427	1.444	1.418
Angles (°)					
M-O1-C4	-	116.6	127.2	121.9	117.9
M-O1-C7	-	129.8	116.8	122.6	126.6
M-S3-C8	-	101.1	97.3	103.0	100.0
O1-M-S3	-	73.7	89.4	77.2	81.7
O1-C4-C3	114.9	119.0	118.8	118.7	118.5
O1-C4-C5	125.1	119.4	119.4	119.3	119.0
O1-C7-C8	110.0	112.4	112.7	112.8	110.7
S3-C8-C7	121.5	122.2	123.0	123.5	120.4
S3-C8-N3	123.9	122.1	120.6	120.4	120.6
C2-C1-C9	120.7	120.4	120.3	120.4	120.4
C6-C1-C9	120.6	120.4	120.3	120.4	120.2
C1-C9-C10	119.7	119.4	120.4	119.6	120.9
C1-C9-C11	119.8	119.5	120.3	119.3	120.7
N1-B-N2	108.3	108.1	106.7	108.1	105.8
N1-B-F1	110.3	110.1	109.9	110.2	109.9
N1-B-F2	110.3	110.1	109.9	110.1	109.8
N2-B-F1	110.3	110.1	109.9	110.1	109.8
N2-B-F2	110.3	110.1	110.0	110.2	109.8
F1-B-F2	107.3	108.2	110.3	108.1	111.5
Dihedral angles (°)					
M-O1-C4-C3	-	88.802	90.035	91.129	85.227
M-O1-C4-C5	-	-88.638	-86.117	-85.228	-91.189
M-O1-C7-C8	-	-6.383	-7.817	-9.178	-4.306
M-S3-C8-C7	-	-8.046	174.237	-8.497	-7.586
M-S3-C8-N3	-	173.786	10.912	173.774	174.126

Table B7 (continued)

Parameter	L7	L7/Na$^+$	L7/Al^{3+}	L7/Cu^{2+}	L7/Ag$^+$
O1-C7-C8-S3	90.921	90.009	90.692	90.251	91.484
C2-C1-C9-C10	-89.308	-90.020	-89.383	-89.832	-89.183
C2-C1-C9-C11	-88.983	-89.957	89.949	-90.633	-89.247
C6-C1-C9-C10	90.788	90.014	-89.976	89.284	90.086
C6-C1-C9-C11	90.921	90.009	90.692	90.251	91.484

Table B8 Geometrical data for the structure of receptor **L8** complexes with various cationic guests obtained by using DFT calculation.

Parameter	L8	L8/Na$^+$	L8/Al^{3+}	L8/Ag$^+$
Distances (Å)				
C3-C4	1.424	1.420	1.401	1.420
C3-O2	1.395	1.419	1.458	1.410
C4-O1	1.395	1.418	1.460	1.410
C4-C5	1.404	1.406	1.393	1.405
O1-M	-	2.338	1.946	2.606
O2-M	-	2.330	1.944	2.590
O3-M	-	2.772	2.334	2.551
O4-M	-	2.770	2.336	2.549
C7-C8	1.524	1.532	1.527	1.530
C7-O1	1.469	1.463	1.494	1.451
C8-S3	1.732	1.736	1.802	1.747
C8-N3	1.357	1.352	1.527	1.529
C12-C13	1.524	1.531	1.527	1.529
C12-O2	1.470	1.464	1.495	1.453
C13-S4	1.731	1.736	1.801	1.747
C13-N4	1.358	1.352	1.315	1.347
N1-B	1.534	1.537	1.545	1.537
N2-B	1.534	1.537	1.547	1.537
B-F1	1.449	1.440	1.419	1.440
B-F2	1.449	1.448	1.443	1.449
Angles (°)				
M-O1-C4	-	116.6	117.0	121.4
M-O1-C7	-	127.9	125.1	121.9
M-O2-C3	-	116.8	117.1	121.8
M-O2-C12	-	127.9	125.1	121.8
M-S3-C8	-	100.4	98.3	107.5
M-S4-C13	-	100.7	98.0	107.4
O1-M-O2	-	71.5	80.6	62.7
O1-M-S3	-	73.2	86.4	72.7
O2-M-S4	-	73.4	86.2	73.2
S3-M-S4	-	142.1	104.7	152.0
O1-C4-C3	115.8	117.4	112.5	117.0

Table B8 (continued)

Parameter	L8	L8/Na$^+$	L8/Al^{3+}	L8/Ag$^+$
Angles (°)				
O1-C4-C5	124.8	123.5	123.9	126.4
O1-C7-C8	109.5	113.0	123.4	125.9
O2-C3-C2	124.6	123.1	117.1	112.5
O2-C3-C4	115.6	117.5	123.4	112.5
O2-C12-C13	109.0	113.4	112.6	110.1
S3-C8-C7	116.9	122.6	123.4	119.8
S3-C8-N3	124.6	122.4	121.1	120.9
S4-C13-C12	117.0	122.9	123.5	119.6
S4-C13-N4	124.6	122.4	121.2	121.1
C2-C1-C9	119.6	118.6	118.4	117.5
C6-C1-C9	121.0	122.4	122.6	122.9
C1-C9-C10	119.7	119.4	119.4	118.9
C1-C9-C11	119.7	119.4	119.4	119.3
N1-B-N2	108.3	108.1	108.2	107.2
N1-B-F1	110.3	110.4	110.4	110.9
N1-B-F2	110.3	109.9	109.9	108.8
N2-B-F1	110.3	110.4	110.4	110.8
N2-B-F2	110.3	109.9	109.9	108.6
F1-B-F2	107.4	108.1	108.1	110.5
Dihedral angles (°)				
M-O1-C4-C3	-	4.099	1.615	4.432
M-O1-C4-C5	-	-175.785	-178.462	-175.105
M-O1-C7-C8	-	-1.351	-0.144	-7.599
M-O2-C3-C2	-	176.001	178.641	175.410
M-O2-C3-C4	-	-3.768	-1.206	-3.163
M-O2-C12-C13	-	2.978	-13.816	3.344
M-S3-C8-C7	-	-18.754	-17.512	179.321
M-S3-C8-N3	-	164.720	165.610	171.714
M-S4-C13-C12	-	-14.264	-13.816	-9.385
M-S4-C13-N4	-	168.069	168.571	-1.731
O1-C7-C8-S3	123.639	15.722	12.328	5.354
O1-C4-C3-O2	-1.433	-0.232	-0.270	-0.781
O2-C12-C13-S4	121.447	9.804	9.259	5.453

Table B8 (continued)

Parameter	L8	L8/Na$^+$	L8/Al^{3+}	L8/Ag$^+$
Dihedral angles (°)				
C2-C1-C9-C10	85.702	88.722	88.413	84.082
C2-C1-C9-C11	-94.037	-89.112	-88.927	-92.404
C6-C1-C9-C10	-94.292	-91.356	-91.648	-95.764
C6-C1-C9-C11	85.969	90.809	91.013	87.751

BIOGRAPHY

BIOGRAPHY

NAME	Mrs Tasawan Keawwangchai
DATE OF BIRTH	April 4th, 1977
PLACE OF BIRTH	Udorn Thani province, Thailand
EDUCATION	

1994	Satree Rachenutid (High School)
1998	Mahasarakham University, B.Sc. (Chemistry)
2000	Chiang Mai University, M.Sc. (Teaching Chemistry)
2012	Mahasarakham University, Ph.D. (Chemistry)

POSITION	Lecturer
WORK PLACE	Department of Chemistry, Faculty of Science, Mahasarakham University, Maha Sarakham, Thailand 44000
ADDRESS	65/2 Raumjit district, Udorn Thani province, 30110, Thailand e-mail : k.tasawan@gmail.com

RESERCH GRANTS & AWARDS

Center of Excellence for Innovation in Chemistry (PERCH-CIC)

LIST OF PUBLICATIONS

CONFERENCES

1. **Tasawan Keawwangchai**, Nongnit Morakot, Banchob Wanno and Somchai Keawwangchai "Theoretical and experimental studies of binitrophenol and binitronaphthol derivatives as Al(III) and Ge(IV) optical sensor" Sokendai Asian Winter School "Molecular Science – Central Role in Multidisciplinary Fields" December 1-4, 2009.

NATIONNAL CONFERENCES

1. **Tasawan Keawwangchai**, Nongnit Morakot and Banchob Wanno, "A Density functional study of Al^{3+} and Ge^{4+} complexs with binitrophenol and binitronaphthol derivatives" PERCH-CIC congress VI, Jomtien Palm Beach Hotel & Resort, Pattaya City, Chonburi, THAILAND, May 3-6, 2009.